The ALS gene TDP-43 induces p53-mediated apoptosis in Neural Stem Cells

A thesis submitted to the University of Sheffield
for the degree of Doctor of Philosophy

Miriam Anna Vogt

October 2013

Department of Biomedical Sciences
University of Sheffield

Acknowledgments

I would like to thank everybody who supported me during my PhD, especially my supervisor Verdon Taylor for giving me the opportunity to work on two exciting projects. I'm very grateful for his advice, trust and support throughout my time in the lab.

For their help and for creating a fun place to work I would like to thank all current and past members of the lab. I especially want to thank Philip who supervised me during my Diploma thesis and who taught me all the basics and more.

I would like to acknowledge all the neighbouring labs over the past 4 years for sharing reagents and knowledge and contributing to a great work environment. Thanks to all members of the Kemler lab, especially Daniel and Stefan, for their patience with the newbie. Thanks to the C-floor and D-floor members for a nice and warm welcome in the UK. And finally thanks to our current neighbours from the Zeller lab for happily sharing their coffee breaks and aperos. I'm very grateful that I have met so many kind, helpful and fun people over the last years.

Special thanks goes to my family and friends for their support. In particular to my parents for their trust and simply for being there whenever I need them.

1 Summary

Neural stem cells (NSCs) give rise to the mammalian central nervous system in a highly regulated process. Notch signalling is critical for the maintenance and fate determination of NSCs and we identified the RNA binding protein TDP-43 as a downstream effector of Notch1. TDP-43 is a key player in various neurodegenerative diseases including Amyotrophic lateral sclerosis (ALS), Frontotemporal lobar degeneration (FTLD) and Alzheimer's disease. Here the protein is a main component of cytoplasmic inclusions accumulating in apoptotic neurons. Point mutations in TDP-43 were recently shown to cause ALS and FTLD and the protein was therefore suggested to play a role in disease onset or progression. However, it is not known how the mutations affect protein function and whether they result in a loss- or gain-of-funtion. Upregulation of p53 has been observed in affected neurons of ALS patients, but no correlation to TDP-43 has been described to date. In this study we show that expression of TDP-43 and its mutant form TDP-43$^{(A315T)}$ in the developing telencephalon results in p53-mediated apoptosis of NSCs. In accordance, we were able to rescue the early lethality of hTDP-43$^{(A315T)}$ mutant mice by pharmacological inhibition of p53. Furthermore, we show in our studies that TDP-43 binds *Cdkn1a* mRNA and demonstrate *Cdkn1a* as being upregulated after TDP-43 expression. This most probably results in altered cell cycle regulation which we observed following TDP-43 and TDP-43$^{(A315T)}$ expression.

2 Abbreviations

ALS	Amyotrophic lateral sclerosis
AVE	Anterior visceral endoderm
bHLH	basic helix-loop-helix
BLBP	Brain lipid-binding protein
BMP	Bone morphogenic protein
BPs	Basal progenitor cells
BrdU	Bromodesoxyuridine
Cdkn1a	Cyclin-dependent kinase inhibitor 1a
cDNA	complementary DNA
cKO	conditional knockout
CLIP	Crosslinked RNA Immunoprecipitation
CNS	Central nervous system
CFTR	Cystic fibrosis transmembrane conductance regulator
CP	Cortical plate
DEPC	Diethylpyrocarbonate
dsRBD	Double-stranded RNA binding domain
dsRNA	Double-stranded RNA
EdU	Ethynyldeoxyuridine
ES	Embryonic stem
EtOH	Ethanol
FACS	Fluorescence-activated cell sorting
FGF	Fibroblast growth factor
FMRP	Fragile X mental retardation protein
FTLD	Frontotemporal lobar degeneration
FUS	Fused in Sarcoma
FXS	Fragile X syndrome
FXTAS	Fragile X tremor ataxia syndrome
GLAST	Astrocyte-specific glutamate transporter
HBSS	Hank's buffered saline solution
INM	Interkinetic nuclear migration
iPS	Induced pluripotent stem
IUE	*In utero* electroporation
ISH	*In situ* Hybridization
IZ	Intermediate zone
KD	Knockdown
KH	K homology
Lcn2	Lipocalin2
miRNA	MicroRNA
MP	Microprocessor
NEs	Neuroepithelial cells
NES	Nuclear export signal
Ngn2	Neurogenin 2
NGS	Normal goat serum
NICD	Notch intracellular domain
NLS	Nuclear localization signal
NPs	Neural progenitors

NS	Neurosphere
NSC	Neural stem cell
PCR	Polymerase chain reaction
PFA	Paraformaldehyde
piRNA	Piwi-interacting RNA
PMSF	Phenylmethylsulfonyl fluoride
PNS	Peripheral nervous system
PVDF	Polyvinylidene fluoride
qRT-PCR	Quantitative real time PCR
RACE	3’ rapid amplification of cDNA ends
RBP	RNA binding protein
RGCs	Radial glial cells
RISC	RNA inducible silencing complex
RNP	Ribonucleoprotein
hnRNP	heterogeneous nuclear ribonucleoprotein
RRM	RNA recognition motif
RT	Room temperature
Sam68	Src associated in mitosis 68 kDa
Shh	Sonic hedgehog
siRNA	Small interfering RNA
SMA	Spinal muscular atrophy
SMN	Survival motor neuron
SOD1	CuZn superoxide dismutase 1
SR	Serine/Arginine-rich
SVZ	Subventricular zone
TDP-43	Tar DNA binding protein 43 kDa
TGF	Transforming growth factor
TN-C	Tenascin-C
TNFR	Tumor necrosis factor receptors
VZ	Ventricular zone

3 Introduction

The introduction will guide the reader through the development of the central nervous system (CNS) with a special focus on the telencephalic development, as most of the experimental work was performed in this brain region. I will briefly touch upon gastrulation, neuronal induction and patterning of the neural tube and thereafter concentrate on cortical development. After I shortly introduce Notch signalling and a transcriptome analysis on Notch1 depleted neural progenitor cells, which will explain the starting point of the project the thesis is composed of. The group of genes we focused on showing altered expression in the transcriptome analysis are RNA binding proteins, which will therefore be commented on in a separate chapter. A detailed chapter on TDP-43 will summarise the state of the art, with a special focus on the known functions of the protein and its role in neurodegenerative disease. Finally, an introduction on p53 and apoptosis will make the reader familiar with cell death mechanisms, as one of the key findings of the thesis is based on p53-mediated apoptosis.

At the end of the introduction the main hypothesis and questions addressed in the thesis will be outlined and an overview of the experiments will be given.

3.1 Development of the Mammalian Cerebral Cortex

The brain is the most complex and least understood mammalian organ. The cerebral cortex, being the most highly evolved part of the human brain, encodes higher functions, determines intelligence and personality and distinguishes us from other mammals. Its massive enlargement through evolution, particularly in surface area, results in the convolution of the cortex and generation of ridges (gyri) and grooves (sulci) (Borrell and Reillo, 2012). Gyrification usually increases with brain size and presumably enhances computational capacities of the cortex, which is probably due to the increased number of neurons and their interaction. Therefore, the level of gyrification reflects the functional development of the cerebral cortex and thus correlates with intelligence (Deng et al., 2011). The importance of proper gyrification is also apparent from various human diseases and a number of neurospychiatric disorders such as autism, epilepsy and schizophrenia (Yang et al., 2010).

3.1.1 Gastrulation and Neural Induction

Gastrulation in mammals occurs after implantation of the blastocyst into the uterine wall. During the process of gastrulation the three germ layers namely ectoderm, mesoderm and endoderm form, these are the precursor structures for organogenesis (Tam et al., 1993). The implanted blastocyst is cylindrical and composed of two structures, the epiblast to the distal and the hypoblast to the proximal side. The hypoblast forms all extraembryonic structures whereas the epiblast gives rise to embryonic ectoderm, endoderm and mesoderm (Gilbert, 2003). Both epi- and hypoblast are surrounded by the visceral endoderm, and the ventral side of the embryo corresponds to the outer surface of the visceral endoderm (Fig. 1).

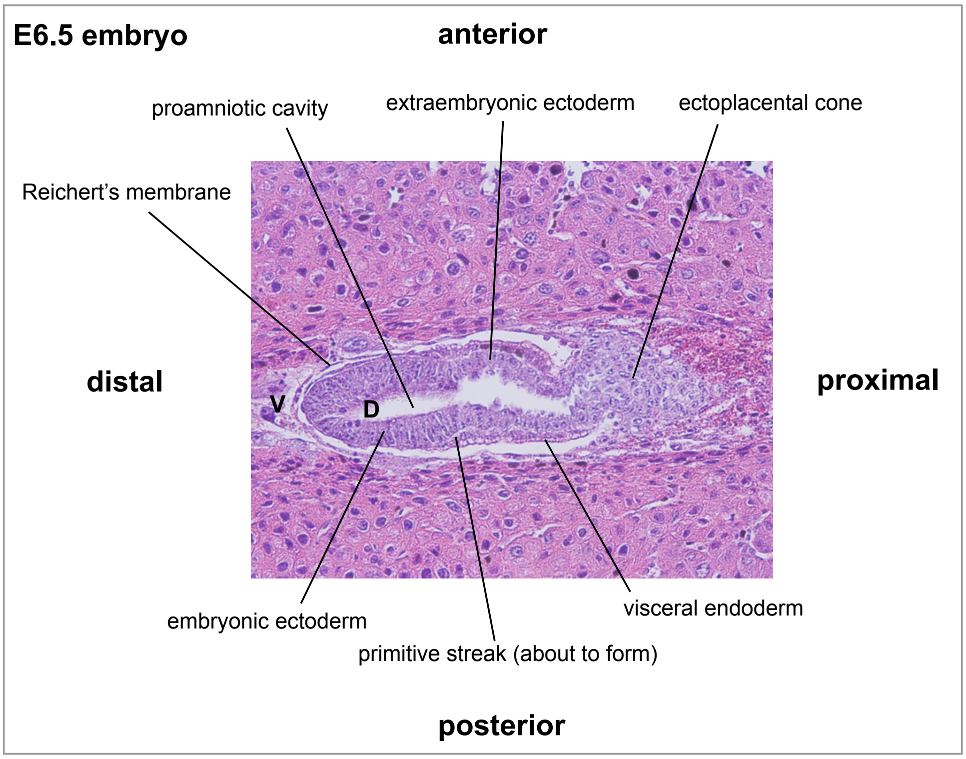

Figure 1. E6.5 embryo at early gastrulation stage Post-implanted embryo at E6.5 displaying early embryonic structures such as extraembryonic ectoderm and embryonic ectoderm. Distal-proximal, anterior-posterior, and ventral (V) -dorsal (D) axis are already determined at this early stage.

The dorsal side corresponds to the epiblast surface directed towards the proamniotic cavity which will form in the centre of the embryo. During the process of gastrulation cells undergo specification and migration, which is mainly coordinated by two signalling centres, the anterior visceral endoderm (AVE) located apically and the node at the tip of the epiblast (Bachiller et al., 2000; Beddington, 1994). On the posterior side of the epiblast the primitive streak forms and prospective mesodermal cells migrate through this streak (Fig. 1). The cell ingression is coordinated by FGFs and the primitive streak will lengthen during this process along the apical-posterior axis until it reaches the node (Ciruna and Rossant, 2001). The extension is probably due to intercalation of some of the recruited cells between the distal and proximal ends of the streak. The definitive endoderm also ingresses through the primitive streak. Prospective neuroectoderm cells migrate through the node giving rise to the notochord at the anterior end of the embryo (Tam and Behringer, 1997).

The first insights into how neural tissue is induced came from pioneering work of Mangold and Spemann in 1924. By means of transplantation experiments they discovered a region of the blastopore, the dorsal lip, whose cells are already determined in their fate. Grafting of the dorsal lip into a recipient gastrula resulted in the induction of a second body axis. Only decades later was the bone morphogenic protein (BMP) antagonist Noggin identified as a molecular mediator that induces neuronal specification (Smith and Harland, 1992). Now many models of neural induction have been proposed, the predominant one being the default model suggested by Levine and Brivanlou (Levine and Brivanlou, 2007). This model is based on the idea that the early mouse embryo exists in a primed neural state that will only form other tissue, if the neural fate is blocked. The block of neural fate occurs initially at the posterior side of the embryo where the formation of mesoderm and endoderm is mediated by BMP/TGF-β (transforming growth factor), Nodal, FGF and Wnt signals, which are antagonised ventrally where the neural tube forms.

In the mouse embryo BMP/TGF-β are inhibited by Chordin and Noggin that are produced by the node (Bachiller et al., 2000). The second signalling center, the AVE expresses Lim-1, Hesx1 and Otx-2, which are necessary for the formation of head structures and generation of an anterior-posterior axis (Perea-Gomez et al., 2001). In addition, anterior-posterior polarity is specified by Hox-gene expression. Hox-genes are highly conserved throughout evolution and are expressed in all vertebrates. The genes are arranged in clusters on the chromosome according to their expression pattern along the head-tail axis, where the genes expressed most anterior are located towards the 3' end of the cluster (Pearson et al., 2005).

3.1.2 Formation of the Neural Tube

Following gastrulation a portion of the dorsal ectoderm is specified to become neural ectoderm and is thereafter referred to as the neural plate. The neural plate forms the mammalian CNS and most of the peripheral nervous system (PNS) and the structure is determined by inductive signals from the notochord, which expresses sonic hedgehog (Shh) (Ybot-Gonzalez et al., 2002). Additionally BMP inhibition through BMP antagonists is necessary for formation of neural ectoderm (Fig. 2) (Wilson and Hemmati-Brivanlou, 1995). The neural plate will undergo a process called neurulation and form the neural tube, whose anterior part gives rise to the brain and posterior part to the spinal cord (Liu and Niswander, 2005). Neurulation is divided into two phases, primary and secondary phases of neurulation (Lowery and Sive, 2004). The portion of the neural tube that forms the brain and most part of the spinal cord is made during primary neurulation and more caudal parts by secondary neurulation (Schoenwolf and Delongo, 1980).

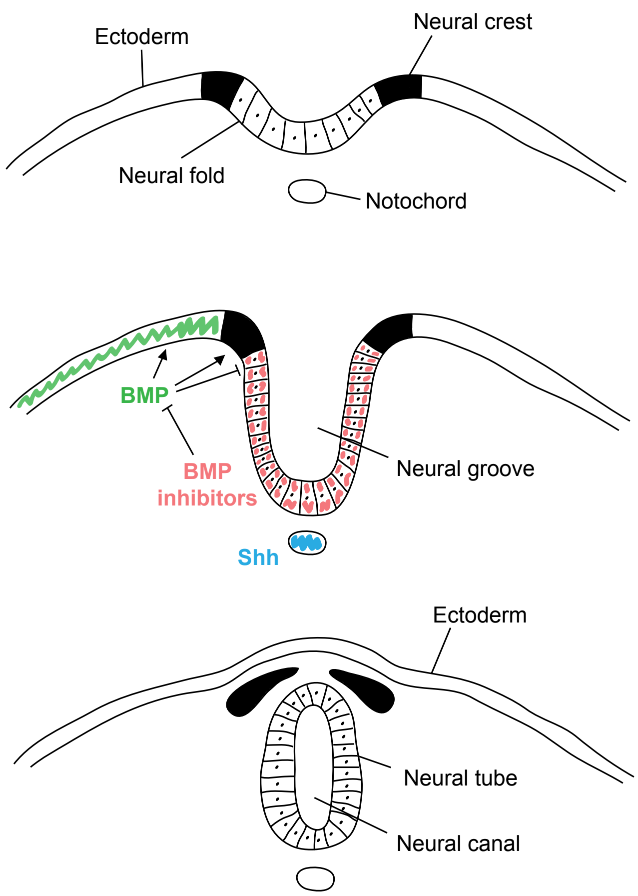

Figure 2. Neural tube formation During primary neurulation the neural folds elevate and fuse dorsally which results in the formation of a tube-like structure. Adapted from (Liu and Niswander, 2005)

During primary neurulation the edges of the neural plate fold upwards forming the neural folds that eventually fuse dorsomedially to form the neural tube beneath the ectoderm (Fig. 2). Neural crest cells derive from the neural folds at the dorsal most region of the neural tube at the junction between the ectoderm and neural ectoderm (Gilbert, 2003). These cells migrate out and differentiate into many cell lineages including Schwann cells, peripheral neurons and melanocytes. In the anterior region of the embryo neural crest cells also give rise to muscle and craniofacial bones. In the process of secondary neurulation the neural tube is formed by hollowing out of a condensed cord of cells that has formed under the ectodermal surface (Knecht and Bronner-Fraser, 2002).

3.1.3 Patterning of the Neural Tube

After formation of the neural tube, the tissue will acquire a defined pattern along the dorsal-ventral and anterior-posterior axis. This process is highly organized both temporally and spatially in order to generate a functional nervous system. The patterning of the spinal cord is determined by two major factors, Shh and proteins of the TGF-β family. Shh originates from the notochord and TGF-β family proteins from the ectoderm. These paracrine factors initiate signalling centres in the neural tube itself at the ventral pole the floor plate that expresses Shh and dorsally the roof plate expressing BMP4 (Gilbert, 2003). Shh functions as a morphogen and generates a gradient along the ventral-dorsal axis which results in the expression of particular transcription factors and the generation of defined neuronal cell types (Fig. 3) (Chamberlain et al., 2008). In this way 5 domains are formed ventrally, termed p3, pMN, p2, p1 and p0 (Briscoe et al., 2000; Ericson et al., 1997). The transcription factors that are expressed at a given time point are determined by the concentration of the morphogen and the duration of the exposure of the cells to the morphogen (Harfe et al., 2004). As these parameters change over time the cells accordingly express different transcription factors. In this way the cells of the floor plate initially express Olig2, but start to express Nkx2.2 and finally Shh as Shh levels increase (Ribes and Briscoe, 2009).

In the dorsal neural tube however, the paracrine factors determining the expression patterns and cell fates are not that well understood. BMPs are expressed and secreted from the roof plate, but they do not function as classical morphogens and were not shown to act over a long distance in the same way that Shh does (Hogan, 1996; Hu et al., 2004). In addition, several members of the TGF-β family are necessary for proper patterning of the dorsal neural tube, as are members of the Wnt family (Le Dreau and Marti, 2012). Thus, formation of the 6 dorsal domains of the neural tube termed dP1-dP6, is very complex and likely depends on an interplay between different inductive signals.

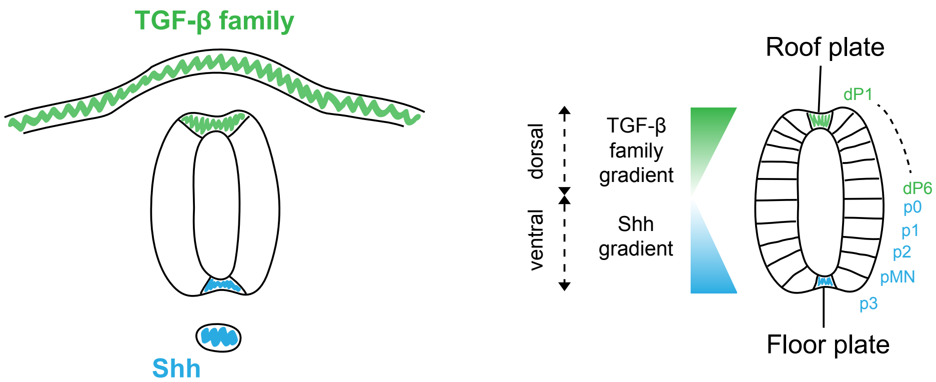

Figure 3. Patterning of the neural tube The notochord induces expression of Shh in the floor plate and the ectoderm induces expression of the TGF-β proteins in the roof plate of the neural tube. A from this expression resulting Shh gradient at the ventral and TGF-β family gradient at the dorsal side results in the generation of distinct domains along the dorsal-ventral axis.

3.1.4 Regional Specification of the Forebrain

Besides establishment of a dorsal-ventral axis the neural tube acquires a defined anterior-posterior pattern. For the most part, the neural tube will give rise to spinal cord while the anterior end will split into distinct areas that compose the brain. From rostral to caudal these are termed forebrain, midbrain and hindbrain. The forebrain can be divided into telencephalon and diencephalon and the hindbrain into metencephalon and myelencephalon (Developmental of the Nervous System, 2006). All of these regions enlarge as development progresses and acquire a distinct and complex structure. Early in brain development an organizing centre located at the boundary of mesencephalon and metencephalon, the midbrain/hindbrain boundary or isthmus establishes the correct regionalization of forebrain and hindbrain

(Alvarado-Mallart, 1993). The midbrain/hindbrain boundary develops from the expression domains of Otx2 in the anterior and Gbx2 in the posterior part of the early embryo (Rhinn and Brand, 2001). The two genes cross-inhibit each other and at the point where this inhibition overlaps *fgf8* is expressed (Crossley et al., 1996). The boundary is maintained by expression of *engrailed* which is induced by FGF8 and also other signalling molecules including Wnt1 and Pax2 (Lee et al., 1997). The specific brain regions will thereafter develop and many more genes are involved but the detailed description exceeds the scope of this thesis.

In the following chapters I will focus on the development of the telencephalon in rodents and therefore more closely explain the organization of this structure before the onset of neurogenesis. The telencephalon consists of 2 hemispheres and their cavities are referred to as the lateral ventricles. Each hemisphere can roughly be divided into the pallium to the dorsal side, which will develop into the cerebral cortex, and the subpallium on the ventral side, which will become the basal ganglia (Fig. 4). Both of these areas can further be subdivided, in the case of the subpallium into the lateral and the medial ganglionic eminence. The lateral surface of the pallium that is directed to the ventricle is also referred to as the apical surface. On the opposite side is the basal surface, the surface of the cortex (Campbell, 2003).

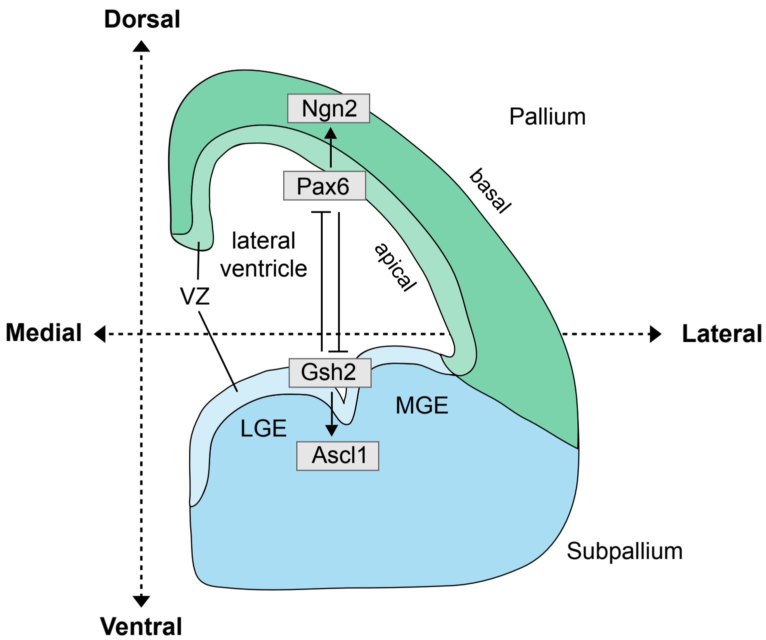

Figure 4. Dorso-ventral patterning of the telencephalon Coronal hemisection through the developing telencephalon of a mouse embryo. Pax6 in the pallium and Gsh2 in the subpallium co-repress each other, resulting in specific expression of transcription factors Ngn2 and Ascl1 in the drosal and ventral domain. VZ = ventricular zone, MGE = medial ganglionic eminence, LGE = lateral ganglionic eminence. Adapted from (Campbell, 2003)

Two key transcriptional regulators Pax6 and Emx2 are regionally expressed in the cortex. The two proteins are expressed in the dorsal part of the cortex in an opposing gradient. Emx2 is highest in the posterior-medial part and diminishes to the anterior-lateral opposite to Pax6 (Bishop et al., 2000). Not only can the telencephalon be divided into different expression domains on the anterior-posterior axis, but also along the dorsal-ventral axis. The restricted expression of transcription factors in pallium and subpallium results in distinct progenitor domains, which give rise to specific neuron subtypes. In the pallium Pax6 and its downstream target Neurogenin2 (Ngn2) are expressed by dorsal progenitor cells (Fig. 4), regulating their identity (Gotz et al., 1998; Kovach et al., 2013). Gsh2 and Ascl1 execute the same function in the subpallium. Pax6 and Gsh2 are key factors in setting up dorsal-ventral polarity and inhibit each other (Yun et al., 2001). Knockout of Pax6 or Gsh2 severely disturb the balance between the two areas and result in expansion of either the dorsal or ventral progenitor domain (Toresson et al., 2000). Additionally Ngn2 restricts *Ascl1* expression to the ventral telencephalon and the two proneural genes are crucial in establishing dorsal and ventral expression domains. Cortical neurons in mice depleted for *Neurog2* acquire ventral characteristics and in addition expression domains of ventral factors are expanded into the dorsal telencephalon (Fode et al., 2000). However, neuronal determination is not abolished after Ngn2 deletion from the pallium as misexpressed Ascl1 compensates to a certain degree for *Neurog2* loss. Similarly Ascl1-deleted progenitors in the subpallium can be fully rescued by *Neurog2* expression (Parras et al., 2002). Many more factors are involved in dorsal and ventral fate determination such as Sox6, which is expressed in the pallium and was shown to be involved in controlling dorsal progenitor identity (Azim et al., 2009).

3.1.5 Transition of Neuroepithelial Cells to Radial Glial Cells.

The cerebral cortex originates from the neuroepithelium, a single layer of NSCs called neuroepithelial cells (NEs). The nucleus of these cells migrates up and down the apical-basal axis according to the different phases of the cell cycle. In S-phase the cell body is located towards the basal surface and migrates back down apically during G_2-phase. Reaching the apical surface the NE will divide symmetrically giving rise to two identical NEs (Fig. 5). This movement is referred to as interkinetic nuclear migration (INM) and gives the neuroepithelium a layered appearance (pseudostratified) (McConnell, 1995; Takahashi et al., 1993). However, it is not clear how positioning of the cell body and cell cycle progression interfere with each other. Recent studies addressing this issue illustrated that arrest of nuclear migration in G_2-phase inhibits mitotic entry (Hu et al., 2013). Proper INM is therefore a requirement for cells to progress from G_2- into M-phase. NEs show typical epithelial features including tight junctions and adherence junctions at the apical end and the expression of neuroepithelial markers such as the intermediate filament Nestin. In addition they express occludin and E-cadherin which are lost before neurogenesis begins (Kriegstein and Gotz, 2003).

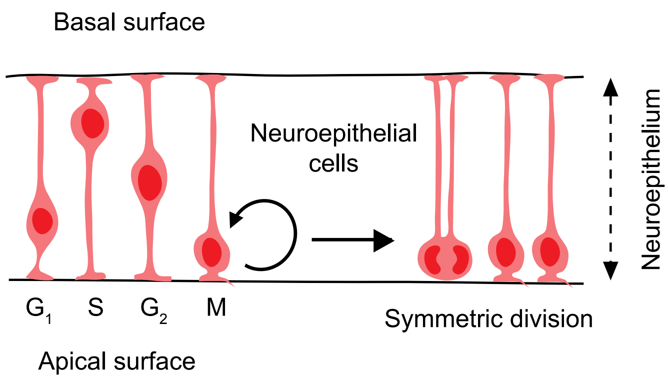

Figure 5. Interkinetic nuclear migration (INM) in the neuroepithelium At E9-10 the neuroepithelium is composed of neuroepithelial cells which are undergoing INM and self-replicate.

At E9-10, which is approximately when cortical neurogenesis begins, the NEs acquire characteristics of glial cells such and expression of astroglial markers and are thereafter referred to as radial glial cells (RGCs) (Kriegstein and Alvarez-Buylla, 2009). RGCs are NSCs as they self-replicate and are multipotent, giving rise to different cell types such as astrocytes, oligodendrocytes and neurons. The RGCs maintain Nestin expression but also begin to express Astrocyte-Specific Glutamate Transporter (GLAST), Tenascin-C (TN-C) and Brain Lipid-Binding Protein (BLBP) (Kriegstein and Gotz, 2003). Tight junctional complexes are lost in RGCs whereas adherens junctions are maintained (Aaku-Saraste et al., 1996). However, the cells retain their apical-basal polarity and the connection of the radial processes to the basal and apical surfaces. RGCs still line the lateral ventricle and undergo

INM although their nucleus only migrates within the ventricular zone (VZ), which is the layer lining the ventricle (Fig. 6). The transition of NEs to RGCs starts around E10 and terminates at around E12. Throughout the process of cortical neurogenesis the initial neuroepithelium will transform into multiple cell layers composed of different cell types (see section 3.1.6 and 3.1.7).

RGCs in the dorsal telencephalon express the stem cell markers Sox2 and Pax6 but are more fate-restricted than NEs. They mainly give rise to neurons, astrocytes or oligodendrocytes in a direct or indirect way. Most astrocytes and oligodendrocytes are generated indirectly, meaning that first an intermediate cell type originates which is more fate restricted than the RGCs that will then differentiate further. NEs can undergo two different modes of division; symmetric or asymmetric. When cells proliferate symmetrically, cell constituents are distributed equally to the two daughter cells giving rise to two identical cells. In the case of NEs and RGCs this type of division is self-replicative and therefore considerably increases the number of NSCs. Symmetric divisions first take place in the neuroepithelium, amplifying the number of NEs, and decrease as development and neurogenesis progresses. RGCs in contrast to NEs mostly divide asymmetrically, giving rise to either a RGC and a neuron or to a RGC and a basal progenitor cell (BP), which is an intermediate in the generation of neurons (Fig. 6). These asymmetric neurogenic divisions are important, as RGCs need to generate a large amount of neurons throughout cortical development, but still have to maintain the stem cell pool.

As mentioned earlier, NEs and RGCs are highly polarized along their apical-basal axis and many constituents are only located to one pole of the cell. The polarized distribution of cell fate components in dividing cells is best studied in *Drosophila* neuroblasts, where it was shown that a group of proteins including Par3, Par6 and aPKC are key in setting up cell polarity (Knoblich, 2008). Par3 was also determined as a crucial factor in maintaining cell polarity and asymmetric division in the developing mammalian cortex (Bultje et al., 2009). In addition, asymmetric distribution of numb, an antagonist of the Notch signalling pathway is important in maintaining cell polarity (Zhong et al., 1996). The general notion therefore is that a division along the apical-basal axis with a vertical cleavage plane results in the equal, symmetric distribution of cell fate determinants to the daughter cells. If the cell divides horizontal to the basal surface, crucial apical constituents will only remain in one of the daughter cells and result in an asymmetric division (Gotz and Huttner, 2005; Huttner and Brand, 1997; Shitamukai and Matsuzaki, 2012). It is still a controversial matter if cleavage plane orientation alone is determining the mode of division but that discussion goes beyond the scope of this introduction.

3.1.6 Early Embryonic Neurogenesis in the Mouse Cerebral Cortex

From E12 onwards RGCs constitute the major pool of progenitor cells in the telencephalon. They divide and amongst others, give rise to BPs, which are located in a layer basal to the VZ that is referred to as the subventricular zone (SVZ) (Fig. 6). This layer is not present in all regions of the mammalian brain but exists in the telencephalon where BPs are most abundant. BPs express the transcription factors Tbr2, Ngn2 and NeuroD1 and are already committed to the neuronal lineage (Englund et al., 2005; Hevner, 2006). In contrast to NE and RGCs, the BPs loose their apical-basal polarity, are multipolar and undergo mitosis in the SVZ without obvious INM. The BPs are not able to self-renew extensively and mostly undergo symmetric neurogenic division giving rise to two immature neurons or neuroblasts. BPs are not pluripotent and are therefore not considered NSCs. However, they are further committed progenitors and one can refer to them as neural progenitor cells since they are able to give rise to neurons. The term neural progenitor can also be applied to NSCs such as NEs and RGCs and if used in the text, it refers to all three cell types. Neuroblasts migrate to the basal surface where they start to differentiate into Tbr1 positive neurons that incorporate into the cortical plate (CP) (Noctor et al., 2004). The newborn neurons use the radial fibre of the RGCs as a guide and migrate radially along them to their final location where they integrate (Noctor et al., 2001). In this inside out fashion the 6 layers of the cortex are consecutively generated until E19 when corticogenesis is completed.

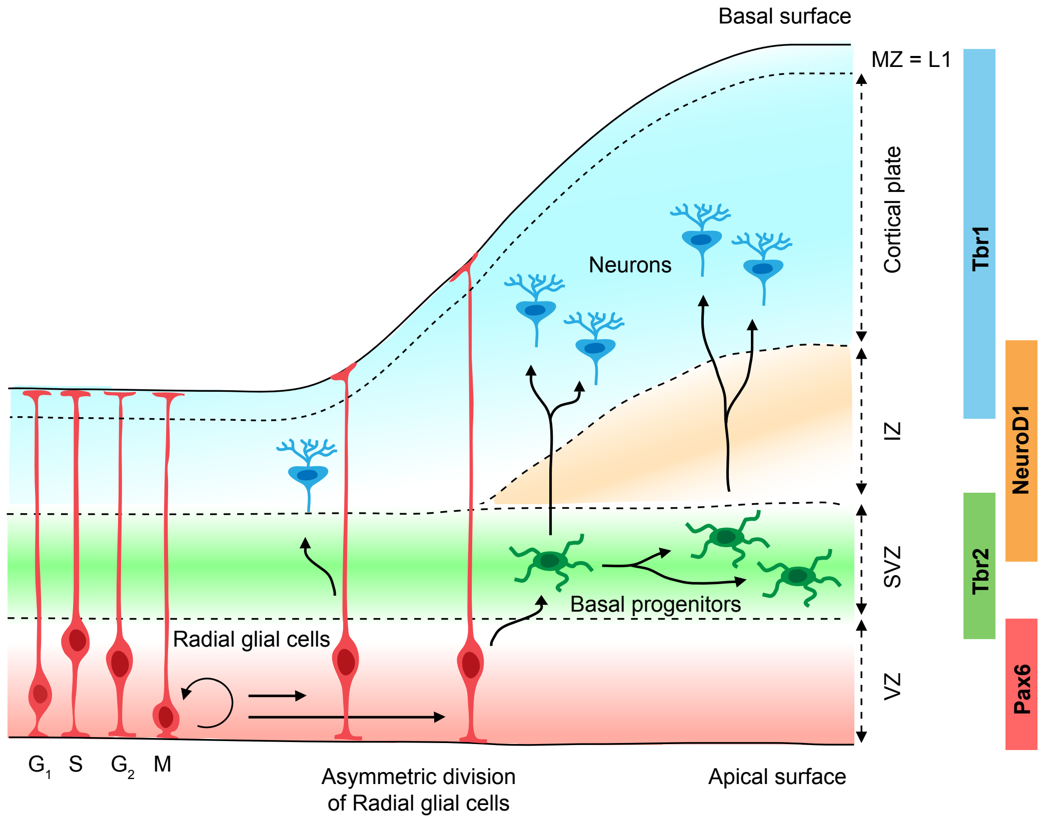

Figure 6. Telencephalic development during the peak of neurogenesis Location and generation of radial glial cells, basal progenitors and neurons in the developing cerebral cortex at E14.5. Through asymmetric division radial glial cells give rise to neurons and basal progenitors. IZ = intermediate zone, SVZ = subventricular zone, VZ = ventricular zone, MZ = marginal zone, L1 = Layer 1. Adapted from (Tiberi et al., 2012)

3.1.7 Layering of the Mammalian Neocortex

Each cortical layer is composed of specific subtypes of neurons, which can be characterised by morphology, electrophysiology and markers. They can broadly be classified into GABAergic inhibitory interneurons and excitatory pyramidal neurons, which are glutamatergic. Pyramidal neurons originate from the VZ and radially migrate outwards to the CP. In contrast interneurons are derived from the ventral telencephalon, predominantly the medial ganglionic eminence from where they migrate tangentially to the cortex (Kriegstein and Noctor, 2004).

Pyramidal projection neurons represent ~80% of the cortical neurons. They have a pyramid-shaped soma, several dendrites towards the basal surface and a single neurite that is directed towards the apical surface (Fig. 6) (Garcia-Lopez et al., 2006). After the migration of the neurons to their final location within the cortex they undergo morphological and molecular differentiation and start to express layer specific genetic markers. Pyramidal neurons of Layer 6 (L6), which is the deepest layer and is therefore generated first, express Tbr1 and Sox5. Mice deficient in these genes show distinct neuronal migration defects resulting in inversion of the deeper layers. Sox5 is not only expressed in L6 but also in L5 and controls positioning of pyramidal neurons in these layers. Therefore, neurons in *Sox5*$^{-/-}$ mice fail to migrate past the early-born neurons, which results in inversion of the upper and lower layers (Kwan et al., 2008). In contrast to Sox5, Tbr1 does not only regulate positioning but also differentiation. This likely causes the distinct phenotype in Tbr1-deficient mice resulting in neuron clusters, which vary from rostral to caudal (Han et al., 2011; Hevner et al., 2001). Brn1 and Brn2 regulate the migration in the upper layers and are expressed in L2-L5. In contrast to most other transcription factors that are expressed in pyramidal neurons, Brn1 and Brn2 are already expressed in the BPs and maintain expression throughout migration and differentiation. Thus, double knockout of the two genes causes not only migration defects but also reduced proliferation of progenitors in the VZ and SVZ from E14.5 onwards, resulting in decreased number of late-born neurons (Sugitani et al., 2002). Satb2 is expressed in pyramidal neurons of all 6 layers and mice deficient in this gene show delayed migration of late-born neurons, a defect that is corrected for postnatally (Alcamo et al., 2008; Britanova et al., 2008). One of the most significant migration defects in cortical development is observed in *Reeler* mutant mice. Here neurons fail to migrate past older neurons which results in an inversion of the layers (Caviness, 1982). However, the mechanism is different from those caused by loss of the layer specific transcription factors. Reelin is a secreted extracellular matrix glycoprotein produced by Cajal-Retzius cells. These neurons are located in the mantel zone, which is the first and most outer layer generated during cortical development (Fig. 5). The mantel zone corresponds to L1 and no neurons migrate past this layer but integrate below. It is interesting to note, that although neurons integrate into the wrong location they still maintain the molecular and projection identity according to their birthdate. Therefore, neurons must be already determined in their fate as they start to migrate radially to their final location. The early commitment of embryonically generated neurons was nicely addressed by Susan McConnell. Performing isochronic and heterochronic transplantation experiments in ferrets, she showed that the birthdate of cortical neurons correlates with their final laminar position and identity (McConnell, 1988).

From mouse models it becomes apparent that proper migration and positioning are crucial in establishing a normal cortical lamination. However, apart from the factors regulating migration there are several other proteins that are necessary for the generation of the functional neocortex. Cux1 and Cux2 for example are expressed in the upper layers and regulate synaptogenesis and spine morphology of pyramidal neurons (Cubelos et al., 2010) and Satb2 controls dendritic arborisation (Zhang et al., 2011).

3.1.8 Sequential Expression of Transcription Factors during Cortical Development

The predominant neuronal cell type in the dorsal cortex are pyramidal projection neurons and a sequential expression of transcription factors is associated with their formation. Pax6, Tbr2, NeuroD1 and Tbr1 are sequentially expressed in a partially overlapping manner (Englund et al., 2005). Pax6 is present in NSCs in the VZ and is crucial in promoting both proliferation and differentiation (Quinn et al., 2007). Loss of Pax6 function leads to the reduction of cortical neurons, which is probably due to reduced Ngn2 expression. Ngn2 is a transcription factor that induces neuronal differentiation and is directly activated by Pax6 (Heins et al., 2002; Scardigli et al., 2001). The T-box transcription factor Tbr2 is expressed by BPs in the SVZ and is also important in establishing neuronal commitment. Moreover, BPs still proliferate to some degree and Tbr2 deletion causes severe behavioural deficits and microcephaly (Arnold et al., 2008). NeuroD1 is detected in some mitotically active cells of the upper SVZ but mainly regulates neuronal migration, survival and maturation of immature postmitotic neurons (Kim, 2013). Finally, Tbr1 is expressed in early born neurons which reside in layer 6 (Hevner et al., 2001). The expression patterns can therefore be linked to certain steps in neurogenesis. However, they are not exclusive but instead show a partial overlap and co-expression in the same cell. The sequential expression of Pax6 → Tbr2 → NeuroD1 → Tbr1 seems to be a conserved program for neurogenesis of glutamatergic neurons as it is also found in the cerebellum (with some modifications) and the adult hippocampus (Hevner et al., 2006).

3.1.9 Morphogens and Pathways Regulating Cortical Development

Besides intrinsic factors, some of which are mentioned above, there are many extrinsic cues that regulate cortical development. These include BMP, TGF, Wnts, Shh, and fibroblast growth factors (FGFs). Many of these morphogens are involved in early patterning of the cortex while some of them act in regulating cortical neurogenesis.

The Wnt pathway plays an important role in patterning of the forebrain and it is crucial for proper dorsalization of the telencephalon (Backman et al., 2005; Grove et al., 1998). Wnt signalling is necessary for maintenance of progenitors at early stages of cortical development, indicated by β-catenin deletion experiments (Woodhead et al., 2006). Conversely, overexpression of stabilized β-catenin leads to overproliferation of cortical progenitors caused by delayed cell cycle exit (Chenn and Walsh, 2002, 2003). In contrast to these findings Wnt signalling promotes neurogenesis at later stages. *In vitro* experiments showed a direct activating effect of a β-catenin/TCF complex on *Neurog1* and *Neurog2* (Hirabayashi and Gotoh, 2005; Hirabayashi et al., 2004). *In vivo* this effect is restricted to late cortical progenitors highlighting the stage and cell type-dependent effects of Wnts. How the different responses to Wnt signalling are timed is still an open question. The dual function of Wnt/β-catenin is possibly dependent on other factors such as varying amounts of Wnts (oscillatory actions of Wnt/β-catenin) or the adhesive function of β-catenin (Junghans et al., 2005). Furthermore, FGF2 signalling was suggested to influence the switch from progenitor maintenance to differentiation, as the presence of FGF2 supports maintenance of cortical progenitors whereas neuronal differentiation is enhanced in the absence of FGF2 (Israsena et al., 2004).

Besides FGF2, which is required for expansion of NEs, FGF10 is expressed in cortical progenitors. It promotes the transition of NEs into RGCs and its deletion results in a delayed appearance of neurogenic progenitors (Sahara and O'Leary, 2009). Interestingly, FGF10 is mainly expressed in the frontal areas of the developing cortex similar to FGF8, which increases survival and proliferation by cortical progenitors. FGF8 was furthermore found to diffuse from anterior to posterior generating a protein gradient (Toyoda et al., 2010). However, it is not clear if it acts as a classical diffusible morphogen and thereby regulates pattern formation. Finally, FGF9 and 18 contribute to the shift from neurogenesis to gliogenesis in the cortex. As neurons are differentiating they start to express the two factors and increasing levels will eventually promote gliogenesis in a feedback mechanism (Iguchi et al., 2013).

3.2 Notch Signalling and Targets of Notch1

Notch signalling is pivotal for the maintenance and cell fate choice of NSCs in the developing brain and in the neurogenic regions of the adult brain (de la Pompa et al., 1997; Lutolf et al., 2002; Nyfeler et al., 2005). Thus, Notch1 is predominantly expressed throughout the neuroepithelium from E9.5 and remains expressed in the neurogenic regions of the mouse brain even into adulthood (Basak and Taylor, 2007; Stump et al., 2002). Conditional gene inactivation of Notch signalling components in the mouse have revealed the requirement for canonical Notch signals to generate a functional nervous system during embryogenesis (Hitoshi et al., 2002; Lutolf et al., 2002). Still, the precise mechanism of how the Notch signal regulates neurogenesis and the formation of the mouse nervous system is not

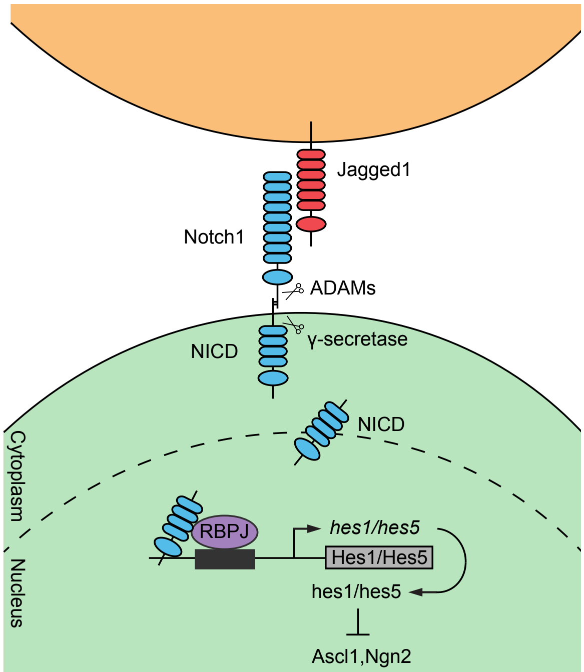

Figure 7. Notch signalling pathway Upon binding of Notch receptor to the ligand the intracellular domain of Notch (NICD) is being cleaved off. The NICD translocates to the nucleus where it associates with RBPJ-kappa, resulting in subsequent activation of canonical Notch target genes. Adapted from (Shimojo et al., 2011)

clear as well as are the target genes of the Notch transcriptional machinery.

Notch family members are transmembrane proteins, which act as receptors. Notch signalling is activated by the binding of canonical ligands of the Delta or Jagged families to Notch receptors. Upon binding of a ligand, an ADAM protease and a Presinilin containing γ-secretase complex sequentially cleave off the ectodomain and intracellular domains of Notch (NICD) (Bray, 2006). The NICD translocates to the nucleus where, in mice, it binds to and induces partial dissociation of the RBPJ-kappa repressor complex (Fig. 7). The NICD-RBPJ-kappa complex recruits chromatin remodelling proteins such as Histone acetyltransferases P300/CBP and Mastermind that recruit the RNA Polymerase II complex and promote transcriptional activation of targets including *Hes* and *Hesr* genes (Mumm and Kopan, 2000). The key targets of the Notch cascade in the mouse CNS are the *Hes/Hey* gene family, which encode basic helix-loop-helix (bHLH) transcription factors including Hes1 and Hes5. Hes5 can negatively regulate neurogenesis by suppressing the expression of the proneural genes *Ascl1*, *Atoh1*, *Neurog1* and *Neurog2*. The proneural genes in turn activate expression of neuronal genes and induce neuronal commitment. Hence, Hes5 and Hes1 are central effectors of Notch signalling that prevent neural progenitor cells from entering neurogenesis (Hatakeyama et al., 2004; Ohtsuka et al., 1999).

3.2.1 Dynamic Regulation of Transcription Factors in NSCs

The bHLH transcriptional activators *Neurog1, Neurog2* and *Ascl1* are expressed in cortical progenitor cells of the telencephalon. *Neurog1* and *Neurog2* are important for development of the dorsal telencephalon (Fode et al., 2000), whereas *Ascl1* controls ventral fates (Casarosa et al., 1999). These factors are implicated in neuronal differentiation whereas Ngn2 is clearly the most important as Ngn2-deficient mice display distinct corticogenesis defects (Fode et al., 2000; Nieto et al., 2001). Notch signalling causes *Ascl1* and *Neurog2* inhibition via *Hes1/Hes5* in a process called lateral inhibition (Beatus and Lendahl, 1998; Kageyama et al., 2005). Thereby NSCs are maintained and neighbouring cells are induced to differentiate. Hes1 levels oscillate with a periodicity of 2-3 hours in NSCs due to a negative feedback loop (Hirata et al., 2002; Shimojo et al., 2008). Because of the oscillating Hes1 levels, Ngn2 is periodically repressed which again results in oscillating Delta1 levels as Delta1 is a directly activated target (Castro et al., 2006; Shimojo et al., 2008). This dynamic expression keeps NSCs in their undifferentiated state and only if Ngn2 expression is sustained will cells undergo neuronal differentiation (Kageyama et al., 2009). The mechanism controlling Ngn2 and Delta1 expression levels however are not known.

3.2.2 Identification of Novel Notch1 Targets

One of the first experiments to address the function of Notch1 in the nervous system was to delete *Notch1* conditionally from the NSCs of midbrain/hindbrain boundary (Lutolf et al., 2002). This ablation resulted in precocious differentiation, apoptosis and loss of well-known Notch targets including Hes5. Targeted mutation of *Notch1* and *RBPJ* similarly results in altered expression of Notch targets and enhanced expression of proneural genes (de la Pompa et al., 1997). Not only is Notch signalling crucial to maintain stem cell potential, activated Notch1 promotes the acquisition of an earlier, less committed cellular phenotype *in vivo* (Gaiano et al., 2000).

In order to analyse the expression profile of cells that were conditionally inactivated for Notch1, a transcriptome analysis was performed. The analysis was executed by a former PhD student in the lab, who crossed Notch1$^{flox/flox}$ onto En2::Cre mice to selectively delete Notch1 from Engrailed2 expressing progenitors of the midbrain/hindbrain boundary (Lutolf et al., 2002). Embryos carrying floxed Notch1 (Notch^{lox}) and En2::Cre alleles were isolated at E10 and individual cerebellar primordia were isolated from Notch1$^{flox/flox}$, En2::Cre (mutant) and Notch1$^{flox/wt}$, En2::Cre (control) animals. RNA was isolated from individual primordia using Trizol (Life Technologies) and RNeasy (Qiagen) columns and RNA was quantified by spectroscopy (NanoDrop) and analysed by 2100 Bioanalyzer (Agilent Technologies). The RNA samples of four mutant and four control animals were labelled and probed on Affymetrix MG430 genechips (Verdon Taylor and Robert Kirch, unpublished), and the data were analysed by Genespringer software (Verdon Taylor and Robert Kirch, unpublished). Regulated genes were determined as those that showed a differential expression of >2 fold on three of the four mutant genechips over all four control samples. Putative regulated genes were analysed further by quantitative RT-PCR on independent samples. Numerous Notch1-regulated gene clusters, which were classified according to gene ontology, were identified. One of these gene clusters encoded members of the RNA binding protein (RBP) family of proteins, which were mostly upregulated following Notch1 ablation (Fig. 8). *Tardbp* and *Fus*, two proteins shown to be involved in onset and progression of neurodegenerative disease were upregulated in the microarray. In addition, genes involved in miRNA biogenesis such as *Sam68* and *Xpo5* were found to be downregulated following Notch1 depletion. The data from this transcriptome analysis provided the basis for two studies. Firstly, the functional analysis of TDP-43 during telencephalon development, which is the topic of this PhD thesis. Secondly, a study I worked on as a side project investigating the function of Drosha and the microprocessor in NSCs. The main findings of this work are summarized in the Appendix.

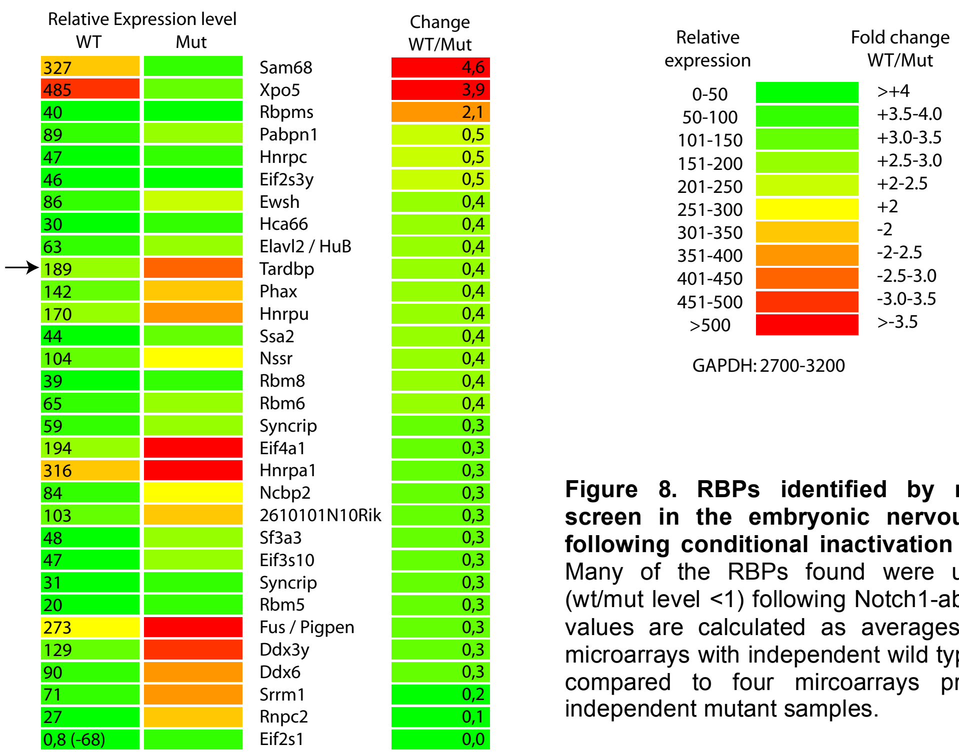

Figure 8. RBPs identified by microarray screen in the embryonic nervous system following conditional inactivation of Notch1 Many of the RBPs found were upregulated (wt/mut level <1) following Notch1-ablation. The values are calculated as averages from four microarrays with independent wild type samples compared to four mircoarrays probed with independent mutant samples.

3.3 Cellular Function of RNA-Binding Proteins

RBPs are localized in the nucleus or cytoplasm and are able to bind to single or double stranded RNA. They can be very diverse and contain one or more RNA-binding domains some of which are well-characterized such as the RNA-recognition motif (RRM), double stranded RNA binding domain (dsRBD) and K homology (KH) domain (Lunde et al., 2007). Additionally, they often contain domains that mediate interaction with other proteins, allowing them to form ribonucleoprotein (RNP) complexes composed of several RBPs (Dreyfuss et al., 2002). The proteins themself can be post-translationally modified which can results in altered RNA-binding function or changed localization within the cell (Glisovic et al., 2008). RBPs can control protein expression by the regulation of numerous cellular functions related to RNA biology. They play a major role at many different steps of pre-mRNA processing such as splicing, polyadenylation, RNA modification, localization, transport, translation and turnover (Glisovic et al., 2008).

Alternative splicing is a process that can lead to the generation of distinct splice variant mRNAs encoding different protein isoforms and is mainly regulated by RBPs. During patterning of the neural tube for example, the midbrain/hindbrain boundary expresses two different isoforms of FGF8, FGF8a and FGF8b (Ghosh et al., 1996; Olsen et al., 2006). FGF8b contains an additional 11 amino acids compared to FGF8a, due to an alternative splice site. This alters their binding affinity to FGF receptors. The two isoforms have different functions during midbrain patterning and misexpression causes distinct phenotypes (Liu et al., 1999; Sato et al., 2004). RNPs bind to immature target RNAs in the nucleus (Giorgi and Moore, 2007) where they regulate the rate and efficiency of RNA splicing to form mature transcripts that can be polyadenylated, capped and exported to the cytoplasm ready for translation. In addition, RBPs can play a role in targeting mRNAs to distinct regions in a cell or to specific structures such as dendrites or synapses of neurons for example (Wells, 2006). It is also likely that RBPs help to shuttle specific target mRNAs to the RNA inducible silencing complex (RISC) found within P-body-like structures (Eulalio et al., 2007a; Eulalio et al., 2007b). In addition, it has been claimed that binding of RBPs to specific regions of target mRNAs modulates the stability of transcripts and this may be by interacting or interfering with the RISC complex. Finally, RBPs play a pivotal role in the initiation and regulation of translation as docking sites or constituents of the ribosome or polysome complex (Glisovic et al., 2008; Kishore et al., 2010). Hence, transcriptional regulation of gene product expression is refined by post-transcriptional mechanisms through which cells can rapidly modulate the expression of specific proteins without the need for changing gene transcription.

3.3.1 RNA-Binding Proteins in Disease

RBPs are key regulators of RNA metabolism, especially pre-mRNA processing. It is therefore not surprising that mutations in RBPs are involved in many human diseases such as cancer and neurodegenerative disorders (Castello et al., 2013). Cancer can be caused by gain- and loss-of-function mutations, chromosomal rearrangement and gene amplifications. Chromosomal translocations of the *Fus (Fused in sarcoma)* gene were identified in human cancer (Crozat et al., 1993), where the promoter and N-terminal domain of the *Fus* gene fuses with the C-terminus of transcription factors such as CHOP. The fusion protein FUS-CHOP looses the RNA-binding domain present in FUS which is replaced by the DNA-binding domain of the transcription factor (Riggi et al., 2007). Thus, the FUS protein acquires a strong transcriptional activation domain, resulting in tumor formation. Altered expression of RBPs such as increased levels of Src associated in mitosis (Sam68) were found in breast and prostate cancer (Bielli et al., 2011). Sam68 is involved in cytoplasmic-nuclear RNA transport (Li et al., 2002) and alternative splicing (Iijima et al., 2011) and binds, among several transcripts, *β-actin* mRNA which is the primary cytoskeletal component of dendritic spines (Itoh et al., 2002). The protein is therefore crucial for proper synaptic function and loss of Sam68 results in severe neurological defects such as Fragile X tremor ataxia syndrome (FXTAS) (Sellier et al., 2010). Loss-of-function in the RNA-binding protein Fragile X mental retardation protein (FMRP) also results in a neurodegenerative disorder called Fragile X syndrome (FXS). The 5' UTR of the *FMR1 (Fragile X mental retardation 1)* gene contains several CGG repeats, which are expanded in the disease to more than 200 repeats. The CpG islands become hypermethylated which causes gene silencing and loss of the protein in patients carrying this mutation (Garber et al., 2008). FMRP is mainly expressed in the brain and has been suggested to play a role in many different processes such as translational regulation at synapses and dendritic mRNA location (Bardoni et al., 2006; Li et al., 2001). Many more RBPs have been linked to neurodegenerative disorders for example the Tar DNA binding protein (TDP-43), which will be discussed in chapter 3.5. Additionally genetic mutations in RBPs cause muscular disorders and the most important one to mention is Spinal muscular atrophy (SMA) that is caused by mutations or deletion of the *Survival motor neuron* (*SMN*) gene (Cartegni and Krainer, 2002). The functional protein encoded by *SMN* is SMN1, which is crucial for splicing and proper localization of RNP complexes in motor neurons. The other transcript variant *SMN2* carries a single nucleotide change in exon 7 that disrupts splicing and results in deletion of exon 7 (Lorson and Androphy, 2000; Monani et al., 1999). Thus, the protein is less stable and becomes rapidly degraded.

3.4 TDP-43

3.4.1 Known Functions of TDP-43

TDP-43 was originally identified as a factor capable of binding to the TAR DNA of human immunodeficiency virus where it is implicated in transcriptional regulation (Ou et al., 1995). It belongs to the family of heterogeneous nuclear ribonucleoproteins (hnRNP) and is ubiquitously expressed (Wang et al., 2004). Deletion of *Tardbp* gene in mice leads to early embryonic lethality between E3.5 and E6.5 (Sephton et al., 2010b; Wu et al., 2010) indicating an important role during early development.

Structurally, TDP-43 is a 414 amino acid protein that contains two RNA-recognition motifs (RRMs), RRM-1 and RRM-2, and a glycine-rich region at its C-terminus (Fig. 9) (Buratti et al., 2001). The RRM-1 is necessary and sufficient for nucleic acid binding activity and the binding of the protein to single stranded RNA is highly specific for GU-rich sequences (Ayala et al., 2005). The C-terminus of TDP-43 is necessary for the formation of hnRNP-rich complexes (Buratti et al., 2005; D'Ambrogio et al., 2009) and contains most of the TDP-43 point mutations that were identified in ALS cases. The ALS-linked mutations were shown to increase the half-life of the protein compared to wild type TDP-43 (Ling et al., 2010). TDP-43 is a 43 kDa protein, has a nuclear localization sequence (NLS) and a predicted nuclear export sequence (NES). It is localized primarily to the nucleus but seems to be continuously shuttled between nucleus and cytoplasm as it was observed for other hnRNPs and SR (serine/arginine-rich) proteins (Wang et al., 2002). The shuttling is necessary as the hnRNPs execute functions in both cellular compartments just like TDP-43. The proper localization of the protein can be disturbed by deletion or insertion of point mutations into the NLS (Ayala et al., 2008b; Barmada et al., 2010).

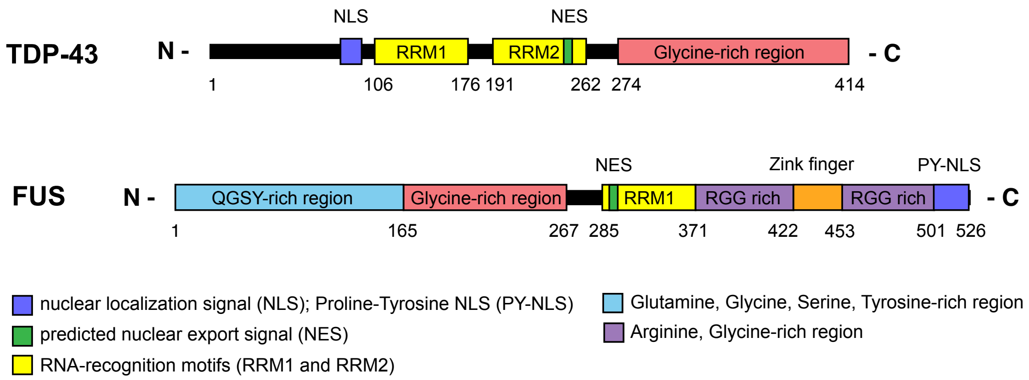

Figure 9. The TDP-43 and FUS proteins Scheme of TDP-43 and FUS, showing the functional domains present in the proteins. Both proteins inherit a nuclear localization signal, nuclear export signal, glycine-rich region and one respectively two RNA-recognition motifs. Adapted from (Lagier-Tourenne et al., 2010)

TDP-43 is one of the main components of cytoplasmic inclusions, which are a characteristic feature of a number of neurodegenerative disorders (Neumann et al., 2006). Several studies have investigated the cause and function of these aggregates, that are mainly composed of C-terminal fragments of TDP-43 of ~25 kDa and ~35 kDa, which are phosphorylated and ubiquitinylated (Inukai et al., 2008; Yang et al., 2010). Recent studies have shown, that the TDP-43 C-terminus inherits prion-like properties (Nonaka et al., 2013; Udan-Johns et al., 2014; Wang et al., 2012). C-terminal fragments of insoluble TDP-43 obtained form ALS or FTLD-TDP patients can act as seeds resulting in aggregation of TDP-43 (Nonaka et al., 2013). Interestingly some studies have shown that mislocalization of TDP-43 to the cytoplasm is insufficient to induce apoptosis (Igaz et al., 2011) and that cytoplasmic TDP-43 aggregates are not necessary for induction of apoptosis *in vivo* (Arnold et al., 2013; Barmada et al., 2010; Igaz et al., 2011; Wegorzewska et al., 2009). It is therefore not clear if the inclusions are in fact causing cell death or whether they are a defense mechanism of the cell to store excessive TDP-43 protein. Apoptotic neurons that display cytoplasmic inclusions show a partial deletion of TDP-43 from the nucleus (Igaz et al., 2011), which was suggested to drive, at least in part, the pathogenesis in diseases such as ALS. A recent study though demonstrated that degeneration of motor neurons due to expression of TDP-43 mutants does not result as a consequence of loss of TDP-43 from the nucleus or accumulation of TDP-43 aggregates *in vivo* (Arnold et al., 2013).

It was reported that the cleavage of TDP-43 can be caspase-mediated (Suzuki et al., 2011) and also other factors of the apoptosis pathway such as Bim, Bax and Bcl were shown to be involved in TDP-43 induced cell death (Gonzalez de Aguilar et al., 2000; Suzuki et al., 2011). Additionally elevated p53 levels were detected in affected neurons of ALS patients (Eve et al., 2007; Martin, 2000; Ranganathan and Bowser, 2010). However, the absence of p53 in a transgenic mouse model for ALS (hSOD1$^{(G93A)}$) did not rescue the apoptosis, suggesting that cell death in these animals occurred in a p53-independent manner (Kuntz et al., 2000; Prudlo et al., 2000). In addition, deletion of Puma, a downstream effector of p53, had no effect on the lifespan of SOD1$^{(G93A)}$ mice (Kieran et al., 2007). A causal link between p53 and TDP-43 induced cell death has not been reported so far.

Many lines of transgenic mice have been generated expressing wild type or mutant forms of TDP-43 (Arnold et al., 2013; Igaz et al., 2011; Iguchi et al., 2013; Tsai et al., 2010; Wegorzewska et al., 2009; Wils et al., 2010; Xu et al., 2010). TDP-43 expression from different promoters at varying levels causes neurodegeneration reminiscent of ALS and FTLD and results in early mortality in mice. One exception is a mouse line where an age-dependent progressive motor neuron death was observed following expression of TDP-43 point mutants close to endogenous TDP-43 levels (Arnold et al., 2013). As the KO of TDP-43 causes early embryonic lethality conditional KO mice have also been generated. Global *Tardbp* deletion in postnatal mice using a Rosa-CreER led to rapid death of the animals due to altered body fat metabolism (Chiang et al., 2010). Mice with *Tardbp* cKO in postnatal motor neurons exhibited an age-dependent progressive motor dysfunction (Iguchi et al., 2013).

Another known function of TDP-43 is in the regulation of pre-mRNA splicing. Currently 4 systems have been described where TDP-43 affects RNA splicing. The first described was the splicing out of exon 9 resulting in exon skipping of the *cystic fibrosis transmembrane conductance regulator* (*CFTR*). To regulate the exon 9 skipping, TDP-43 specifically binds to the GU-rich exon-intron junction sequences of the *CFTR* pre-mRNA (Ayala et al., 2006). TDP-43 also acts as a negative splicing regulator for *Apo AII* exon 3 by binding to UG-repeated elements (Mercado et al., 2005). However, molecular analysis show that the splicing inhibition through TDP-43 is partially dependent on the interaction with other hnRNP proteins including A1/A2/B1/C (Buratti et al., 2005). TDP-43 can also have a positive role in splicing as it enhances exon 7 inclusion during the *SMN2* pre-mRNA splicing (Bose et al., 2008). In addition, it was shown that TDP-43 and hnRNP H repress splicing of *SC35* transcripts by competing with *SC35* for binding to the terminal 3' splice site of *SC35* mRNA (Dreumont et al., 2010).

TDP-43 can also regulate the transcript levels of genes such as *Cyclin-dependent kinase 6 (Cdk6)* (Ayala et al., 2008a*), Histone deacetylase 6 (Hdac6)* (Fiesel et al., 2010), *Neurofilament light polypeptide (Nefl)* (Strong et al., 2007), *Autophagy related 7 (Atg7)* (Bose et al., 2011) and *Tardbp* (Ayala et al., 2010; Sephton et al., 2010a). In the case of *Tardbp*, TDP-43 binds to the 3´ UTR of its own mRNA and thus promotes RNA instability. In addition, several groups have performed high throughput screening analysis in various systems that have revealed many additional transcripts that are bound and potentially regulated by TDP-43 (Buratti et al., 2013; Polymenidou et al., 2011; Tollervey et al., 2011). The relevance and function of TDP-43-binding to these many RNAs remains to be shown as does the relevance of the binding in disease.

3.4.2 TDP-43 in Neurodegenerative Disease

ALS is a neurodegenerative disease characterized by the progressive death of motor neurons of the spinal cord, motor cortex and brainstem (Kirby et al., 2010). Patients suffering from ALS display progressive muscle weakening and eventually die due to respiratory failure or pneumonia within 2-5 years of diagnosis (Mulder and Howard, 1976). ALS is a late onset disease with an incidence of 1-2 per 100,000 whereas it strikes most people between the age of 50-65. Most ALS cases are sporadic (~90% sALS) and are pathologically and clinically indistinguishable from familial ALS (fALS), which is inherited in an autosomal-dominant mode (Kirby et al., 2010). Nearly all of the sALS cases display TDP-43 pathology (ALS-TDP), manifesting in ubiquitin-positive inclusions in the cytoplasm of affected motor neurons, whose main constituent is TDP-43 (Neumann et al., 2006). In 5% of fALS and sALS cases point mutations in the TDP-43 protein have been found, mainly localized to the highly conserved C-terminal region. Up to now more than 30 *Tardbp* point mutations have been identified in ALS-TDP (Dormann and Haass, 2011; Pesiridis et al., 2009). ALS cases with familial history are also associated with mutations in other genes, including *CuZn superoxide dismutase 1* (*SOD1*) (Battistini et al., 2005), *FUS* (Kwiatkowski et al., 2009; Vance et al., 2009), *Progranuline* (Schymick et al., 2007), *Valosine containing protein (VCP)* (Johnson et al., 2010), *Optineurin* (Maruyama et al., 2010), *Ubiquilin 2* (Deng et al., 2011), *Profilin 1* (Wu et al., 2012) and *Angiogenin* (*Ang*) (Thiyagarajan et al., 2012), of which *SOD1* is the most common of all mutations. Interestingly the inclusions occurring in patients with *SOD1* mutations are TDP-43- and FUS-negative which suggests a different mechanism of pathology (Dormann and Haass, 2011). In addition, expanded GGGGCC hexanucleotide repeats in the noncoding region of C9ORF72 on Chromosome 9p were recently found in ALS and FTLD patients. These repeats were detected in several patients and are suggested to cause both ALS and FTLD (DeJesus-Hernandez et al., 2011). The interrelationship between these different mutations and genes remains unknown however, TDP-43 aggregates seem to occur in many cases.

Not only is TDP-43 a key factor in ALS but also in other neurodegenerative diseases including Alzheimer's disease, Parkinson's disease, FTLD and Huntington's disease (Chen-Plotkin et al., 2010). The disease affected neurons also display cytoplasmic inclusions consistent of TDP-43 and it is still under debate whether these inclusions are a cause or a secondary feature of the disease. It is still not known how TDP-43 triggers disease or contributes to observed phenotypes of other neurological disease. The prevailing question at the moment is, whether TDP-43 mutations result in loss-, gain-of-function or gain-of-amorphic function. Despite intensive research on ALS and TDP-43 we are far from understanding the disease mechanism and the role of TDP-43 during disease onset and progression.

3.4.3 TDP-43 pathology in ALS patients

ALS is the most common motor neuron disease, that goes along with muscle weakness and atrophy caused by degeneration of lower and upper motor neurons. α-motor neurons of the spinal cord as well as brainstem motor neurons of cranial nerves V, VII and X-XII display TDP-43 pathology, which is characterized by cytoplasmic inclusions consistend of ubiquitinylated and phosphorylated TDP-43 protein (Brettschneider et al., 2013). In addition, neurons of the frontal and motor cortex, striatum and hippocampal dentate granular neurons are affected (Neumann et al., 2006). In the cortex mainly layer 5 pyramidal neurons display TDP-43 pathology. At later disease stages TDP-43 inclusions are also present in projection neurons of layer II, III and VI whereas layer IV neurons are unaffected (Brettschneider et al., 2013). Besides neurons, TDP-43 immunopositive inclusions are present in oligendroglial cells in the subcortical white matter and cortex.

15% of ALS patients develop symptoms such as behavioral and cognitive impairment that are typically defining FTLD (Ringholz et al., 2005). Conversely, 50% of FTLD patients show ALS pathology characterized by TDP-43 inclusions, thus showing the clinical and pathological link between the two diseases (Ling et al., 2013).

Mouse models expressing wild type or mutant TDP-43 develop ALS and FTLD pathology to a certain extent. The mice display cognitive deficits an motor neuron dysfunction (Swarup et al., 2011; Tsai et al., 2010). In addition TDP-43 inclusions are observed in the spinal cord, hippocampus and cortex (Igaz et al., 2011; Swarup et al., 2011; Wils et al., 2010). In the motor and somatosensory cortex ubiquitin pathology is only present in layer V neurons although TDP-43 is ubiquitiously expressed (Wegorzewska et al., 2009; Wils et al., 2010). Additionally increased GFAP reactivity in layer V is observed suggesting local activation of astrocytes caused by neuronal degeneration.

3.4.4 The Role of Astrocytes in ALS

Astrocytes are star-shaped glial cells present in the spinal cord and brain. They are involved in physical structuring of the brain and closely interact with neurons providing them with nutrients like lactate and glycogen and control extracellular levels of neurotransmitters and ions which are essential for neuron function (Ransom and Ransom, 2012). Astrocytes can become activated which occurs in response to injury of the CNS and also in neurodegenerative diseases, and this results in proliferation and characteristic phenotypic changes of the cells. Reactive astrocytes display an increased GFAP expression, extended processes and altered expression of extracellular matrix proteins. Active astrocytes can trigger motor neuron death by secretion of pro-apoptotic factors and nitric oxide, which results in mitochondrial damage (Barbeito et al., 2004). Astrocytosis is a pathological characteristic of ALS and was long considered to be a secondary feature of the disease (Hirano, 1996). Resent publications however indicate that glial cells play a critical role during neurodegeneration. Astrocytes derived from SOD1 mutant mice were shown to affect survival of wild type and SOD1 mutant motor neurons whereas interneurons and dorsal root ganglion neurons were unaffected (Di Giorgio et al., 2007; Nagai et al., 2007). Similar results were observed in two other studies where human motor neurons derived from embryonic stem cells or ALS patients displayed sensitivity to co-cultured SOD1 mutant astrocytes (Di Giorgio et al., 2008; Haidet-Phillips et al., 2011). In addition, wild type nonneuronal cells were found to extend the survival of SOD1 mutant motor neurons, indicating a protective effect (Clement et al., 2003). A possible factor mediating the toxic function of activated astrocytes is

Lipocalin2 (Lcn2) that was identified in two independent studies employing TDP-43 mutant rats (Bi et al., 2013; Tong et al., 2013). Lcn2 was secreted by reactive astrocytes and was selectively toxic to neurons. However, the expression of Lcn2 was independent of mutant TDP-43 expression and might therefore be caused by the reactive status of astrocytes (Tong et al., 2013). Collectively these studies indicate a non-cell autonomous effect of glial cells on motor neurons whereas the only *in vivo* data on the matter was obtained from Tong et al. 2003. This group used transgenic rats that selectively expressed TDP-43$^{(M337V)}$ in astrocytes. The animals displayed progressive motor neuron death and progressive paralysis. Contradicting data was published by Serio et al. as they observed no adverse effects of TDP-43 mutant astrocytes on co-cultured motor neurons (Serio et al., 2013). Most of the studies convincingly demonstrating a non-cell autonomous neurodegeneration were obtained using SOD1 mutant cells. fALS cases with SOD1 mutations do not show TDP-43 pathology and TDP-43 and SOD1 mutant astrocytes might influence motor neurons differently. However, Tong et al. showed non-cell autonomous effects of TDP-43 mutant astrocytes on neighbouring motor neurons. These differing findings could be due to dose dependent effects. Induced pluripotent stem (iPS) cells derived form ALS patients carry one copy of the mutated gene and therefore express mutant protein at a much lower level than the TDP-43$^{(M337V)}$ transgenic rats. Thus, a certain level of mutant TDP-43 expression in astrocytes might be necessary to induce apoptosis in neighbouring motor neurons.

A recent study investigated the adverse effect of oligodendrocytes on motor neurons. Oligodendrocytes are a type of glial cells, located in the CNS providing support and insulation for neurons (Kang et al., 2013). Degenerating oligodendrocytes were identified in the gray matter of SOD1$^{(G93A)}$ mice prior to disease onset. SOD1 deletion increased survival of the mice by delaying disease onset. These results also support the concept of non-cell autonomous degeneration of motor neurons and further studies will be needed to resolve the problem.

3.4.5 TDP-43 and FUS Regulate miRNA Processing

A protein that has several structural and functional analogies with TDP-43 is the hnRNP protein FUS (Fig. 9). It was shown that mutations in this protein similar to TDP-43 trigger premature degeneration of motor neurons and are responsible for 4-5% of familial ALS cases (Kwiatkowski et al., 2009; Vance et al., 2009). Inclusions containing FUS are also present in FTLD and ALS, though they are less frequent than TDP-43 inclusion (Kwiatkowski et al., 2009; Vance et al., 2009). FUS is a DNA/RNA binding protein with an RRM, a glycine rich region and a NES that has been implicated in RNA maturation and splicing (Fig. 10). These striking similarities between TDP-43 and FUS and the linkage of the very to neurodegenerative diseases suggest a similar function in the onset of ALS.

By mass spectrometry both proteins have been found to associate with Drosha, suggesting an involvement of TDP-43 and FUS in miRNA processing (Lagier-Tourenne and Cleveland, 2009). In fact, it was shown that the cellular levels of let-7b and miR-663 are affected by TDP-43 deletion (Buratti et al., 2001). There is also evidence for the involvement of FUS in miRNA biogenesis. FUS interacts with Drosha and specific pri-miRNA sequences and helps Drosha recruitment to chromatin, allowing for efficient miRNA processing (Kang et al., 2013; Morlando et al., 2012). Similarly TDP-43 was shown to simultaneously bind to the Drosha complex and pri-miRNAs, which results in efficient cleavage into pre-miRNAs (Serio et al., 2013). Another hnRNP protein very similar to TDP-43, hnRNP A1, was shown to regulate the processing of pre-miR-18a (Guil and Caceres, 2007). All this data suggests a general function of hnRNPs in miRNA processing. Whether Drosha, the microprocessor or miRNAs play a role in sALS or fALS-TDP-43 remains to be clarified.

3.5 The Apoptosis Pathway and the Key Factor p53

The tumor suppressor protein p53 encoded by *Trp53* in mice regulates cell cycle, apoptosis and numerous other processes (Matlashewski et al., 1984). During normal homeostasis p53 is inactivated by its inhibitor Mdm2, an E3-ligase that mediates ubiquitination of p53 and thus proteasomal degradation. Another critical regulator of p53 is Mdm4, a protein structurally very similar to Mdm2. Mdm4 contains a C-terminal Ring domain via which it interacts with Mdm2 to promote E3-ligase activity (Marine and Jochemsen, 2005). However, the protein itself lacks the E3-ligase activity. Despite repressing p53 function Mdm4 is an important regulator of Mdm2, and Mdm2 as well as Mdm4 knockout mice display embryonic lethality which can be rescued by p53 deletion (Montes de Oca Luna et al., 1995; Parant et al., 2001). Upon cellular stresses including DNA damage, hypoxia or cell cycle abnormalities, p53 can be phosphorylated by a number of kinases including ATM, ATR, Chk1 or Chk2. p53-phosphorylation at the N-terminus disrupts binding of Mdm2 and thus degradation of the protein (Kruse and Gu, 2009). Stabilized p53 can bind to transcriptional coactivators in the nucleus and activate transcription of genes including *Cdkn1a (Cyclin-dependent kinase inhibitor 1)* (Fig. 10). *Cdkn1a* encodes p21, a regulator of cell cycle progression. Increased levels of p21 result in cell cycle arrest at the two main checkpoints, G_2/M and G_1/S-phase. The arrest allows for DNA damage repair and other repair mechanism to occur and the cell can thereafter progress through cell cycle (Woo and Poon, 2003). However, apoptosis can be initiated if the cell damage is irreparable.

Besides phosphorylation other posttranslational modifications of p53 are regulating the function of the protein. p53 can be acetylated by the histone acetyltransferase CBP/p300 which allows for recruitment of cofactors and activation of target genes. Although p53 inherits a DNA-binding domain, cofactors are needed for the transcription of certain genes such as p21, Bax, and Puma. In addition, p53 can be sumoylated, methylated and neddylated whereas most of posttraslational modifications occur at the C-terminus of the protein (Kruse and Gu, 2009).

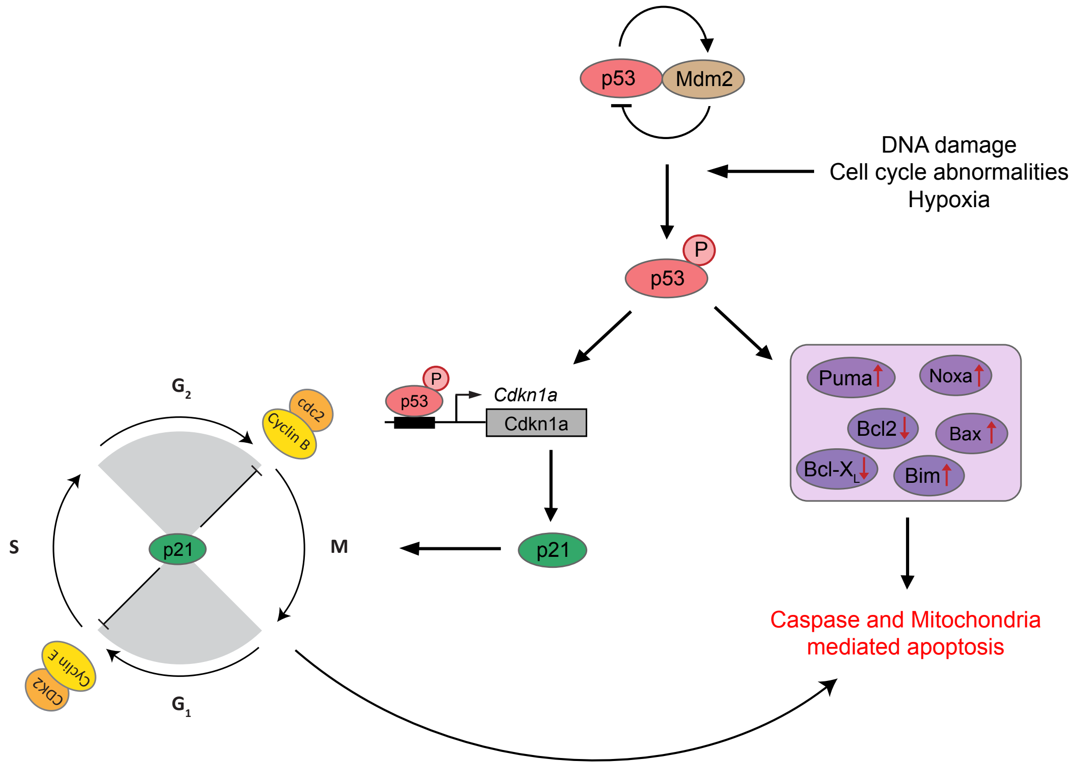

Figure 10. Apoptosis pathway p53 is inhibited by Mdm2 and becomes phosphorylated upon cellular stresses such as DNA damage. The phosphorylated and therefore stabilized protein acts as a transcriptional activator for *Cdkn1a* and other genes and can induce cell cycle arrest via increased p21 levels. Additionally pro-apoptotic proteins can be activated such as Puma and Bax, which causes caspase and mitochondria mediated apoptosis.

Programmed cell death or apoptosis goes along with characteristic cell changes such as membrane blebbing, DNA and nuclear fragmentation and cell shrinkage (Kerr et al., 1972). Apoptosis can also be induced by phosphorylated p53 protein through activation of pro-apoptotic factors such as Puma, Noxa, Bax and proteins of the anti-apoptotic Bcl2 family. Anti-apoptotic Bcl2 proteins like Bcl2 and Bcl-X$_L$ are located at the mitochondrial surface where they inhibit the pro-apoptotic proteins Bax and Bak and thereby promote survival of the cell (Kubli and Gustafsson, 2012). Activation of Puma and the effector proteins Bax and Bak results in binding and neutralisation of anti-apoptotic BCL-2 proteins. Thus Bax and Bak are freed and they can form pores in the outer mitochondrial membrane, which results in permeabilization of the membrane and release of pro-apoptotic factors from the mitochondria (Green and Kroemer, 2009). One of this factors is cytochrome C which interacts with Apaf1 and thereby initiates the formation of the apoptosome. The apoptosome recruits and activates the initiator caspase pro-caspase-9 through cleavage of the pro-caspase. Activated caspase-9 thereafter activates downstream effector caspases such as caspase-3 which degrade cellular targets (McIlwain et al., 2013). In addition, death receptors that belong to the group of tumor necrosis factor receptors (TNFR) can trigger apoptosis. The receptors contain an intracellular death domain that can initiate a signalling cascade, which will ultimately lead to apoptosis (Mc Guire et al., 2011). The major proteins of this cascade are caspases, which play also a central role in p53-mediated apoptosis, necrosis and inflammation. In contrast to p53-activated apoptosis, the caspases involved in death receptor–mediated apoptosis are caspase 8, 7 and 3.

Programmed cell death is a complex process in which many different signalling pathways and factors are involved. However, p53 is the central protein in cell death induction and its function has been addressed in numerous studies (Levine and Oren, 2009). Mouse models with p53 deletion, activated p53 or mutant p53 have been employed to study the protein, especially during tumor formation (Donehower and Lozano, 2009; Lozano, 2010). In many cancers the protein was found to be absent or inactive due to missense mutations (Muller and Vousden, 2013), and it also plays a major role during neuronal apoptosis. p53 is implicated in apoptosis occurring in Alzheimer’s disease (de la Monte et al., 1997), Parkinson’s disease (Duan et al., 2002) and ALS (Martin, 2000; Ranganathan and Bowser, 2010) and inhibition of p53 in stroke and ischemia models rescues apoptosis (Culmsee et al., 2001).

3.6 Hypothesis

NSCs are capable of self renewal and differentiation. They are found throughout the embryonic development of the brain and Notch signalling is critical for the maintenance of NSCs. Performing a transcriptome analysis on Notch1 depleted tissue we identified a group of RBPs that showed altered expression upon loss of Notch1. A gene from this analysis that particularly caught our interest was *Tardbp*. The gene was found to be mutated in ALS and FTLD patients and the encoded protein TDP-43 is one of the main constituents of cytoplasmic inclusions residing in affected neurons. Studies on

TDP-43 have linked the protein to several cellular processes such as transcription, translation, splicing, mRNA export and miRNA biogenesis. However, TDP-43 function during brain development has not been addressed. We therefore decided to study the function of TDP-43 protein during development of the telencephalon, and in particular in NSCs. We found TDP-43 as being upregulated following Notch1 depletion indicating a role for TDP-43 in NSC maintenance and/or differentation. Thus, we intended to analyse the endogenous expression of *Tardbp* mRNA and protein in the different cell types of the developing brain by performing *In Situ* Hybridisation and immunohistochemistry. In order to address the function of TDP-43 and TDP-43$^{(A315T)}$ we performed loss- and gain-of-function experiments. By *In Utero* Electroporation one can express or knockdown proteins of interest in the NSCs of the developing telencephalon. Thus, we employed this powerful technique to investigate the effect of modulated TDP-43 expression *in vivo*. Based on the results of these experiments we addressed the observed apoptosis phenotype following TDP-43 and TDP-43$^{(A315T)}$ expression in more detail. In addition, we investigated the function of TDP-43 and TDP-43$^{(A315T)}$ on cell cycle regulation, as we noticed a block in cell cycle progression after expression of TDP-43. Taken together we investigated the role of TDP-43 and TDP-43$^{(A315T)}$ in the developing telencephalon *in vivo*, and found that expression of TDP-43 and the point mutant in NSCs results in an apoptosis phenotype that is p53-dependent. In addition TDP-43 binds *Cdkn1a* mRNA which results in the upregulation of the transcript and a block of the cell cycle at G_1/S and G_2/M phase.

4 Materials

4.1 Chemicals

All used chemicals were obtained from the following companies if not indicated differently:
Amersham Pharmacia Biotech, J.T.Baker, Carl Roth GmbH, Fluka, GibcoBRL, GE Healthcare, Invitrogen, Merck KGaA, Qiagen GmbH, Roche Diagnostics GmbH, Sigma-Aldrich.

4.2 Buffers and Solutions

All buffers and solutions were prepared with water purified in a Millipore filter system (Biocel A10 century). For the work with RNA all solutions were prepared RNAse free with Diethylpyrocarbonate (DEPC) treated water and autoclaved before use.

4.2.1 Animal Treatment

BrdU solution	10 mg/ml 5,5´-diaminobenzidine and 0,0024% H_2O_2 in 0.05 M Trizma-HCl, pH7.4
HBSS/PenStrept	1x Hank´s buffered saline solution (HBSS, Gibco), 1% PenStrept
PFT-α solution	20 mM PFT-α in DMSO

4.2.2 Histological and *In Situ* Hybridization (ISH) Procedures

Blocking buffer	0.3% Triton, 2% NGS in PBS
Buffer B1	100 mM Tris-HCl pH7.5, 150 mM NaCl
Buffer B2	Buffer B1, 1% Blocking Reagent (Roche)
Buffer B3	100 mM Tris-HCl pH9.5, 100 mM NaCl, 50 mM $MgCl_2$
Borate buffer	0.1 M Boric acid (in H_2O), adjust to pH8.5
DEPC H_2O	DEPC treated H_2O
0.2 M EDTA	0.2 M EDTA in H_2O
0.15% Eosin solution	0.15% (w/v) Eosin in 100% EtOH
40% EtOH	40% EtOH in PBS
70% EtOH	70% EtOH in PBS
95% EtOH	95% EtOH in H_2O (PBS cannot be used as it would result in precipitation of the salt)
2 N HCl	2N HCl in H_2O

Hybridisation mix	50% Formamide, 5x SSC, 5x Denhardt´s solution (Invitrogen), 250 µg/ml yeast tRNA (Roche)
4 M Lithium chloride	4 M Lithium chloride in H_2O
NBT/BCIP	10 ml buffer B3, 45 µl NBT (Roche), 33 µl BCIP (Roche), the solution was filtered sterile after preparation
PB buffer	0.1 M Phosphate buffer, adjust to pH7.4
PBS	2.7 mM KCl pH7.4, 1.5 mM KH_2PO_4, 8.1 mM Na_2PO_4, 137 mM NaCl, (1 tablet) in 0.5 l H_2O
4% PFA	4% (w/v) Paraformaldehyde in 0.1 M PB buffer
Sodium citrate	10 mM NaCitrate-2H_2O, 0.05% Tween
15% Sucrose in PBS	15% (w/v) Sucrose in PBS
30% Sucrose in PBS	30% (w/v) Sucrose in PBS
20x SSC	3 M NaCl, 0.3 M Na_3Citrate-2H_2O, adjust to pH7

4.2.3 Cell Culture

Blasticidin solution	10 mg/ml blasticidin S HCl in sterilized water
Cell culture medium for N2A cells	DMEM (Gibco), 1% Pen/Strept (Gibco), 10% fetal calf serum (FCS) (Life Technologies), FCS was heat inactivated for 30 min at 56°C before use
Digestion mix	Papain Mix, Ovomucoid Mix 1:1
DMEM/F12	DMEM/F12 + GlutaMax™-I (Gibco)
L15	L15 (Leibovitz) + GlutaMax™-I (Gibco)
Neurosphere medium NS medium	49 ml DMEM/F12 + GlutaMax™-I (Gibco), 1 ml B27 supplement (Gibco), 20 ng/ml FGF-2 (R&D), NS medium cannot be filtered sterile
Ovomucoid mix	45 mg Trypsin inhibitor (Sigma), 21 mg BSA (Sigma), 40 µg/ml DNAse I (cell culture grade, Roche), 39 ml L15 medium, has to be filtered sterile and can be used one week if stored at 4°C
Papain mix	30 U/ml Papain (Sigma), 40 µg/ml DNAse I, 0.24 mg/ml Cystein (diluted in L15) (Sigma); has to be prepared fresh and filtered sterile
0.25% Trypsin	2.5% Trypsin (Gibco) 1:10 diluted in Versene (Gibco)

4.2.4 Biochemical Procedures

5x AP I buffer	300 mM Tris-HCl, adjust to pH9.4
1x AP II buffer	30 mM Tris-HCl, adjust to pH9.4
Blocking buffer	5% (w/v) milk in TBST
IP buffer	50 mM Hepes pH7.5, 0.4 M NaCl, 1 mM EDTA, 1 mM DTT, 0.5% Triton-X-100, 10% Glycerol, add fresh 1x Complete from 50x stock solution
1x KP buffer	30 mM Tris-HCl pH9.4, 40 mM ε-capronacid, 0.1%

	SDS
Lysis buffer	20 mM Tris-HCl pH7.6, 150 mM NaCl, 2 mM EDTA, 0.5% Triton-X-100, 0.5% Nonidet P40, 10% Glycerol, add fresh 1x Complete from 50x stock solution
RIPA buffer	50 mM Tris-HCl pH8, 150 mM NaCl, 1% Triton-X-100, 0.5% Sodium deoxychelate, 0.1% SDS, add fresh 1x Complete from 50x stock solution
RIP buffer	50 mM Hepes pH7.5, 0.1 M NaCl, 5 mM EDTA, 10 mM DTT, 0.5% Triton-X-100, 10% Glycerol, 1% SDS
Running buffer	25mM Tris-HCl pH9.4, 192 mM Glycine, 0.1% SDS
Sample loading buffer	62.5 mM Tris-HCl pH6.8, 2% SDS, 0.01% Bromophenolblue, 25% Glycerol
TBS	10 mM Tris-HCl pH8, 150 mM NaCl
TBST	10 mM Tris-HCl pH8, 150 mM NaCl, 1%Tween20

Recipes for SDS-acrylamide gel preparation:

Separation gel (15%)	**Stacking gel (4%)**
2.5 ml 30% Acrylamid/Bis Acrylamid	0.555 ml 30% Acrylamid/Bis Acrylamid
1.25 ml 1,5 M Tris-HCl (pH8,8)	1.055 ml 0,5 M Tris-HCl (pH6,8)
25 µl 20% SDS	11.1 µl 20% SDS
50 µl 10% APS	22.2 µl 10% APS
5 ml H_2O	2 ml H_2O
5 µl TEMED	2 µl TEMED

4.2.5 Molecular Biology

DNA loading buffer	15% Ficoll, 2.5% Bromphenolblue, 2.5% Xylene
dNTPs	10 mM of each dATP, dGTP, dCTP, dTTP (Fermentas) in H_2O
2 M Glycine	2 M Glycine in H_2O
LB medium	10 g Bacto-tryptone, 5 g Bacto-Yeast Extract, 5g NaCl, add H_2O up to 1 l (was prepared in the in-house media kitchen)
Saturated NaCl	~6 M NaCl in H_2O
0.1 M PMSF	0.1 M Phenylmethylsulfonyl fluoride
RNA loading buffer	1 µl 10x TAE, 10 µl Formamide, 3.5 µl; 37% Formaldehyde, Ethidiumbromide 1:2000
Tail lysis buffer	50 mM Tris-HCl pH8, 0.1 M EDTA, 0.1 M NaCl, 1% SDS, 0.5 mg/ml Proteinase K freshly added before use.
50x TAE	242 g Trizma-Base, 57.1 ml CH_3COOH, 100 ml 0.5 M EDTA pH8, to a total volume of 1 l

1 M TEA	1 M Triethanolamine, HCl 37%, adjust to pH8
0.25% Trypsin	2.5% Trypsin (Gibco) 1:10 diluted in Versene (Gibco)

4.3 Antibodies

Antibodies used for ISH and Immunoprecipitation

anti-DIG Fab-Fragments (Roche)

anti-FLAG® M2 Affinity Gel (Sigma)

Primary antibodies used for Immunostaining

Antigen	Origin	Dilution	Source
BrdU	rat	1:500	Serotec abD OBT0030CX
activated caspase-3	rabbit	1:200	Cell Signaling, ASP1755A1E
Pax6	mouse	1:500	Covance PRB-278P
phospho-Histone 3	rabbit	1:300	Upstate 06-570
Tbr1	rabbit	1:500	Abcam 31940
Tbr2	rabbit	1:500	Abcam 9618
TDP-43	rabbit	1:500	Proteintech 12892-1-AP

Secondary antibodies used for Immunostaining

Antigen	Origin	Dilution	Source
FITC conjugated anti-mouse Immunoglobulin	donkey	1:1000	Jackson ImmunoResearch
FITC conjugated anti-rabbit Immunoglobulin	donkey	1:1000	Jackson ImmunoResearch
Cy™3 conjugated anti-mouse Immunoglobulin	donkey	1:1000	Jackson ImmunoResearch
Cy™3 conjugated anti-rabbit Immunoglobulin	donkey	1:1000	Jackson ImmunoResearch
Cy™5 conjugated anti-rabbit Immunoglobulin	donkey	1:1000	Jackson ImmunoResearch
Biotin-SP-conjugated anti-rat Immunoglobulin	donkey	1:1000	Jackson ImmunoResearch
Cy™3 conjugated Streptavidin		1:1000	Jackson ImmunoResearch

Primary antibodies used for Immunoblotting

Description	Origin	Dilution	Source
Flag	mouse	1:2000	Sigma F3165
GAPDH	mouse	1:10000	Calbiochem (6C5)
GFP	mouse	1:1000	Roche 11814460001
p21	rabbit	1:120	Abcam 7960
p53	rabbit	1:1000	Santa Cruz (FL393)
TDP-43	rabbit	1:2000	Proteintech 12892-1-AP

Secondary antibodies used for Immunoblotting

Description	Origin	Dilution	Source
Peroxidase-conjugated anti-mouse Immunoglobulin	donkey	1:10000	Jackson ImmunoResearch
Peroxidase-conjugated anti-rabbit Immunoglobulin	donkey	1:10000	Jackson ImmunoResearch

4.4 Primers

Primers for cloning of ISH probes

Description	Forward 5'-3'	Reverse 5'-3'
Tardbp	attccttcccgtctgtgctt	ggctgttgtcggattcctt

qRT-PCR primers

Description	Forward 5'-3'	Reverse 5'-3'
Actin	aggtgacagcattgcttctg	gggagaccaaagccttc
Bax	tgaagacagggcctttttg	aattcgccggagacactcg
Bcl2	cctgtggtcatggatctgtt	ggaagaccaggctttcttgt
GAPDH	tccatgacaactttggcattgtgg	gttgctgttgaagtcgcaggagac
Puma	agcagcacttcgcgtcgcc	cctgggtaaggggaggagt
p21-3'UTR	aaggccagctaggatgacag	agagacccacaggagaggtg
p21-CDR	caaagtgtgccgttgtctct	aggaagtactgggcctcttg
p53-3'UTR	cccagcgaaattctatccag	cagacaggctttgcagaatg
TDP-43-3'UTR	gcccacaaactgaggggataa	tgtcctcctgcacacaagtc
TDP-43-CDR	aggttgcccagtctctttgt	agttcatccctccacccata

Genotyping primer

Description	Forward 5'-3'	Reverse 5'-3'
hTDP-43$^{(A315T)}$	#1 ctgttgtcggattccttccc #2 ctcgtcaatttcttacctggag	caactgcaagagggtttattgg
Trp53	#1 cgggaaatagagacgctgagtccg #2 ggtggggtgggattagataaatgcc	agtgtgatgatggtaaggatag gtcggc

4.5 Enzymes

BioScript™ kit (Bioline)

Cloned *Pfu* DNA Polymerase (Stratagene)

Dnase I recombinant, Rnase free (Roche)

pGEM-T Easy Vector System (Promega)

Kappa2G polymerase (Peqlab)

KOD DNA Polymerase (Novagen®)

Proteinase K (Roche)

Rnase-Inhibitor recombinant (Invitrogen)

Sp6 RNA-Polymerase (Roche)

SensiMix SYBR Kit (Bioline)

SuperScript™ III First-Strand Synthesis System for RT-PCR (Invitrogen)

T4 DNA-Ligase (Promega)

T3 and T7 RNA-Polymerase (Roche)

TaqDNA-Polymerase Kit (Invitrogen)

4.6 Reagents

Immunohistochemistry

1,4-diazabicyclo(2.2.2)octane mounting medium (DABCO, Sigma)

4',6-Diamino-2-phenylindol (DAPI) (Roche)

Normal Goat Serum (NGS) (Gibco)

Tissue-Tek® O.C.T™ Compound (Sakura)

Eukitt®-quick-hardening mounting media (Fluka)

Cell Culture

Lipofectamine™ 2000 Reagent (Invitrogen)

Poly-L-Lysin hydrobromide (Sigma-Aldrich)

TransFectin™ Lipid Reagent (Biorad)

Molecular Biology

cOmplete, EDTA-free (Roche)

1 Kb Plus DNA Ladder (Invitrogen)

GlycoBlue™ (Applied Biosystems)

Protein G Sepharose 4 Fast Flow (GE Healthcare)

Precision Plus Protein™ Standards (BioRad)

4.7 Plasmids

Plasmid	Cloned by / obtained from
pBS-Beta2 NeuroD1::mCherry	(Philip Knuckles)
pBS-Beta2 NeuroD1::TDP-43	(Philip Knuckles)
pCAGGS-eGFP	(laboratory Prof. R. Kemler)
pCAGGS-p21	(Miriam Vogt)
pCAGGS-TDP-43	(Miriam Vogt)
pCAGGS-TDP-43$^{(A315T)}$	(Miriam Vogt)
pCAGGS-ΔRRM1	(Miriam Vogt)
p3X-GFP-flag	(laboratory Prof. S. Wilson)
p3X-FLAG-myc-CMV™-26 (Sigma)	
p3X-TDP-43-flag	(Miriam Vogt)
pFucci mKO-hCdt1 (Addgene)	
pMI-Tomato	(Sebastian Lugert)
pMI-TDP-43-Tomato	(Miriam Vogt)
pMI-TDP-43$^{(A315T)}$-Tomato	(Miriam Vogt)
pSuper-shRenilla (Oligoengine)	(Philip Knuckles)
pSuper-shTDP-43 (Oligoengine)	(Miriam Vogt)

pCAGGS-TDP-43 and pCAGGS-ΔRRM1 were subcloned into the pCAGGS vector from expression constructs obtained from Francisco E. Baralle (Ayala et al., 2008b).

pCAGGS-TDP-43$^{(A315T)}$ was subloned into the pCAGGS vector from an expression construct obtained from Pamela Shaw (SITraN, University of Sheffield.

4.8 Kits

Amersham™ ECL™ Western Blotting Detection Reagents (GE Healthcare)
Click-iT® EdU Imaging Kit (Invitrogen)
CalPhos™ Mammalian Transfection Kit (Clontech)
10x DIG RNA labelling mix (Roche)
EndoFree® Plasmid Maxi Kit (Qiagen)
Pierce® BCA Protein Assay Kit (Thermo Scientific)
Retro-X™ Concentrator (Clontech)
QIAGEN Plasmid Midi Kit (Qiagen)
QIAprep® Spin Miniprep Kit (Qiagen)
QIA quick® Gel Extraction Kit (Qiagen)
TRIZOL® Reagent (Invitrogen)

5 Methods

5.1 Animal Treatment

5.1.1 Animal Husbandry

Mice were kept on a 12-hour day/night cycle with adequate food and water under SPF (specific pathogen free) conditions. Adult mice 8-12 weeks of age were used in the experiments. The day of vaginal plug was considered as embryonic day 0.5 (E0.5).

C57Bl/6J, Trp53^{tm1Tyj} and hTDP-43$^{(A315T)}$ (Schebelle et al., 2010), mice were used in the experiments.

5.1.2 Intraperitoneal Injection of BrdU

BrdU solution was stored in aliquots of 1 ml at -20°C. During use it was kept at 4°C in tubes wrapped with aluminum foil since BrdU is light sensitive. A final dose of 50 mg/kg bodyweight of the BrdU solution was injected intraperitoneally before sacrificing the mouse and isolation of the embryos.

5.1.3 Intraperitoneal Injection of PFT-α

PFT-α solution was stored in aliquots of 20 µl at -20°C. During use it was kept at 4°C and a final dose of 2.2 mg/kg bodyweight of the PFT-α solution was injected intraperitoneally into pregnant mice.

5.1.4 *In Utero* Electroporation (IUE)

For injections of plasmid DNA into embryonic brains *in utero*, a microinjector (Pneumatic Pico Pump, WPI Rnage) and Borosilicate glass capillaries (Kwick-Fil™) were used. The capillaries were pulled in a micropipette puller (Sutter Instrument Co.) at: heat = 540°C; pull = 50; velocity = 50; time = 200 sec. The tip of the capillaries was broken off and sharpened using a capillary sharpener (Bachofer). The capillaries were back end-loaded with 10 µl of the plasmid solutions.

Plasmid stocks were prepared endotoxin free and resuspended in PBS at a high concentration (2-4 μg/μl). Fast green contrast dye diluted in PBS (10%) was added to the plasmids to control the targeting of the injection. For cell tracing the expression vector was injected together with a second vector coding for a fluorescent protein in a ratio of 3:1. Thereby, one can later trace the cells that were electroporated *in vivo*.

Mice were anesthetized with Isofluran (Baxter), diluted in O_2 and secured on a heated operating table. The eyes of the animals were covered with Bepanthene crème to avoid drying-out. The fur was removed from the stomach using depilation cream and the skin disinfected with 70% Ethanol (EtOH) thereafter. Before opening the abdomen, the skin was moistened with HBSS/PenStrept. This was repeated continuously, especially during the electroporation, to prevent drying-out. After the capillary was checked for clogging a cut of about 2 cm was made from the bottom of the abdomen upwards. The uterine horns containing the embryos (E13.5) were pulled out of the abdominal cavity and 1–2 μl of DNA solution were injected into one of the lateral ventricle of each embryo (Fig. 11). A cold light source was used for illuminating the developing embryos. The embryos were electroporated (Electro Square Pavator™, BTX® Harvard Apparatus) with 40 V, a pulse length of 50 ms and 5 pulses in an interval of 950 ms. The positive pole of the electrode was oriented towards the injection side, thereby DNA enters stem cells lining the lateral ventricle. Paddles were stored in cell culture PBS when not used.

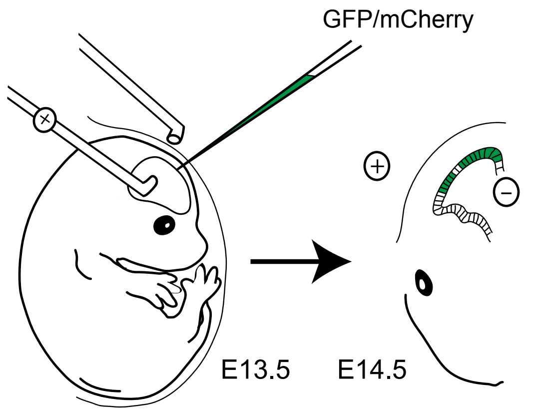

Figure 11: IUE scheme Embryos are electroporated at E13.5 and cells can be traced by expression of a fluorescent protein from a co-electroporated plasmid.

After injection and electroporation embryos were returned into the abdomen and the abdomen was filled with HBSS/PenStrept to disinfect it. Excess of HBSS/PenStrept and bubbles were gently pushed out of the thoracic cavity. Then the muscle and afterwards the skin were sutured. The animals were allowed to recover under a heat lamp.

5.2 Histology

5.2.1 Postnatal Tissue Fixation

After mice were sacrificed in CO_2, the embryos were isolated and fixed in 4% PFA at 4°C overnight. Then the tissue was cryoprotected in a sucrose gradient. First the tissue was incubated in 15% sucrose solution until it was equalized and sank to the bottom, followed by the same procedure using 30% solution. Thereafter, the tissue was embedded in tissue O.C.T. over dry ice and stored at -80°C.

For paraffin embedding E6.5 embryos were washed twice in PBS after fixation in 4% PFA for 1 h at 4°C. Thereafter the embryos were consecutively incubated in 40%, 80% and 100% EtOH to dehydrate them. Each incubation was performed for 1 h at 4°C with constant agitation. Then the 100% EtOH was replaced with xylene for 2-5 min and embryos were put into hot paraffin before the tissue turned completely yellow or transparent. The embryos were left in hot paraffin overnight and were embedded the day after using fresh paraffin. The paraffin with the embryos was put to 4°C to harden and thereafter stored at 4°C.

5.2.2 Cryosectioning

After tissue equilibration to -20°C for 30 min, transverse sections were made at -21°C and 20 μm thickness using a cryostat (Leica CM3050S). The sections were collected on pre-cleaned and ground edged glass slides (SuperFrost Thermo Scientific). After air drying for 15 min, the sections were stored at 4°C in PBS.

5.2.3 Paraffin-Sectioning

Paraffin embedded embryos were sectioned at room temperature (RT) at a thickness of 7 μm using a microtome (Reichert-Jung 2030 Biocut). The sections were collected on pre-cleaned and ground edged glass slides (SuperFrost Thermo Scientific), dried at 37°C and finally stored at 4°C.

5.2.4 Antigen Retrieval

Antigen retrieval was performed for anti-BrdU, activated caspase-3, TDP-43, Tbr1 and Tbr2 stainings.

Antigen retrieval for activated caspase-3, TDP-43, Tbr1 and Tbr2
Sections were incubated in sodium citrate buffer for 30 min at 80°C in a water bath, cooled afterwards to RT for 50 min and washed in PBS for 10 min.

Antigen retrieval for BrdU
Since BrdU is integrated into the genome sections were incubated in 2N HCl for 30 min at 37°C, cooled afterwards to RT for 15 min, incubated in borate buffer for 15 min at RT and finally washed in PBS for 10 min.

5.2.5 Staining of Cryopreserved Tissue Fixed in 4% PFA

To inhibit unspecific binding the tissue was blocked using normal goat serum (NGS). Therefore 300 μl of blocking solution was added to each slide and incubated for 1 h at RT. The blocking solution was removed and 250 μl of primary antibody diluted in blocking solution were added to each slide. The slides were covered with parafilm to avoid drying out and incubated at 4°C overnight in a moist chamber. The next day, slides were washed (3x10 min, PBS, RT) and 250 μl blocking solution with secondary antibodies were added to each slide, covered with parafilm and incubated in the dark for 3 h at RT. After, the slides were washed (3x10 min, PBS, RT) and the nuclei were stained using DAPI diluted in PBS (1 μg/ml) for 15 min at RT. The slides were washed one more time with PBS, air-dried for 15 min and mounted with DABCO. All steps following the application of the secondary antibody were performed in the dark to avoid fading of the fluorescent signal.
For the BrdU staining a biotinylated secondary antibody was used in combination with a Cy™3-conjugated streptavidin to enhance the signal. The sections were incubated with the biotinylated anti-rat antibody for 3 h at RT and with the Cy™3-conjugated streptavidin for 1 h at RT, whereas both were diluted in blocking solution.

5.2.6 Ethynyldeoxyuridine (EdU) Staining

EdU is an uridinederivate like BrdU and is integrated into the DNA during replication of the genome which allows measuring of DNA synthesis. The advantage of using EdU over BrdU is that the chemical compound Alexa Flour® azide can bind covalently to EdU via a copper-catalyzed reaction. This allows direct binding of a primary antibody, without denaturing of the DNA.
For EdU staining the Click-iT® EdU Imaging Kit was used according to the manufacturer's instructions.

5.2.7 Hematoxylin & Eosin (H&E) Staining of Paraffin Embedded Tissue Fixed in 4% PFA

H&E staining was performed to identify broad morphological changes in transgenic mouse embryos. With this staining method cell nuclei are coloured blue by oxidation of Hematoxylin which is added first to the slides. After a counterstaining using Eosin, eosinophilic parts of the cell such as collagen, cytoplasm, muscle fibres and red blood cells will be labelled in red.
In order to perform H&E staining paraffin sections were re-hydrated by two times incubation in xylene for 5 min each followed by immersion of the slides in an EtOH series. The slides were incubated consecutively in 100%, 95% and 70% EtOH for 5 min each and finally transferred to H_2O for 5 min. Then the sections were incubated in Mayer's Hematoxylin solution for 2 min and washed in running tap water for 10 min. Next slides were counterstained in 0.15% Eosin solution for 10 min and de-hydrated with 95% and 100% EtOH for 2 min each, cleared in two changes of xylene for 5 min each, air-dried for 10 min and finally mounted in xylene based mounting media.
The incubation times of the sections with Hematoxylin and Eosin varies dependent of the thickness of the sections. The incubation times mentioned above were used for 7 µm sections.

5.3 *In Situ* Hybridization (ISH)

5.3.1 Preparation of ISH probe

cDNA containing vectors were linearized using appropriate restriction enzymes (section 5.6.3) and the digest was analysed on a 0.6% agarose gel (section 5.6.4). The adequate bands were cut from the gel, purified and the concentration measured. To obtain Digoxygenine (DIG)-labelled RNA probes, linearized DNA was used as template in the RNA-labelling reaction mix. The mix was comprised of 7 μg template DNA, 1x reaction buffer (10x), 0.05 μg/μl RNase Inhibitor (1 μg/μl), 1x DIG RNA labelling Mix (10x) and 4 U/μl RNA Polymerase (40 U/μl) (T3 or T7). The final volume of the mix was adjusted to 20 μl with DEPC H_2O and incubated at 37°C overnight. The newly synthesized RNA-probes were precipitated by addition of 2 μl 0.2 M EDTA, 2.4 μl 4 M lithium chloride and 75 μl 100% EtOH. The sample was mixed and incubated at -20°C for 30 min. Labelled RNA was precipitated by centrifugation (13000 rpm, 30 min, 4°C) and the supernatant carefully removed. RNA was washed with 75 μl 70% EtOH (chilled at -20°C) and centrifuged (13000 rpm, 30 min, 4°C). The supernatant was removed and the pellet air-dried for ~5 min. Thereafter, the cRNA-probes were dissolved in 100 μl DEPC H_2O and the RNA concentration measured using a NanoDrop ND-1000 Spectrophotometer. To analyse the size of the probes they were run on a 1% RNA gel (section 5.6.5). The cDNA probes were stored at -20°C after adding one volume of formamide.

5.3.2 ISH Procedure

For acetylation a glass tray with slides was filled with 250 ml 0.1 M TAE and a magnetic stirrer added. 625 μl acetic anhydride was added dropwise with constant stirring and after 20 min, slides were washed (3x5 min, PBS, RT). For pre-hybridization, the slides were placed horizontally in a moistened chamber (50% formamide) with 400 μl of hybridisation-mix (without DIG-labelled probes) for 3-4 h at RT. Prior hybridisation DIG-labelled probes were denatured by incubation of 100 ng/ml probe diluted in hybridisation–mix at 85°C for 5 min and kept on ice thereafter. The pre-hybridisation-mix was replaced by the DIG-labelled probe containing hybridisation-mix (400 µl per slide) and covered with hybri-slips (Sigma). The moist chamber was sealed with parafilm and incubated in a pre-heated incubator at 68°C overnight. Bottles with 5x and 0.2x SSC, a glass tray and an 80 ml glass beaker were also put into the incubator overnight to equilibrate.

The next day, slides were rinsed in pre-warmed 5x SSC (68°C) in an 80 ml glass beaker and washed in 5x SSC for 5 min at 68°C. Afterwards, they were incubated in 0.2x SSC for 1 h at 68°C and finally cooled to RT for 5 min. Slides were placed in a moistened chamber and incubated for 1 h at RT with 400 µl buffer B2. Next, hybridized DIG-labelled probes were detected with 400 µl alkaline phosphatase coupled anti-DIG Fab-Fragments dissolved 1:2000 in the buffer B2, covered with hybri-slips for 4 h at RT. Afterwards, slides were washed twice for 20 min in buffer B1. To provide suitable conditions for the colour reaction and to suppress endogenous alkaline phosphatase activity, the samples were briefly rinsed and subsequently equilibrated overnight at 4°C in buffer B3.

The colour reaction was carried out in a moistened chamber by adding 400 µl of NBT/BCIP solution, an alkalinephosphate substrate. The slides were covered with hybri-slips and incubated at 37°C for developing. As the staining developed the slides were put to RT to slow down the reaction. For overnight reactions slides were kept at 4°C. The developing time varied, dependent on the used probe. Therefore the staining was controlled under the light microscope.

A sense probe was always included and as here background staining appeared, slides were transferred to PBS to stop the reaction. After washing for 1 h in PBS, the slides were mounted with DABCO.

5.4 Cell culture

5.4.1 Transfection of Cells with Lipofectamine or Transfectin

For transfection, N2A cells were grown to a confluency of 70-80%. Lipofectamine™ 2000 Reagent or TransFectin™ Lipid Reagent were used and prepared according to the manufacturer's instructions.

5.4.2 Generation of Stable Cell Lines

The stable N2A cell line N2A-hCdt1 was generated using the pFucci mKO-hCdt1 (Sakaue-Sawano et al., 2008) expression plasmid. Cells were transfected with the plasmid and kept under blasticidin selection to eliminate all non-transfected cells. The medium containing blasticidin (10 μg/ml) was changed every 3-4 days and cells were sorted using FACS (section 5.4.6.) after 4 weeks of selection. Single cells were seeded in 96 well plates, expanded and analysed to confirm adequate expression of the plasmid.

5.4.3 Antibody Staining of Cells

Cells were plated on Poly-L-Lysine coated glass plates in a 12 well plate. Before staining the cells were washed twice in PBS to remove all serum which would result in a strong background signal after staining. Next, cells were fixed in 4% PFA for 20 min at RT with shaking. After, they were washed (3x10 min, PBS, RT) and blocked with blocking solution for 30 min. The primary antibody diluted in blocking buffer was added for 1.5 h at RT with gentle shaking. The antibody solution was removed, the cells washed (3x10 min, PBS, RT) and next incubated with the secondary antibody in blocking buffer for 1.5 h at RT shaking. After washing (3x10 min, PBS, RT) the nuclei were stained using DAPI diluted in PBS (1 μg/ml) for 15 min at RT. The cells were washed once more with PBS and mounted with DABCO on glass slides. All steps following the application of the secondary antibody were performed in the dark to avoid fading of the fluorescent signal.
For staining of cells the primary antibody anti-phospho-Histone 3 was used in the concentration of 1:400. As secondary antibody Cy™5 conjugated anti-rabbit Immunoglobulin was used in a concentration of 1:1000.

5.4.4 Isolation and Culturing of Embryonic Forebrain NSCs

Embryonic and adult NSCs can be cultured and expanded *in vitro* as neurospheres. For generation of embryonic neurospheres, the region of the dorsal forebrain where NSCs are located was micro-dissected.
Before starting the dissection 5 ml sterile glass vials were prepared and labelled. Under the cell culture hood and under sterile conditions 150 µl of ovomucoid mix and 150 µl of papain mix were added to each vial.

Isolation of the embryonic forebrain and NSCs:
The uterus containing the embryos (E12.5-E18.5) was placed into a sterile 10 cm dish with L15 medium. In a sterile cell culture hood the embryos were removed from the uterus and transferred to a fresh sterile 10 cm dish containing L15 medium. Embryos were decapitated and transferred to a fresh sterile 10 cm dish containing L15 medium. The micro-dissection of embryonic forebrain was performed with fine forceps with a scissor action under sterile conditions in a cell culture hood, using a binocular. The dissected tissue was transferred to a 5 ml glass vial with screw cap using the forceps or a sieve and lightly homogenized in the digestion mix with the tips of the forceps to assist the enzyme penetrating the tissue. Thereafter, the tissue was kept at room temperature until all of the dissections were completed. Between dissections of the embryos, any tissue sticking to the forceps and scissors was removed and the tools were sterilized by submersion in 70% ethanol. Care was taken not to damage the tips of the fine forceps. Therefore, a tissue paper was pushed to the bottom of the 50 ml bottle to protect the tips of the forceps. The dissection was continued until all of the embryos were prepared and tissue was digested in the 300 µl digestion mix for 10 min at 37˚C.
The total volume of the digestion mix was increased relative to the size of the tissue isolated. Preparing the tissue from individual embryos reduced the risk of contaminating all of the preparation if the dissected tissue was pooled. If mutant mice were being used for the preparation, the donor embryos were genotyped and preparations with the same genotype pooled at a later stage if necessary.

After incubation an equal volume (300 µl) of ovomucoid mix was added and the tissue dissociated in the digestion/ovomucoid mix using fire-polished glass pipettes. Either a rubber bulb or electronic pipetting device was used and it was taken care not to aspirate the cells into the pipetter. The cells were pipetted 10-20 times until the solution was homogeneous and no clumps of tissue were visible. If the tissue did not dissociate easily, the tip of the Pasteur pipette was gently pressed against the bottom of the tube to reduce the opening and increase the pressure on the cells.

Preparation of fire-polishing pipettes:

The tips of sterile glass Pasteur pipettes were held on the edge of a Bunsen flame and rotated until the tip started to melt, removing the sharp edge, and reducing the diameter of the opening. The longer the tip was flamed the smaller the opening became. The diameter of the opening should not be too small to avoid damaging the cells due to shear forces. At least one fire-polished pipette was prepared for each embryo to be dissected and the pipettes were sterilized by flaming prior to use.

The dissociated cells were added to 9 ml DMEM/F12 in a 15 ml conical tube at room temperature and cells were centrifuged (80-100 xg, 5 min, RT) in a swing-out rotor. The supernatant was removed (leave a little – 100 µl – over the cells to avoid losing neural stem cells), and the cells were suspended in 4 ml of neurosphere (NS)-Medium using a 1 ml pipette. 300.000 cells were transferred to a 25 cm^2 flask for culture and it was assure that they were single cells.

Culturing of NSCs as NS:

Cells were fed every 4 d (addition of 4 ml NS-Medium) and passaged after 7 d. Flasks were shaken every day to avoid clustering of the NS as this would falsify the number and size of NS formed after a given time point. Healthy NS are spherical with a smooth regular surface and are shiny under transmitted light (Fig. 12). If the cells attached to the plastic and spread out, the concentration of FGF-2 was too low and the cells were differentiating. This mostly happens if too many cells are taken into culture after dissociation of the tissue. In such an instance ½ of the cells were discarded and fresh NS-Medium was added up to the original volume.

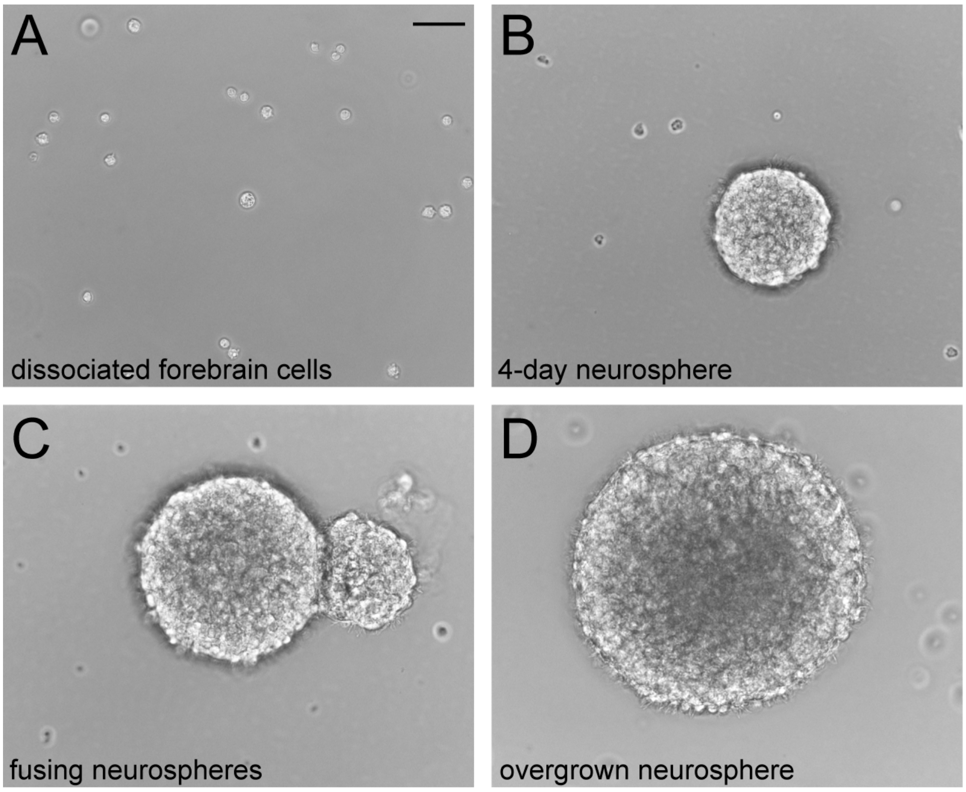

Figure 12. Images of developing neurospheres as well as fused and overgrown spheres A. Cells were isolated as described and plated in neurosphere medium. Most of the cells should be single and the culture should be devoid of aggregates. **B**. After 4 d in culture, neurospheres will have formed and should be relatively uniform in size. Neurospheres should be compact and homogeneous in texture as well as luminosity. **C.** If maintained at high density neurospheres will aggregate and fuse. **D.** Large and fused neurospheres can have rough edges and can be non-homogenous in texture. Also they sometimes display a dark or vacuolated center. Scale bar = 50 µm.

Passage of NS:

NS were transferred in a 15 ml falcon and centrifuged (800 rpm, 5 min, RT). Supernatant was removed, 200 µl Trypsin added and incubated at 37˚C for 5-10 min. Thereafter 500 µl ovomucoid mix was added and the cells singularized using a fire-polished glass pipette. 5 ml of DMEM/F12 was added, the cells centrifuged (800 rpm, 5 min, RT) and the supernatant removed. Cells were dissociated in 1 ml and 300.000 cells used for re-culturing in a 25 cm^2 flask. It was assured that the cells were singularized properly as the newly formed NS would otherwise not be clonal and not representative for the neural stem cell potential of the cells.

Freezing of NS:

NS were frozen 3-4 d after the last passage when small spheres were already formed. Optional the cells can also be frozen directly after passaging. For freezing the cells were harvested in a 15 ml falcon, the supernatant removed and cells frozen in NS-Medium + 10 % DMSO.

5.4.5 Viral Infection of Neurospheres

Retroviruses were generated using the packaging cell line Plat-E (Morita et al., 2000). Plat-E cells were transfected with the viral plasmid constructs using CalPhos™ Mammalian Transfection Kit according to the manufacturer's instructions. Viral supernatants were collected 48 and 72 h after transfection and the virus was purified using the Retro-X™ Concentrator according to the manufacturer's instructions.
For viral infection neurospheres were passaged and allowed to recover for 24 h. Then virus (50 virus particles/cell) was added in a small volume (~200 µl) of NS-medium for 4 h and the cells were afterwards cultured in an adequate volume until analysis or sorting.

5.4.6 FACS (Fluorescence-activated cell sorting)

FACS was performed by the staff of the in-house FACS facility using a FACSAria™ III (BD Biosciences).

5.5 Biochemical Methods

5.5.1 Lysis of Cells for Immunoblot Analysis

To obtain cell lysates cells were first washed with ice cold PBS and an adequate volume of lysis buffer was added. The lysis buffer contained detergents and proteinase inhibitors to avoid the degradation of the proteins. Next, the cell suspension was transferred to an eppendorf tube, cells were lysed by trituration and incubated at 4°C with constant agitation. After the cell suspension was centrifuged (13000 rpm, 5 min, 4°C) to sediment the insoluble parts of the cells. The supernatant containing all soluble proteins was transferred to a new tube and the protein concentration measured using a BCA Protein Assay Kit according to the manufacturer's instructions. For storage, lysates were kept at -20°C.

5.5.2 Immunoprecipitation

A 6 cm^2 plate of N2A cells was transfected with expression plasmids (p3X-TDP-43-flag or p3X-GFP-flag as control). After 24 h cells were washed with cold PBS, 500 µl IP lysis buffer added and the plates incubated at 4°C for 20 min with gentle agitation. Thereafter, the cell suspension was transferred to an eppendorf tube and centrifuged (13000 rpm, 10 min, 4°C) to sediment the insoluble parts. The supernatant containing the soluble proteins was transferred to a new tube and 1/10 was used as input control. The remaining lysate was added to pre-blocked beads coupled to anti-flag antibody (ANTI-FLAG® M2 Affinity Gel) or to un-coupled beads (Sepharose-G beads) and incubated at 4°C for 2 h with constant agitation. For pre-blocking 40 µl beads were washed twice with 900 µl cold H_2O (2000 rpm, 1 min, RT), then 400 µl IP lysis buffer + 1% BSA was added and incubated at 4°C (on a rotating wheel) overnight. After incubation of lysate and beads the samples were centrifuged (2000 rpm, 5 min, 4°C) the supernatant discarded and the beads with the bound proteins washed twice with IP lysis buffer. For the release of the bound proteins from the beads 100 µl of RIP buffer was added and incubated at 70°C for 1 h. The supernatant containing the immunoprecipitated proteins was then analysed on a SDS-gel.

5.5.3 SDS-Polyacrylamide-Gel-Electrophoresis (SDS-page) of Proteins

To separate proteins according to their molecular weight SDS-acrylamide gels were used. For low molecular weight proteins like TDP-43 15% separation gel and 4% stacking gel were used. The gel was casted into a gel apparature (BioRad) according to the manufacturer’s instruction and allowed to polymerise.

20-40 µg proteins with 2x sample loading buffer were denatured at 95°C for 5 min and loaded on the gel. To determine the molecular weight a standard weight marker was loaded on the gel. The proteins were separated at 35 mA constant current per gel. Electrophoresis was performed in running buffer until the bromophenolblue band of the loading buffer reached the bottom of the gel.

5.5.4 Blotting of Proteins from SDS Page Gels

For blotting onto a Polyvinylidene fluoride (PVDF) membrane, proteins were transferred electrophoretically from an SDS-gel. To do so, one Whatman paper, moistened in AP I buffer, was placed onto the negative cathode of a blotting apparatus. A second Whatman paper moistened in AP II buffer was put on top, followed by a PVDF membrane that was activated for 1 min in Methanol and after soaked in AP II buffer. The SDS-gel and three Whatman paper soaked in KP buffer were added. To allow a proper transfer of the protein onto the membrane bubbles were avoided. The positive anode was put on top and the proteins were blotted for 30 min at 0.8 mA/cm^2.

5.5.5 Immunodetection of Proteins on PVDF Membrane

To detect specific proteins the PVDF membrane was incubated with specific antibodies. First the membrane was incubated with blocking buffer for 1 h at RT with shaking. Second, primary antibodies diluted in blocking buffer were added and incubated overnight at 4°C shaking. The next day, the membrane was washed (3x10 min, TBST, RT) and the secondary antibodies coupled to horse reddish peroxidase, diluted in blocking buffer were added to the membrane. After incubation for 1 h at RT with shaking the membrane was washed again 2 times in TBST and finally one time using TBS.
For antibody detection the Amersham™ ECL™ Western Blotting Detection Reagent was used. The peroxidase catalyzes the oxidation of luminol, which is present as a substrate leading to chemiluminescence. The signal was detected by an X-ray film or the ChemiDoc™ MP Imaging System (BioRad). The amount of protein was quantified using the ImageLab™ Software Version 4.0.

5.6 Molecular Biology Methods

5.6.1 Transformation of Bacteria

For transformation of bacteria electro-competent E.coli bacteria from the line XL1 blue or TOP 10 were used. 40 μl bacteria were thawed and kept on ice. DNA was added to the bacteria and after mixing gently they were incubated

on ice for 1 min. The bacteria were transferred to a cooled electroporation cuvette (1 mm) and electroporated with 1.8 kV using a MicroPulser (BioRad). Afterwards, 600 µl of LB medium was added and bacteria were transferred to an eppendorf tube and incubated for 1 h at 37°C. The transformed bacteria were plated on agar plates with the corresponding resistance and incubated at 37°C overnight. For re-transformation of bacteria with plasmid 0.1 µg of DNA was used. 10 µl of the transformed cells in LB medium were diluted 1:10 in LB medium and plated. For transforming bacteria with a ligation, 1/3 (~2 µl) of the ligation was used and 200 µl of the bacteria were plated.
50 mg/ml Kanamycin- and 80 mg/ml Ampicillin-Stocks were prepared in H_2O, stored in 1 ml aliquots at -20°C and used 1:1000.

5.6.2 DNA Isolation from Tail Biopsies

In order to perform genotyping of mice, DNA was isolated form tail biopsies. Therefore, 500 µl of tail lysis buffer was added to each sample and incubated at 55°C overnight with shaking. The next day 250 µl saturated NaCl (6 M) was added, mixed gently and centrifuged (13000 rpm, 7 min, RT). After 600 µl of the supernatant were transferred to a new tube and 400 µl Isopropanol added to precipitate the DNA. DNA was centrifuged (13000 rpm, 5 min, RT), washed with 200 µl 70% EtOH (-20°C) and the supernatant was discarded after another round of centrifugation (13000 rpm, 1 min, RT). Thereafter, the DNA was dried, resuspended in 500 µl H_2O and stored at -20°C.

5.6.3 Restriction Digest of DNA Constructs

For restriction digestion enzymes and appropriate buffers from BioLabs® were used. Control digest was performed with 0.1 – 1 µg DNA together with 2-5 U restriction enzyme per µg DNA, the appropriate 1x buffer (10x) and if recommended BSA (100 µg/ml) in a total volume of 20 µl. To obtain a linearized vector for the generation of ISH probes or cloning experiments, a total volume of 50 µl and 5 µg of DNA were used. The digestion mix was incubated for 1-2 h at 37°C and analysed on an agarose gel.

5.6.4 DNA Agarose Gel Electrophoresis

DNA fragments were analysed by using agarose gel electrophoresis. Agarose was dissolved in 1x TAE buffer to a final concentration of 1% by boiling. The hot solution was allowed to cool to 65°C, 2.5 ng/ml ethidium bromide added and the gel was casted. Gel electrophoresis was performed submerged in an electrophoresis tank filled with 1x TAE buffer between two electrodes. DNA samples loaded were with 5x DNA loading buffer. Fragments were separated in an electric field of maximum 120 V and a current of 0.2 A. To assign the DNA fragments, 2-10 µl of 1 Kb ladder was used.

5.6.5 Denaturing RNA Agarose Gel Electrophoresis

For preparation of a RNA agarose gel, 1.2 g agarose was added to 75 ml H_2O (DNAse free) and 10 ml 10x TAE buffer. The agarose was melted by heating it in the microwave and cooled to about 60°C. Afterwards 18 ml 37% formaldehyde was added. The gel was casted and allowed to solidify. Before loading RNA was resuspended in 2 µl DEPC H_2O. Then 15 µl of fresh RNA loading buffer was added and incubated at 65°C for 5 min. The DNA samples were loaded on the gel with 5x DNA loading buffer and run at 60 V.

5.6.6 Sequencing of DNA Constructs

Plasmids were sequenced externally using sequence specific primers.

5.6.7 RNA Purification for Quantitative Real Time PCR (qRT-PCR)

RNA was purified from cells or tissue using TRIZOL® Reagent according to the manufacturer’s instructions. Next RNA was precipitated using isopropanol and dried for ~10 min until all EtOH had evaporated and the pellet was resuspended in RNase free water. The amount of RNA was measured using a NanoDrop ND-1000 Spectrophotometer.

5.6.8 cDNA Preparation

The reverse transcription to generate cDNA was performed using the SuperScript III First-Strand Synthesis kit. For the reaction, 1 µg of total RNA was incubated with 1 µl oligodeoxythymidine primers (50 µM) and 1 µl dNTPs

(10 mM) and filled up to 13 µl with H_2O. The reaction was incubated at 65°C for 5 min in a light cycler and thereafter put on ice. 6 µl of Premix consisting of 4µl 5x first strand buffer, 1 µl 0.1 M DTT, 1 µl reverse transcriptase and 1 µl RNase inhibitor (1 µg/µl) was added to the sample and the reaction incubated at 50°C for 60 min. Thereafter the reverse transcriptase was inactivated at 70°C for 15 min and cDNA was stored at -20°C.

5.6.9 Polymerase Chain Reaction (PCR)

PCR was performed according to this general protocol. Per reaction 1x Buffer (10x), 1.5 µM $MgCl_2$ (50 mM), 200 µM dNTPs (10 mM), 0.2 µM each forward and reverse Primer (20 pM), 1 U/µl Polymerase (5 U/µl) and 0.1 - 0.5 µg template DNA was used. The PCR reaction was run in a light cycler at which the strands were first separated by heating the reaction to 94°C for 5 min. Annealing was performed for 1 min with the appropriate annealing temperature, which was adjusted dependent on the melting temperature of the primers. For extension of the PCR fragments a temperature of 72°C was used and the extension time was adjusted to the length of the expected PCR fragment (1 min/kb). 30-35 cycles were run in order to receive an appropriate amount of DNA. For the final extension the reaction was incubated at 72°C for 7 min after the last cycle and the reaction was cooled to 4°C thereafter.
For genotyping of mice Taq-Polymerase was used. For cloning purposes proof reading Polymerases such as KOD DNA Polymerase or Cloned *Pfu* DNA Polymerase were used according to the manufacturer's instruction.

5.6.10 Crosslinked RNA Immunoprecipitation (CLIP)

This method is for the immunoprecipitation of Flag-tagged RNA binding proteins from mammalian cell lines and isolation of the bound RNAs for analysis by quantitative real-time PCR. The RNA binding protein of interest was tagged with the M2 Flag-tag and expressed in N2A cells. However, specific antibodies for the protein of interest can be used in conjunction with Sepharose G-beads.
This method is also published online at http://www.bio-protocol.org/wenzhang.aspx?id=398

Blocking of the beads:

40 µl Anti-Flag M2 Affinity Gel beads coupled to antibody were washed twice with 900 µl of pure H_2O (cold). 400 µl IP lysis buffer + 1% BSA was added and incubated at 4°C (on a rotating wheel) overnight. Alternatively 30 µl Sepharose G-Beads + specific antibody was used. The amount of antibody and beads to be used in the pre-coupling need to be determined in preliminary experiments.

Cell transfection:

2 x 10 cm^2 tissue culture plates were used per condition (this might vary depending on the cell type and the level of expression of the protein of interest). No more than 10 plates were processed at a time in order to assure that every experiment was treated the same. Cells were transfected with the appropriate plasmids and incubated for 48 h to express the tagged protein.

Formaldehyde crosslinking and preparation of cell extracts:

Medium was removed, cells washed once with PBS and 1 ml 0.25% Trypsin (pre-heated to 37°C) added. Cells were incubated with the Trypsin until they lost cell-cell contact and 5 ml DMEM including 10% fetal calf serum (pre-warmed to 37°C) was added to inhibit the trypsin. After, cells were transferred to a 15 ml conical tube by pipetting and incubated on ice for 5 min. Thereafter, cells were harvested (100 xg, 2 min) the supernatant discarded and the cell pellet resuspended in 5 ml ice-cold PBS. A 250 µl aliquot of the cell suspension was kept for Western blot analysis to be used as a transfection control. 143 µl 37% formaldehyde (over a period of approximately 10 seconds, all of the samples were treated in the same way) was added to the cell suspension and the 15 ml conical tubes were thereafter placed on a rocking plate and shaken for 10 min at room temperature. 685 µl 2 M Glycine (over a period of approximately 10 s, all of the samples were treated in the same way) was added to block the formaldehyde. The tubes were again placed on a rocking plate and shaken for 5 min at room temperature. Cells were harvested (100 xg, 2 min, RT), supernatant discarded and the cell pellet transferred to ice. Cells were washed twice with 5 ml ice-cold PBS and harvested (100 xg, 2 min, 4°C). The supernatant was removed from the cells after the last wash and 1 ml of IP lysis buffer + 20 µl 0.1 M phenylmethylsulfonyl fluoride (PMSF) + 20 µl complete protease inhibitor

(50x) + 5 µl RNase inhibitor (40 U/ul) was added to each sample. For sonication the cells were kept on ice at all times and sonication was performed 10x (10 s on, 10 s off, Amplitude 15 µm) until the lysate was clear. Probe sonicator was cleaned with RNaseZap between the samples to avoid contamination with RNases. The lysed cells were transferred to a 1.5 ml snap-cap tube and kept on ice. After centrifugation of the lysates (14000 xg, 3 min, RT) 50 µl of the supernatant was kept as an INPUT control (used to standardize the qPCR analysis). The rest of the lysate was added to the blocked beads and incubated overnight at 4°C on a rotating wheel.

Reverse crosslink and RNA extraction:

The beads were washed 5 times with 900 µl of IP lysis buffer collecting the beads by centrifugation (1000 xg, 1 min, RT). All of the supernatant was removed after the last wash and 100 µl of RIP buffer + 1 µl RNase inhibitor added. 50 µl of RIP buffer was added to the INPUT control. The samples and INPUT controls were incubated for 1 h at 70°C to reverse the cross-link, centrifuged (400 xg, 1 min, RT) to sediment the beads and 100 µl of the supernatant collected. The RNA was extracted with Trizol reagent (proceed according to the manufacturer's instruction, see section 5.6.7). Optionally 1 µl of Glycogen blue was added before precipitation of the RNA with Isopropanol to make the pellet visible. Precipitation was performed at -20°C for 1 h to increase the amount of precipitated RNA.

DNAse treatment of the RNA to avoid contamination with genomic DNA.

The RNA pellet was directly diluted in DNAse mastermix (per sample: 16 µl DEPC treated H_2O, 2 µl DNAase buffer, 2 µl DNAse) in order to use all RNA in the following RT reaction and it was proceeded after the manufacturer's instruction.

Reverse transcription of the RNA into cDNA:

BioScript^{TM} kit works well but other reverse transcriptase kits may also be used. 9 µl of the DNAse treated RNA was used in a reverse transcriptase-containing and a reverse transcriptase-minus (negative control) reaction for each sample. cDNA was primed with random hexamer primers and the reaction performed according to the manufacturer's instructions. The cDNA was diluted 1:4 and continued with quantitative real-time PCR analysis of the target gene to identify specific changes in target mRNA level. Alternatively the cDNA can be used to generate a library.

5.6.11 Quantitative Real-time PCR (qRT-PCR)

Quantitative real-time PCR was performed using the SensiMix SYBR Kit. Primers for detection of specific targets were designed using Primer3Plus software (http://www.bioinformatics.nl). The pipetting robot QIAgility (Qiagen) was used to pipette the master mix and to transfer it into the reaction tubes. 1 µl of template was added manually to 9 µl master mix. The reaction was run in a Rotor-Gene™ 6000 Real-time PCR machine (Corbett) and analysed using Rotor-gene 6000 series software 1.7.

5.7 Imaging

Sections were analysed with an Apoptom (Zeiss Observer.Z1) or confocal (Zeiss LSM510) fluorescence microscope. Images were acquired using Zen pro 2012 (Zeiss) or Zeiss LSM 4.2 (Zeiss) and processed with ImageJ64 or Photoshop CS5 (Adobe) software. Images of hTDP-43$^{(A315T)}$ embryos were acquired using a Leica MZFIIII and H&E stainings were acquired using an Axioskop2 plus (Zeiss).

5.8 Quantification and Statistical Analysis of the Data

Randomly selected, stained cells were analysed with fixed photomultiplier settings on a Zeiss LSM510 confocal microscope (Zeiss). In order to ensure an unbiased analysis, countings were performed in a blind manner at which images of control and experiment were labelled randomly. For IUE experiments data of at least 3 embryos were analysed per experiment whereas 3-5 sections were quantified per embryo and staining. Embryos with a very low number of electroporated cells as well as embryos with an electroporation area too close to the MGE or the medial midline were excluded from the analysis. Data are presented as average percentages of co-labelled cells. Statistical comparisons were conducted by two-tailed unpaired Student's t-test. Significance was established at $P < 0.05$. In all graphs, error bars are standard error of the mean (s.e.m.)

6 Results

6.1 Background and Key Findings

The mammalian central nervous system arises from neural stem cells (NSCs). This process is highly regulated and Notch signalling plays a key role in the maintenance and fate of NSCs (see section 3.1.2-9 and 3.2). The RNA binding protein TDP-43 is regulated downstream of Notch1 in NSCs (see section 3.2). Point mutations in TDP-43 were recently shown to cause ALS and affected neurons show cytoplasmic inclusions of TDP-43 protein. Accumulation of TDP-43 in apoptotic neurons is also a characteristic of other neurodegenerative diseases including Alzheimer’s disease. Therefore, TDP-43 is suggested to play a role in disease onset or progression but it is not known how it triggers or contributes to the disease phenotypes. We have investigated the function of wild type and mutant TDP-43 protein in NSCs *in vivo* and *in vitro* by gain- and loss-of-function approaches.

We performed *in utero* electroporation to both express and knockdown TDP-43 transiently in NSCs in the forebrains of mouse embryos. We could show that expression of TDP-43 and the TDP-43 point mutant TDP-43$^{(A315T)}$ results in rapid death of NSCs *in vivo*. This effect can be rescued by p53 inhibition using a specific p53 inhibitor or by genetically ablating p53. Moreover, we are able to rescue the early lethality in a transgenic mouse model in which hTDP-43$^{(A315T)}$ is expressed from the endogenous *Tardbp* regulatory elements by pharmacological inhibition of p53. Analysing the apoptosis pathway further we found *p53* as well as the downstream factors *Cdkn1a, Bax* and *Bbc3/Puma* upregulated upon TDP-43 and TDP-43$^{(A315T)}$ expression. In addition, expression of TDP-43 and TDP-43$^{(A315T)}$ results in cell cycle arrest of neural progenitors in S- and M-phase *in vitro*. p21 is a key regulator of cell cycle progression and we determined that *Cdkn1a* mRNA is bound by TDP-43 and upregulated after TDP-43 expression. Thus, TDP-43 might directly regulate p21 levels explaining our findings that TDP-43 gain-of-function experiments lead to cell cycle arrest in G_1 and G_2-phase. To date this work represents the first study demonstrating a direct link between TDP-43 and p53-mediated neuronal cell death as well as presenting insights into p21 dependent cell cycle regulation via TDP-43.

6.2 Statement of Contributions

I performed all experiments except for the injection of hTDP-43$^{(A315T)}$ mutant mice with the p53-inhibitor PFT-α, which was done in collaboration with Andrea Huber at the Helmholtz Zentrum München. I participated in the experimental design, data analysis and contributed to the writing of the manuscript, which is currently finalized.

6.3 Results

The following result part is subdivided into three sections, including the three main findings of the work.

6.3.1 Performing gain- and loss-of-function experiments for TDP-43 *in vivo,* we show that loss of TDP-43 does not affect survival of NSCs. However, increased TDP-43 level in NSCs induces cell death whereas TDP-43 expression in BPs does not affect survival.

6.3.2 Apoptosis induced by TDP-43 is p53 dependent and pharmacological inhibition of p53 rescues early lethality of hTDP-43$^{(A315T)}$ transgenic mice.

6.3.4 TDP-43 binds *Cdkn1a* mRNA, which results in increased *Cdkn1a* transcript levels and altered cell cycle regulation.

6.3.1 Gain- and loss-of-function experiments for TDP-43

TDP-43 is expressed in neural progenitor cells of the developing CNS

We have previously found that *Tardbp* is upregulated upon deleting Notch1 from embryonic neural stem cells (Fig. 8). Therefore, we first analysed the expression levels of TDP-43 in the developing CNS by performing *in situ* hybridisation analysis for *Tardbp* in the developing CNS of E11.5 embryos. We found TDP-43 transcripts expressed by progenitor cells of the spinal cord, midbrain and telencephalon (Fig. 13a). TDP-43 protein was detected in the cytoplasm of NSCs lining the ventricle (Fig. 13b,b’ arrows). Most of the TDP-43 high expressing cells were in M-phase of the cell cycle, shown by pH3 staining (Fig. 13c, arrowheads). Additionally, TDP-43 protein was present in neuroblasts in the SVZ and CP (Fig. 13b).

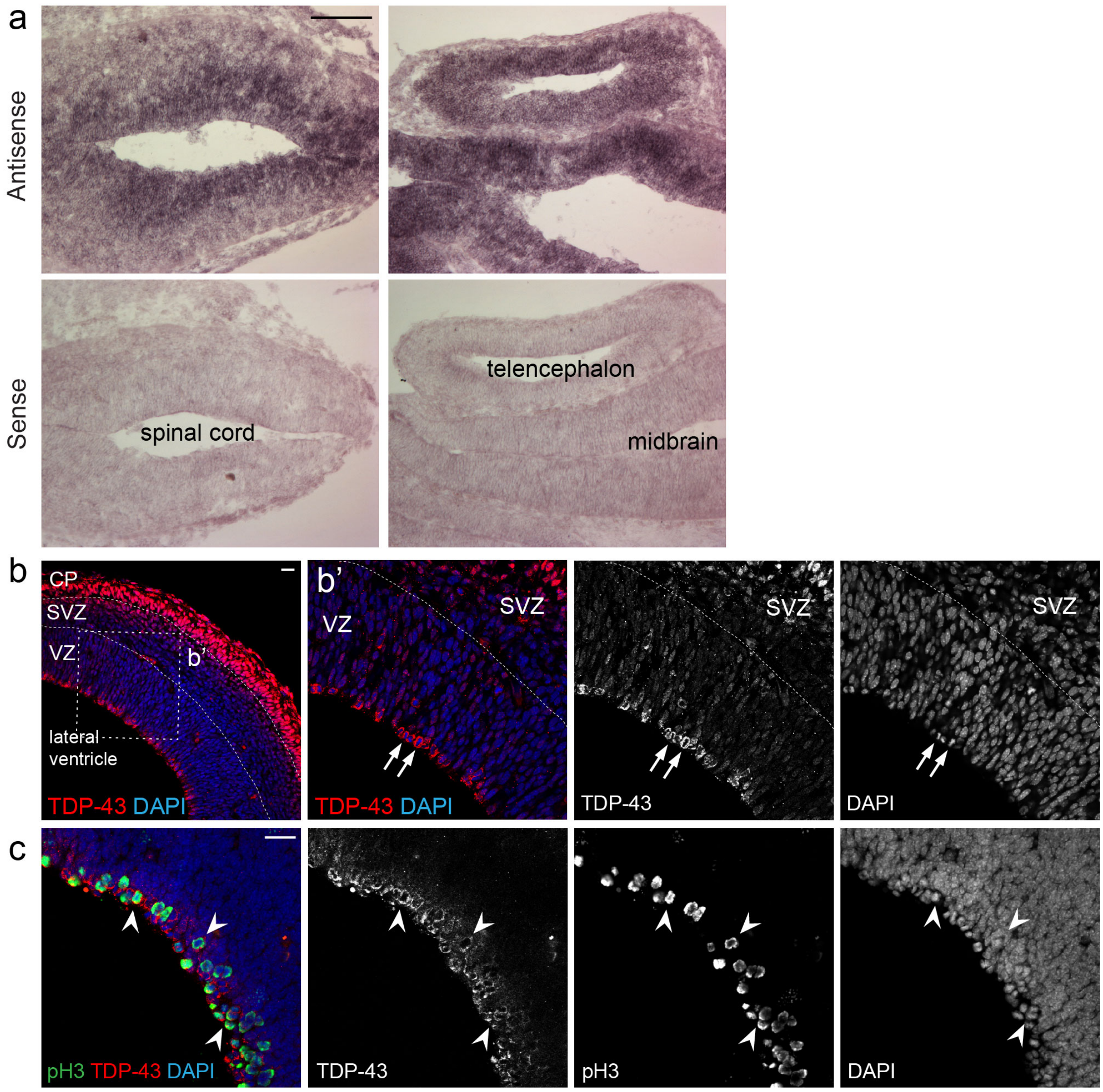

Figure 13: TDP-43 is expressed in neural progenitor cells in the developing CNS

a. *In situ* hybridization analysis using RNA probes generated against the 5' UTR of *Tardbp*. *Tardbp* is highly expressed in NPs of the spinal cord, telencephalon and midbrain of E11.5 embryos. **b,b'.** TDP-43 is expressed by NSCs lining the lateral ventricle of the telencephalon (arrows) and neurons in the CP at E13.5. **c.** Most of the NSCs are in M-phase, which was confirmed by immunostaining for pH3 (arrowheads). VZ = ventricular zone, SVZ = subventricular zone and CP = cortical plate. Scale bars in a = 100 µm, in b and c = 20 µm.

Expression of TDP-43 and TDP-43$^{(A315T)}$ in NSCs induces cell death *in vivo*

To address the function of TDP-43 in NSCs during development of the telencephalon we performed gain- and loss-of-function experiments. For *in vivo* analysis we used *in utero* electroporation (IUE) for transfection of plasmid

DNA into NSCs of the developing telencephalon, allowing expression or knockdown of proteins. Electroporations were performed at embryonic day E13.5 for two reasons. First, E13.5 is the time point whereafter neurogenesis peaks in the developing telencephalon and secondly the embryos are big enough to be manipulated easily enabling high electroporation efficiency. For this TDP-43 as well as TDP-43$^{(A315T)}$ expression plasmids (Fig. 14a) were co-electroporated with a GFP expression plasmid allowing for the identification of transfected cells. TDP-43$^{(A315T)}$ causes in an autosomal dominant ALS in patients, however, it is not known whether the mutation results in loss-, gain-of-function or gain-of-amorphic function.

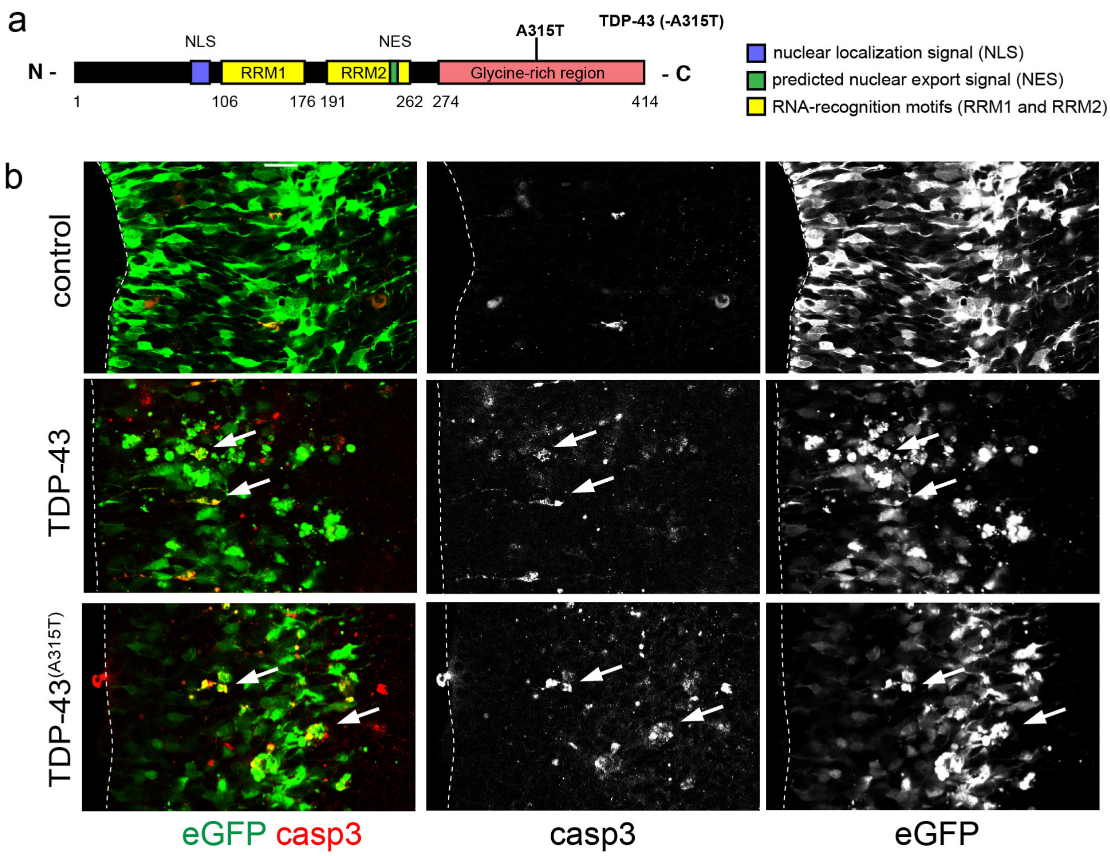

Figure 14: Expression of TDP-43 and TDP-43$^{(A315T)}$ results in apoptosis

a. Scheme of TDP-43 and TDP-43$^{(A315T)}$. The corresponding cDNAs were cloned into the pCAGGS expression vector. **b.** Expression of TDP-43 and TDP-43$^{(A315T)}$ by IUE drives cells into apoptosis after 24 hours, confirmed by immunostaining against cleaved caspase-3. Scale bars = 20 µm. Dashed line marks the ventricular lining.

Expression of TDP-43 as well as TDP-43$^{(A315T)}$ by IUE resulted in an increase in apoptosis as indicated by pycnotic and fragmented nuclei of transfected cells within 24 hours (Fig. 14b arrows). Antibody staining against cleaved caspase3 confirmed that GFP^{+} cells were undergoing cell death (Fig.

14b). Although no quantification was performed to determine the amount of apoptotic cells, we observed an increase in apoptosis based on cellular phenotypic changes.

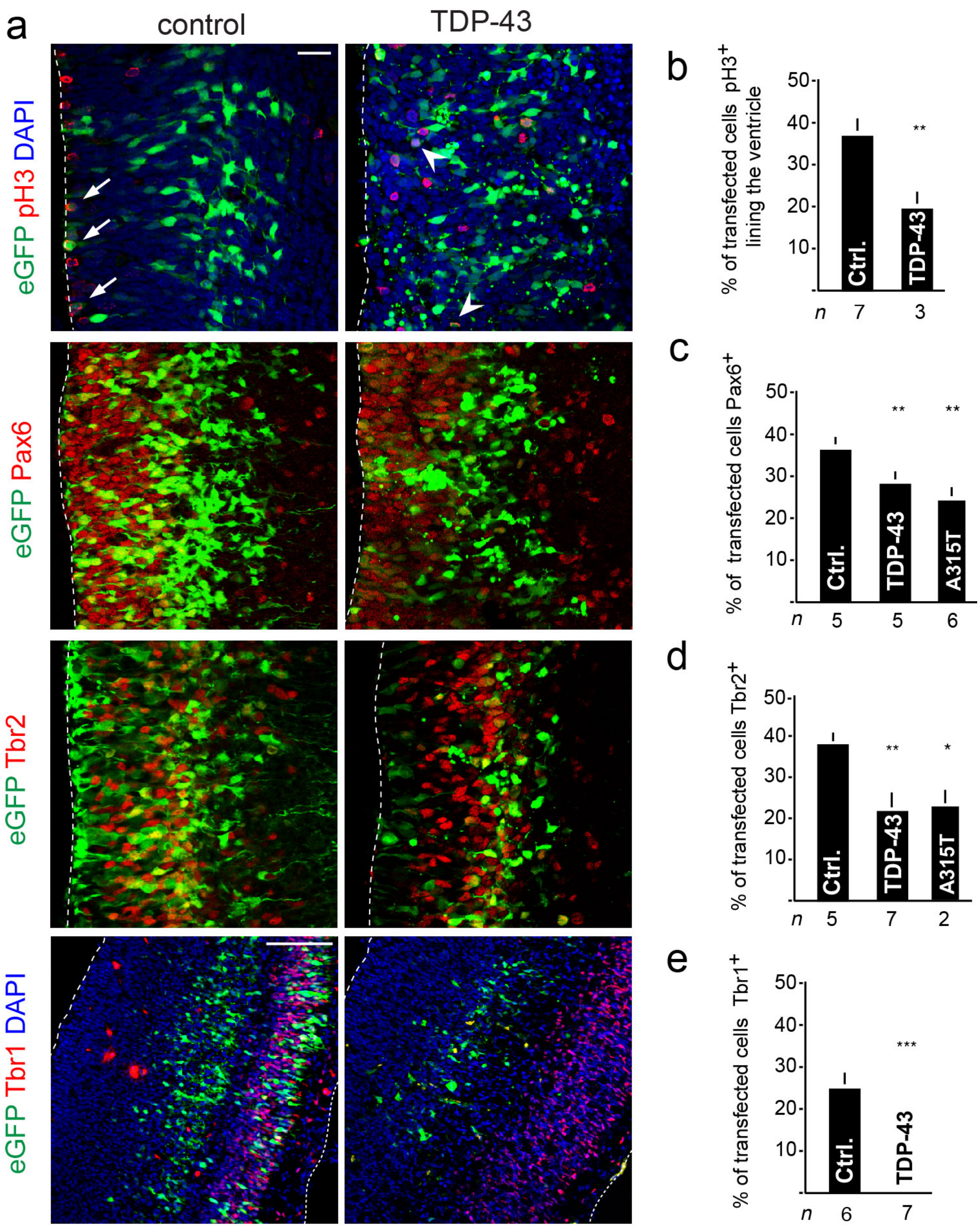

Figure 15: TDP-43 and TDP-43$^{(A315T)}$ expression results in loss of NPs

a. Immunostaining of embryos after expression of TDP-43 or control against pH3, Pax6, Tbr2 and Tbr1. TDP-43 expression leads to a reduced number of cells in M-phase (pH3^{+}) and mislocalization from the ventricular lining (arrowheads). **b**. Quantification of pH3 positive cells expressing TDP-43 or control plasmids. tTest **P<0.005. **c**. Quantification of Pax6 positive cells expressing TDP-43, TDP-43$^{(A315T)}$ or control plasmids. tTest *P<0.05 and **P<0.005. **d.** Quantification of Tbr2 positive cells expressing TDP-43, TDP-43$^{(A315T)}$ or control plasmids. tTest ***P<0.001 and *P<0.05. **e.** Quantification of Tbr1 positive cells expressing TDP-43 or control plasmids. tTest ***P<0.001. Scale bars = 20 µm. Dashed line marks the ventricular lining.

In order to investigate how the few transfected (GFP^+, $TDP\text{-}43^+$) surviving cells were affected by the expression of TDP-43 and $TDP\text{-}43^{(A315T)}$ respectively, we performed immunostaining with different antibodies. Some of the electroporated cells were still mitotically active as they expressed the M-phase marker pH3 (Fig. 15a,b). Interestingly, these $pH3^+$ cells were mislocalized within the VZ (Fig. 15a arrowheads) and were no longer at the ventricular lining as seen in control and wild type embryos (Fig. 15a arrows). Furthermore, we found that the $Pax6^+$ NSC population was also reduced in number after 24 hours after onset of TDP-43 and $TDP\text{-}43^{(A315T)}$ expression (Fig. 15a,c). In addition, we observed that neuronal differentiation was impaired, marked by a significant reduction in basal progenitors ($Tbr2^+$) in the SVZ and differentiated neurons ($Tbr1^+$) in the CP (Fig. 15a,d,e).

Expression of TDP-43 in basal progenitors (BPs) does not result in apoptosis

Expression of TDP-43 in NSCs leads to apoptosis within 24 hours, based on observed changes in cellular morphology. In order to address whether exogenous expression of TDP-43 is generally toxic and to test if this effect is cell type specific we expressed wild type TDP-43 in BPs using NeuroD1 regulatory elements (Fig. 16e). These cells are already committed towards the neuronal lineage but are still able to undergo one round of cell division. NeuroD1 is a transcription factor that starts to be expressed as BPs undergo differentiation in the SVZ. 48 hours post IUE apoptotic cells were not detectable and TDP-43 expressing cells looked normal. In the control condition most of the electroporated cells were located to the SVZ and very few had reached the CP (Fig. 16a arrows). In contrast several cells were located in the CP after TDP-43 expression in BPs (arrows). To address whether the increased number of cells in the CP was due to the transfection efficiency, we quantified the number of Tbr2 and Tbr1-positive cells and found them strongly increased after TDP-43 expression (Fig. 16b,c). More self-replicative divisions of BPs instead of symmetric neurogenic divisions can cause the elevated numbers of BPs ($Tbr2^+$), whereas increased numbers of newborn neurons ($Tbr1^+$) might result from precocious differentiation or exit of BPs from the SVZ.

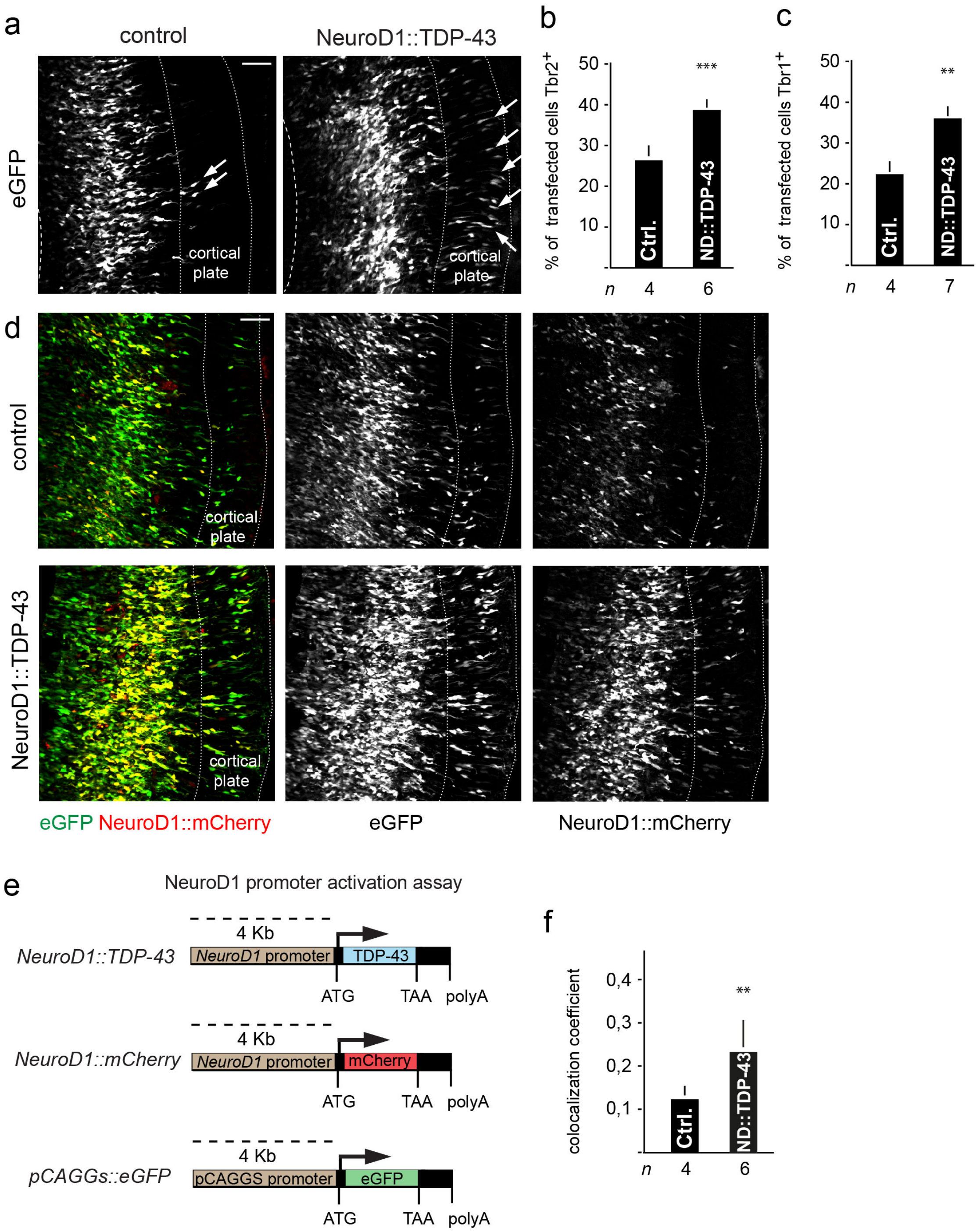

Figure 16: Expression of TDP-43 in BPs leads to an increased number of neurons

a. Expression of TDP-43 under the control of a NeuroD1 promoter element results in an increased number of GFP^{+} cells in the CP after 48 hours. **b,c.** Quantification of Tbr2 and Tbr1 positive cells show an increase after TDP-43 expression in BPs. tTest ***P<0.001, tTest **P<0.05 **d.** Electroporated cells with an active NeuroD1 promoter were identified by expression of mCherry from the NeuroD1 promoter. After expression of TDP-43 in BPs the overall number of mCherry/GFP double positive cells is strongly increased. **e.** Schemes of the expression construct NeuroD1::TDP-43 and the reporter constructs NeuroD1::mCherry and pCAGGS::eGFP **f.** Calculation of the colocalization coefficient = area where mCherry and GFP are co-expressed. tTest **P<0.005. Dashed line marks the ventricular lining, dotted line marks the CP. Scale bars = 50 µm.

Co-electroporation with a construct expressing mCherry under the same NeuroD1 promoter elements used for TDP-43 allowed us to check the activity of the promoter and potential activation of the neurogenic pathway. We therefore electroporated the animals with 3 constructs: pCAGGS::eGFP to report for transfected cells, NeuroD1::mCherry to report for NeuroD1 promoter activity and NeuroD1::TDP-43 or a control plasmid (Fig. 16e). We detected proportionally many more mCherry^{+} cells after expression of TDP-43 compared to control after 48 hours (Fig. 16d). This was quantified by calculating the colocalization coefficient of mCherry and GFP positive cells, which displayed an increase after TDP-43 expression in BPs (Fig. 16f). The increased number of mCherry^{+} cells suggests an enhancing effect of TDP-43 on the NeuroD1 promoter and an increased proliferation of TDP-43 expressing BP cells. However, BPs expressing exogenous TDP-43 did not die.

Cell survival is not affected by knockdown of TDP-43

TDP-43 interacts with several target mRNAs, one of which is its own mRNA. Binding of TDP-43 protein to a RNA binding region located within the 3' UTR of the *Tardbp* mRNA leads to destabilization and degradation of its own mRNA (Ayala et al., 2010). In order to test whether the apoptotic phenotype we observed following TDP-43 expression might be caused by degradation of the endogenous *Tardbp* mRNA we applied direct knockdown (KD) experiments of the endogenous TDP-43 protein. Therefore, we used an *in vivo* shRNA approach by expressing a shRNA in NSCs from a plasmid vector that specifically targets *Tardbp* mRNA by IUE. To confirm the specific downregulation we first isolated transfected E14.5 embryonic forebrain cells 24 hours post-electroporation. We took advantage of a co-electroporated GFP-reporter plasmid and sorted for GFP^{+} cells by FACS and analysed their mRNA expression levels by qRT-PCR (Fig. 17a). To control for specificity of the TDP-43 shRNA approach an irrelevant shRNA construct was used targeting Renilla luciferase mRNA. We found *Tardbp* mRNA levels decreased down to 30% after hairpin-mediated downregulation *in vivo* compared to control conditions (Fig. 17b).

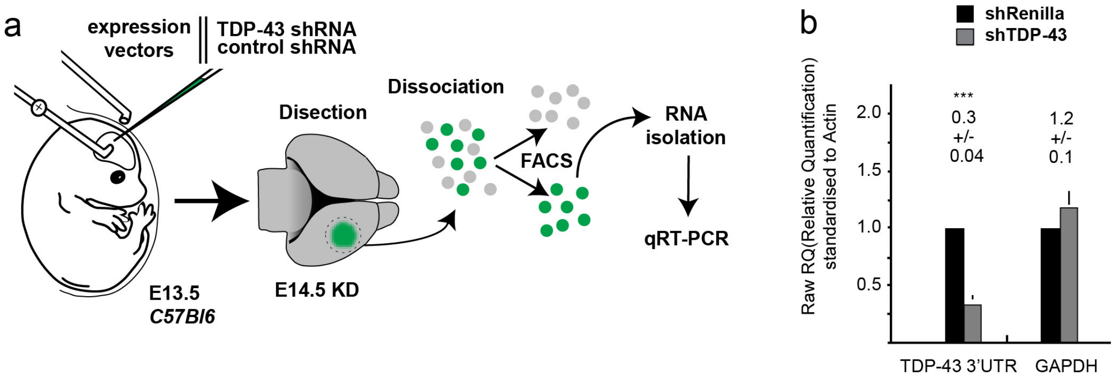

Figure 17: TDP-43 KD does not affect survival of NPs

a. Cartoon of experimental procedure applied to isolate electroporated (green) embryonic day (E) 14.5 (shRNA KD) NPs for qRT-PCR analysis. Wild type embryos were electroporated with TDP-43 shRNA or control (Renilla) shRNA expression vectors. Forebrain cells were isolated and FACSorted for GFP^+ cells after 24 hours. **b.** TDP-43 mRNA levels are reduced down to 30% after expression of TDP-43 shRNA in *in vivo* electroporated neural progenitors (sorted by Flow cytometry). tTest: *P<0.001

To address whether specific cell populations were affected by the downregulation of *Tardbp* mRNA we performed immunohistochemical marker analysis. Importantly, we did not observe an increase in apoptosis in transfected cells 24 hours after IUE and TDP-43 KD. Instead we detected an increase in the number of proliferating cells already 24 hours after downregulation of endogenous *Tardbp,* as shown by an increase in BrdU we observed pulse labelling for 1.5 hours and by increased pH3 staining (Fig. 18a-c). In contrast, the $Pax6^+$ cell population was reduced whereas the $Tbr2^+$ cells exhibited no significant change (Fig. 18a,d,e). These data demonstrate that the cell death we observed in our TDP-43 expression experiments was not due to a downregulation of endogenous *Tardbp* levels and therefore unlikely due to a dominant negative or loss-of-function. Moreover, our shRNA studies provide evidence for a role of TDP-43 in regulating cell proliferation *in vivo.*

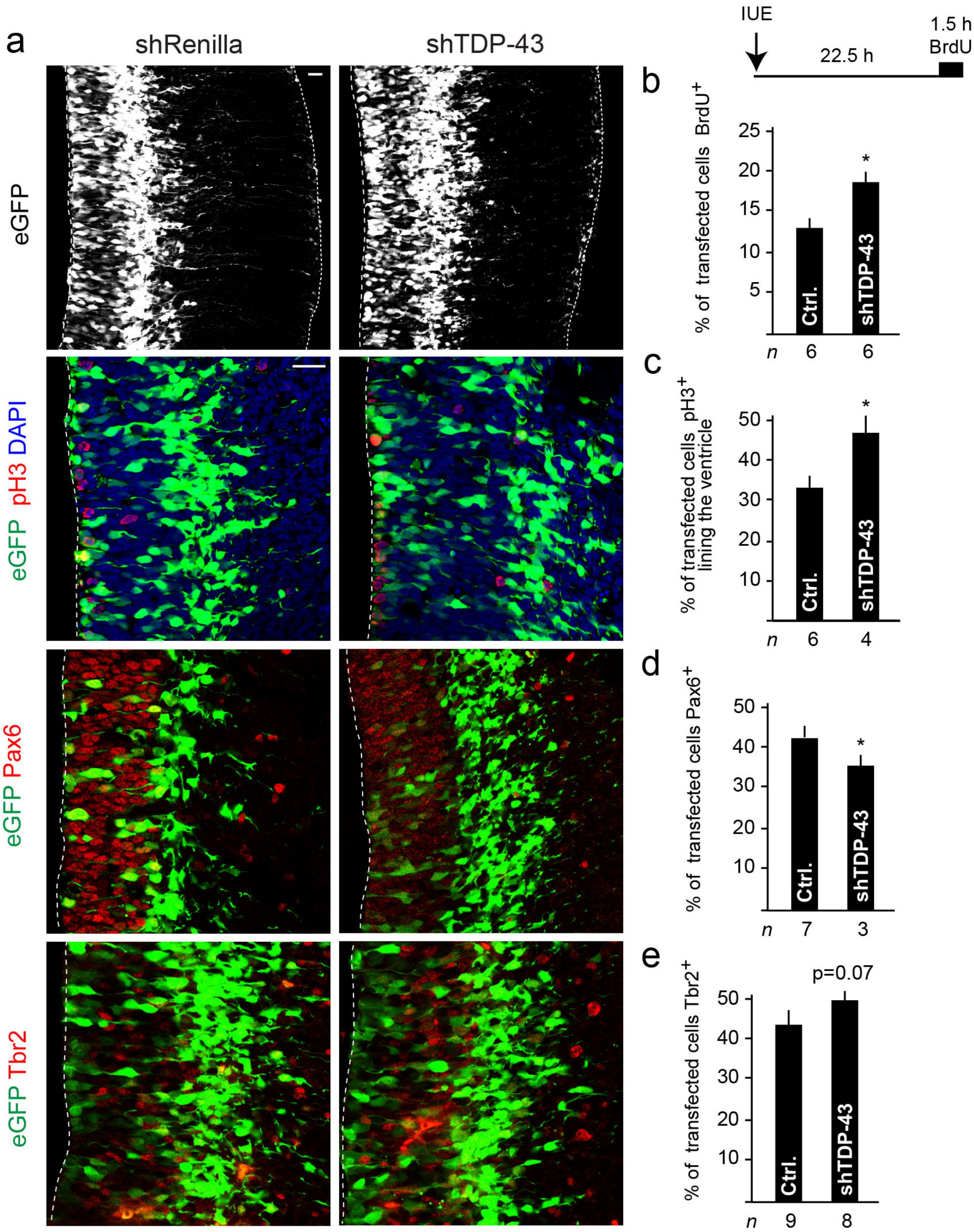

Figure 18: TDP-43 KD does not affect survival but leads to an increase in proliferating cells

a. Embryos immunostained against Pax6, pH3 and Tbr2 24 hours after expression of TDP-43 KD or Renilla KD (control). The number of cells in M- and S-phase are increased after TDP-43 KD. The number of NSCs is decreased whereas BPs is not affected by the reduction of TDP-43. **b.** Quantification of BrdU positive cells in TDP-43 KD and control cells. tTest *P<0.05. Scheme of BrdU labelling procedure of E13.5 embryos with a BrdU pulse 22.5 hours post-electroporation and 1.5 hours prior to sacrifice. **c.** Quantification of pH3 positive cells in TDP-43 KD and control cells. tTest *P<0.05. **d.** Quantification of Pax6 positive cells in TDP-43 KD and control cells. tTest *P<0.05. **e.** Quantification of Tbr2 positive cells in TDP-43 KD and control cells. tTest P=0.07. Dashed line marks the ventricular lining, dotted line marks the basal surface. Scale bars = 20 µm.

6.3.2 TDP-43 induces p53-dependent apoptosis

TDP-43 induced apoptosis in NSCs is p53-dependent

p53 is a central factor of the apoptosis pathway and able to activate various downstream targets (see section 3.6). Although elevated p53 protein levels were reported in ALS patients a causal molecular link to the onset of cell death during progression of the disease is still missing (Martin, 2000; Ranganathan and Bowser, 2010). To investigate whether the onset of apoptosis by NSCs we observed after expression of TDP-43 (Fig 19b,a arrows) and TDP-43$^{(A315T)}$ is dependent on p53 we performed IUE in p53-deficient mice. Interestingly no cell death was detectable in p53$^{-/-}$ and p53$^{+/-}$ embryos 24 hours after expression of TDP-43 and TDP-43$^{(A315T)}$ (Fig. 19a,b).

It should be mentioned here, that apoptosis was not determined by immunostaining against apoptosis markers such as cleaved caspase3, but simply by the observation of cell phenotypic changes such as membrane blebbing, nuclear fragmentation and cell shrinkage. Apototic cells were not quantified after TDP-43 and TDP-43$^{(A315T)}$ expression or after rescue by p53 deletion.

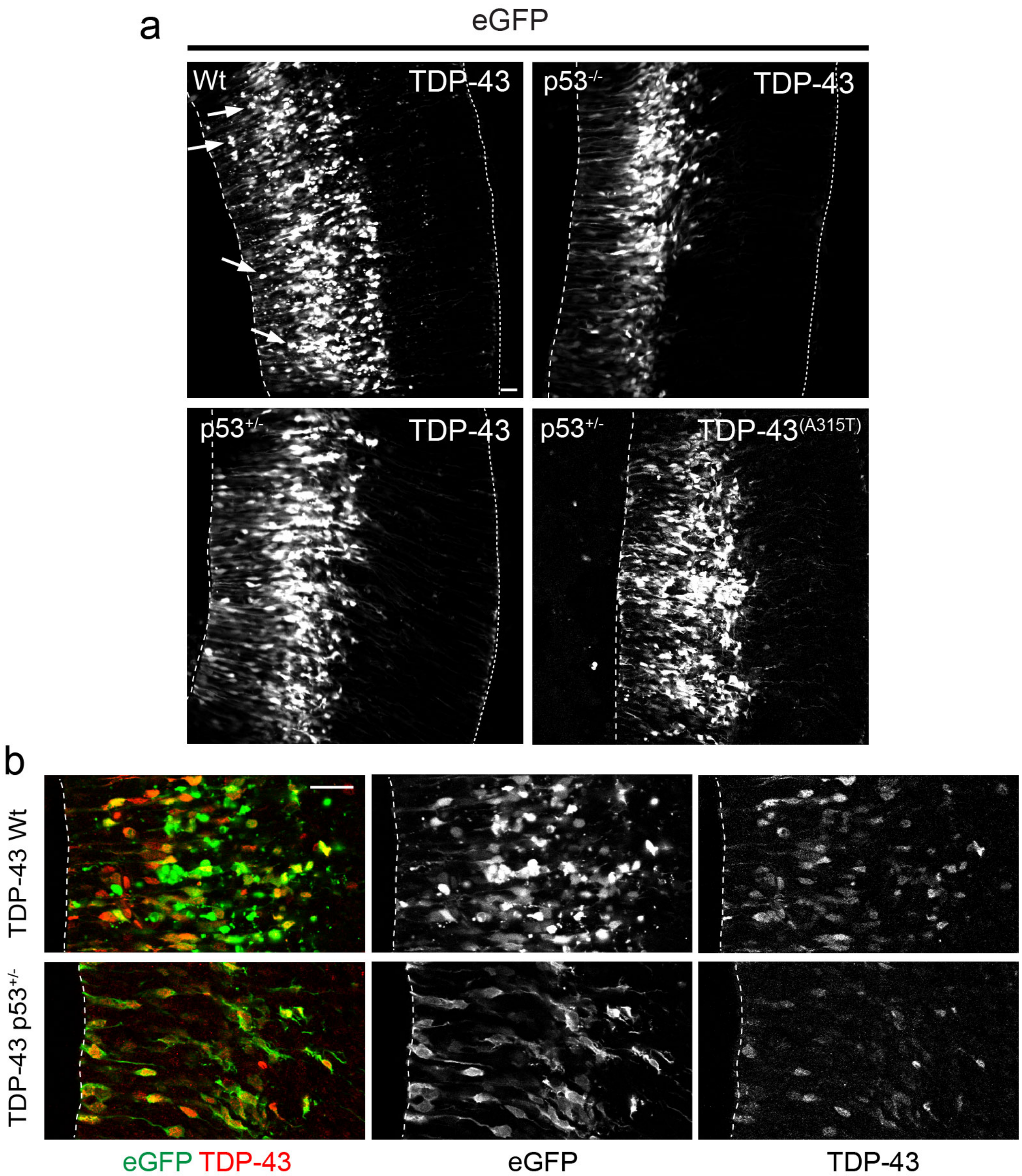

Figure 19: Toxicity mediated by TDP-43 can be rescued by deletion of p53

a. Expression of TDP-43 in wild type embryos induces apoptosis (arrows) of transfected cells (GFP^{+}) whereas expression in $p53^{+/-}$ and $p53^{-/-}$ does not affect cell survival. **b.** TDP-43 staining is present in transfected cells 24 hours after IUE. In wild type embryos this results in apoptosis whereas cell survival in $p53^{-/+}$ is not affected. Dashed line marks the ventricular lining, dotted line marks the apical basal surface. Scale bars = 20 µm.

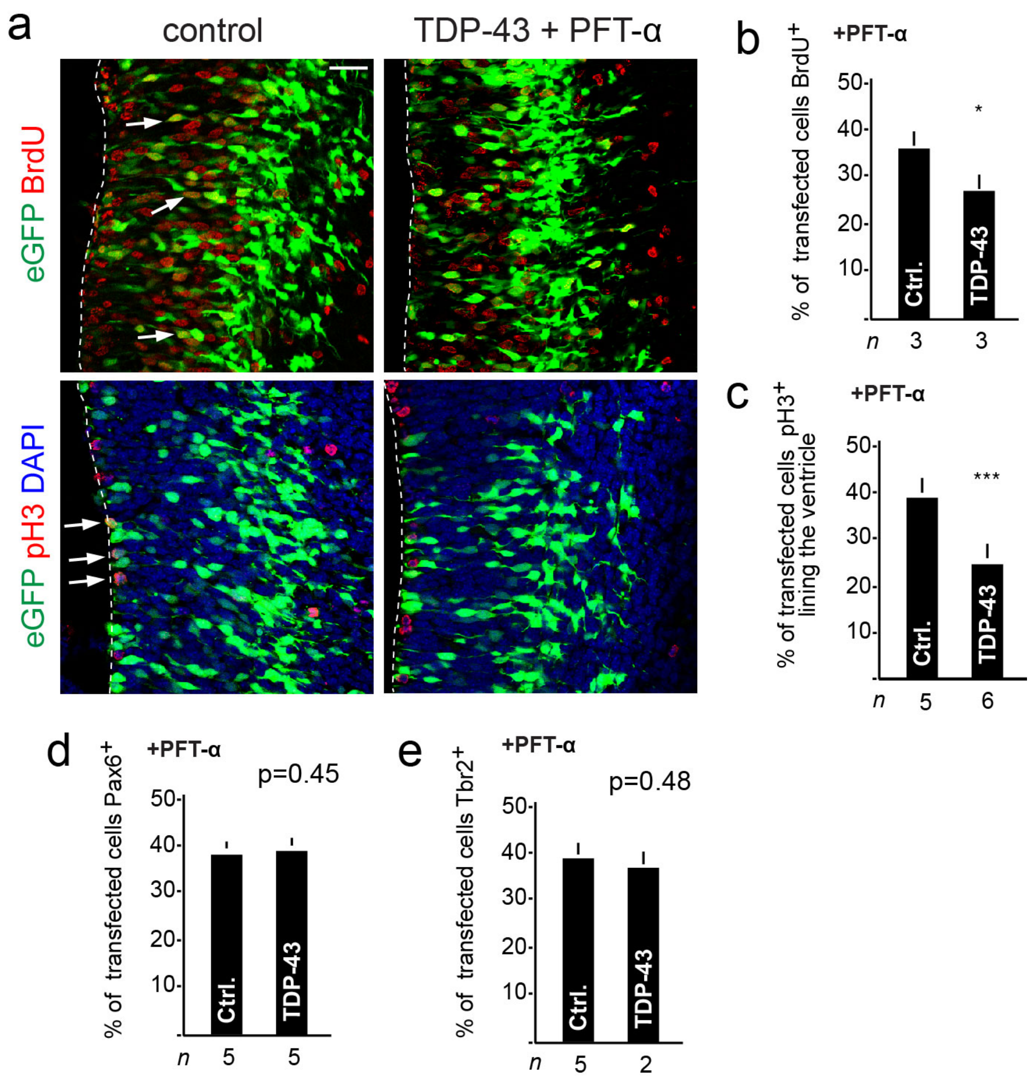

Figure 20: Toxicity mediated by TDP-43 can be rescued by pharmacological inhibition of p53

a. p53 inhibition by PFT-α *in vivo* into pregnant wild type mice after IUE inhibits apoptosis. Embryos were analysed by staining for BrdU and pH3. TDP-43 transfection led to a decreased number of cells in S- and M-phase. **b.** Quantification of BrdU positive cells expressing TDP-43 or control plasmids. BrdU administration to the mice 3 hours prior analysis. tTest $^{*}P<0.05$. **c.** Quantification of pH3 positive cells expressing TDP-43 or control plasmids. tTest $P<0.45$.**d**. Quantification of Pax6 positive cells expressing TDP-43 or control plasmids. tTest $^{**}P<0.005$. **e.** Quantification of Tbr2 positive cells expressing TDP-43 or control plasmids. tTest $P<0.48$. Dashed line marks the ventricular lining. Scale bars = 20 µm.

In a second approach, we injected the p53-inhibitor PFT-α into pregnant wild type mice directly after IUE and expression of TDP-43 and 8 hours before harvesting the embryos. We again observed a rescue of the TDP-43 induced cell death (Fig. 20), as we did not observe any cellular phenotypic changes in electroporated cells. By investigating in more detail the TDP-43 positive cells after IUE and pharmacological inhibition of p53 we found that the number of NSCs ($Pax6^{+}$) and BPs ($Tbr2^{+}$) were unchanged in p53 inhibition rescued animals (Fig. 20d,e). However, we noticed a reduction of proliferating cells. We performed BrdU pulse labelling experiments and pH3 immunoanalysis to assess changes in proliferation and observed a reduction of $BrdU^+$ cells within the TDP-43 transfected population (monitored by GFP-expression) (Fig. 20a,b arrows). In addition, a decrease of $pH3^+$ cells lining the ventricle was detectable (Fig. 20a,c arrows). Hence, loss of p53 rescued the apoptosis induced by TDP-43 but progenitor proliferation was still affected.

Pharmacological inhibition of p53 rescues hTDP-43$^{(A315T)}$ mice

Several TDP-43 mutant transgenic mice have been generated in the past. These mice develop features of ALS and FTLD and early lethality of the animals (Arnold et al., 2013; Igaz et al., 2011; Iguchi et al., 2013; Tsai et al., 2010; Wegorzewska et al., 2009; Wils et al., 2010; Xu et al., 2010). In our study we used a transgenic TDP-43 animal model in which a mutant form of human TDP-43 carrying the A315T point mutation is inserted via knock-in into exon 1 of the mouse TDP-43 genomic locus (Schebelle et al., 2010). Expression of hTDP-43$^{(A315T)}$ from both alleles resulted in embryonic lethality as no live homozygous mutant mice were born. We analysed the embryos more closely in order to identify the cause and time point of the death of the embryos. Homozygous E6.5 embryos did not display any morphological changes indicating that blastocyst formation and implantation were not affected (Fig. 21a). E9.5 homozygous mutant embryos showed a developmental delay compared to wild type and heterozygous littermates. Many of the homozygous mutant embryos were misformed and pale at the time point of harvesting. However, homozygous hTDP-43$^{(A315T)}$ mice were obtained at a normal mendelian ratio at this point (Fig. 21b). By E12.5 mutant embryos were rare and we did not find mutants after E12.5. Lethality of embryos at E9 is mostly due to heart defects, which we did not investigate further.

In the IUE experiments TDP-43 induced cell death *in vivo* was rescued upon deletion or suppression of p53. To test if the lethality of the hTDP-43$^{(A315T)}$ transgenic embryos is also due to a p53-mediated pathway we pharmacologically inhibited p53 in pregnant hTDP-43$^{(A315T)}$ mice. PFT-α was injected daily into pregnant hTDP-43$^{(A315T)}$ mice from day 5.5 post coitum. We were able to collect homozygous mutant embryos up to E14.5, the last stage analysed, at a normal mendelian ratio (Fig. 21d). The rescued embryos were slightly smaller than their heterozygous or wild type littermates but apart from that did not show any morphological abnormalities (Fig. 21c).

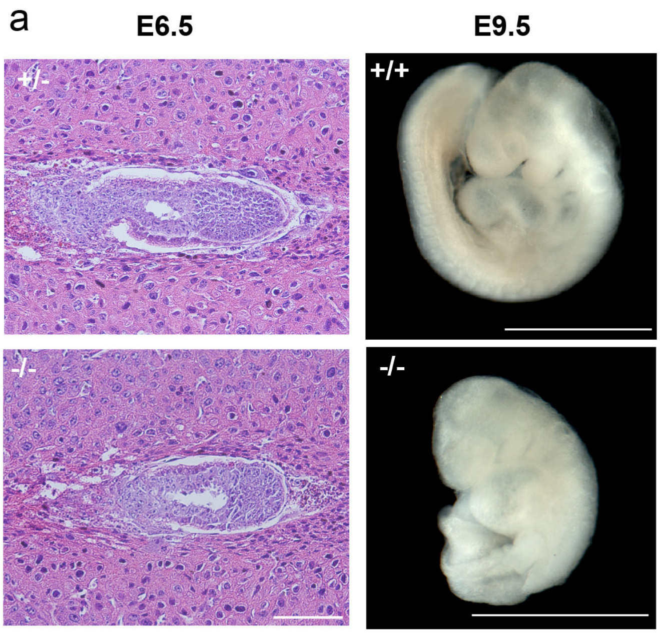

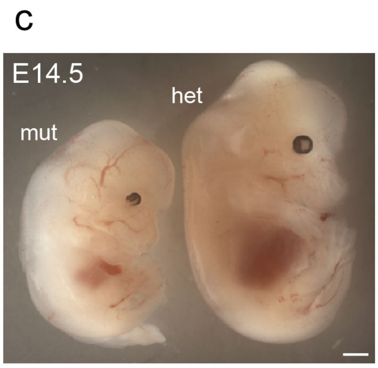

d + PFT-α

	E12.5	E13.5	E14.5
mutant	6 (2)	1	6
het / WT	18 (38)	4	31

b

	E6.5	E9.5
mutant	1	6
het / WT	3	16

Figure 21: Pharmacological inhibition of p53 rescues hTDP-43$^{(A315T)}$ mice

a. Implantation of hTDP-43$^{(A315T)}$ homozygous embryos is normal whereas E9.5 embryos display severe developmental defects. **b.** Table displaying the proportion of mutant vs. het/WT offspring at E6.5 and E9.5 **c**. PFT-α injection of pregnant hTDP-43$^{(A315T)}$ rescues survival of mutant embryos until E14.5. Mutant embryos are significantly smaller than heterozygous littermates. **d.** Table displaying the proportion of mutant vs. het/WT offspring with (black) and without (red) p53 inhibition. Scale bars in a and c = 1 mm, 200 µm for E6.5.

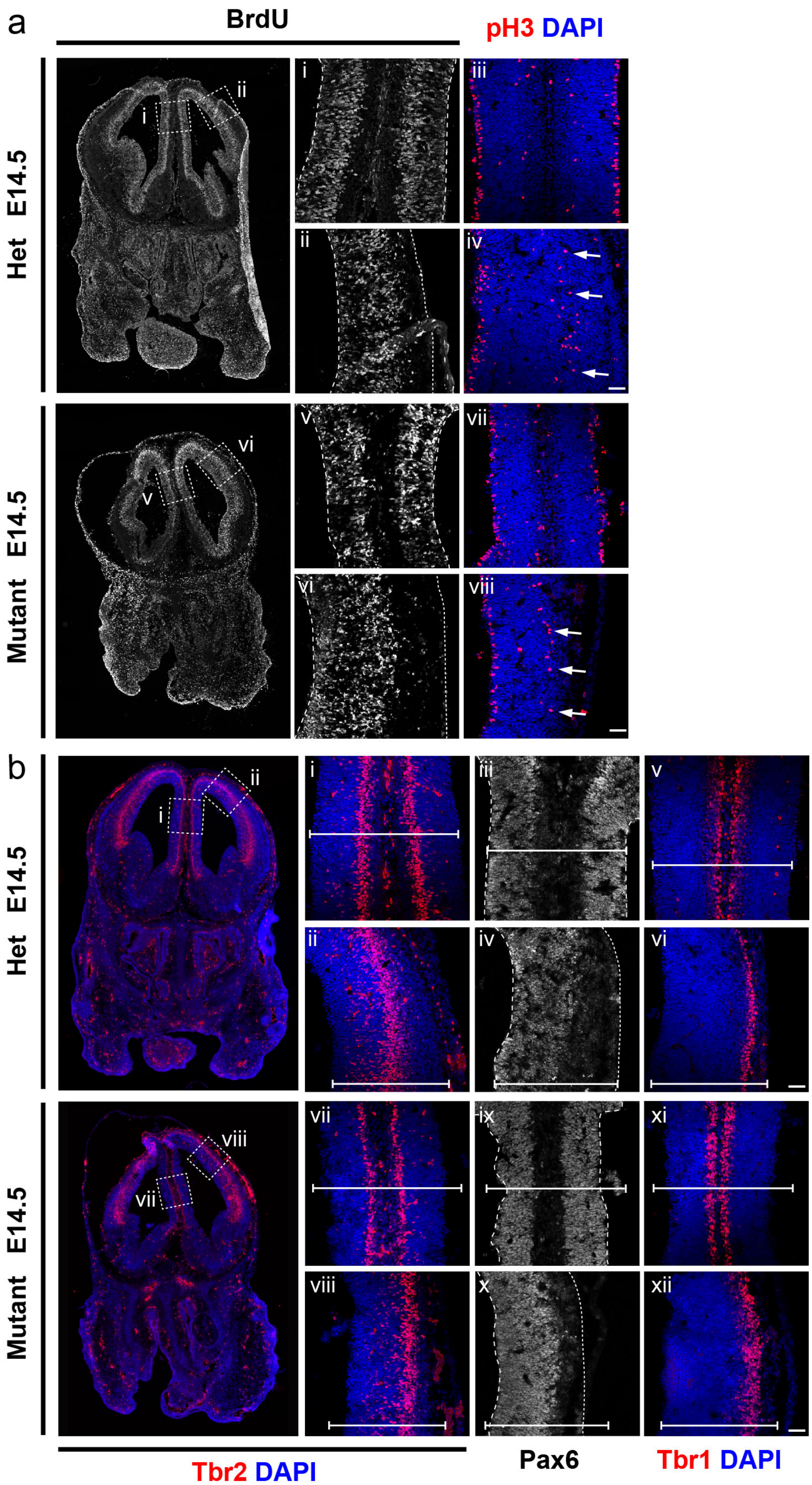

Figure 22: Pharmacological inhibition of p53 rescues hTDP-43$^{(A315T)}$ mice

a,b Immunostainings of hTDP-43$^{(A315T)}$ embryos after PFT-α mediated rescue for BrdU, pH3, Tbr2 and Pax6. No changes in NSCs (Pax6^{+}), BPs (Tbr2^{+}) or neurons (Tbr1^{+}) are visible. Additionally no alterations are detectable in proliferating cells (pH3^{+} and BrdU^{+}). Dashed line marks the ventricular lining, dotted line marks the basal surface. Scale bars = 20 µm.

The brains of the homozygous mutant embryos showed a normal dorsal-ventral and anterior-posterior patterning and all brain regions were present. As our previous expression and knockdown studies of TDP-43 were performed in the forebrain we analysed the telencephalon of the rescued embryos. We therefore performed immunohistochemical analysis of the different cell types present in the telencephalon of E14.5 brains. Pax6^{+} NSCs were present and localized in the VZ and BPs (Tbr2^{+}) and differentiated neurons (Tbr1^{+}) were detected by immunostaining and displayed a normal localization (Fig. 22b). The cerebral cortex of the mutants displayed a regular layering, though the layers of cortex and lateral wall are thinner compared to control littermates (Fig 22b). Most of the NSCs in the mutant VZ were proliferating and had entered S-phase during a 3 hour BrdU pulse as in the control. NSCs in M-phase (pH3^{+}) were localized correctly to the ventricular lining and few proliferating pH3^{+} BPs were detected in the SVZ (Fig. 22a, arrows) of control and homozygous mutant embryos. In addition, no distinct areas of apoptotic or necrotic cells were observed in the telencephalon of the rescued embryos. Thus, the rescued hTDP-43$^{(A315T)}$ embryos do not display any defects except for the growth retardation.

6.3.3 TDP-43 regulates cell cycle progression through binding to *Cdkn1a* mRNA

TDP-43 expression results in cell cycle arrest of N2A cells in G_2- and S-phase

In *in vivo* experiments we observed alterations in the number of cells going through M- and S-phase after KD and expression of TDP-43. We investigated the effect of TDP-43 on cell cycle regulation. There are two cell cycle checkpoints ensuring proper progression through cell cycle. One checkpoint is located at the end of G_1-phase, deciding whether cells are ready to divide and to progress into S-phase. The second checkpoint is at the end of G_2-phase and ensures that the genome has doubled properly and that the cell is ready for mitosis (Jung et al., 2010; Woo and Poon, 2003). Both checkpoints are regulated by p21, which is a direct target of p53. Upon phosphorylation and stabilization of p53, the p53 protein translocates to the nucleus where it acts as a transcription factor and activates the p21 gene among others (Fig. 10). Because of the link of p21 to p53 and the important function of p21 during cell cycle progression we included p21 in our further studies on cell cycle regulation by TDP-43.

To investigate the cell cycle phenotype we used a neural progenitor cell line N2A and expressed TDP-43, TDP-43$^{(A315T)}$ or p21. The transfection efficiency of N2A cells was high (~95%), still we made use of a GFP expression plasmid to identify the transfected cells. 24 hours post-transfection the cells were fixed and analysed for their cell cycle status. N2A cells express TDP-43 endogenously (Fig. 26d) and an increased TDP-43 protein level or expression of TDP-43$^{(A315T)}$ resulted in a modest number of apoptotic cells, determined by morphological changes (Fig. 23a,c and Fig 24a arrows). Similarly, expression of p21 induced cell death in a few cells comparable to the number of apoptotic cells after expression of TDP-43, TDP-43$^{(A315T)}$ and showed a significant increase over control transfected cells (Fig. 23c). However, the total number of apoptotic cells was very low, allowing for further analysis of the transfected cells.

To analyse cells in S-phase, EdU was added to the medium 1 hour prior to fixation and staining of the cells. Within this hour about 33% of control transfected cells had gone through S-phase and intercalated EdU in the newly synthesised DNA strands (Fig. 23a,b empty arrowhead). This number was strongly reduced by expression of TDP-43 and TDP-43$^{(A315T)}$, indicating that less cells had entered S-phase. As expected, expression of p21 in N2A cells completely blocked cells from progressing into S-phase. Only non-transfected (GFP$^-$) cells displayed an EdU staining under these conditions (Fig. 23a filled arrows).

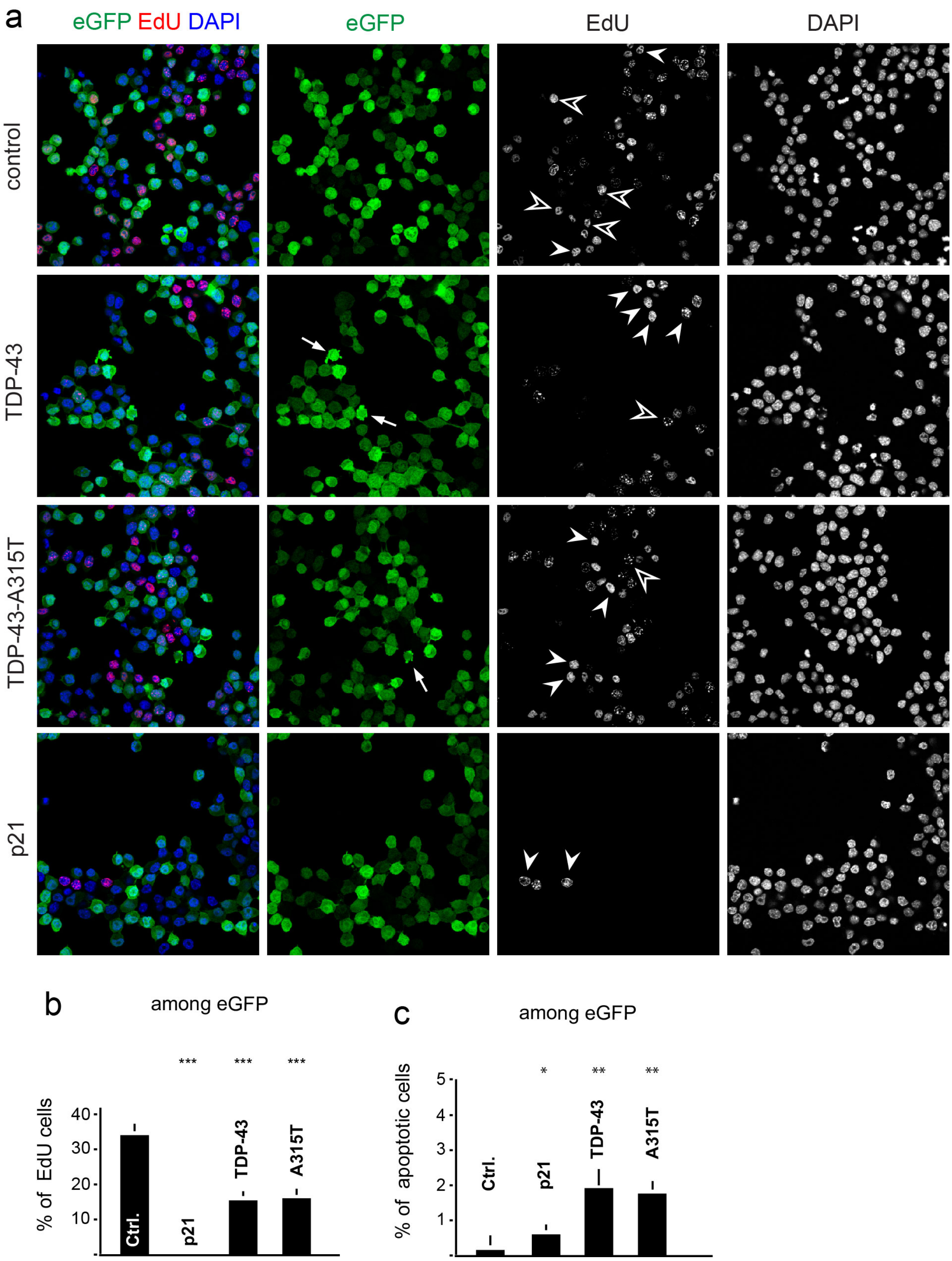

Figure 23: Expression of TDP-43 and TDP-43$^{(A315T)}$ in N2A cells decrease the number of cells in S-phase

a. Immunostaining of N2A cells 24 hours after TDP-43 and TDP-43$^{(A315T)}$ for EdU displays a reduced number of transfected cells in S-phase (empty arrowheads) following a 1 hour EdU pulse. Most EdU^{+} cells under these conditions are untransfected (GFP^{-}) (filled arrows). Expression of TDP-43 and TDP-43$^{(A315T)}$ induces apoptosis in some cells (arrows). **b.** Quantification of EdU^{+} cells after expression of p21, TDP-43, TDP-43$^{(A315T)}$ and control plasmids. tTest ***P=0.001 **c.** Quantification of apoptotic cells after expression of p21, TDP-43, TDP-43$^{(A315T)}$ and control plasmids. tTest *P=0.05 and tTest **P=0.005.

In IUE experiments we found that the number of cells labelled with pH3 was decreased following TDP-43 expression and increased after *Tardbp* KD. Phosphorylation of Histone 3 increases already in late-replicating/early-condensing heterochromatin and can therefore be detected as a dotty staining in cells in G_2-phase. To check whether entry into M-phase was affected after TDP-43 expression we analysed cells for pH3 more closely by distinguishing those cells with a dotty (G_2-phase) and a more homogeneously stained nucleus (M-phase). Cells were considered as having a dotty staining, as long as single dots could clearly be identified in the stained nucleus. In control conditions about 5% of the cells were in M-phase (Fig. 24a filled arrowheads and 24c) and 10% in G_2-phase (Fig. 24a empty arrowheads and 24b). After expression of TDP-43 and TDP-43$^{(A315T)}$ double the amount of cells was in G_2 whereas nearly no cells with a fully stained nucleus were present 24 hours after transfection. We conclude that expression of TDP-43 as well as the TDP-43$^{(A315T)}$ point mutant arrests cells in late G_2. Similarly, p21 expression resulted in a reduction of cells in M-phase but in addition also cells in G_2-phase were completely lost as increased p21 levels block cells in G_1-phase.

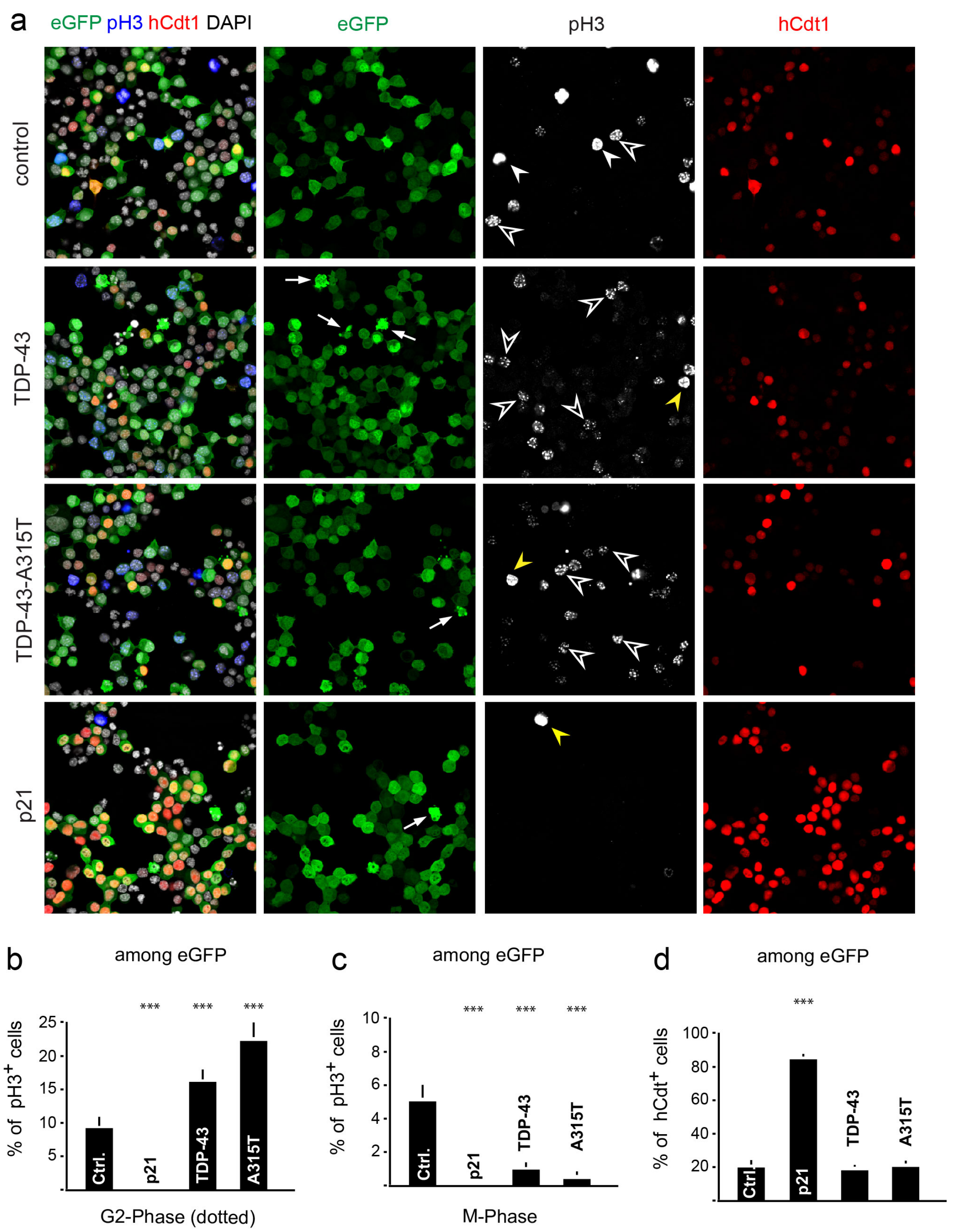

Figure 24: Expression of TDP-43 and TDP-43$^{(A315T)}$ in N2A cells arrests cells in G_2-phase

a. Immunostaining of N2A cells 24 hours after TDP-43 and TDP-43$^{(A315T)}$ results in reduced number of transfected (GFP$^+$) cells in M-phase, labelled with anti-pH3 antibody (complete staining of the nucleus; filled arrowheads). In contrast transfected (GFP$^+$) cells in G_2-phase are increased (dotty pH3 staining of the nucleus; empty arrows). Expression of TDP-43 and TDP-43$^{(A315T)}$ induces apoptosis in some cells (arrows). Number of cells in G_0/G_1 reflected by hCdt1-KO2 expression are not altered after TDP-43 and TDP-43$^{(A315T)}$ expression. **b.** Quantification of pH3$^+$ cells in G_2-phase after expression of p21, TDP-43, TDP-43$^{(A315T)}$ and control plasmids. tTest ***P=0.001 **c.** Quantification of pH3$^+$ cells in M-phase after expression of p21, TDP-43, TDP-43$^{(A315T)}$ and control plasmids. tTest ***P=0.001 **d.** Quantification of hCdt1$^+$ cells after expression of p21, TDP-43, TDP-43$^{(A315T)}$ and control plasmids. tTest ***P=0.001 P=0.45 and tTest P=0.28.

In order to check for cells in G_1-phase we stably transfected N2A cells with the hCdt1-KO2 plasmid (Sakaue-Sawano et al., 2008). Cdt1 is expressed in cells in G_0/G_1-phase and the protein is gradually degraded as the cell continues to cycle into S-phase. The hCdt1-KO2 plasmid expresses a fragment of the human Cdt1 protein fused to the fluorescent protein Kusabira Orange. Therefore, the stably transfected N2A cells express Kusabira Orange in G_0/G_1-phase of the cell cycle. Quantifying the Kusabira Orange-positive cells after expression of TDP-43 or TDP-43$^{(A315T)}$ we could not detect a change in cell numbers compared to control (Fig. 24a,d). The expression level of the hCdt1-KO2 varies heavily and for the quantifications only cells with a strong Kusabira Orange expression were included in order to avoid implication of negative cells. The hCdt1-KO2 construct is expressed reliably in G_0/G_1-phase, as we found all GFP$^+$ cells arrested in G_1 after expression of p21 (Fig. 24a,d). Only non-transfected (GFP$^-$) cells displayed a pH3 staining and were hCdt1$^-$ (Fig. 24a yellow arrowhead).

RNA binding ability of TDP-43 is crucial in mediating apoptosis

The mechanism through which TDP-43 induces apoptosis and alters cell cycle is unclear and in order to define which part of the TDP-43 protein is functionally important in inducing the observed effects we employed a TDP-43 mutant where the RNA recognition motive 1 (RRM1) had been deleted (Fig. 25a). TDP-43 was recently shown to regulate not only his own but also other mRNAs (Ayala et al., 2010; Polymenidou et al., 2011; Tollervey et al., 2011). The RRM1 is necessary and sufficient to mediate binding of TDP-43 to RNA and we therefore deleted this domain in order to investigate the importance of the RNA binding ability of the protein. We performed IUE and expressed TDP-43-ΔRRM1 *in vivo*. TDP-43-ΔRRM1 expression did not induce apoptosis of electroporated cells within 24 hours (Fig. 25b). We did not observe significant changes in the numbers of NSCs (Pax6$^+$) or basal progenitors (Tbr2$^+$) (Fig. 25c-e). This suggests that the RNA binding ability of the protein is crucial to induce apoptosis and observed changes in neuron numbers. These data also support that the mutant TDP-43 has a gain or amorphic rather than loss-of-function.

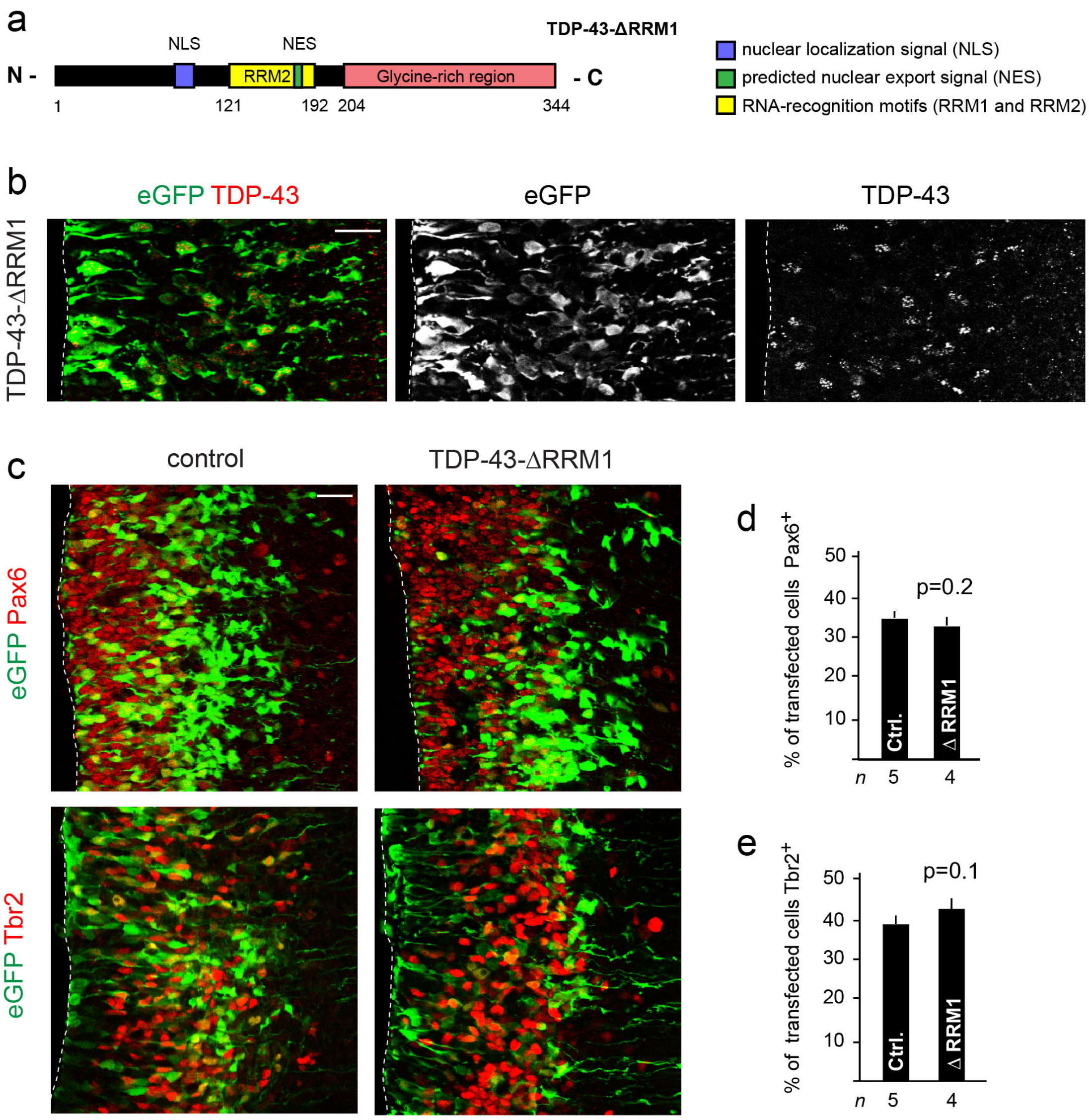

Figure 25: Toxic effect of TDP-43 is dependent on the binding to RNA

a. Scheme of TDP-43-ΔRRM1. The corresponding cDNA was cloned into the pCAGGS expression vector. **b.** Expression of TDP-43-ΔRRM1 does not result in apoptosis. **c.** Embryos immunostained against Pax6 and Tbr2 24 hours after expression of TDP-ΔRRM1 or control. Localization and number of BPs ($Tbr2^+$) and NSCs ($Pax6^+$) are not changed 24 h post-electroporation. **d.** Quantification of Pax6 positive cells expressing TDP-43-ΔRRM1 or control plasmid. tTest P=0.2. **e.** Quantification of Tbr2 positive cells expressing TDP-43-ΔRRM1 or control plasmid. tTest P=0.1. Dashed line marks the ventricular lining. Scale bars = 20 µm.

TDP-43 binds and regulates *Cdkn1a* mRNA

TDP-43 and TDP-43$^{(A315T)}$ expression induced apoptosis *in vivo* and blocked cells from progressing into S- and M-phase of the cell cycle. Increased p21 levels similarly cause cell cycle arrest at which activated p53 can induce *Cdkn1a* transcription. Many RBPs bind *Cdkn1a* mRNA, regulate its stability and thereby affect p21 protein levels (Jung et al., 2010). TDP-43 is an RBP reported to bind and regulate several RNAs, therefore, we tested if

TDP-43 binds *Cdkn1a* specifically. We performed crosslinked RNA immunoprecipitation (CLIP) experiments in N2A cells after expression of a flag-tagged TDP-43 protein or flag-tagged GFP as a control. 48 hours after transfection cells were crosslinked with PFA and CLIP performed with beads coupled to anti-flag antibodies. After pull-down of the proteins, reverse cross-link and purification of the pulled-down RNA, the bound RNAs were reverse transcribed into cDNA and analysed by qRT-PCR. qRT-PCR values of the CLIPed products were corrected relative to the input RNA concentration of each condition and primers specific for *Cdkn1a, Tardbp* (positive control) and *β-actin* (negative control) were used. TDP-43 bound to *Cdkn1a* as well as *Tardbp* mRNA (Fig. 26a,b), showing that TDP-43 does indeed bind its own mRNA, but also *Cdkn1a. β-actin* levels were not pulled down with TDP-43.

In order to investigate how binding of TDP-43 affects *Cdkn1a* mRNA levels and vice versa we performed qRT-PCR analysis *in vitro*. N2A cells were transfected with expression plasmids (TDP-43, TDP-43$^{(A315T)}$, p21 or control) and the cells harvested 24 hours post-transfection. Total RNA was isolated and reverse transcribed into cDNA. TDP-43 and TDP-43$^{(A315T)}$ expression resulted in downregulation of *Tardbp* mRNA levels as has already been demonstrated (Ayala et al., 2010; Polymenidou et al., 2011; Sephton et al., 2010a; Tollervey et al., 2011). Additionally, *Tardbp* was decreased after p21 expression which also translated into reduced TDP-43 protein levels (Fig. 26c,d). Next we analysed *Cdkn1a* mRNA levels and detected an increase in *Cdkn1a* transcripts following expression of TDP-43 and TDP-43$^{(A315T)}$ (Fig. 26c) and p21 itself. It was not possible to test if the changes on the mRNA level were translated into increased p21 protein because endogenous p21 was expressed at very low levels in N2A cells. This made it difficult to detect the protein per se or quantify changes at protein level. Binding of TDP-43 and TDP-43$^{(A315T)}$ to *Cdkn1a* mRNA resulted in an increase in p21 transcript levels. In contrast, p21 downregulated *Tardbp* and also *Cdkn1a* levels. In addition, we identified a negative feedback loop for p21 which regulates its own transcript levels.

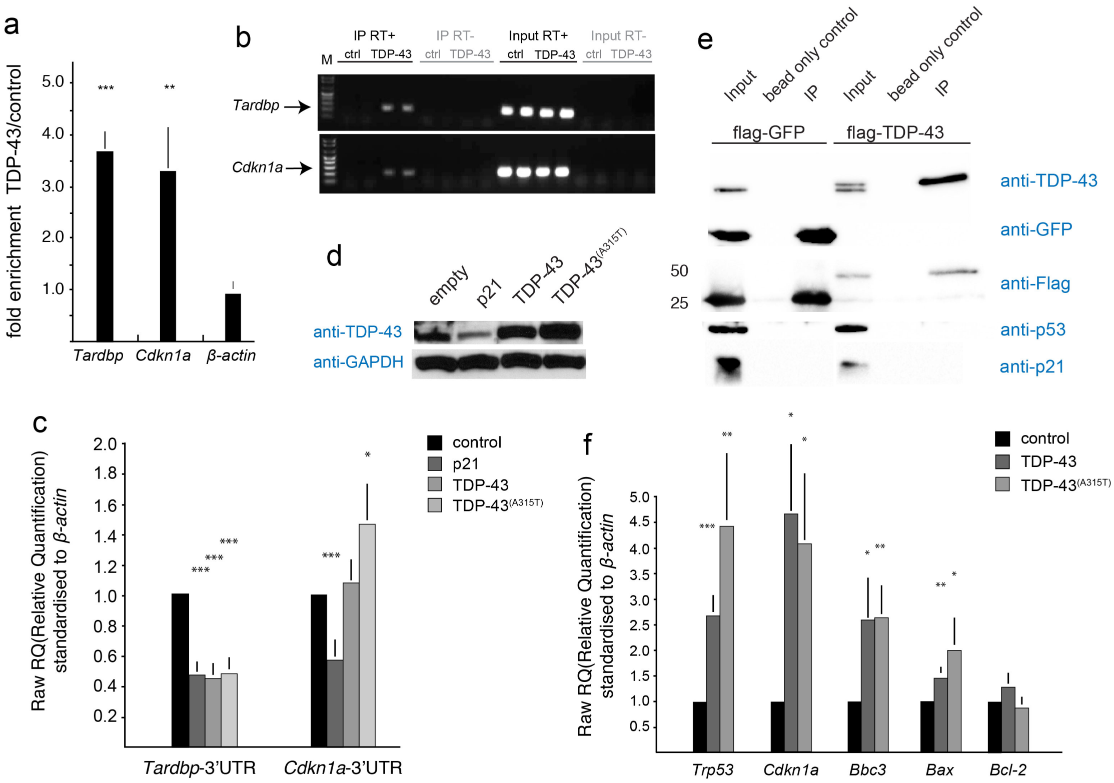

Figure 26: TDP-43 binds p21 mRNA

a. Quantitative qRT-PCR analysis of *Tardbp, p21* and *β-actin* transcripts CLIPed from N2A cells transfected with flag-TDP-43. Values are fold enrichment over control CLIPed (flag-GFP) transcripts. Statistical analysis of CLIPed products corrected relative to input RNA concentrations compared to flag-GFP CLIPed samples. **b.** Gel analysis of amplicons for TDP-43 and p21 after CLIP with TDP-43. Flag-tagged GFP was CLIPed as a control. The agarose gels are representative experiments performed in duplicate (2 lanes per CLIP). CLIP RT+ shows amplification of precipitated TDP-43 and p21 RNAs. CLIP RT- and Input RT+ are controls for RNA amplification and absence of genomic DNA contamination. **c.** qRT-PCR analysis of N2A cells transfected with control, p21, TDP-43 or TDP-43$^{(A315T)}$. Expression of p21, TDP-43 and TDP-43$^{(A315T)}$ results in decrease of *Tardbp* mRNA. *Cdkn1a* mRNA is downregulated by p21 whereas TDP-43 and TDP-43$^{(A315T)}$ results in an upregulation of *Cdkn1a*. **d.** Expression of p21 downregulates TDP-43 protein levels in N2A cells. **e.** IP of flag-tagged TDP-43 and GFP demonstrates no protein interaction between TDP-43 and p21 or p53. **f.** qRT-PCR analysis of NSCs expressing control, TDP-43 or TDP-43$^{(A315T)}$. Expression of TDP-43 and TDP-43$^{(A315T)}$ results in an increase of *Trp53*, *Cdkn1a, Bbc3* and *Bax* levels, whereas *Bcl-2* levels are slightly decreased. tTest *P<0.05, **P<0.01 and ***P<0.001

Addressing if TDP-43 also interacts with p21 or p53 on protein level we performed immunoprecipitation experiments. Therefore, flag-tagged TDP-43 and flag-tagged GFP as a control, were expressed in N2A cells for 30 hours. The cells were then lysed and the proteins separated on an SDS-page and transferred to a membrane. Blotting of the membrane with anti-TDP-43 antibody we detected the endogenous and exogenous protein in the Input lane of cells transfected with flag-tagged TDP-43, whereas only the endogenous protein was present in the Input of flag-GFP transfected cells (Fig. 26e). In addition, we detected a prominent band for flag-tagged TDP-43 after IP of flag-tagged TDP-43 (IP lane). We were able to pull-down the two flag-tagged proteins using beads coupled to anti-flag antibody, whereas no GFP, TDP-43 or Flag-protein was detected in the bead-only control. We analysed the pulled-down proteins using anti-p53 antibody but did not detect p53 in the IP lane of neither flag-GFP nor flag-TDP-43. Thus, we were not able to show an interaction between TDP-43 and p53 at the protein level. We could also not detect an interaction between p21 and TDP-43 or GFP proteins.

Exogenous expression of TDP-43 and TDP-43$^{(A315T)}$ results in apoptosis *in vivo,* a phenotype that can be rescued by inhibition of p53. Therefore, we addressed whether p53 levels are changed upon TDP-43 and TDP-43$^{(A315T)}$ expression in primary NSCs. In order to test the effects of TDP-43 and TDP-43$^{(A315T)}$ on p53 and downstream factors of the apoptosis pathway in NSCs cultured as neurospheres TDP-43 and TDP-43$^{(A315T)}$ were expressed in NSCs using retroviruses, which resulted in a stable integration and expression of genes including an IRES Tomato reporter in the actively proliferating cells. Embryonic neurospheres were infected with pMI-TDP-43-Tomato, pMI-TDP-43$^{(A315T)}$-Tomato or pMI-Tomato (control) and the unsorted cells were analysed 4 days after infection. Expression of TDP-43 and TDP-43$^{(A315T)}$ did not affect survival of the NSCs most probably due to the high concentration of growth factors present in the neurosphere medium (see method section 5.4.4). The RNA of the infected NSCs was isolated and analysed by qRT-PCR. We found *Trp53* and *Cdkn1a* to be upregulated after TDP-43 and TDP-43$^{(A315T)}$ expression compared to controls (Fig. 26f). We also observed an increase in *Bbc3* and *Bax* levels though not as pronounced. *Bcl-2* levels were not significantly changed following TDP-43 and TDP-43$^{(A315T)}$ expression. Hence, expression of TDP-43 and TDP-43$^{(A315T)}$ in NSCs *in vitro* results in an increase of *Trp53* and also affects downstream factors of the apoptosis pathway such as the direct p53 target *Cdkn1a*.

Expression of p21 does not induce apoptosis *in vivo*

We have demonstrated a binding of TDP-43 to *Cdkn1a* mRNA, which results in upregulation of the transcript. In addition, expression of TDP-43 resulted in apoptosis of transfected cells *in vivo*. In order to test if TDP-43 triggers cell death through increased p21 levels, we expressed p21 by IUE *in* *vivo*. 24 hours post-electroporation no apoptotic cells were detected following p21 expression (Fig. 27a) and BP ($Tbr2^+$) numbers were unchanged (Fig. 27d) . However, as expected p21 expression arrested cell cycle and actively proliferating cells were completely lost. All transfected cells were $pH3^-$ and after a BrdU pulse for 2 hours only 2% of the cells had passed through S-phase (Fig. 27a-c arrows). Thus, increased p21 protein levels induced cell cycle arrest which may also be part of the TDP-43 induced phenotype, but did not trigger apoptosis *in vivo*.

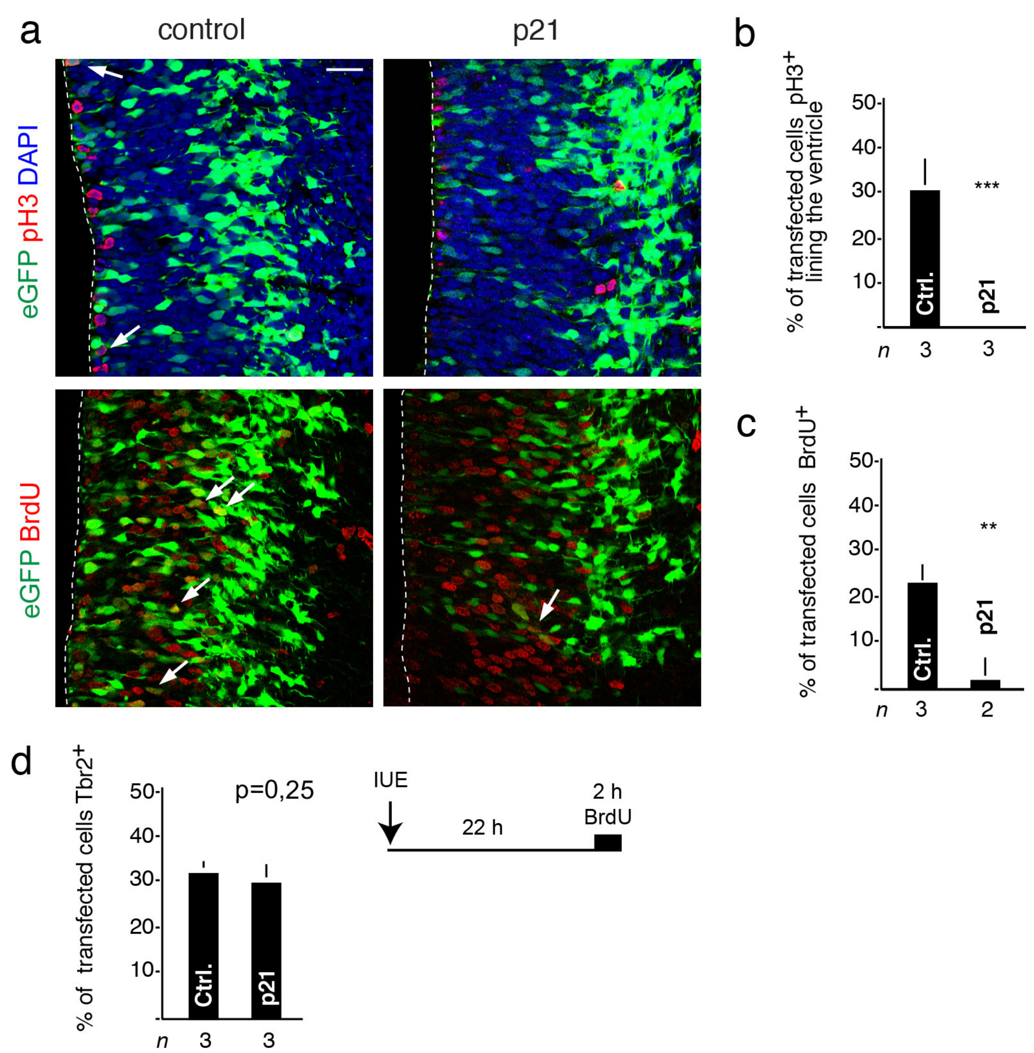

Figure 27: p21 expression *in vivo* does not induce apoptosis

a. Immunostaining of electroporated embryos 24 hours after expression of p21 or control plasmids. Embryos were stained against pH3 and BrdU. Following p21 expression the number of proliferating cells is strongly reduced (arrows). **b.** Quantification of pH3 positive cells expressing p21 or control plasmids. tTest ***P<0.001. **c.** Quantification of BrdU positive cells expressing p21 or control plasmids. Scheme of BrdU labelling procedure of E13.5 embryos with a BrdU pulse 22 hours post-electroporation and 2 hours prior to sacrifice. tTest **P<0.01. **d.** Quantification of Tbr2 positive cells expressing p21 or control plasmids. tTest P<0.25. Dashed line marks the ventricular lining. Scale bars = 20 µm.

7 Discussion

Since the last century a growing number of people develop neurodegenerative diseases mostly due to the higher life expectancy of humans. These primarily late onset diseases can occur sporadic or due to an inherited mutation. A large number of mutated genes has been identified in the last years and provided more insight into the pathogenesis of these disorders. Still, the high heterogeneity of neurodegenerative diseases makes it difficult to understand the mechanism causing the neuron loss. In ALS patients for instance, more than 9 different genetic mutations have been linked to disease onset. One of the mutated genes is *Tardbp,* but it is not known how the point mutations affect the function of the TDP-43 protein or how TDP-43 mutations cause disease. Furthermore the cytoplasmic inclusions residing in affected neurons of ALS, Alzheimer's disease and FTLD patients are partially composed of TDP-43. Neither the cause of the inclusions nor their effect on the cells are clear.

Notch signalling is an important pathway in several developmental processes including brain development. Notch plays a key role in the maintenance and fate of NSCs. By performing a microarray analysis we identified several novel targets regulated upon Notch1 deletion. One of the genes affected was *Tardbp*, which we found to be upregulated following Notch1 ablation. Because of the particular interest of the protein and the link to NSC regulation we sought to study the function of TDP-43 in NSCs.

To analyse the expression of TDP-43 we performed ISH and found *Tardbp* present at high levels in progenitor cells of the midbrain, telencephalon and spinal cord in E11.5 embryos. This coincides with the *Tardbp* expression pattern published by Sephton et al. where TDP-43 was knocked-out using a gene trap which carried a β-galactosidase reporter gene (Sephton et al., 2010b). The group reported *Tardbp* expression in progenitor cells of the midbrain, hindbrain, telencephalon and spinal cord at embryonic stages. In addition, they detected a decrease of β-galactosidase expression in postnatal brains. Still, a distinct X-gal staining was observed in the hippocampus, olfactory bulb, neocortex and granule cell layer of the cerebellum of adult animals. This reduced expression of *Tardbp* at postnatal stages coincides with the gradual loss of NSCs after birth. Analysing TDP-43 protein expression we detected a cytoplasmic staining in mitotically active NSCs lining the lateral ventricle. Additionally TDP-43 staining was detected in neuroblasts in the CP and at lower levels in the SVZ.

To address the function of TDP-43 we employed IUE. With this method proteins of interest can be expressed or knocked-down in NSCs of the developing telencephalon. Importantly, IUE transfects the cells that line the ventricles of the brain by default, which at this stage are RGCs, thus targeting NSCs within a wildtype environment. The analysis of the electroporated cells can be performed at any given time point although one has to keep in mind that the transiently transfected DNA will be diluted out with every cell division. In addition, the number of cells are variable implying that quantifications must be performed as percentages of total electroporated cells. Another limitation of the method in our set up is, that we are co-electroporating two expression plasmids in parallel. One plasmid encodes the fluorescent protein GFP to trace the cells and the other plasmid the protein of interest. Thus, it is possible that cells are taking up only one of the two plasmids. In order to ensure, that all GFP^+ cells are expressing the protein of interest the plasmids are used in a ratio of 3:1. However, it is still possible, although very unlikely, that some of the GFP^+ cells are not expressing the second plasmid and vice versa. To address this issue one could perform IUE with plasmids encoding for different fluorescent proteins. One could therefore clearly determine how many of the cells are double or single positive. Alternatively one could express both proteins from the same plasmid, using an internal ribosomal entry site (IRES) to circumvent the problem.

Expression of TDP-43 and TDP-43$^{(A315T)}$ *in vivo* triggered cell death within 24 hours. The persistent surviving cells missed to express the adequate NSC (Pax6) and BP (Tbr2) markers and after 48 hours almost no surviving cells were detected, reflected by a complete loss of $Tbr1^+$ neurons. Selective expression of TDP-43 in BPs did not induce apoptosis even after 48 hours. Instead TDP-43 induced an increase in $Tbr2^+$ and $Tbr1^+$ cells. In addition, immature neurons expressing the proneural gene NeuroD1 were strongly increased. This can be explained by an enhancing effect of TDP-43 on NeuroD1 expression or an increased production of $NeuroD1^+$ cells due to altered proliferation or differentiation. The microarray data coincides with this result as Notch1 deletion induces precocious differentiation and upregulated *Tardbp* levels. Thus, increased TDP-43 levels can be linked to differentiation or proliferation of neural progenitor cells. However, the two opposing findings indicate a cell type specific effect of TDP-43 in NSCs and BPs. While NSCs rapidly underwent apoptosis the expression of TDP-43 in BPs increased the number of differentiated neurons and did not cause cell death. The two cell types are in fact very different concerning their proliferative potential, marker expression, location and cell cycle regulation. The proliferation of NSCs is tightly regulated compared to BPs and a disturbance of the timing might have a severe effect on the survival of these cells. Another possible explanation for the different effects on cell survival are the differing TDP-43 expression levels due to the different promoters used in the experiments.

The apoptosis phenotype following TDP-43 and TDP-43$^{(A315T)}$ expression in NSCs is conflicting with a recent study where a TDP-43-GFP fusion protein was expressed by IUE (Akamatsu et al., 2013). The authors did not observe significant cell death in the analysed animals. We used TDP-43-GFP for IUE and did not detect an effect on cell survival after 48 hours. Thus, the GFP protein must alter TDP-43 function, possibly through disturbance of correct protein folding.

Many groups suggest a connection between the partial clearance of TDP-43 from the nucleus of apoptotic neurons and the onset of cell death. We therefore performed loss-of-function experiments to analyse the effect on NSCs *in vivo*. No cell death was observed 24 hours after *Tardbp* KD. TDP-43 is indispensable for early development (Sephton et al., 2010b), yet at the time point analysed it did not seem to have a crucial function in NSC maintenance. In addition, we can conclude from this experiment that potential loss of endogenous TDP-43 after TDP-43 expression by IUE did not cause the apoptosis phenotype. This would have been a possibility as TDP-43 regulates its own levels by destabilization of the mRNA through binding of the protein to the 3’ UTR. We expressed the coding region of TDP-43 in the electroporated cells, which therefore only allowed for a negative regulation of the endogenous protein and not the transgene, thus circumventing the autoregulatory feedback loop.

Classically apoptosis is induced by various stressors, which eventually results in stabilization of p53 protein through phosphorylation. Phosphorylated p53 will then translocate to the nucleus and activate different downstream factors resulting in cell cycle arrest and cell death (Fig. 28). We therefore tried to rescue the TDP-43 induced apoptosis by inhibition of p53. *In vivo* p53 was either inhibited pharmacologically using PFT-α or by genetic ablation of p53. Both approaches fully rescued the apoptosis phenotype. In addition, the early lethality of hTDP-43$^{(A315T)}$ homozygous mutant mice was rescued by p53 inhibition. Similar rescue experiments were performed more then 10 years ago in hSOD1$^{(G93A)}$ mice. Interestingly p53 deletion did not rescue the early lethality in those animals (Kuntz et al., 2000; Prudlo et al., 2000). Apoptosis and embryonic lethality must have occurred in a p53-independent way possibly through death receptors such as Fas (Mc Guire et al., 2011). This notion is supported by a recent study in which death receptor 6 (DR6) levels were found to be elevated in SOD1$^{(G93A)}$ transgenic mice (Huang et al., 2013). Additionally, treatment with antagonist antibody against DR6 increased motor neuron survival and therefore provided a neuroprotective effect in these animals. In line with this, TDP-43 is not present in cytoplasmic inclusions in ALS cases with SOD1 mutations and TDP-43 is thus not contributing to the pathogenesis (Dormann and Haass, 2011). Presenting an intriguing explanation for why p53 inhibition may not rescue SOD1 induced cell death. One can therefore suggest that neuronal cell death in ALS is induced through different mechanisms, dependent on the mutated genes present. In several of our rescue experiments we made use of the p53 inhibitor PFT-α and it is therefore important to consider how the small molecule inhibits p53 function. The drug is a specific inhibitor of p53 and blocks transcription and activation of the protein (Komarov et al., 1999). PFT-α was shown to rescue apoptosis in rodent models of stroke (Leker et al., 2004), kainate-induced seizures (Culmsee et al., 2001) and Parkinson’s disease (Duan et al., 2002). Although it is not clear how the drug interacts with p53 it is very unlikely that PFT-α affects any other protein or signalling pathway in the cell. In addition we observed the same rescue after genetic ablation of p53 and pharmacological inhibition of p53, and therefore conclude that off-target effects by the drug can be excluded.

Although p53-deletion rescued the apoptosis phenotype, changes in the number of proliferating cells could still be observed. We detected a reduction of cells in M- and S-phase *in vivo* even after p53-inhibition. In line with this proliferative cells were increased after *Tardbp* KD which was also reported in an independent study (Ayala et al., 2008a). Performing *in vitro* experiments we found that cells were blocked in the cell cycle at the end of G_2- and G_1-phase following TDP-43 and TDP-43$^{(A315T)}$ expression. In addition, another study reported G_2/M arrest after expression of TDP-43 *in vitro (Lee et al., 2012)*. However, in this study the effect was partially dependent on p53 and apoptosis could not be rescued by p53-deletion. The contradicting results can be explained by the cell line that was used in those experiments. The group employed HeLa cells for their study, which have an altered cell cycle regulation and might not respond adequately to inhibition of p53.

p21 regulates the transition from G_2- into M-phase and G_1- into S-phase and expression of p21 resulted in a complete block at these two checkpoints *in vitro* and *in vivo*. Similar cell cycle alterations were observed after TDP-43 and TDP-43$^{(A315T)}$ expression (Fig. 28). This was most likely caused by the interaction of TDP-43 and *Cdkn1a*, which we observed by performing CLIP experiments. TDP-43 binds *Cdkn1a* mRNA resulting in an upregulation of p21 mRNA and protein in N2A cells and NSCs. The increase was more pronounced in NSCs than in N2A cells and can be explained by the different cells types used in the experiments. N2A cells are originally derived form a neuroblastoma and have an altered cell cycle regulation due to genetic mutations and adaptations that might have occurred over time in culture. In contrast NSCs are a primary cell line that is only cultured for short time and the cell cycle as well as apoptosis pathway is still unaffected. Elevated p21 levels triggered by TDP-43 and TDP-43$^{(A315T)}$ expression most likely caused cell cycle arrest in our experiments. Sustained growth arrest of cells can trigger apoptosis and for that reason we analysed how expression of p21 affects cell survival. Increased p21 levels *in vivo* did not cause apoptosis within 24 hours and the cell death observed after TDP-43 and TDP-43$^{(A315T)}$ expression must thus be due to a different or additional mechanism. Still, RNA binding ability of TDP-43 seems to be crucial in mediating the apoptosis phenotype since expression of TDP-43-ΔRRM1 did not induce cell death.

However, one has to consider that deletion of the RRM1 might also affect protein folding. The RRM1 comprises 70 amino acids and therefore constitutes a big part of the TDP-43 protein (414 amino acids). Deletion of this domain might, in addition to RNA-binding ability also alter interaction with other proteins. If time allowed one could have rendered the RRM1 non-functional by site-directed mutation and could have more accurately addressed RNA-binding function of TDP-43.

To investigate how TDP-43 and TDP-43$^{(A315T)}$ expression affects the apoptosis pathway, downstream effectors of p53 were analysed. The experiments were performed in primary NSC cultures instead of N2A cells, as the cancer cell line N2A presumably does not reliably represent occurring changes in the p53 pathway. It has not been addressed whether tumor suppressor genes are deleted or mutated in N2A cells, which makes it very difficult to study apoptosis in such a cell line. NSCs can be isolated and cultured as neurospheres and experiments were performed after passaging the cells for 3-4 times, ensuring that the cultured cells are all residing from self-replicating NSCs. After 3-4 passages cells are in culture for 4-5 weeks and most likely have not acquired any sporadic mutations to their genome, which would give them a growth advantage and affect the read-out of the experiment. TDP-43 and TDP-43$^{(A315T)}$ expression in NSCs resulted in upregulation of *Trp53.* In line with this, downstream effectors of p53 such as *Cdkn1a, Bbc3 and Bax* were upregulated*.* Here the strongest increase was observed in *Cdkn1a* levels. This is probably caused by a dual activation of *Cdkn1a* through p53 and TDP-43. *Bbc3,* another direct target of p53 also showed a strong upregulation. Puma is important for p53 function in the cytoplasm as it releases the protein from its binding to Bcl2 proteins at the mitochondrial membrane. Thus, p53 can interact with pro-apoptotic proteins like Bax and trigger permeabilization of the mitochondrial membrane and apoptosis. *Bax* levels were also increased in our study, however, not as strongly as *Bbc3*, probably due to the hierarchy of the signalling cascade. *Bcl-2* transcript levels were not significantly altered in NSCs, yet, we did not analyse the expression levels of other members of the Bcl2 family.

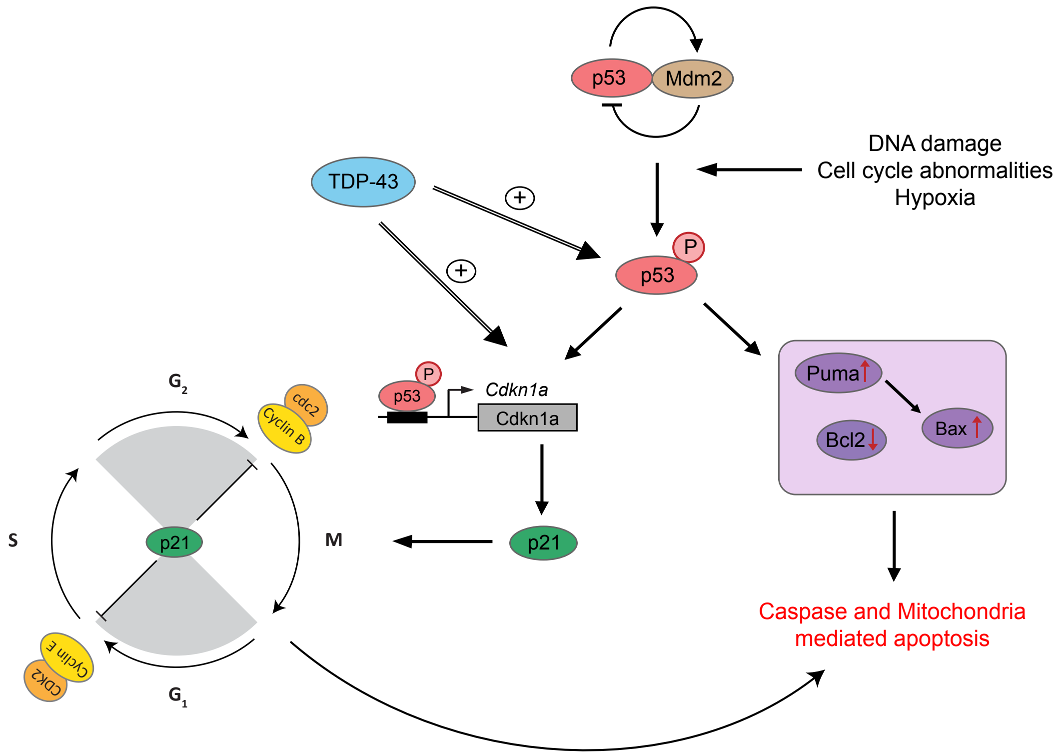

Figure 28. The TDP-43 and FUS proteins TDP-43 interacting with p53 results in an upregulation of *Trp53* and therefore induces apoptosis. Additionally TDP-43 activates *Cdkn1a* transcription resulting in cell cycle arrest, which possibly contributes to apoptosis.

Trp53 transcript levels were upregulated following TDP-43 expression. However, we did not analyse the p53 protein for posttranscriptional modifications or altered levels. Stress signals trigger phosphorylation, ubiquitinylation and acetylation of p53 and it would be interesting to see if these modifications are occurring after TDP-43 expression. Specific posttranslational modifications trigger different effects on target genes. The degree of p53 acetylation for example can be linked to different p53 target genes (Kruse and Gu, 2009). Genes involved in DNA repair and growth arrest are activated by partially acetylated p53 whereas full acetylation is required for activation of pro-apoptotic genes. Thus, analysing the posttranslational modifications of p53 following TDP-43 expression would give more insight into the effects triggered in the cell. Different modifications of p53 may enhance or counteract TDP-43 induced activation in a cell and cortex specific manner. In addition, we need to analyse how TDP-43 interacts with p53. Performing immunoprecipitation experiments we ruled out an interaction of p53 and TDP-43 on protein level. We therefore intend to analyse if TDP-43 interacts with *Trp53* mRNA by performing CLIP experiments in NSCs.

Besides *Cdkn1a* and potentially *Trp53,* additional mRNA targets are bound by TDP-43. CLIP-Seq experiments have been performed to identify the bound transcripts in different cell lines and also in mouse brains and brains from FTLD patients (Buratti et al., 2013). These experiments did not shed light on the role of TDP-43 in disease. Performing a similar experiment in N2A cells or NSC neurospheres is therefore unlikely to bring new insights. It would be interesting though to check the targets identified in the CLIP-Seq experiments for *Trp53* and *Cdkn1a* or other cell cycle regulators and apoptosis factors. However, only the data from Xiao et al. is currently available to us and here *Trp53* and *Cdkn1a* were not included in the list of 127 targets identified to bind to TDP-43 (Xiao et al., 2011).

Performing expression experiments of TDP-43 and TDP-43$^{(A315T)}$ we observed two phenotypes. Firstly an apoptosis phenotype that was rescued upon p53 deletion or inhibition and secondly a cell cycle phenotype that occurred independent of p53. It is not clear if these two mechanisms are connected and if cell cycle arrest is necessary to induce apoptosis. This question could be addressed by expression of TDP-43 and simultaneously knockdown of *Cdkn1a* mRNA. A more challenging approach would be the replacement of the endogenous p21 with a p21 that is lacking the binding domain for TDP-43. Therefore, it would be necessary to determine the protein binding domain in the *Cdkn1a* mRNA, yet most RBPs bind to the 3’ UTR of target transcripts. One could thus simply delete the endogenous p21 and express the coding region of the protein with a synthetic 3’ UTR.

In our study we performed rescue experiments of homozygous mutant hTDP-43$^{(A315T)}$ embryos that normally die at around E9.5. Embryonic death at this time point of development is mostly due to heart or vasculature failures. We did not investigate this further but it is certainly very unlikely that embryonic death is caused by brain defects. In order to investigate the effects of the point mutant TDP-43$^{(A315T)}$ on neuronal cells one could rescue the embryos until a specific time point by PFT-α injection. The treatment could then be stopped and the developing brains analysed thereafter with a special focus on NSCs and neuronal differentiation.

TDP-43 point mutations trigger ALS and the affected motor neurons display cytoplasmic inclusions composed of the protein. It was reported that the point mutations cause a higher stability of the protein compared to the wild type protein. Increased levels of mutated TDP-43 might therefore be present in the nucleus of the cell and we showed in our study that increased levels of TDP-43 and TDP-43$^{(A315T)}$ induce apoptosis. Thus TDP-43 increase could cause a defense mechanism of the cell that is shuttling and storage of the excess protein in the cytoplasm. However, this might not be sufficient and eventually the cell will undergo apoptosis. In neurodegenerative disorders specifically neurons are affected, although the mutated proteins are ubiquitously expressed. Why is it, that pathology selectively targets neuronal subtypes? Neurons are vulnerable cells, due to their long neurites and axons in which cargos such as neurotransmitters, proteins and synaptic vesicle precursors are constantly transported back and forth (Hirokawa et al., 2010). Thus storage of proteins in the cytoplasm might increase the stress level of neurons and have a tremendous effect on the survival of these cells (Roy et al., 2005). However, this issue is still under debate and requires further investigation (Saxena and Caroni, 2011). In our experiments we also observed a cell type specific effect of TDP-43. Whereas survival of BPs was not affected by TDP-43 expression, NSCs rapidly underwent apoptosis. Yet, we were able to rescue these cells by p53 inhibition and it is thus evident to suggest, that p53 inhibition might also rescue affected neurons in ALS patients. First one would of course have to confirm the TDP-43-induced apoptosis and rescue in human cells, preferentially differentiated neurons.

8 References

Aaku-Saraste, E., Hellwig, A., and Huttner, W.B. (1996). Loss of occludin and functional tight junctions, but not ZO-1, during neural tube closure--remodeling of the neuroepithelium prior to neurogenesis. Dev Biol *180*, 664-679.
Akagi, K., Sandig, V., Vooijs, M., Van der Valk, M., Giovannini, M., Strauss, M., and Berns, A. (1997). Cre-mediated somatic site-specific recombination in mice. Nucleic Acids Res *25*, 1766-1773.
Akamatsu, M., Takuma, H., Yamashita, T., Okada, T., Keino-Masu, K., Ishii, K., Kwak, S., Masu, M., and Tamaoka, A. (2013). A unique mouse model for investigating the properties of amyotrophic lateral sclerosis-associated protein TDP-43, by in utero electroporation. Neuroscience research.
Alcamo, E.A., Chirivella, L., Dautzenberg, M., Dobreva, G., Farinas, I., Grosschedl, R., and McConnell, S.K. (2008). Satb2 regulates callosal projection neuron identity in the developing cerebral cortex. Neuron *57*, 364-377.
Alvarado-Mallart, R.M. (1993). Fate and potentialities of the avian mesencephalic/metencephalic neuroepithelium. J Neurobiol *24*, 1341-1355.
Ambros, V. (2004). The functions of animal microRNAs. Nature *431*, 350-355.
Arnold, E.S., Ling, S.C., Huelga, S.C., Lagier-Tourenne, C., Polymenidou, M., Ditsworth, D., Kordasiewicz, H.B., McAlonis-Downes, M., Platoshyn, O., Parone, P.A., *et al.* (2013). ALS-linked TDP-43 mutations produce aberrant RNA splicing and adult-onset motor neuron disease without aggregation or loss of nuclear TDP-43. Proc Natl Acad Sci U S A *110*, E736-745.
Arnold, S.J., Huang, G.J., Cheung, A.F., Era, T., Nishikawa, S., Bikoff, E.K., Molnar, Z., Robertson, E.J., and Groszer, M. (2008). The T-box transcription factor Eomes/Tbr2 regulates neurogenesis in the cortical subventricular zone. Genes Dev *22*, 2479-2484.
Ayala, Y.M., De Conti, L., Avendano-Vazquez, S.E., Dhir, A., Romano, M., D'Ambrogio, A., Tollervey, J., Ule, J., Baralle, M., Buratti, E., *et al.* (2010). TDP-43 regulates its mRNA levels through a negative feedback loop. EMBO J.
Ayala, Y.M., Misteli, T., and Baralle, F.E. (2008a). TDP-43 regulates retinoblastoma protein phosphorylation through the repression of cyclin-dependent kinase 6 expression. Proc Natl Acad Sci U S A *105*, 3785-3789.
Ayala, Y.M., Pagani, F., and Baralle, F.E. (2006). TDP43 depletion rescues aberrant CFTR exon 9 skipping. FEBS Lett *580*, 1339-1344.
Ayala, Y.M., Pantano, S., D'Ambrogio, A., Buratti, E., Brindisi, A., Marchetti, C., Romano, M., and Baralle, F.E. (2005). Human, Drosophila, and C.elegans TDP43: nucleic acid binding properties and splicing regulatory function. J Mol Biol *348*, 575-588.
Ayala, Y.M., Zago, P., D'Ambrogio, A., Xu, Y.F., Petrucelli, L., Buratti, E., and Baralle, F.E. (2008b). Structural determinants of the cellular localization and shuttling of TDP-43. J Cell Sci *121*, 3778-3785.
Azim, E., Jabaudon, D., Fame, R.M., and Macklis, J.D. (2009). SOX6 controls dorsal progenitor identity and interneuron diversity during neocortical development. Nat Neurosci *12*, 1238-1247.
Babiarz, J.E., Hsu, R., Melton, C., Thomas, M., Ullian, E.M., and Blelloch, R. (2011). A role for noncanonical microRNAs in the mammalian brain revealed

by phenotypic differences in Dgcr8 versus Dicer1 knockouts and small RNA sequencing. Rna *17*, 1489-1501.

Babiarz, J.E., Ruby, J.G., Wang, Y., Bartel, D.P., and Blelloch, R. (2008). Mouse ES cells express endogenous shRNAs, siRNAs, and other Microprocessor-independent, Dicer-dependent small RNAs. Genes Dev *22*, 2773-2785.

Bachiller, D., Klingensmith, J., Kemp, C., Belo, J.A., Anderson, R.M., May, S.R., McMahon, J.A., McMahon, A.P., Harland, R.M., Rossant, J.*, et al.* (2000). The organizer factors Chordin and Noggin are required for mouse forebrain development. Nature *403*, 658-661.

Backman, M., Machon, O., Mygland, L., van den Bout, C.J., Zhong, W., Taketo, M.M., and Krauss, S. (2005). Effects of canonical Wnt signaling on dorso-ventral specification of the mouse telencephalon. Dev Biol *279*, 155-168.

Barbeito, L.H., Pehar, M., Cassina, P., Vargas, M.R., Peluffo, H., Viera, L., Estevez, A.G., and Beckman, J.S. (2004). A role for astrocytes in motor neuron loss in amyotrophic lateral sclerosis. Brain research Brain research reviews *47*, 263-274.

Bardoni, B., Davidovic, L., Bensaid, M., and Khandjian, E.W. (2006). The fragile X syndrome: exploring its molecular basis and seeking a treatment. Expert reviews in molecular medicine *8*, 1-16.

Barmada, S.J., Skibinski, G., Korb, E., Rao, E.J., Wu, J.Y., and Finkbeiner, S. (2010). Cytoplasmic mislocalization of TDP-43 is toxic to neurons and enhanced by a mutation associated with familial amyotrophic lateral sclerosis. J Neurosci *30*, 639-649.

Basak, O., and Taylor, V. (2007). Identification of self-replicating multipotent progenitors in the embryonic nervous system by high Notch activity and Hes5 expression. Eur J Neurosci *25*, 1006-1022.

Battistini, S., Giannini, F., Greco, G., Bibbo, G., Ferrera, L., Marini, V., Causarano, R., Casula, M., Lando, G., Patrosso, M.C.*, et al.* (2005). SOD1 mutations in amyotrophic lateral sclerosis. Results from a multicenter Italian study. Journal of neurology *252*, 782-788.

Beatus, P., and Lendahl, U. (1998). Notch and neurogenesis. J Neurosci Res *54*, 125-136.

Beddington, R.S. (1994). Induction of a second neural axis by the mouse node. Development *120*, 613-620.

Bernstein, E., Kim, S.Y., Carmell, M.A., Murchison, E.P., Alcorn, H., Li, M.Z., Mills, A.A., Elledge, S.J., Anderson, K.V., and Hannon, G.J. (2003). Dicer is essential for mouse development. Nat Genet *35*, 215-217.

Bi, F., Huang, C., Tong, J., Qiu, G., Huang, B., Wu, Q., Li, F., Xu, Z., Bowser, R., Xia, X.G.*, et al.* (2013). Reactive astrocytes secrete lcn2 to promote neuron death. Proc Natl Acad Sci U S A *110*, 4069-4074.

Bielli, P., Busa, R., Paronetto, M.P., and Sette, C. (2011). The RNA-binding protein Sam68 is a multifunctional player in human cancer. Endocr Relat Cancer *18*, R91-R102.

Bishop, K.M., Goudreau, G., and O'Leary, D.D. (2000). Regulation of area identity in the mammalian neocortex by Emx2 and Pax6. Science *288*, 344-349.

Bohnsack, M.T., Czaplinski, K., and Gorlich, D. (2004). Exportin 5 is a RanGTP-dependent dsRNA-binding protein that mediates nuclear export of pre-miRNAs. Rna *10*, 185-191.
Borrell, V., and Reillo, I. (2012). Emerging roles of neural stem cells in cerebral cortex development and evolution. Developmental neurobiology *72*, 955-971.
Bose, J.K., Huang, C.C., and Shen, C.K. (2011). Regulation of autophagy by neuropathological protein TDP-43. J Biol Chem *286*, 44441-44448.
Bose, J.K., Wang, I.F., Hung, L., Tarn, W.Y., and Shen, C.K. (2008). TDP-43 overexpression enhances exon 7 inclusion during the survival of motor neuron pre-mRNA splicing. J Biol Chem *283*, 28852-28859.
Bray, S.J. (2006). Notch signalling: a simple pathway becomes complex. Nature reviews Molecular cell biology *7*, 678-689.
Brettschneider, J., Del Tredici, K., Toledo, J.B., Robinson, J.L., Irwin, D.J., Grossman, M., Suh, E., Van Deerlin, V.M., Wood, E.M., Baek, Y.*, et al.* (2013). Stages of pTDP-43 pathology in amyotrophic lateral sclerosis. Ann Neurol *74*, 20-38.
Briscoe, J., Pierani, A., Jessell, T.M., and Ericson, J. (2000). A homeodomain protein code specifies progenitor cell identity and neuronal fate in the ventral neural tube. Cell *101*, 435-445.
Britanova, O., de Juan Romero, C., Cheung, A., Kwan, K.Y., Schwark, M., Gyorgy, A., Vogel, T., Akopov, S., Mitkovski, M., Agoston, D.*, et al.* (2008). Satb2 is a postmitotic determinant for upper-layer neuron specification in the neocortex. Neuron *57*, 378-392.
Bultje, R.S., Castaneda-Castellanos, D.R., Jan, L.Y., Jan, Y.N., Kriegstein, A.R., and Shi, S.H. (2009). Mammalian Par3 regulates progenitor cell asymmetric division via notch signaling in the developing neocortex. Neuron *63*, 189-202.
Buratti, E., Brindisi, A., Giombi, M., Tisminetzky, S., Ayala, Y.M., and Baralle, F.E. (2005). TDP-43 binds heterogeneous nuclear ribonucleoprotein A/B through its C-terminal tail: an important region for the inhibition of cystic fibrosis transmembrane conductance regulator exon 9 splicing. J Biol Chem *280*, 37572-37584.
Buratti, E., Dork, T., Zuccato, E., Pagani, F., Romano, M., and Baralle, F.E. (2001). Nuclear factor TDP-43 and SR proteins promote in vitro and in vivo CFTR exon 9 skipping. Embo J *20*, 1774-1784.
Buratti, E., Romano, M., and Baralle, F.E. (2013). TDP-43 high throughput screening analyses in neurodegeneration: Advantages and pitfalls. Mol Cell Neurosci.
Bushati, N., and Cohen, S.M. (2007). microRNA functions. Annual review of cell and developmental biology *23*, 175-205.
Campbell, K. (2003). Dorsal-ventral patterning in the mammalian telencephalon. Curr Opin Neurobiol *13*, 50-56.
Cartegni, L., and Krainer, A.R. (2002). Disruption of an SF2/ASF-dependent exonic splicing enhancer in SMN2 causes spinal muscular atrophy in the absence of SMN1. Nat Genet *30*, 377-384.
Casarosa, S., Fode, C., and Guillemot, F. (1999). Mash1 regulates neurogenesis in the ventral telencephalon. Development *126*, 525-534.
Castello, A., Fischer, B., Hentze, M.W., and Preiss, T. (2013). RNA-binding proteins in Mendelian disease. Trends Genet *29*, 318-327.

Castro, D.S., Skowronska-Krawczyk, D., Armant, O., Donaldson, I.J., Parras, C., Hunt, C., Critchley, J.A., Nguyen, L., Gossler, A., Gottgens, B.*, et al.* (2006). Proneural bHLH and Brn proteins coregulate a neurogenic program through cooperative binding to a conserved DNA motif. Developmental cell *11*, 831-844.

Caviness, V.S., Jr. (1982). Development of neocortical afferent systems: studies in the reeler mouse. Neurosciences Research Program bulletin *20*, 560-569.

Chamberlain, C.E., Jeong, J., Guo, C., Allen, B.L., and McMahon, A.P. (2008). Notochord-derived Shh concentrates in close association with the apically positioned basal body in neural target cells and forms a dynamic gradient during neural patterning. Development *135*, 1097-1106.

Chen-Plotkin, A.S., Lee, V.M., and Trojanowski, J.Q. (2010). TAR DNA-binding protein 43 in neurodegenerative disease. Nat Rev Neurol *6*, 211-220.

Chenn, A., and Walsh, C.A. (2002). Regulation of cerebral cortical size by control of cell cycle exit in neural precursors. Science *297*, 365-369.

Chenn, A., and Walsh, C.A. (2003). Increased neuronal production, enlarged forebrains and cytoarchitectural distortions in beta-catenin overexpressing transgenic mice. Cerebral cortex *13*, 599-606.

Chiang, P.M., Ling, J., Jeong, Y.H., Price, D.L., Aja, S.M., and Wong, P.C. (2010). Deletion of TDP-43 down-regulates Tbc1d1, a gene linked to obesity, and alters body fat metabolism. Proc Natl Acad Sci U S A *107*, 16320-16324.

Chong, M.M., Rasmussen, J.P., Rudensky, A.Y., and Littman, D.R. (2008). The RNAseIII enzyme Drosha is critical in T cells for preventing lethal inflammatory disease. J Exp Med *205*, 2005-2017.

Chong, M.M., Zhang, G., Cheloufi, S., Neubert, T.A., Hannon, G.J., and Littman, D.R. (2010). Canonical and alternate functions of the microRNA biogenesis machinery. Genes Dev *24*, 1951-1960.

Ciruna, B., and Rossant, J. (2001). FGF signaling regulates mesoderm cell fate specification and morphogenetic movement at the primitive streak. Developmental cell *1*, 37-49.

Clement, A.M., Nguyen, M.D., Roberts, E.A., Garcia, M.L., Boillee, S., Rule, M., McMahon, A.P., Doucette, W., Siwek, D., Ferrante, R.J.*, et al.* (2003). Wild-type nonneuronal cells extend survival of SOD1 mutant motor neurons in ALS mice. Science *302*, 113-117.

Crossley, P.H., Martinez, S., and Martin, G.R. (1996). Midbrain development induced by FGF8 in the chick embryo. Nature *380*, 66-68.

Crozat, A., Aman, P., Mandahl, N., and Ron, D. (1993). Fusion of CHOP to a novel RNA-binding protein in human myxoid liposarcoma. Nature *363*, 640-644.

Cubelos, B., Sebastian-Serrano, A., Beccari, L., Calcagnotto, M.E., Cisneros, E., Kim, S., Dopazo, A., Alvarez-Dolado, M., Redondo, J.M., Bovolenta, P.*, et al.* (2010). Cux1 and Cux2 regulate dendritic branching, spine morphology, and synapses of the upper layer neurons of the cortex. Neuron *66*, 523-535.

Culmsee, C., Zhu, X., Yu, Q.S., Chan, S.L., Camandola, S., Guo, Z., Greig, N.H., and Mattson, M.P. (2001). A synthetic inhibitor of p53 protects neurons against death induced by ischemic and excitotoxic insults, and amyloid beta-peptide. J Neurochem *77*, 220-228.

D'Ambrogio, A., Buratti, E., Stuani, C., Guarnaccia, C., Romano, M., Ayala, Y.M., and Baralle, F.E. (2009). Functional mapping of the interaction between TDP-43 and hnRNP A2 in vivo. Nucleic Acids Res *37*, 4116-4126.
Davis, T.H., Cuellar, T.L., Koch, S.M., Barker, A.J., Harfe, B.D., McManus, M.T., and Ullian, E.M. (2008). Conditional loss of Dicer disrupts cellular and tissue morphogenesis in the cortex and hippocampus. J Neurosci *28*, 4322-4330.
de la Monte, S.M., Sohn, Y.K., and Wands, J.R. (1997). Correlates of p53- and Fas (CD95)-mediated apoptosis in Alzheimer's disease. Journal of the neurological sciences *152*, 73-83.
de la Pompa, J.L., Wakeham, A., Correia, K.M., Samper, E., Brown, S., Aguilera, R.J., Nakano, T., Honjo, T., Mak, T.W., Rossant, J.*, et al.* (1997). Conservation of the Notch signalling pathway in mammalian neurogenesis. Development *124*, 1139-1148.
De Pietri Tonelli, D., Pulvers, J.N., Haffner, C., Murchison, E.P., Hannon, G.J., and Huttner, W.B. (2008). miRNAs are essential for survival and differentiation of newborn neurons but not for expansion of neural progenitors during early neurogenesis in the mouse embryonic neocortex. Development *135*, 3911-3921.
DeJesus-Hernandez, M., Mackenzie, I.R., Boeve, B.F., Boxer, A.L., Baker, M., Rutherford, N.J., Nicholson, A.M., Finch, N.A., Flynn, H., Adamson, J.*, et al.* (2011). Expanded GGGGCC hexanucleotide repeat in noncoding region of C9ORF72 causes chromosome 9p-linked FTD and ALS. Neuron *72*, 245-256.
Deng, H.X., Chen, W., Hong, S.T., Boycott, K.M., Gorrie, G.H., Siddique, N., Yang, Y., Fecto, F., Shi, Y., Zhai, H.*, et al.* (2011). Mutations in UBQLN2 cause dominant X-linked juvenile and adult-onset ALS and ALS/dementia. Nature *477*, 211-215.
Di Giorgio, F.P., Boulting, G.L., Bobrowicz, S., and Eggan, K.C. (2008). Human embryonic stem cell-derived motor neurons are sensitive to the toxic effect of glial cells carrying an ALS-causing mutation. Cell stem cell *3*, 637-648.
Di Giorgio, F.P., Carrasco, M.A., Siao, M.C., Maniatis, T., and Eggan, K. (2007). Non-cell autonomous effect of glia on motor neurons in an embryonic stem cell-based ALS model. Nat Neurosci *10*, 608-614.
Doench, J.G., and Sharp, P.A. (2004). Specificity of microRNA target selection in translational repression. Genes Dev *18*, 504-511.
Donehower, L.A., and Lozano, G. (2009). 20 years studying p53 functions in genetically engineered mice. Nat Rev Cancer *9*, 831-841.
Dormann, D., and Haass, C. (2011). TDP-43 and FUS: a nuclear affair. Trends Neurosci.
Dreumont, N., Hardy, S., Behm-Ansmant, I., Kister, L., Branlant, C., Stevenin, J., and Bourgeois, C.F. (2010). Antagonistic factors control the unproductive splicing of SC35 terminal intron. Nucleic Acids Res *38*, 1353-1366.
Dreyfuss, G., Kim, V.N., and Kataoka, N. (2002). Messenger-RNA-binding proteins and the messages they carry. Nature reviews Molecular cell biology *3*, 195-205.
Duan, W., Zhu, X., Ladenheim, B., Yu, Q.S., Guo, Z., Oyler, J., Cutler, R.G., Cadet, J.L., Greig, N.H., and Mattson, M.P. (2002). p53 inhibitors preserve dopamine neurons and motor function in experimental parkinsonism. Ann Neurol *52*, 597-606.

Englund, C., Fink, A., Lau, C., Pham, D., Daza, R.A., Bulfone, A., Kowalczyk, T., and Hevner, R.F. (2005). Pax6, Tbr2, and Tbr1 are expressed sequentially by radial glia, intermediate progenitor cells, and postmitotic neurons in developing neocortex. J Neurosci *25*, 247-251.

Ericson, J., Rashbass, P., Schedl, A., Brenner-Morton, S., Kawakami, A., van Heyningen, V., Jessell, T.M., and Briscoe, J. (1997). Pax6 controls progenitor cell identity and neuronal fate in response to graded Shh signaling. Cell *90*, 169-180.

Eulalio, A., Behm-Ansmant, I., and Izaurralde, E. (2007a). P bodies: at the crossroads of post-transcriptional pathways. Nature reviews Molecular cell biology *8*, 9-22.

Eulalio, A., Behm-Ansmant, I., Schweizer, D., and Izaurralde, E. (2007b). P-body formation is a consequence, not the cause, of RNA-mediated gene silencing. Mol Cell Biol *27*, 3970-3981.

Eve, D.J., Dennis, J.S., and Citron, B.A. (2007). Transcription factor p53 in degenerating spinal cords. Brain Res *1150*, 174-181.

Fiesel, F.C., Voigt, A., Weber, S.S., Van den Haute, C., Waldenmaier, A., Gorner, K., Walter, M., Anderson, M.L., Kern, J.V., Rasse, T.M.*, et al.* (2010). Knockdown of transactive response DNA-binding protein (TDP-43) downregulates histone deacetylase 6. EMBO J *29*, 209-221.

Fode, C., Ma, Q., Casarosa, S., Ang, S.L., Anderson, D.J., and Guillemot, F. (2000). A role for neural determination genes in specifying the dorsoventral identity of telencephalic neurons. Genes Dev *14*, 67-80.

Gaiano, N., Nye, J.S., and Fishell, G. (2000). Radial glial identity is promoted by Notch1 signaling in the murine forebrain. Neuron *26*, 395-404.

Garber, K.B., Visootsak, J., and Warren, S.T. (2008). Fragile X syndrome. Eur J Hum Genet *16*, 666-672.

Garcia-Lopez, P., Garcia-Marin, V., and Freire, M. (2006). Three-dimensional reconstruction and quantitative study of a pyramidal cell of a Cajal histological preparation. J Neurosci *26*, 11249-11252.

Ghosh, A.K., Shankar, D.B., Shackleford, G.M., Wu, K., T'Ang, A., Miller, G.J., Zheng, J., and Roy-Burman, P. (1996). Molecular cloning and characterization of human FGF8 alternative messenger RNA forms. Cell growth & differentiation : the molecular biology journal of the American Association for Cancer Research *7*, 1425-1434.

Giorgi, C., and Moore, M.J. (2007). The nuclear nurture and cytoplasmic nature of localized mRNPs. Semin Cell Dev Biol *18*, 186-193.

Glisovic, T., Bachorik, J.L., Yong, J., and Dreyfuss, G. (2008). RNA-binding proteins and post-transcriptional gene regulation. FEBS Lett *582*, 1977-1986.

Gonzalez de Aguilar, J.L., Gordon, J.W., Rene, F., de Tapia, M., Lutz-Bucher, B., Gaiddon, C., and Loeffler, J.P. (2000). Alteration of the Bcl-x/Bax ratio in a transgenic mouse model of amyotrophic lateral sclerosis: evidence for the implication of the p53 signaling pathway. Neurobiol Dis *7*, 406-415.

Gotz, M., and Huttner, W.B. (2005). The cell biology of neurogenesis. Nature reviews Molecular cell biology *6*, 777-788.

Gotz, M., Stoykova, A., and Gruss, P. (1998). Pax6 controls radial glia differentiation in the cerebral cortex. Neuron *21*, 1031-1044.

Green, D.R., and Kroemer, G. (2009). Cytoplasmic functions of the tumour suppressor p53. Nature *458*, 1127-1130.

Grove, E.A., Tole, S., Limon, J., Yip, L., and Ragsdale, C.W. (1998). The hem of the embryonic cerebral cortex is defined by the expression of multiple Wnt genes and is compromised in Gli3-deficient mice. Development *125*, 2315-2325.

Guil, S., and Caceres, J.F. (2007). The multifunctional RNA-binding protein hnRNP A1 is required for processing of miR-18a. Nature structural & molecular biology *14*, 591-596.

Guillemot, F. (2005). Cellular and molecular control of neurogenesis in the mammalian telencephalon. Curr Opin Cell Biol *17*, 639-647.

Haidet-Phillips, A.M., Hester, M.E., Miranda, C.J., Meyer, K., Braun, L., Frakes, A., Song, S., Likhite, S., Murtha, M.J., Foust, K.D*., et al.* (2011). Astrocytes from familial and sporadic ALS patients are toxic to motor neurons. Nature biotechnology *29*, 824-828.

Han, J., Lee, Y., Yeom, K.H., Kim, Y.K., Jin, H., and Kim, V.N. (2004). The Drosha-DGCR8 complex in primary microRNA processing. Genes Dev *18*, 3016-3027.

Han, J., Lee, Y., Yeom, K.H., Nam, J.W., Heo, I., Rhee, J.K., Sohn, S.Y., Cho, Y., Zhang, B.T., and Kim, V.N. (2006). Molecular basis for the recognition of primary microRNAs by the Drosha-DGCR8 complex. Cell *125*, 887-901.

Han, W., Kwan, K.Y., Shim, S., Lam, M.M., Shin, Y., Xu, X., Zhu, Y., Li, M., and Sestan, N. (2011). TBR1 directly represses Fezf2 to control the laminar origin and development of the corticospinal tract. Proc Natl Acad Sci U S A *108*, 3041-3046.

Harfe, B.D., McManus, M.T., Mansfield, J.H., Hornstein, E., and Tabin, C.J. (2005). The RNaseIII enzyme Dicer is required for morphogenesis but not patterning of the vertebrate limb. Proc Natl Acad Sci U S A *102*, 10898-10903.

Harfe, B.D., Scherz, P.J., Nissim, S., Tian, H., McMahon, A.P., and Tabin, C.J. (2004). Evidence for an expansion-based temporal Shh gradient in specifying vertebrate digit identities. Cell *118*, 517-528.

Hatakeyama, J., Bessho, Y., Katoh, K., Ookawara, S., Fujioka, M., Guillemot, F., and Kageyama, R. (2004). Hes genes regulate size, shape and histogenesis of the nervous system by control of the timing of neural stem cell differentiation. Development *131*, 5539-5550.

Heins, N., Malatesta, P., Cecconi, F., Nakafuku, M., Tucker, K.L., Hack, M.A., Chapouton, P., Barde, Y.A., and Gotz, M. (2002). Glial cells generate neurons: the role of the transcription factor Pax6. Nat Neurosci *5*, 308-315.

Hevner, R.F. (2006). From radial glia to pyramidal-projection neuron: transcription factor cascades in cerebral cortex development. Mol Neurobiol *33*, 33-50.

Hevner, R.F., Hodge, R.D., Daza, R.A., and Englund, C. (2006). Transcription factors in glutamatergic neurogenesis: conserved programs in neocortex, cerebellum, and adult hippocampus. Neuroscience research *55*, 223-233.

Hevner, R.F., Shi, L., Justice, N., Hsueh, Y., Sheng, M., Smiga, S., Bulfone, A., Goffinet, A.M., Campagnoni, A.T., and Rubenstein, J.L. (2001). Tbr1 regulates differentiation of the preplate and layer 6. Neuron *29*, 353-366.

Hirabayashi, Y., and Gotoh, Y. (2005). Stage-dependent fate determination of neural precursor cells in mouse forebrain. Neuroscience research *51*, 331-336.

Hirabayashi, Y., Itoh, Y., Tabata, H., Nakajima, K., Akiyama, T., Masuyama, N., and Gotoh, Y. (2004). The Wnt/beta-catenin pathway directs neuronal differentiation of cortical neural precursor cells. Development *131*, 2791-2801.

Hirano, A. (1996). Neuropathology of ALS: an overview. Neurology *47*, S63-66.

Hirata, H., Yoshiura, S., Ohtsuka, T., Bessho, Y., Harada, T., Yoshikawa, K., and Kageyama, R. (2002). Oscillatory expression of the bHLH factor Hes1 regulated by a negative feedback loop. Science *298*, 840-843.

Hirokawa, N., Niwa, S., and Tanaka, Y. (2010). Molecular motors in neurons: transport mechanisms and roles in brain function, development, and disease. Neuron *68*, 610-638.

Hitoshi, S., Alexson, T., Tropepe, V., Donoviel, D., Elia, A.J., Nye, J.S., Conlon, R.A., Mak, T.W., Bernstein, A., and van der Kooy, D. (2002). Notch pathway molecules are essential for the maintenance, but not the generation, of mammalian neural stem cells. Genes Dev *16*, 846-858.

Hogan, B.L. (1996). Bone morphogenetic proteins in development. Current opinion in genetics & development *6*, 432-438.

Hu, D.J., Baffet, A.D., Nayak, T., Akhmanova, A., Doye, V., and Vallee, R.B. (2013). Dynein recruitment to nuclear pores activates apical nuclear migration and mitotic entry in brain progenitor cells. Cell *154*, 1300-1313.

Hu, Q., Ueno, N., and Behringer, R.R. (2004). Restriction of BMP4 activity domains in the developing neural tube of the mouse embryo. EMBO reports *5*, 734-739.

Huang, G., Lee, X., Bian, Y., Shao, Z., Sheng, G., Pepinsky, R.B., and Mi, S. (2013). Death receptor 6 (DR6) antagonist antibody is neuroprotective in the mouse SOD1G93A model of amyotrophic lateral sclerosis. Cell death & disease *4*, e841.

Huttner, W.B., and Brand, M. (1997). Asymmetric division and polarity of neuroepithelial cells. Curr Opin Neurobiol *7*, 29-39.

Igaz, L.M., Kwong, L.K., Lee, E.B., Chen-Plotkin, A., Swanson, E., Unger, T., Malunda, J., Xu, Y., Winton, M.J., Trojanowski, J.Q.*, et al.* (2011). Dysregulation of the ALS-associated gene TDP-43 leads to neuronal death and degeneration in mice. J Clin Invest.

Iguchi, Y., Katsuno, M., Niwa, J., Takagi, S., Ishigaki, S., Ikenaka, K., Kawai, K., Watanabe, H., Yamanaka, K., Takahashi, R.*, et al.* (2013). Loss of TDP-43 causes age-dependent progressive motor neuron degeneration. Brain *136*, 1371-1382.

Iijima, T., Wu, K., Witte, H., Hanno-Iijima, Y., Glatter, T., Richard, S., and Scheiffele, P. (2011). SAM68 regulates neuronal activity-dependent alternative splicing of neurexin-1. Cell *147*, 1601-1614.

Inukai, Y., Nonaka, T., Arai, T., Yoshida, M., Hashizume, Y., Beach, T.G., Buratti, E., Baralle, F.E., Akiyama, H., Hisanaga, S.*, et al.* (2008). Abnormal phosphorylation of Ser409/410 of TDP-43 in FTLD-U and ALS. FEBS Lett *582*, 2899-2904.

Ishizu, H., Siomi, H., and Siomi, M.C. (2012). Biology of PIWI-interacting RNAs: new insights into biogenesis and function inside and outside of germlines. Genes Dev *26*, 2361-2373.

Israsena, N., Hu, M., Fu, W., Kan, L., and Kessler, J.A. (2004). The presence of FGF2 signaling determines whether beta-catenin exerts effects on proliferation or neuronal differentiation of neural stem cells. Dev Biol *268*, 220-231.

Itoh, M., Haga, I., Li, Q.H., and Fujisawa, J. (2002). Identification of cellular mRNA targets for RNA-binding protein Sam68. Nucleic Acids Res *30*, 5452-5464.

Ivey, K.N., and Srivastava, D. (2010). MicroRNAs as regulators of differentiation and cell fate decisions. Cell stem cell *7*, 36-41.

Johnson, J.O., Mandrioli, J., Benatar, M., Abramzon, Y., Van Deerlin, V.M., Trojanowski, J.Q., Gibbs, J.R., Brunetti, M., Gronka, S., Wuu, J.*, et al.* (2010). Exome sequencing reveals VCP mutations as a cause of familial ALS. Neuron *68*, 857-864.

Jung, Y.S., Qian, Y., and Chen, X. (2010). Examination of the expanding pathways for the regulation of p21 expression and activity. Cell Signal *22*, 1003-1012.

Junghans, D., Hack, I., Frotscher, M., Taylor, V., and Kemler, R. (2005). Beta-catenin-mediated cell-adhesion is vital for embryonic forebrain development. Developmental dynamics : an official publication of the American Association of Anatomists *233*, 528-539.

Kageyama, R., Ohtsuka, T., Hatakeyama, J., and Ohsawa, R. (2005). Roles of bHLH genes in neural stem cell differentiation. Exp Cell Res *306*, 343-348.

Kageyama, R., Ohtsuka, T., Shimojo, H., and Imayoshi, I. (2009). Dynamic regulation of Notch signaling in neural progenitor cells. Curr Opin Cell Biol *21*, 733-740.

Kanellopoulou, C., Muljo, S.A., Kung, A.L., Ganesan, S., Drapkin, R., Jenuwein, T., Livingston, D.M., and Rajewsky, K. (2005). Dicer-deficient mouse embryonic stem cells are defective in differentiation and centromeric silencing. Genes Dev *19*, 489-501.

Kang, S.H., Li, Y., Fukaya, M., Lorenzini, I., Cleveland, D.W., Ostrow, L.W., Rothstein, J.D., and Bergles, D.E. (2013). Degeneration and impaired regeneration of gray matter oligodendrocytes in amyotrophic lateral sclerosis. Nat Neurosci *16*, 571-579.

Karginov, F.V., Cheloufi, S., Chong, M.M., Stark, A., Smith, A.D., and Hannon, G.J. (2010). Diverse endonucleolytic cleavage sites in the mammalian transcriptome depend upon microRNAs, Drosha, and additional nucleases. Mol Cell *38*, 781-788.

Kawase-Koga, Y., Otaegi, G., and Sun, T. (2009). Different timings of Dicer deletion affect neurogenesis and gliogenesis in the developing mouse central nervous system. Developmental dynamics : an official publication of the American Association of Anatomists *238*, 2800-2812.

Kerr, J.F.R., Wyllie, A.H., and Currie, A.R. (1972). Apoptosis - Basic Biological Phenomenon with Wide-Ranging Implications in Tissue Kinetics. Brit J Cancer *26*, 239-&.

Kieran, D., Woods, I., Villunger, A., Strasser, A., and Prehn, J.H. (2007). Deletion of the BH3-only protein puma protects motoneurons from ER stress-induced apoptosis and delays motoneuron loss in ALS mice. Proc Natl Acad Sci U S A *104*, 20606-20611.

Kim, W.Y. (2013). NeuroD regulates neuronal migration. Molecules and cells *35*, 444-449.

Kirby, J., Goodall, E.F., Smith, W., Highley, J.R., Masanzu, R., Hartley, J.A., Hibberd, R., Hollinger, H.C., Wharton, S.B., Morrison, K.E.*, et al.* (2010).

Broad clinical phenotypes associated with TAR-DNA binding protein (TARDBP) mutations in amyotrophic lateral sclerosis. Neurogenetics *11*, 217-225.

Kishore, S., Luber, S., and Zavolan, M. (2010). Deciphering the role of RNA-binding proteins in the post-transcriptional control of gene expression. Brief Funct Genomics *9*, 391-404.

Knecht, A.K., and Bronner-Fraser, M. (2002). Induction of the neural crest: a multigene process. Nature reviews Genetics *3*, 453-461.

Knoblich, J.A. (2008). Mechanisms of asymmetric stem cell division. Cell *132*, 583-597.

Komarov, P.G., Komarova, E.A., Kondratov, R.V., Christov-Tselkov, K., Coon, J.S., Chernov, M.V., and Gudkov, A.V. (1999). A chemical inhibitor of p53 that protects mice from the side effects of cancer therapy. Science *285*, 1733-1737.

Kovach, C., Dixit, R., Li, S., Mattar, P., Wilkinson, G., Elsen, G.E., Kurrasch, D.M., Hevner, R.F., and Schuurmans, C. (2013). Neurog2 simultaneously activates and represses alternative gene expression programs in the developing neocortex. Cerebral cortex *23*, 1884-1900.

Kriegstein, A., and Alvarez-Buylla, A. (2009). The glial nature of embryonic and adult neural stem cells. Annual review of neuroscience *32*, 149-184.

Kriegstein, A.R., and Gotz, M. (2003). Radial glia diversity: a matter of cell fate. Glia *43*, 37-43.

Kriegstein, A.R., and Noctor, S.C. (2004). Patterns of neuronal migration in the embryonic cortex. Trends Neurosci *27*, 392-399.

Kruse, J.P., and Gu, W. (2009). Modes of p53 regulation. Cell *137*, 609-622.

Kubli, D.A., and Gustafsson, A.B. (2012). Mitochondria and mitophagy: the yin and yang of cell death control. Circulation research *111*, 1208-1221.

Kuntz, C.t., Kinoshita, Y., Beal, M.F., Donehower, L.A., and Morrison, R.S. (2000). Absence of p53: no effect in a transgenic mouse model of familial amyotrophic lateral sclerosis. Exp Neurol *165*, 184-190.

Kwan, K.Y., Lam, M.M., Krsnik, Z., Kawasawa, Y.I., Lefebvre, V., and Sestan, N. (2008). SOX5 postmitotically regulates migration, postmigratory differentiation, and projections of subplate and deep-layer neocortical neurons. Proc Natl Acad Sci U S A *105*, 16021-16026.

Kwiatkowski, T.J., Jr., Bosco, D.A., Leclerc, A.L., Tamrazian, E., Vanderburg, C.R., Russ, C., Davis, A., Gilchrist, J., Kasarskis, E.J., Munsat, T.*, et al.* (2009). Mutations in the FUS/TLS gene on chromosome 16 cause familial amyotrophic lateral sclerosis. Science *323*, 1205-1208.

Lagier-Tourenne, C., and Cleveland, D.W. (2009). Rethinking ALS: the FUS about TDP-43. Cell *136*, 1001-1004.

Lagier-Tourenne, C., Polymenidou, M., and Cleveland, D.W. (2010). TDP-43 and FUS/TLS: emerging roles in RNA processing and neurodegeneration. Hum Mol Genet *19*, R46-64.

Le Dreau, G., and Marti, E. (2012). Dorsal-ventral patterning of the neural tube: a tale of three signals. Developmental neurobiology *72*, 1471-1481.

Lee, K., Suzuki, H., Aiso, S., and Matsuoka, M. (2012). Overexpression of TDP-43 causes partially p53-dependent G2/M arrest and p53-independent cell death in HeLa cells. Neurosci Lett *506*, 271-276.

Lee, R.C., Feinbaum, R.L., and Ambros, V. (1993). The C. elegans heterochronic gene lin-4 encodes small RNAs with antisense complementarity to lin-14. Cell *75*, 843-854.
Lee, S.M., Danielian, P.S., Fritzsch, B., and McMahon, A.P. (1997). Evidence that FGF8 signalling from the midbrain-hindbrain junction regulates growth and polarity in the developing midbrain. Development *124*, 959-969.
Lee, Y., Kim, M., Han, J., Yeom, K.H., Lee, S., Baek, S.H., and Kim, V.N. (2004). MicroRNA genes are transcribed by RNA polymerase II. Embo J *23*, 4051-4060.
Leker, R.R., Aharonowiz, M., Greig, N.H., and Ovadia, H. (2004). The role of p53-induced apoptosis in cerebral ischemia: effects of the p53 inhibitor pifithrin alpha. Exp Neurol *187*, 478-486.
Leonardo, T.R., Schultheisz, H.L., Loring, J.F., and Laurent, L.C. (2012). The functions of microRNAs in pluripotency and reprogramming. Nat Cell Biol *14*, 1114-1121.
Levine, A.J., and Brivanlou, A.H. (2007). Proposal of a model of mammalian neural induction. Dev Biol *308*, 247-256.
Levine, A.J., and Oren, M. (2009). The first 30 years of p53: growing ever more complex. Nat Rev Cancer *9*, 749-758.
Li, J., Liu, Y., Kim, B.O., and He, J.J. (2002). Direct participation of Sam68, the 68-kilodalton Src-associated protein in mitosis, in the CRM1-mediated Rev nuclear export pathway. J Virol *76*, 8374-8382.
Li, L., and Liu, Y. (2011). Diverse small non-coding RNAs in RNA interference pathways. Methods Mol Biol *764*, 169-182.
Li, Z., Zhang, Y., Ku, L., Wilkinson, K.D., Warren, S.T., and Feng, Y. (2001). The fragile X mental retardation protein inhibits translation via interacting with mRNA. Nucleic Acids Res *29*, 2276-2283.
Ling, S.C., Albuquerque, C.P., Han, J.S., Lagier-Tourenne, C., Tokunaga, S., Zhou, H., and Cleveland, D.W. (2010). ALS-associated mutations in TDP-43 increase its stability and promote TDP-43 complexes with FUS/TLS. Proc Natl Acad Sci U S A *107*, 13318-13323.
Ling, S.C., Polymenidou, M., and Cleveland, D.W. (2013). Converging mechanisms in ALS and FTD: disrupted RNA and protein homeostasis. Neuron *79*, 416-438.
Liu, A., Losos, K., and Joyner, A.L. (1999). FGF8 can activate Gbx2 and transform regions of the rostral mouse brain into a hindbrain fate. Development *126*, 4827-4838.
Liu, A., and Niswander, L.A. (2005). Bone morphogenetic protein signalling and vertebrate nervous system development. Nature reviews Neuroscience *6*, 945-954.
Liu, J., Carmell, M.A., Rivas, F.V., Marsden, C.G., Thomson, J.M., Song, J.J., Hammond, S.M., Joshua-Tor, L., and Hannon, G.J. (2004). Argonaute2 is the catalytic engine of mammalian RNAi. Science *305*, 1437-1441.
Lorson, C.L., and Androphy, E.J. (2000). An exonic enhancer is required for inclusion of an essential exon in the SMA-determining gene SMN. Hum Mol Genet *9*, 259-265.
Lowery, L.A., and Sive, H. (2004). Strategies of vertebrate neurulation and a re-evaluation of teleost neural tube formation. Mech Dev *121*, 1189-1197.
Lozano, G. (2010). Mouse models of p53 functions. Cold Spring Harb Perspect Biol *2*, a001115.

Lund, E., Guttinger, S., Calado, A., Dahlberg, J.E., and Kutay, U. (2004). Nuclear export of microRNA precursors. Science *303*, 95-98.
Lunde, B.M., Moore, C., and Varani, G. (2007). RNA-binding proteins: modular design for efficient function. Nature reviews Molecular cell biology *8*, 479-490.
Lutolf, S., Radtke, F., Aguet, M., Suter, U., and Taylor, V. (2002). Notch1 is required for neuronal and glial differentiation in the cerebellum. Development *129*, 373-385.
Macias, S., Plass, M., Stajuda, A., Michlewski, G., Eyras, E., and Caceres, J.F. (2012). DGCR8 HITS-CLIP reveals novel functions for the Microprocessor. Nature structural & molecular biology *19*, 760-766.
Makeyev, E.V., Zhang, J., Carrasco, M.A., and Maniatis, T. (2007). The MicroRNA miR-124 promotes neuronal differentiation by triggering brain-specific alternative pre-mRNA splicing. Mol Cell *27*, 435-448.
Maniataki, E., and Mourelatos, Z. (2005). A human, ATP-independent, RISC assembly machine fueled by pre-miRNA. Genes Dev *19*, 2979-2990.
Marine, J.C., and Jochemsen, A.G. (2005). Mdmx as an essential regulator of p53 activity. Biochem Biophys Res Commun *331*, 750-760.
Martin, L.J. (2000). p53 is abnormally elevated and active in the CNS of patients with amyotrophic lateral sclerosis. Neurobiol Dis *7*, 613-622.
Maruyama, H., Morino, H., Ito, H., Izumi, Y., Kato, H., Watanabe, Y., Kinoshita, Y., Kamada, M., Nodera, H., Suzuki, H.*, et al.* (2010). Mutations of optineurin in amyotrophic lateral sclerosis. Nature *465*, 223-226.
Matlashewski, G., Lamb, P., Pim, D., Peacock, J., Crawford, L., and Benchimol, S. (1984). Isolation and Characterization of a Human P53 Cdna Clone - Expression of the Human P53 Gene. Embo Journal *3*, 3257-3262.
Mc Guire, C., Beyaert, R., and van Loo, G. (2011). Death receptor signalling in central nervous system inflammation and demyelination. Trends Neurosci *34*, 619-628.
McConnell, S.K. (1988). Fates of visual cortical neurons in the ferret after isochronic and heterochronic transplantation. J Neurosci *8*, 945-974.
McConnell, S.K. (1995). Constructing the cerebral cortex: neurogenesis and fate determination. Neuron *15*, 761-768.
McIlwain, D.R., Berger, T., and Mak, T.W. (2013). Caspase functions in cell death and disease. Cold Spring Harb Perspect Biol *5*, a008656.
Mercado, P.A., Ayala, Y.M., Romano, M., Buratti, E., and Baralle, F.E. (2005). Depletion of TDP 43 overrides the need for exonic and intronic splicing enhancers in the human apoA-II gene. Nucleic Acids Res *33*, 6000-6010.
Monani, U.R., Lorson, C.L., Parsons, D.W., Prior, T.W., Androphy, E.J., Burghes, A.H., and McPherson, J.D. (1999). A single nucleotide difference that alters splicing patterns distinguishes the SMA gene SMN1 from the copy gene SMN2. Hum Mol Genet *8*, 1177-1183.
Montes de Oca Luna, R., Wagner, D.S., and Lozano, G. (1995). Rescue of early embryonic lethality in mdm2-deficient mice by deletion of p53. Nature *378*, 203-206.
Morita, S., Kojima, T., and Kitamura, T. (2000). Plat-E: an efficient and stable system for transient packaging of retroviruses. Gene therapy *7*, 1063-1066.
Morlando, M., Dini Modigliani, S., Torrelli, G., Rosa, A., Di Carlo, V., Caffarelli, E., and Bozzoni, I. (2012). FUS stimulates microRNA biogenesis by facilitating co-transcriptional Drosha recruitment. EMBO J *31*, 4502-4510.

Mulder, D.W., and Howard, F.M., Jr. (1976). Patient resistance and prognosis in amyotrophic lateral sclerosis. Mayo Clinic proceedings Mayo Clinic *51*, 537-541.

Muller, P.A., and Vousden, K.H. (2013). p53 mutations in cancer. Nat Cell Biol *15*, 2-8.

Mumm, J.S., and Kopan, R. (2000). Notch signaling: from the outside in. Dev Biol *228*, 151-165.

Nagai, M., Re, D.B., Nagata, T., Chalazonitis, A., Jessell, T.M., Wichterle, H., and Przedborski, S. (2007). Astrocytes expressing ALS-linked mutated SOD1 release factors selectively toxic to motor neurons. Nat Neurosci *10*, 615-622.

Neumann, M., Sampathu, D.M., Kwong, L.K., Truax, A.C., Micsenyi, M.C., Chou, T.T., Bruce, J., Schuck, T., Grossman, M., Clark, C.M.*, et al.* (2006). Ubiquitinated TDP-43 in frontotemporal lobar degeneration and amyotrophic lateral sclerosis. Science *314*, 130-133.

Nieto, M., Schuurmans, C., Britz, O., and Guillemot, F. (2001). Neural bHLH genes control the neuronal versus glial fate decision in cortical progenitors. Neuron *29*, 401-413.

Noctor, S.C., Flint, A.C., Weissman, T.A., Dammerman, R.S., and Kriegstein, A.R. (2001). Neurons derived from radial glial cells establish radial units in neocortex. Nature *409*, 714-720.

Noctor, S.C., Martinez-Cerdeno, V., Ivic, L., and Kriegstein, A.R. (2004). Cortical neurons arise in symmetric and asymmetric division zones and migrate through specific phases. Nat Neurosci *7*, 136-144.

Nonaka, T., Masuda-Suzukake, M., Arai, T., Hasegawa, Y., Akatsu, H., Obi, T., Yoshida, M., Murayama, S., Mann, D.M., Akiyama, H.*, et al.* (2013). Prion-like properties of pathological TDP-43 aggregates from diseased brains. Cell reports *4*, 124-134.

Nowakowski, T.J., Mysiak, K.S., Pratt, T., and Price, D.J. (2011). Functional dicer is necessary for appropriate specification of radial glia during early development of mouse telencephalon. PLoS One *6*, e23013.

Nyfeler, Y., Kirch, R.D., Mantei, N., Leone, D.P., Radtke, F., Suter, U., and Taylor, V. (2005). Jagged1 signals in the postnatal subventricular zone are required for neural stem cell self-renewal. Embo J *24*, 3504-3515.

Ohtsuka, T., Ishibashi, M., Gradwohl, G., Nakanishi, S., Guillemot, F., and Kageyama, R. (1999). Hes1 and Hes5 as notch effectors in mammalian neuronal differentiation. Embo J *18*, 2196-2207.

Olsen, S.K., Li, J.Y., Bromleigh, C., Eliseenkova, A.V., Ibrahimi, O.A., Lao, Z., Zhang, F., Linhardt, R.J., Joyner, A.L., and Mohammadi, M. (2006). Structural basis by which alternative splicing modulates the organizer activity of FGF8 in the brain. Genes Dev *20*, 185-198.

Ou, S.H., Wu, F., Harrich, D., Garcia-Martinez, L.F., and Gaynor, R.B. (1995). Cloning and characterization of a novel cellular protein, TDP-43, that binds to human immunodeficiency virus type 1 TAR DNA sequence motifs. J Virol *69*, 3584-3596.

Parant, J., Chavez-Reyes, A., Little, N.A., Yan, W., Reinke, V., Jochemsen, A.G., and Lozano, G. (2001). Rescue of embryonic lethality in Mdm4-null mice by loss of Trp53 suggests a nonoverlapping pathway with MDM2 to regulate p53. Nat Genet *29*, 92-95.

Parras, C.M., Schuurmans, C., Scardigli, R., Kim, J., Anderson, D.J., and Guillemot, F. (2002). Divergent functions of the proneural genes Mash1 and

Ngn2 in the specification of neuronal subtype identity. Genes Dev *16*, 324-338.
Pauli, A., Rinn, J.L., and Schier, A.F. (2011). Non-coding RNAs as regulators of embryogenesis. Nature reviews Genetics *12*, 136-149.
Pearson, J.C., Lemons, D., and McGinnis, W. (2005). Modulating Hox gene functions during animal body patterning. Nature reviews Genetics *6*, 893-904.
Perea-Gomez, A., Lawson, K.A., Rhinn, M., Zakin, L., Brulet, P., Mazan, S., and Ang, S.L. (2001). Otx2 is required for visceral endoderm movement and for the restriction of posterior signals in the epiblast of the mouse embryo. Development *128*, 753-765.
Pesiridis, G.S., Lee, V.M., and Trojanowski, J.Q. (2009). Mutations in TDP-43 link glycine-rich domain functions to amyotrophic lateral sclerosis. Hum Mol Genet *18*, R156-162.
Polymenidou, M., Lagier-Tourenne, C., Hutt, K.R., Huelga, S.C., Moran, J., Liang, T.Y., Ling, S.C., Sun, E., Wancewicz, E., Mazur, C.*, et al.* (2011). Long pre-mRNA depletion and RNA missplicing contribute to neuronal vulnerability from loss of TDP-43. Nat Neurosci *14*, 459-468.
Prudlo, J., Koenig, J., Graser, J., Burckhardt, E., Mestres, P., Menger, M., and Roemer, K. (2000). Motor neuron cell death in a mouse model of FALS is not mediated by the p53 cell survival regulator. Brain Res *879*, 183-187.
Quinn, J.C., Molinek, M., Martynoga, B.S., Zaki, P.A., Faedo, A., Bulfone, A., Hevner, R.F., West, J.D., and Price, D.J. (2007). Pax6 controls cerebral cortical cell number by regulating exit from the cell cycle and specifies cortical cell identity by a cell autonomous mechanism. Dev Biol *302*, 50-65.
Ranganathan, S., and Bowser, R. (2010). p53 and Cell Cycle Proteins Participate in Spinal Motor Neuron Cell Death in ALS. Open Pathol J *4*, 11-22.
Ransom, B.R., and Ransom, C.B. (2012). Astrocytes: multitalented stars of the central nervous system. Methods Mol Biol *814*, 3-7.
Rhinn, M., and Brand, M. (2001). The midbrain--hindbrain boundary organizer. Curr Opin Neurobiol *11*, 34-42.
Ribes, V., and Briscoe, J. (2009). Establishing and interpreting graded Sonic Hedgehog signaling during vertebrate neural tube patterning: the role of negative feedback. Cold Spring Harb Perspect Biol *1*, a002014.
Riggi, N., Cironi, L., Suva, M.L., and Stamenkovic, I. (2007). Sarcomas: genetics, signalling, and cellular origins. Part 1: The fellowship of TET. The Journal of pathology *213*, 4-20.
Ringholz, G.M., Appel, S.H., Bradshaw, M., Cooke, N.A., Mosnik, D.M., and Schulz, P.E. (2005). Prevalence and patterns of cognitive impairment in sporadic ALS. Neurology *65*, 586-590.
Roy, S., Zhang, B., Lee, V.M., and Trojanowski, J.Q. (2005). Axonal transport defects: a common theme in neurodegenerative diseases. Acta Neuropathol *109*, 5-13.
Ruby, J.G., Jan, C.H., and Bartel, D.P. (2007). Intronic microRNA precursors that bypass Drosha processing. Nature *448*, 83-86.
Sahara, S., and O'Leary, D.D. (2009). Fgf10 regulates transition period of cortical stem cell differentiation to radial glia controlling generation of neurons and basal progenitors. Neuron *63*, 48-62.
Sakaue-Sawano, A., Kurokawa, H., Morimura, T., Hanyu, A., Hama, H., Osawa, H., Kashiwagi, S., Fukami, K., Miyata, T., Miyoshi, H.*, et al.* (2008).

Visualizing spatiotemporal dynamics of multicellular cell-cycle progression. Cell *132*, 487-498.

Sato, T., Joyner, A.L., and Nakamura, H. (2004). How does Fgf signaling from the isthmic organizer induce midbrain and cerebellum development? Development, growth & differentiation *46*, 487-494.

Saxena, S., and Caroni, P. (2011). Selective neuronal vulnerability in neurodegenerative diseases: from stressor thresholds to degeneration. Neuron *71*, 35-48.

Scardigli, R., Schuurmans, C., Gradwohl, G., and Guillemot, F. (2001). Crossregulation between Neurogenin2 and pathways specifying neuronal identity in the spinal cord. Neuron *31*, 203-217.

Schebelle, L., Wolf, C., Stribl, C., Javaheri, T., Schnutgen, F., Ettinger, A., Ivics, Z., Hansen, J., Ruiz, P., von Melchner, H.*, et al.* (2010). Efficient conditional and promoter-specific in vivo expression of cDNAs of choice by taking advantage of recombinase-mediated cassette exchange using FlEx gene traps. Nucleic Acids Res *38*, e106.

Schoenwolf, G.C., and Delongo, J. (1980). Ultrastructure of secondary neurulation in the chick embryo. The American journal of anatomy *158*, 43-63.

Schymick, J.C., Yang, Y., Andersen, P.M., Vonsattel, J.P., Greenway, M., Momeni, P., Elder, J., Chio, A., Restagno, G., Robberecht, W.*, et al.* (2007). Progranulin mutations and amyotrophic lateral sclerosis or amyotrophic lateral sclerosis-frontotemporal dementia phenotypes. Journal of neurology, neurosurgery, and psychiatry *78*, 754-756.

Seila, A.C., and Sharp, P.A. (2008). Small RNAs tell big stories in Whistler. Nat Cell Biol *10*, 630-633.

Sellier, C., Rau, F., Liu, Y., Tassone, F., Hukema, R.K., Gattoni, R., Schneider, A., Richard, S., Willemsen, R., Elliott, D.J.*, et al.* (2010). Sam68 sequestration and partial loss of function are associated with splicing alterations in FXTAS patients. EMBO J *29*, 1248-1261.

Sephton, C.F., Cenik, C., Kucukural, A., Dammer, E.B., Cenik, B., Han, Y.H., Dewey, C.M., Roth, F.P., Herz, J., Peng, J.*, et al.* (2010a). Identification of neuronal RNA targets of TDP-43-containing Ribonucleoprotein complexes. J Biol Chem.

Sephton, C.F., Good, S.K., Atkin, S., Dewey, C.M., Mayer, P., 3rd, Herz, J., and Yu, G. (2010b). TDP-43 is a developmentally regulated protein essential for early embryonic development. J Biol Chem *285*, 6826-6834.

Serio, A., Bilican, B., Barmada, S.J., Ando, D.M., Zhao, C., Siller, R., Burr, K., Haghi, G., Story, D., Nishimura, A.L.*, et al.* (2013). Astrocyte pathology and the absence of non-cell autonomy in an induced pluripotent stem cell model of TDP-43 proteinopathy. Proc Natl Acad Sci U S A *110*, 4697-4702.

Shimojo, H., Ohtsuka, T., and Kageyama, R. (2008). Oscillations in notch signaling regulate maintenance of neural progenitors. Neuron *58*, 52-64.

Shimojo, H., Ohtsuka, T., and Kageyama, R. (2011). Dynamic expression of notch signaling genes in neural stem/progenitor cells. Frontiers in neuroscience *5*, 78.

Shitamukai, A., and Matsuzaki, F. (2012). Control of asymmetric cell division of mammalian neural progenitors. Development, growth & differentiation *54*, 277-286.

Smith, W.C., and Harland, R.M. (1992). Expression cloning of noggin, a new dorsalizing factor localized to the Spemann organizer in Xenopus embryos. Cell *70*, 829-840.

Strong, M.J., Volkening, K., Hammond, R., Yang, W., Strong, W., Leystra-Lantz, C., and Shoesmith, C. (2007). TDP43 is a human low molecular weight neurofilament (hNFL) mRNA-binding protein. Mol Cell Neurosci *35*, 320-327.

Stump, G., Durrer, A., Klein, A.L., Lutolf, S., Suter, U., and Taylor, V. (2002). Notch1 and its ligands Delta-like and Jagged are expressed and active in distinct cell populations in the postnatal mouse brain. Mech Dev *114*, 153-159.

Sugitani, Y., Nakai, S., Minowa, O., Nishi, M., Jishage, K., Kawano, H., Mori, K., Ogawa, M., and Noda, T. (2002). Brn-1 and Brn-2 share crucial roles in the production and positioning of mouse neocortical neurons. Genes Dev *16*, 1760-1765.

Suzuki, H., Lee, K., and Matsuoka, M. (2011). TDP-43-induced death is associated with altered regulation of BIM and Bcl-xL and attenuated by caspase-mediated TDP-43 cleavage. J Biol Chem *286*, 13171-13183.

Swarup, V., Phaneuf, D., Bareil, C., Robertson, J., Rouleau, G.A., Kriz, J., and Julien, J.P. (2011). Pathological hallmarks of amyotrophic lateral sclerosis/frontotemporal lobar degeneration in transgenic mice produced with TDP-43 genomic fragments. Brain *134*, 2610-2626.

Takahashi, T., Nowakowski, R.S., and Caviness, V.S., Jr. (1993). Cell cycle parameters and patterns of nuclear movement in the neocortical proliferative zone of the fetal mouse. J Neurosci *13*, 820-833.

Tam, P.P., and Behringer, R.R. (1997). Mouse gastrulation: the formation of a mammalian body plan. Mech Dev *68*, 3-25.

Tam, P.P., Williams, E.A., and Chan, W.Y. (1993). Gastrulation in the mouse embryo: ultrastructural and molecular aspects of germ layer morphogenesis. Microscopy research and technique *26*, 301-328.

Tchorz, J.S., Suply, T., Ksiazek, I., Giachino, C., Cloetta, D., Danzer, C.P., Doll, T., Isken, A., Lemaistre, M., Taylor, V*., et al.* (2012). A modified RMCE-compatible Rosa26 locus for the expression of transgenes from exogenous promoters. PLoS One *7*, e30011.

Teta, M., Choi, Y.S., Okegbe, T., Wong, G., Tam, O.H., Chong, M.M., Seykora, J.T., Nagy, A., Littman, D.R., Andl, T*., et al.* (2012). Inducible deletion of epidermal Dicer and Drosha reveals multiple functions for miRNAs in postnatal skin. Development *139*, 1405-1416.

Thiyagarajan, N., Ferguson, R., Subramanian, V., and Acharya, K.R. (2012). Structural and molecular insights into the mechanism of action of human angiogenin-ALS variants in neurons. Nature communications *3*, 1121.

Tiberi, L., Vanderhaeghen, P., and van den Ameele, J. (2012). Cortical neurogenesis and morphogens: diversity of cues, sources and functions. Curr Opin Cell Biol *24*, 269-276.

Tollervey, J.R., Curk, T., Rogelj, B., Briese, M., Cereda, M., Kayikci, M., Konig, J., Hortobagyi, T., Nishimura, A.L., Zupunski, V*., et al.* (2011). Characterizing the RNA targets and position-dependent splicing regulation by TDP-43. Nat Neurosci *14*, 452-458.

Tong, J., Huang, C., Bi, F., Wu, Q., Huang, B., Liu, X., Li, F., Zhou, H., and Xia, X.G. (2013). Expression of ALS-linked TDP-43 mutant in astrocytes causes non-cell-autonomous motor neuron death in rats. EMBO J *32*, 1917-1926.

Toresson, H., Potter, S.S., and Campbell, K. (2000). Genetic control of dorsal-ventral identity in the telencephalon: opposing roles for Pax6 and Gsh2. Development *127*, 4361-4371.

Toyoda, R., Assimacopoulos, S., Wilcoxon, J., Taylor, A., Feldman, P., Suzuki-Hirano, A., Shimogori, T., and Grove, E.A. (2010). FGF8 acts as a classic diffusible morphogen to pattern the neocortex. Development *137*, 3439-3448.

Tsai, K.J., Yang, C.H., Fang, Y.H., Cho, K.H., Chien, W.L., Wang, W.T., Wu, T.W., Lin, C.P., Fu, W.M., and Shen, C.K. (2010). Elevated expression of TDP-43 in the forebrain of mice is sufficient to cause neurological and pathological phenotypes mimicking FTLD-U. J Exp Med *207*, 1661-1673.

Udan-Johns, M., Bengoechea, R., Bell, S., Shao, J., Diamond, M.I., True, H.L., Weihl, C.C., and Baloh, R.H. (2014). Prion-like nuclear aggregation of TDP-43 during heat shock is regulated by HSP40/70 chaperones. Hum Mol Genet *23*, 157-170.

Vance, C., Rogelj, B., Hortobagyi, T., De Vos, K.J., Nishimura, A.L., Sreedharan, J., Hu, X., Smith, B., Ruddy, D., Wright, P.*, et al.* (2009). Mutations in FUS, an RNA processing protein, cause familial amyotrophic lateral sclerosis type 6. Science *323*, 1208-1211.

Wang, H.Y., Wang, I.F., Bose, J., and Shen, C.K. (2004). Structural diversity and functional implications of the eukaryotic TDP gene family. Genomics *83*, 130-139.

Wang, I.F., Chang, H.Y., Hou, S.C., Liou, G.G., Way, T.D., and James Shen, C.K. (2012). The self-interaction of native TDP-43 C terminus inhibits its degradation and contributes to early proteinopathies. Nature communications *3*, 766.

Wang, I.F., Reddy, N.M., and Shen, C.K. (2002). Higher order arrangement of the eukaryotic nuclear bodies. Proc Natl Acad Sci U S A *99*, 13583-13588.

Wang, Y., Medvid, R., Melton, C., Jaenisch, R., and Blelloch, R. (2007). DGCR8 is essential for microRNA biogenesis and silencing of embryonic stem cell self-renewal. Nat Genet *39*, 380-385.

Wegorzewska, I., Bell, S., Cairns, N.J., Miller, T.M., and Baloh, R.H. (2009). TDP-43 mutant transgenic mice develop features of ALS and frontotemporal lobar degeneration. Proc Natl Acad Sci U S A *106*, 18809-18814.

Wells, D.G. (2006). RNA-binding proteins: a lesson in repression. J Neurosci *26*, 7135-7138.

Wils, H., Kleinberger, G., Janssens, J., Pereson, S., Joris, G., Cuijt, I., Smits, V., Ceuterick-de Groote, C., Van Broeckhoven, C., and Kumar-Singh, S. (2010). TDP-43 transgenic mice develop spastic paralysis and neuronal inclusions characteristic of ALS and frontotemporal lobar degeneration. Proc Natl Acad Sci U S A *107*, 3858-3863.

Wilson, P.A., and Hemmati-Brivanlou, A. (1995). Induction of epidermis and inhibition of neural fate by Bmp-4. Nature *376*, 331-333.

Winter, J., Jung, S., Keller, S., Gregory, R.I., and Diederichs, S. (2009). Many roads to maturity: microRNA biogenesis pathways and their regulation. Nat Cell Biol *11*, 228-234.

Woo, R.A., and Poon, R.Y. (2003). Cyclin-dependent kinases and S phase control in mammalian cells. Cell Cycle *2*, 316-324.

Woodhead, G.J., Mutch, C.A., Olson, E.C., and Chenn, A. (2006). Cell-autonomous beta-catenin signaling regulates cortical precursor proliferation. J Neurosci *26*, 12620-12630.

Wu, C.H., Fallini, C., Ticozzi, N., Keagle, P.J., Sapp, P.C., Piotrowska, K., Lowe, P., Koppers, M., McKenna-Yasek, D., Baron, D.M.*, et al.* (2012). Mutations in the profilin 1 gene cause familial amyotrophic lateral sclerosis. Nature.

Wu, L.S., Cheng, W.C., Hou, S.C., Yan, Y.T., Jiang, S.T., and Shen, C.K. (2010). TDP-43, a neuro-pathosignature factor, is essential for early mouse embryogenesis. Genesis *48*, 56-62.

Xiao, S., Sanelli, T., Dib, S., Sheps, D., Findlater, J., Bilbao, J., Keith, J., Zinman, L., Rogaeva, E., and Robertson, J. (2011). RNA targets of TDP-43 identified by UV-CLIP are deregulated in ALS. Mol Cell Neurosci *47*, 167-180.

Xu, Y.F., Gendron, T.F., Zhang, Y.J., Lin, W.L., D'Alton, S., Sheng, H., Casey, M.C., Tong, J., Knight, J., Yu, X.*, et al.* (2010). Wild-type human TDP-43 expression causes TDP-43 phosphorylation, mitochondrial aggregation, motor deficits, and early mortality in transgenic mice. J Neurosci *30*, 10851-10859.

Yang, C., Tan, W., Whittle, C., Qiu, L., Cao, L., Akbarian, S., and Xu, Z. (2010). The C-terminal TDP-43 fragments have a high aggregation propensity and harm neurons by a dominant-negative mechanism. PLoS One *5*, e15878.

Ybot-Gonzalez, P., Cogram, P., Gerrelli, D., and Copp, A.J. (2002). Sonic hedgehog and the molecular regulation of mouse neural tube closure. Development *129*, 2507-2517.

Yun, K., Potter, S., and Rubenstein, J.L. (2001). Gsh2 and Pax6 play complementary roles in dorsoventral patterning of the mammalian telencephalon. Development *128*, 193-205.

Zamore, P.D., and Haley, B. (2005). Ribo-gnome: the big world of small RNAs. Science *309*, 1519-1524.

Zhang, J., Tu, Q., Grosschedl, R., Kim, M.S., Griffin, T., Drissi, H., Yang, P., and Chen, J. (2011). Roles of SATB2 in osteogenic differentiation and bone regeneration. Tissue engineering Part A *17*, 1767-1776.

Zhong, W., Feder, J.N., Jiang, M.M., Jan, L.Y., and Jan, Y.N. (1996). Asymmetric localization of a mammalian numb homolog during mouse cortical neurogenesis. Neuron *17*, 43-53.

9 Appendix

During my tenure as a PhD student I worked on a side project investigating the function of Drosha and the microprocessor in NSCs. The project was published in 2012, and the following chapters include the data I have contributed to the paper: 'Drosha regulates neurogenesis by controlling Neurogenin 2 expression independent of microRNAs'. In addition a short introduction to the topic as well as additional Material & Methods are listed.

9.1 Introduction

9.1.1 Small, non-coding RNAs

Small, non-coding RNA species including microRNAs (miRNAs), small interfering RNAs (siRNAs), small nucleolar RNAs (snoRNAs), small nuclear RNAs (snRNAs) and Piwi-interacting RNAs (piRNAs) control gene expression in plants and animals (Li and Liu, 2011). Small RNAs have been shown to be implicated in a wide range of cellular processes (Pauli et al., 2011). They regulate mRNA stability and translation through distinct RNA silencing pathways and are mainly distinguished by their different origins and biogenesis pathways (Zamore and Haley, 2005). siRNAs are generated from exogenous or endogenous double-stranded RNAs (dsRNAs) whereas the piRNAs derive from single-stranded precursors independent of RNase III enzymes (Ishizu et al., 2012). piRNAs form complexes with Piwi proteins and silence retrotransposons and other genetic elements in germ cells, mainly during spermatogenesis (Bushati and Cohen, 2007). miRNAs, another group of small, non-coding species of RNAs originate from hairpin-containing transcripts and play a crucial role in the regulation of gene expression. Discovered initially by loss-of-function mutations in *C. elegans* (Lee et al., 1993), miRNAs have also been identified in higher vertebrates. In animals hundreds of miRNAs are described although the function of only a few have been explored.

9.1.2 MicroRNA Biogenesis

Most miRNAs are encoded as solitary genes and are under the control of their own promoters and regulatory sequences. Yet, others are closely clustered on the genome and may be co-regulated with other members of the cluster. Some miRNAs are also found within the non-coding or coding region of larger genes (Ambros, 2004). miRNAs are derived from long, largely unstructured transcripts (pri-miRNA) that are primarily, although not exclusively, transcribed by RNA-Polymerase II (Lee et al., 2004). Pri-miRNAs contain a stem-loop or "hairpin" structure of about ~70 nt in length. This sequence is recognised by a protein complex termed the "microprocessor" (Ayala et al., 2006) that is composed of two key factors: Drosha, a member of the ribonuclease III family and DGCR8. Drosha contains a double-stranded RNA binding domain (dsRBD) and two RNase III domains which form an intramolecular dimer and cleave the 3' and 5' strands of the stem (Han et al., 2004). Because the dsRBD of Drosha is insufficient for substrate binding, Drosha needs a partner protein, DGCR8, surrogating the RNA recognition function.

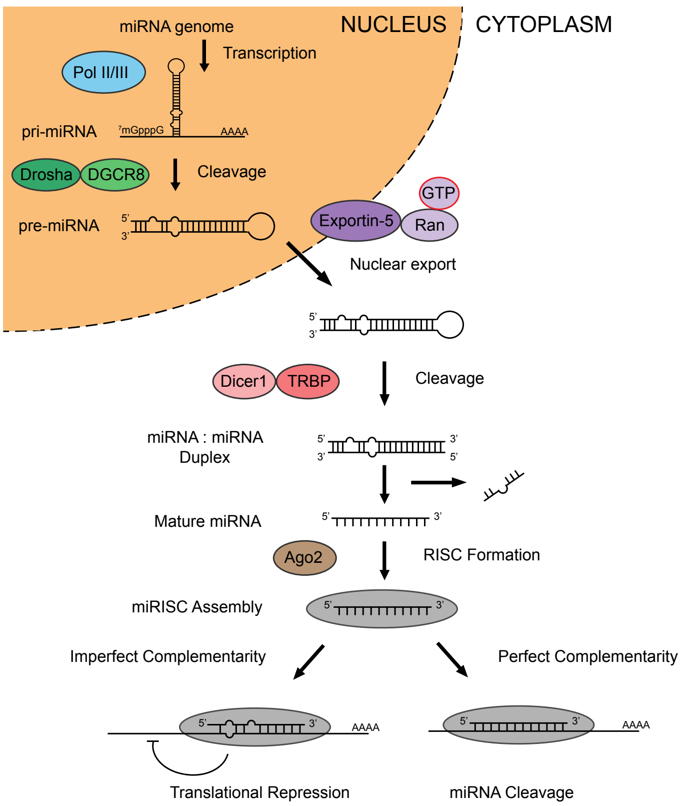

Figure 29: Biogenesis of miRNA Scheme outlining the stepwise cleavage and maturation of miRNA. Drosha/DGCR8 cleave the initial pri-miRNA, which is then transported into the cytoplasm, further processed by Dicer/TRBP and loaded onto the RISC complex. Adapted from (Winter et al., 2009)

DGCR8 contains two dsRBDs and recognises the unique features of the pri-miRNA, which include the ssRNA segments flanking a stem of appropriate length. DGCR8 anchors at the ssRNA-dsRNA junction and directs Drosha to cleave 11 bp away from the junction (Han et al., 2006). The hairpin is cut out by the microprocessor to yield a precursor miRNA (pre-miRNA). Exportin-5 transports the pre-miRNA via a Ran-GTP-dependent mechanism into the cytoplasm (Bohnsack et al., 2004; Lund et al., 2004), where it is cleaved by another RNase III endonuclease, Dicer1. Dicer1 together with the dsRBD protein TRBP release the 2 nt 3´overhang containing a ~22 nt miRNA : miRNA complex. Usually a single “leader” strand is finally loaded onto the RISC composed of proteins of the Argonaute family (Maniataki and Mourelatos, 2005) (Fig. 29) .

In the cytoplasm, the miRNA can specifically interact with the complementary mRNA, which results in translational repression, mRNA cleavage or de-adenylation (Seila and Sharp, 2008). The base-pair complementarity between the miRNA and the mRNA dictates which mechanism of silencing will predominate. In cases where complementarity is near perfect, as happens primarily in plants, degradation is mediated through direct cleavage of the mRNA. The catalytic component of the RISC that performs the cleavage is thought to be Argonaute 2 in vertebrates (Liu et al., 2004). In animals, degradation of mRNA following perfect base-pairing is very rare. Most miRNAs in animals base-pair imperfectly resulting in translational silencing and overall downregulation of protein levels (Bushati and Cohen, 2007). The mechanisms by which miRNAs regulate gene expression are still under debate. Published studies indicate that miRNAs inhibit translational initiation, block elongation or cause premature termination of translation (ribosome drop-off) (Bushati and Cohen, 2007; Seila and Sharp, 2008). Obviously perfect base-pair recognition of the entire 22 nt miRNA is not a requirement for mRNA silencing. Instead a short “seed sequences” between base 2 and 7 of the miRNA is essential for correct target recognition (Doench and Sharp, 2004) and translational inhibition. Interestingly, the imperfect recognition of targets by miRNA programmed RISC results in the possibility for a single miRNA to regulate the expression of several genes simultaneously.

9.1.3 Function of miRNAs during Mouse Development

Silencing of genes mediated by miRNAs is a mechanism involved in many physiological processes such as muscle differentiation, hematopoiesis, bone formation and neurogenesis (Ivey and Srivastava, 2010). Additionally miRNAs are involved in cancer and are important for maintenance of pluripotency in stem cells (Leonardo et al., 2012). Some studies address the function of individual miRNAs, however, loss of single miRNAs very rarely results in a detectable phenotype in mice. This may, in part, be explained by the duplication and redundancy among miRNAs with similar seed sequences in higher vertebrates. Many factors are involved in miRNA biogenesis and deletion or knockdown (KD) of the very results in much more severe phenotypes. Therefore, miRNA function in different cell systems has been investigated using global impairment strategies. However, these approaches are limited, as many factors are not only involved in the biogenesis of one small, non-coding RNA species but instead participate in the maturation of several different ones.

The *Dicer1* gene was used in many studies and *Dicer1* knockout (KO) in mice results in embryonic lethality at E7.5 possibly due to a loss of pluripotent stem cells (Bernstein et al., 2003). Conditional deletion of *Dicer1* from different cell types of the developing mouse cortex causes death of mice shortly after weaning and the cortex displays a high degree of apoptosis and impaired differentiation (Davis et al., 2008; De Pietri Tonelli et al., 2008; Kawase-Koga et al., 2009; Nowakowski et al., 2011). The changes observed following *Dicer1* ablation are possibly not only due to the loss of miRNAs as Dicer1 is also implicated in other cellular processes such as maturation of small interfering RNAs (siRNAs) or noncanonical miRNAs (Babiarz et al., 2008; Ruby et al., 2007). In order to achieve a more selective impairment of miRNA biogenesis, factors upstream of Dicer1 such as Drosha and DGCR8 have been deleted. *Dgcr8* conditional knockout (cKO) in mice results in a phenotype distinct from *Dicer1* cKO and the comparison of the two identified novel noncanonical miRNAs (Babiarz et al., 2011). KO of *Dgcr8* from embryonic stem (ES) cells similarly differs from the *Dicer1* KO in ES cells. *Dgcr8* KO ES cells fail to downregulate pluripotency markers and early differentiation markers are partially absent (Wang et al., 2007). Still, survival and growth is not affected whereas *Dicer1* KO ES cells stop growing after 8 days in culture (Kanellopoulou et al., 2005). Dicer1-null ES cells similarly to *Dgcr8* KO ES cells display differentiation defects and in addition reduction of epigenetic silencing of centromeric repeat sequences. The observed *Dicer1* KO phenotype, however, is conflicting with the published data from Bernstein et al. 2003, where *Dicer1*-deficient ES cells could not be obtained, which was possibly due to differences in the experimental procedure. Drosha-null ES cell lines have been generated, however, it was not reported whether they exhibit phenotypes (Karginov et al., 2010). *Drosha* cKO was also analysed in the immune system, where miRNAs are indispensable for functional regulatory T cells (Chong et al., 2008), and in the postnatal skin of mice (Teta et al., 2012).

9.2 Materials

In addition to the Materials described in chapter 4 the following reagents were used in this set of experiments.

9.2.1 Primers

Primers for 3' Rapid Amplification of cDNA Ends (3' RACE)

Anchored 3' RACE oligo-dT primer: gaccacgcgtatcgatgtcgacttttttttttttttttv

Ngn2_fwd: ttgtaggcttttgtaagggttg

Binding primer_rev: gaccacgcgtatcgatgtcgac

Primers for cloning of ISH probes

Description	Forward 5'-3'	Reverse 5'-3'
Drosha	taatgatccggaccttcgag	cttagaaaggcaatgctccg

qRT-PCR primers

Description	Forward 5'-3'	Reverse 5'-3'
Actin	aggtgacagcattgcttctg	gggagaccaaagccttc
DGCR8	gccacaggtggaagaagaa	acactggcggcttagtcaa
GAPDH	tccatgacaactttggcattgtgg	gttgctgttgaagtcgcaggagac
NeuroD1	gcgttgccttagcacttctt	ctcttgagtgttatgggtctgg
NeuroD6	ggatcacatggctctctctg	gagtgtcgcatcgtctcct
Ngn2	gaaacacgtgtgtggctga	gccacaggtggaagaagaa
hRluc	tgatcggaatgggtaagtcc	ggccttgatcttgtcttggt
Sox2	ccgtgatgccgactagaaa	gaagcgcctaacgtaccact

Genotyping primer

Description	Forward 5'-3'	Reverse 5'-3'
Dicer$^{flox/flox}$	#1 cctgacagtgacggtccaaag #2 catgactcttcaactcaaact	cctgagcaaggcaagtcattc
Drosha$^{flox/flox}$	gcagaaagtctcccactcctaaccttc	ccaggggaaattaaacgagac tcc

9.2.2 Enzymes

Poly(A) Polymerase (NEB)

9.2.3 Plasmids

Plasmid	Cloned by / obtained from
Hes5::Cre	(Onur Basak)
pCAGGS-mCherry	(Philip Knuckles)
pCK-Flag-Drosha	(laboratory Prof. V. Narry. Kim)
pCK-Flag-TNDrosha	(laboratory Prof. V. Narry. Kim)
psiCHECK2	(Philip Knuckles)
psiCHECK2-Neurog2-3’ UTR	(Philip Knuckles)
psiCHECK2-Neurog2-HP	(Miriam Vogt)
pSuper-shDrosha (Oligoengine)	(Philip Knuckles)
shNgn2	(laboratory Prof. F. Guillemot)

9.3 Methods

In addition to the Methods described in chapter 5 the following methods were used in this set of experiments.

9.3.1 Animal Husbandry

Mice were kept on a 12-hour day/night cycle with adequate food and water under SPF (specific pathogen free) conditions. Adult mice 8-12 weeks of age were used in the experiments. The day of vaginal plug was considered as embryonic day 0.5 (E0.5).

Rosa-CAGS-Stop-eGFP (Tchorz et al., 2012), Drosha$^{flox/flox}$ (Chong et al., 2008) and Dicer$^{flox/flox}$ (Harfe et al., 2005) mice were used in the experiments.

9.3.2 3’ Rapid Amplification of cDNA Ends (3’ RACE)

For 3’ RACE, RNA of total RNA extract were 3’ polyadenylated using Poly(A) Polymerase following the manufacturer’s instructions. Next, 1 µg of polyadenylated total RNA was used for cDNA synthesis using the SuperScript III First-Strand Synthesis kit and an anchored 3’ RACE oligo-dT primer (gaccacgcgtatcgatgtcgactttttttttttttttttv). The PCR amplification from cDNA was performed using Kappa2G polymerase according to the manufacturer’s instructions with forward (Ngn2) specific primers (ttgtaggcttttgtaagggttg) and an anchor binding primer as reverse primer (gaccacgcgtatcgatgtcgac).

9.1 Results

9.1.1 Background and Key Findings

Canonical Notch signalling is essential to maintain NSCs as it regulates transcription factors of the Hes and proneural gene families. Proneural genes including the transcription factor Neurogenin2 induce the neuronal differentiation program and are negatively regulated by Hes proteins in NSCs. Hes proteins are expressed in an oscillatory fashion which results in opposing degradation of proneural gene mRNAs and thereby oscillatory expression of proneural proteins. The mechanism controlling the instability of proneural gene mRNA such as *Neurog2* and thus preventing precocious accumulation and differentiation of NSCs are not known. miRNAs have been shown to regulate gene expression on post-transcriptional level and therefore would have been a potential candidate to regulate mRNA levels of proneural genes in NSCs. However, Dicer1, a key factor in the RNA biogenesis pathway has been shown not to be required for maintenance or differentiation of NSCs. In general the role of miRNAs and the components necessary for miRNA production have not been explored in NSC biology. We investigated the function of Drosha and DGCR8, the two components of the microprocessor, through loss-of-function strategies. We found that *Drosha* and *Dgcr8* are highly expressed in forebrain progenitors and conditional deletion or small hairpin-mediated knockdown in NSCs *in vivo* induces precocious differentiation. This effect occurs independently of Dicer1 and miRNA levels are unchanged at the time point when the phenotype is observed. We uncovered that the microprocessor components Drosha and DGCR8 function to destabilize *Neurog2* mRNA and thus prevent accumulation of the mRNA and protein which would result in differentiation of NSCs. Mechanistically Drosha directly binds conserved hairpin structures in the 3’ UTR of *Neurog2* which leads to the destabilization and degradation of the mRNA. We identified a novel mechanism that regulates proneural gene expression in NSCs, which is possibly also conserved in other systems where post-transcriptional regulation of mRNAs is essential.

9.1.2 Statement of Contributions

For the paper 'Drosha regulates neurogenesis by controlling Neurogenin2 expression independent of miRNAs' I participated in the execution of several experiments, in particular in the biochemical analysis of the interaction of Drosha with *Neurog2* mRNA. I also participated in the experimental design and data analysis and contributed to the writing of the final manuscript. In the following chapter the reader will find the results I contributed to the paper. For better understanding of the study some data generated by Philip Knuckles and Verdon Taylor are shown which are clearly labelled. Furthermore the paper is included as not all experiments of the study are mentioned in this chapter.

9.1.3 Results

The miRNA microprocessor is critical for embryonic neurogenesis

The MP controls initial stages of miRNA biogenesis. The central components of the MP, DGCR8 and Drosha, form a multimeric complex that binds double-stranded hairpins of pri-miRNAs and cleaves them to release the hairpin pre-miRNA. Pre-miRNAs generated by the MP in the nucleus are exported and processed to mature miRNAs by Dicer1 (Bernstein et al., 2003). To analyse the expression pattern of *Drosha* in the developing telencephalon we performing *in situ* hybridisation assays. We found *Drosha* being expressed by forebrain progenitors in the VZ and differentiating neurons in the CP (Fig. 30). The RNA levels of Drosha seem to show a dynamic expression pattern during the differentiation of progenitors in the VZ to SVZ/IZ and differentiating immature neurons in the CP.

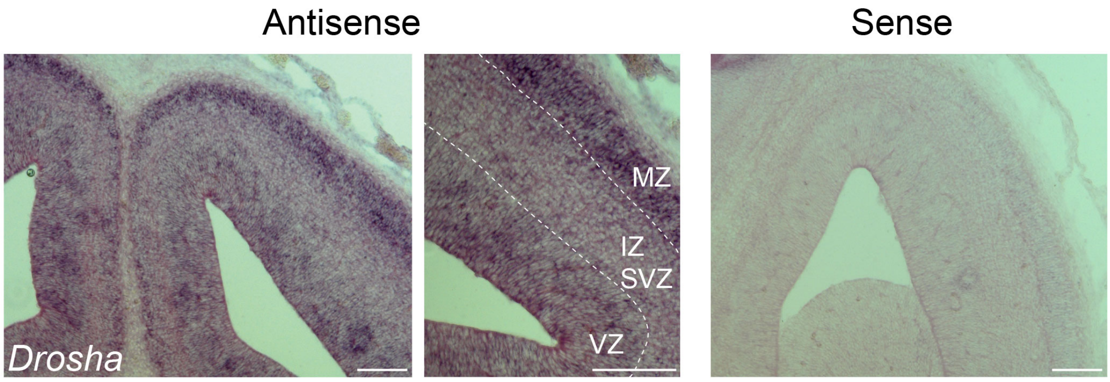

Figure 30: *Drosha* is expressed in the developing dorsal telencephalon

In situ hybridization analysis displaying *Drosha* mRNA expression in the dorsal telencephalon of E14.5 mouse embryos. VZ = ventricular zone, SVZ = subventricular zone, IZ = intermediate zone and MZ = marginal zone. Scale bars = 100 µm.

NSCs in the developing telencephalon have active Notch signalling and express the Notch target *Hes5*. In order to address the function of Drosha in Notch signalling neural progenitors (NPs) we expressed Cre recombinase from the *Hes5* regulatory elements in *loxP*-flanked (floxed) *Drosha* embryos by IUE (Fig. 31a). This resulted in recombination and deletion of the *Drosha* locus specifically in transfected NPs. A mCherry expression plasmid was co-electroporated to trace the transfected and recombined cells. NPs conditionally deleted for Drosha showed reduced expression of the progenitor protein Pax6 after 24 hours (Fig. 31b). Unlike control cells most Drosha depleted cells had exited from the VZ and entered into the SVZ/IZ or CP. To address whether the Drosha effects required the core MP components we knocked-down *Dgcr8* by shRNA expression. Therefore, IUE of wild type animals was performed using a plasmid that expresses a hairpin shRNA that specifically targets *Dgcr8* mRNA. *Dgcr8* KD phenocopied the cKO of *Drosha*, as it resulted in rapid loss of progenitor markers and exit from the VZ within 24 hours (Fig. 31d).

The effect of inactivating Drosha or DGCR8 on NPs was distinct to the *Dicer* cKO phenotype described previously (De Pietri Tonelli et al., 2008; Makeyev et al., 2007). We therefore also performed cKO of *Dicer1* from Notch signalling NPs to analyse the resulting phenotype in our system. Again, the *Hes5::cre* construct was used for electroporation of *loxP*-flanked (floxed) *Dicer1* embryos in order to achieve recombination selectively in NPs. In contrast to Drosha and DGCR8 deleted NPs, *Dicer1* cKO cells did not precociously exit the VZ and retained progenitor-marker expression after 24 hours (Fig. 31c). Comparing *Dicer1* depleted NPs to control cells we observed no obvious changes in cell location, survival or marker expression.

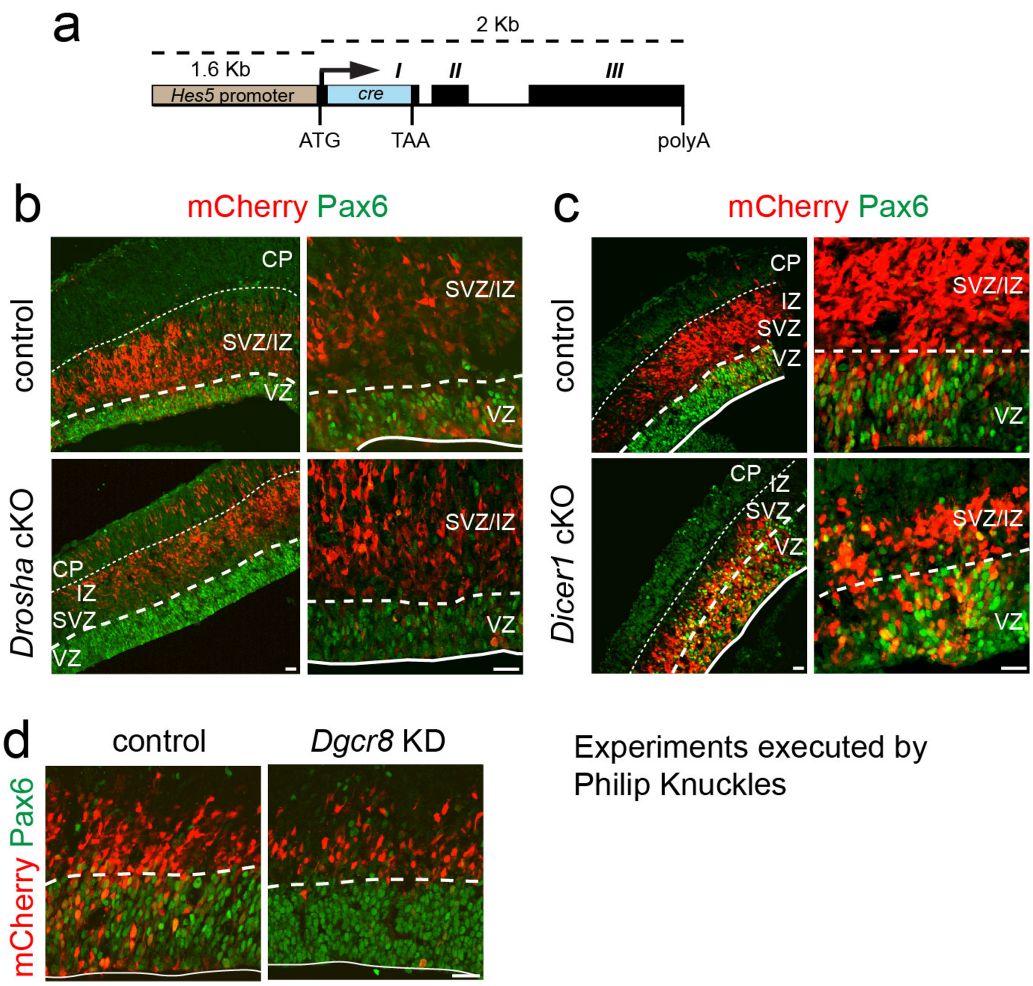

Figure 31: Inactivation of the MP at E13.5 results in NP differentiation in contrast to *Dicer1* cKO

a. *Hes5::cre* construct driving expression of Cre-recombinase from the mouse *Hes5* regulatory elements including promoter, exons *I, II, III,* introns, the endogenous 3' UTR and polyA **b.** *Drosha* cKO results in NPs downregulating Pax6 and exiting the VZ, lineage traced by mCherry **c.** *Dicer1* cKO NPs do not precociously exit the VZ and express the progenitor marker Pax6. **d.** shRNA mediated KD of Dgcr*8* results in downregulation of Pax6 and exit of NPs from the VZ. VZ = ventricular zone, SVZ = subventricular zone, IZ = intermediate zone and CP = cortical plate. Scale bars = 20 µm.

miRNAs are unaffected by *Drosha* KD at the point of phenotypic effects

The MP and Dicer1 are involved in different steps of miRNA biogenesis. Whereas the microprocessor recognises and cleaves hairpin structures in the nucleus and therefore decides which RNA is processed into miRNA, Dicer1 acts in the cytoplasm where it undertakes the final cleavage giving rise to the mature miRNA. Both steps however are crucial to yield mature miRNAs. The different phenotypes observed after MP inactivation and *Dicer1* ablation suggest that the induced effects may not result from changes in mature miRNA levels. Additionally the phenotypic changes induced by Drosha and DGCR8 deletion were already distinguishable after 24 hours. This time-frame is too short to be an effect dependent on changes in miRNA levels. We therefore analysed the miRNA levels of 381 miRNAs *in vivo* after Drosha deletion. Therefore, *Drosha* floxed embryos were electroporated using the *Hes5::cre* and a mCherry expressing construct. The embryos were harvested after 24 hours and transfected NPs (mCherry$^+$) were isolated and sorted by FACS. Subsequently the RNA of the sorted cells was isolated and analysed using TaqMan® array cards, allowing for the analysis of 381 rodent miRNAs. 187 of the analysed miRNAs were expressed in NPs and none showed substantial changes after 24 hours of *Drosha* cKO (Fig. 32). This suggested that mature miRNAs are quite stable in NPs and blocking MP function for 24 hours does not significantly affect their levels.

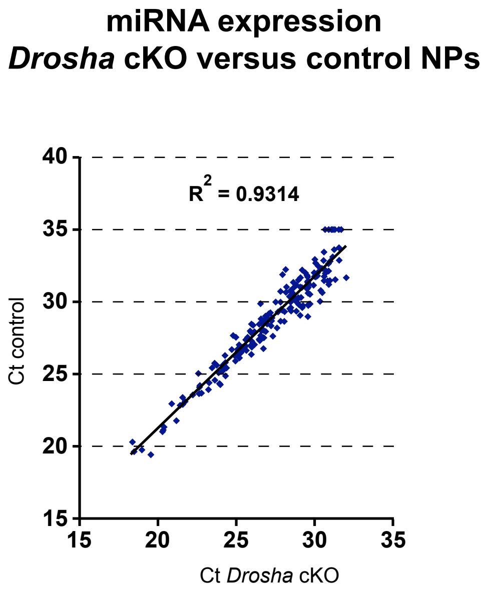

Figure 32: miRNA levels are unchanged after 24 hours of *Drosha* cKO

Change in cycle threshold (ΔCt) plot of relative miRNA expression profiles of control (*Drosha*$^{flox/WT}$) and *Drosha* cKO NPs. R^2 =0.9314 indicates no change in miRNA levels 24 hours after *Drosha* cKO

Experiment executed by Philip Knuckles and Verdon Taylor

Drosha deletion results in increased cell death over time

Dicer1 KO in the dorsal telencephalon was reported to result in a striking phenotype. Whereas neural stem/progenitor cells are unaffected, differentiation and survival of newborn neurons are impaired. At E14.5 a massive apoptosis in the cerebral cortex of Dicer1-deleted mice occurs (Davis et al., 2008; De Pietri Tonelli et al., 2008). We therefore, checked for apoptotic cells after *Drosha* and *Dicer1* deletion in the electroporated embryos.

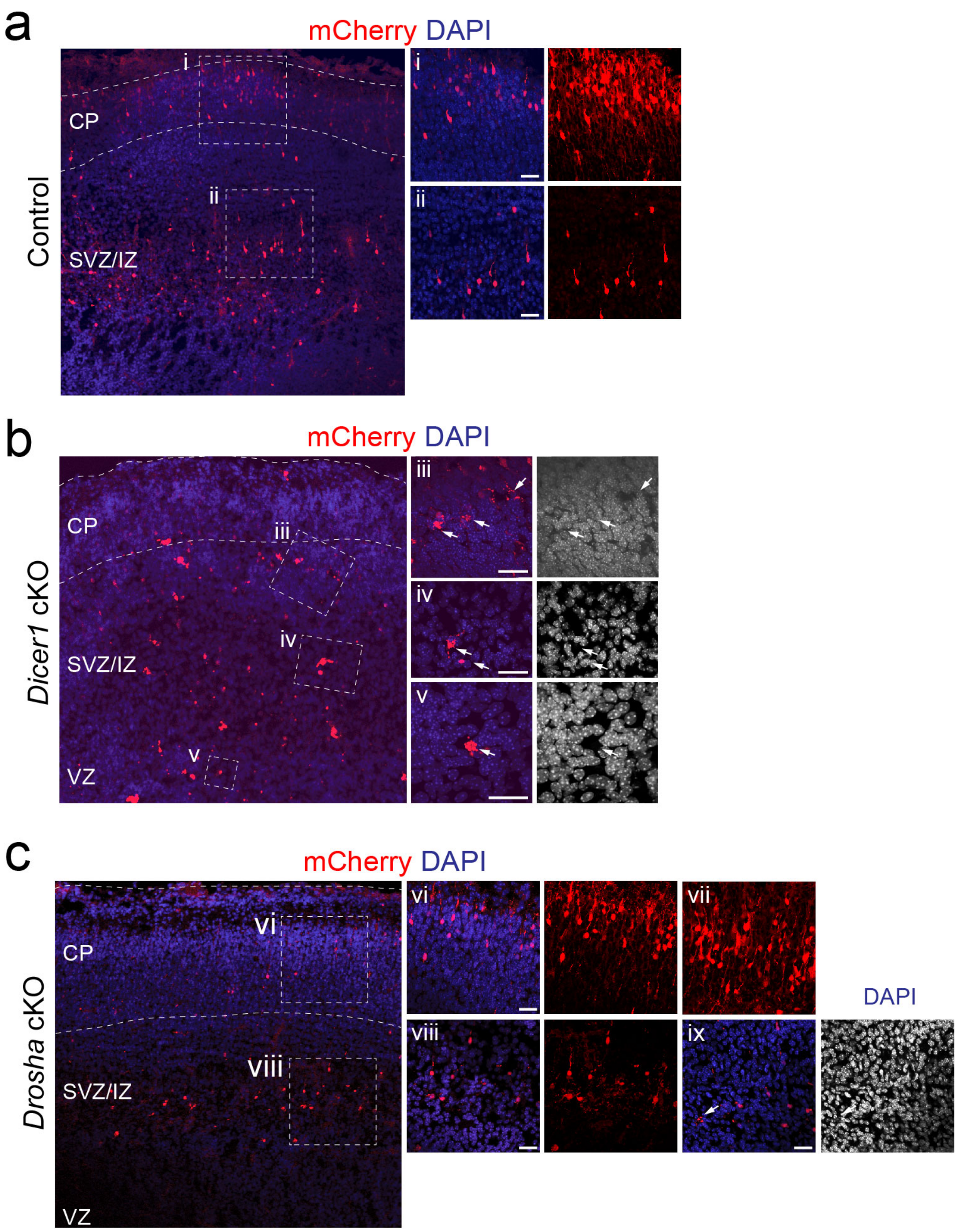

Figure 33: Over time *Drosha* cKO results in increased cell death

a. In the control no morphological changes are observed 4 days post-transfection (i). Cells in the SVZ/IZ are reminiscent of migratory neuroblasts on their way to the CP (ii) **b.** 4 days after *Dicer* cKO very few cells are found in the CP. Massive cell death has occurred detectable by left over cell debris in the SVZ/IZ (iii and iv) arrow. **c.** 4 days after Drosha deletion cells have migrated to the CP and show a normal neuronal morphology (vi, vii). Some cells in the SVZ/IZ show aberrant morphology and cell debris is evident (viii and xi) indicative of cell death (arrow). VZ = ventricular zone, SVZ = subventricular zone, IZ = intermediate zone and CP = cortical plate. Scale bars = 20 µm.

At early time point no apoptotic cells were detected in *Drosha* or *Dicer1* cKO embryos (Fig. 31a,b and data not shown), whereas 4 days after *Dicer1*-ablation many cells had undergone cell death (Fig. 33b). Very few intact cells were found in the CP and only cell debris remained in the SVZ/IZ indicative of cell death. 4 days after *Drosha* cKO some apoptotic cells were detectable in the SVZ/IZ though the effect was less severe than in *Dicer1* cKO mice (Fig. 33c). cKO of *Dgcr8* in neurons resulted in a similar phenotype displaying modest cell death (Babiarz et al., 2011), which indicates that the apoptosis occurring after 4 days is the result of reduced miRNA levels. Thus, we detect apoptotic cells 4 days after *Dicer1* and *Drosha* deletion from NPs, similarly to the published *Dicer1* KO phenotype.

Proneural gene mRNA levels are regulated by Drosha

Next we wanted to analyse how NSC gene expression is affected after *Drosha* cKO. We addressed the role of Drosha in cultured NSCs (neurospheres) by conditional inactivation. Therefore, NSCs were isolated from *Drosha*$^{flox/flox}$ and *Drosha*$^{flox/wt}$ littermates that were crossed onto GFP-Cre reporter mice. NSCs were expanded in cell culture and *Drosha* was efficiently ablated by infection of dissociated cells with Cre-recombinase expressing Adenovirus (Akagi et al., 1997), reported by GFP expression of recombined cells (data not shown). RNA of the unsorted cells was isolated, reverse transcribed into cDNA and analysed by qRT-PCR. Drosha deletion resulted in a 2.8-fold increase in *Dgcr8* mRNA levels (Fig. 34), in line with the published findings of Narry Kim's lab (Han et al., 2004). The Kim lab showed a direct and miRNA independent regulation of *Dgcr8* expression by Drosha, which results in hairpin cleavage and degradation of the mRNA. Upon deletion of Drosha, *Dgcr8* mRNA is not cleaved and degraded which leads to an increased transcript level. The proneural transcription factor *Neurog2* and its downstream effector *NeuroD1* were also increased after *Drosha* cKO in NSCs whereas *Sox2* mRNA levels were decreased (Fig. 34). *Neurog2* and *NeuroD1* are possibly regulated by a mechanism similar to the one reported in Han et al. 2009. The observed changes following *Drosha* deletion were not seen after *Dicer1* cKO where *Dgcr8, Sox2, Neurog2* and *NeuroD1* mRNA levels were unchanged. Therefore, *Drosha* but not *Dicer1* cKO affects transcript levels of the proneural genes *Neurog2* and *NeuroD1* as well as *Dgcr8 and Sox2*.

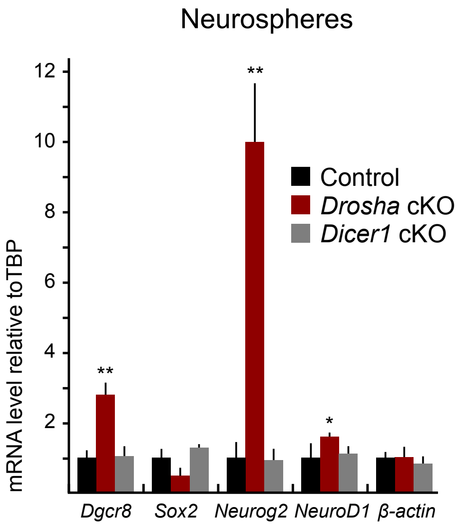

Figure 34: Drosha regulates proneural mRNA levels unlike Dicer1

a. qRT-PCR analysis of *Drosha* cKO and *Dicer1* cKO neurospheres. *Drosha* cKO increased mRNA levels of the proneural genes *Neurog2* and *NeuroD1* and resulted in loss of progenitor-associated *Sox2. DGCR8* mRNA levels are also increased. These changes were not seen after *Dicer1* cKO. tTest *$P<0.05$ and **$P<0.001$

Experiment executed by Miriam Vogt and Philip Knuckles

NP differentiation after *Drosha* cKO is mediated by increased Ngn2 expression

To test whether the changes in mRNA levels are also translated into protein, we analysed Ngn2 expression after *Drosha* cKO *in vivo*. Therefore, *Drosha* and *Dgcr8* were deleted by IUE from NPs similar to the previous experiments and Ngn2 expression was analysed 24 hours later. We found a strong increase in Ngn2-expressing cells after deletion of Drosha or DGCR8 compared to control, and the cells maintained the expression ectopically into the SVZ/IZ (Fig. 35a,b arrowheads). We next addressed if expression of Ngn2 *in vivo* can phenocopy *Drosha* cKO. Therefore, Ngn2 was expressed by IUE, which resulted in exit of the transfected (mCherry$^+$) cells from the VZ and loss of progenitor marker Pax6 after 24 hours (Fig. 35c,d arrowheads). This shows that increased Ngn2 expression is sufficient to induce differentiation of NPs and precocious exit from the VZ.

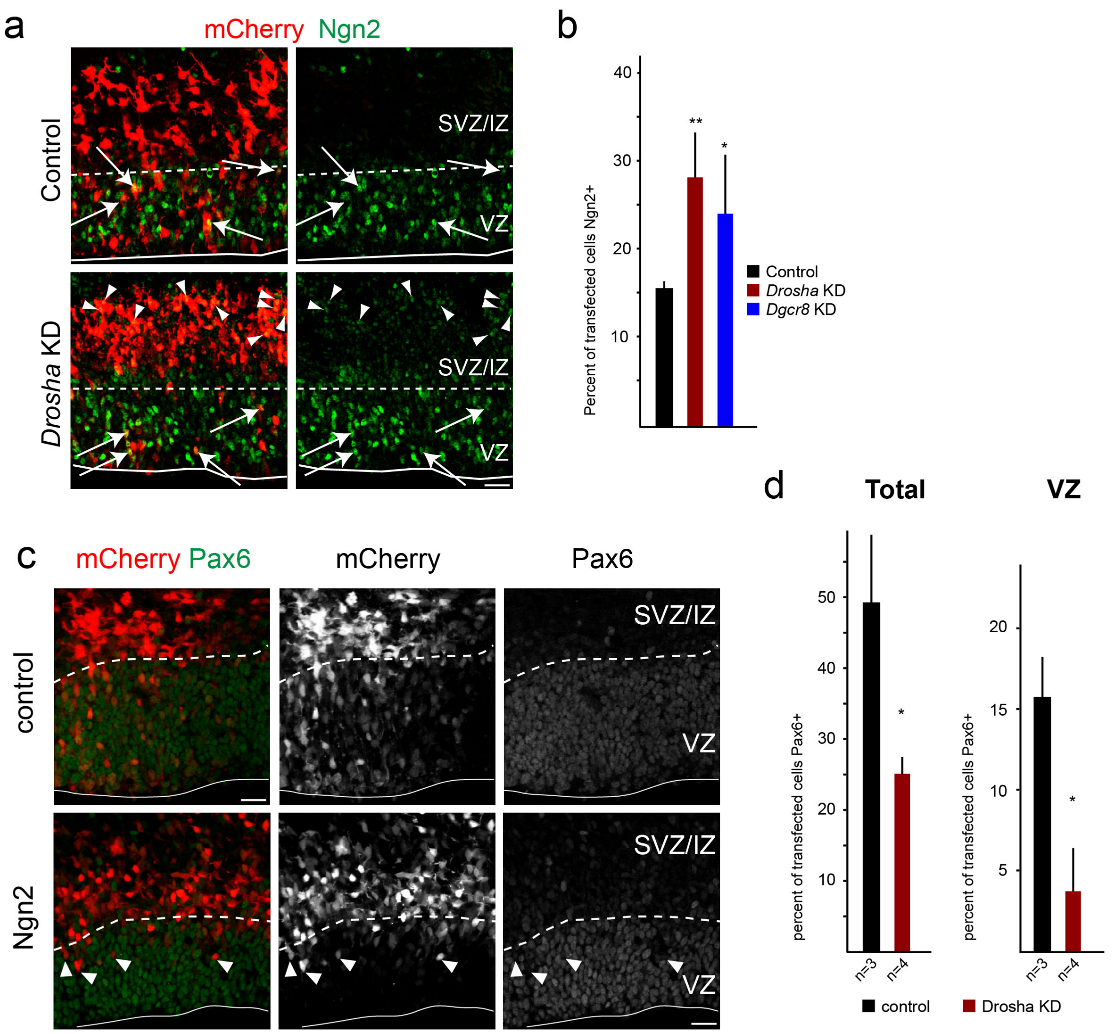

Experiments executed by Philip Knuckles

Figure 35: NP differentiation after *Drosha* cKO is mediated by increased Ngn2 expression

a. Following *Drosha* KD cells in the VZ express Ngn2 (arrows) and maintain expression ectopically into the SVZ/IZ (arrowheads) unlike control cells. **b.** Quantification of cells expressing Ngn2 after *Drosha* and *DGCR8* KD compared to control. tTest *P<0.05 and **P<0.001 **c.** Expression of Ngn2 by IUE in NSCs results in loss of the progenitor marker Pax6. Electroporated cells precociously exit the VZ after Ngn2 expression similar to *Drosha* cKO and *Dgcr8* KD. **d.** Quantification of Pax6^{+} cells after Ngn2 expression. tTest *P<0.05 VZ = ventricular zone, SVZ = subventricular zone and IZ = intermediate zone. Scale bars = 20 µm.

Drosha KD neural progenitors can be rescued by *Neurog2* KD

Drosha-ablation in NPs leads to increased Ngn2 levels, which results in differentiation of NPs. We tried to rescue the phenotype by KD of *Neurog2*, to confirm that precocious differentiation and exit of NPs from the VZ is driven by increased Ngn2. Therefore, small hairpin RNAs targeting *Drosha* and *Neurog2* were expressed simultaneously *in vivo* by IUE. This resulted in a rescue of NPs as the transfected (mCherry^{+}) cells were normally distributed in the SVZ and VZ compared to control where a scrambled shRNA was used (Fig. 36a,b). This result confirms that increased Ngn2 levels alone cause precocious exit of NPs from the VZ.

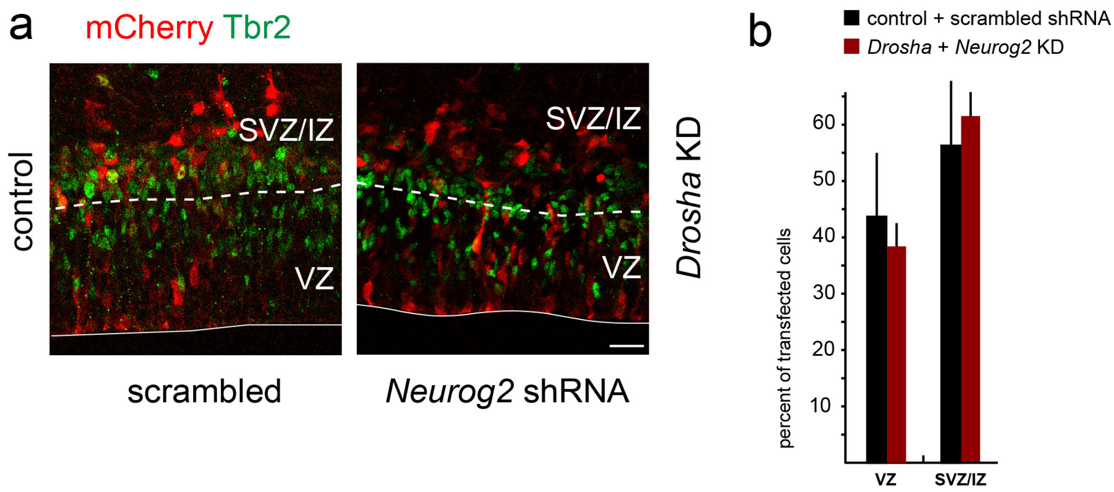

Figure 36: shRNA mediated KD of *Neurog2* can rescue *Drosha* KD NPs

a. Simultaneous KD of *Drosha* and *Neurog2* rescues NPs. Electroporated cells are localized in a normal distribution in the SVZ/IZ and VZ compared to control (scrambled shRNA). **b.** Quantification of $Pax6^+$ cells in the VZ and total cortical area after Ngn2 expression in NSCs. VZ = ventricular zone, SVZ = subventricular zone and IZ = intermediate zone. Scale bars = 20 µm.

Drosha binds to *Neurog2* mRNA via conserved hairpins in the 3' UTR

Loss of the MP by *Drosha* cKO or *Dgcr8* KD resulted in NP differentiation and exit from the VZ within 24 hours, a phenotype distinct from *Dicer1* cKO. Considering the early manifestation of the phenotype and the unchanged levels of miRNAs we speculated that the MP has a miRNA-independent function. *Neurog2* mRNA levels were upregulated following deletion of the MP and *Neurog2* KD rescued the Drosha and Dgcr8 phenotype. We therefore checked the transcripts of the proneural gene *Neurog2* for conserved hairpin structures. The *in silico* analysis revealed multiple secondary stem loop structures in the 3' UTR of *Neurog2* (Fig. 37a). To address if Drosha binds to *Neurog2* mRNA we performed a crosslinked RNA immunoprecipitation (CLIP) experiment. pCK-Flag-Drosha, a transdominant version of Drosha, which has a mutation in the enzyme domain (pCK-Flag-TNDrosha) and Flag-GFP (control) were expressed in N2A cells and the CLIPed RNA was analysed by qRT-PCR. qRT-PCR values of the CLIPed products were corrected relative to the input RNA concentration of each condition and compared to flag-GFP CLIPed samples. We found that *Neurog2* mRNA was bound by Drosha resulting in a 2.5 fold increase over control. Additionally *Dgcr8* mRNA (positive control) was pulled down with Drosha protein whereas no enrichment was detected for *Gapdh*. Hairpin structures were also predicted for *NeuroD1* and *NeuroD6* transcripts, which were also bound by Drosha (Fig. 37b). Drosha therefore directly binds to *Neurog2* mRNA as well as *Dgcr8, NeuroD1* and *NeuroD6.*

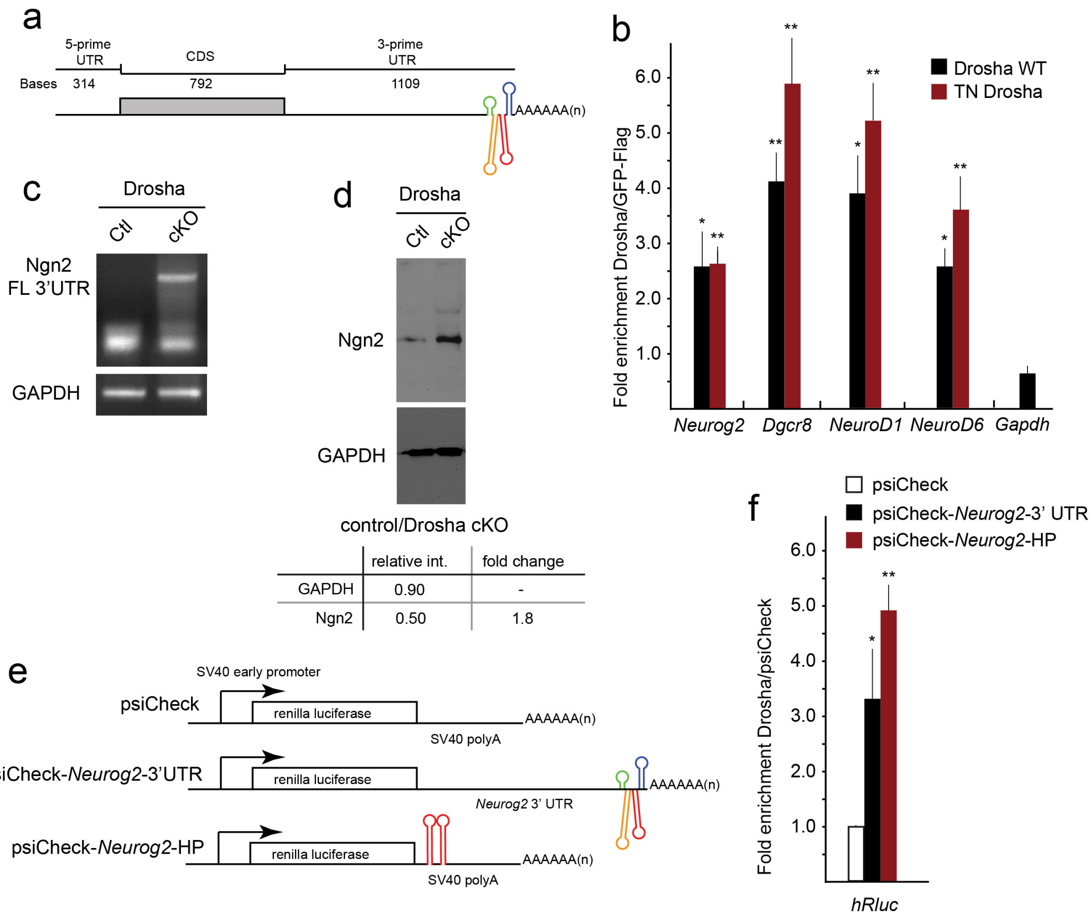

Figure 37: *Neurog2* mRNA contains hairpins bound by Drosha

a. Schematic representation of the mouse *Neurog2* mRNA, which contains 4 conserved hairpins in the 3' UTR (EvoFold prediction) **b.** qRT-PCR analysis of *Neurog2, DGCR8, NeuroD1, NeuroD6* and *GAPDH* transcripts CLIPed from N2A cells after Drosha-flag or transdominant (TN) Drosha-flag expression. Statistical analysis of CLIPed products corrected relative to input RNA concentrations compared to flag-GFP CLIPed samples. tTest *P<0.05 and **P<0.001 **c.** 3'-RACE analysis of full-length 3'*Neurog2* mRNA (FL 3' UTR) in control (Ctrl: Drosha$^{flox/WT}$) and *Drosha* cKO neurospheres. **d.** *Drosha* cKO results in increase in Ngn2 protein in neurospheres compared to control. Values standardized to GAPDH levels using ImageJ software. **e.** Scheme of the mouse *Renilla luciferase* constructs expressing mRNAs containing either synthetic SV40 Poly(A) sequences (psiCheck), psiCheck-*Neurog2*-3' UTR or a synthetic SV40 Poly(A) containing a tandem repeat of the *Ngn2* hairpin (psiCheck-*Neurog2*-HP) **f.** qRT-PCR analysis of humanized *Renilla luciferase* (*hRluc*) mRNA from psiCheck-*Neurog2*-3' UTR and psiCheck-*Neurog2*-HP CLIPed from N2A relative to psiCheck. Values are fold enrichment over CLIPed control (psiCheck). CLIPed products are corrected relative to input RNA concentrations compared to Flag-Drosha. tTest *P<0.05 and **P<0.001

Investigating if binding of Drosha to *Neurog2* mRNA affects transcript stability we tested if intact 3' ends were still present in control conditions or after *Drosha* cKO. Therefore, sorted NPs from electroporated *Drosha*$^{flox/flox}$ and control (*Drosha*$^{flox/Wt}$) embryos, which were deleted for Drosha upon cre-mediated recombination of the floxed locus, were used. RNA of the sorted NPs was isolated and the transcripts were polyadenylated *in vitro*, followed by 3' rapid amplification of cDNA ends (RACE) rt-PCR, using an anchored oligo(dt) RACE primer. For the amplification a *Neurog2*-specific 5' primer that spanned the hairpin region, and an anchored binding primer as reverse primer were used. After *Drosha* cKO an amplicon of the predicted size was detected whereas no *Neurog2* transcripts containing the intact 3' end of the *Neurog2* mRNA were detected in the presence of Drosha (Fig. 37c). This change is also reflected in Ngn2 protein level, which is increased nearly two fold after Drosha deletion (Fig. 33d). Therefore, intact 3' ends of the *Neurog2* transcript, which include the conserved hairpin, are present after Drosha deletion, whereas they are absent in the presence of a functional MP.

To assess if the hairpin structures in the 3' end of *Neurog2* are bound by the MP we again performed CLIP. This time Flag-tagged Drosha was expressed together with a *Renilla luciferase (hRluc)* reporter. The *hRluc* constructs contained either *Neurog2* 3' UTR or two copies of the hairpin present in the 3' UTR of their downstream sequence (Fig. 37e). qRT-PCR analysis of the precipitated mRNA was performed using specific primers against *hRluc*. *hRluc* mRNA bound to Drosha via the *Neurog2* 3' UTR as well as *Neurog2* HP and we detected a 3 and 5 fold increase over control (Fig. 33e,f). No mRNA was pulled down with the control construct (psiCheck) with Flag-tagged Drosha. We therefore conclude that the conserved hairpin (bases 2044 – 2022) in the 3' end of *Neurog2* is sufficient to mediate binding to Drosha and the MP.

9.1 Discussion

Neurogenesis is a multistep developmental process that is key to CNS function and plasticity. The mammalian cortex, one of the most complex structures of the brain, is composed of various cell types which arise from NSCs during embryonic development (Guillemot, 2005). Canonical Notch signalling maintains NSCs by regulation of transcription factors of the Hes and proneural gene families. *Hes* genes are expressed in an oscillatory fashion and negatively regulate neurogenic transcription factors including *Neurog2* (Fig. 38). In fact, mRNA and protein levels of Hes1 and Ngn2 were shown to oscillate in NSCs in a complementary manner (Kageyama et al., 2009; Shimojo et al., 2008). Paradoxically, mRNAs of neurogenic transcription factors are readily expressed in NSCs and it has been hypothesized, that the lack of induction of neuronal differentiation is the consequence of post-transcriptional mechanisms that destabilize mRNAs. In our study we show that the mRNA levels of the proneural transcription factor Ngn2 is regulated by direct binding and destabilization by the MP, which happens independent of miRNA and Dicer1.

Expression analysis of *Drosha* by *in situ* hybridisation displayed high *Drosha* levels in NPs in the VZ and differentiating neurons in the CP, which is in agreement with independently reported data from a genome wide transcription atlas (http://www.eurexpress.org). The same database shows a correlating *Dgcr8* expression, whereas *Dicer1* is not present in NPs of the developing forebrain. This explains partly why Dicer1 ablation did not affect NPs. In fact, comparison of *Dicer1* and *Dgcr8* KO revealed distinct phenotypic differences (Babiarz et al., 2011). *Dicer1* cKO from the developing telencephalon resulted in impaired differentiation and cell death (De Pietri Tonelli et al., 2008). Likewise we observed apoptosis 4 days after *Dicer1*-depletion, as only fragmented cell debris remained in the SVZ and CP. In comparison, cKO of *Drosha* resulted in a less severe phenotype since only few apoptotic cells were found after 4 days. Apoptosis was therefore occurring upon loss of mature miRNAs, therefore no cell death could be detected at early time points after *Drosha* or *Dgcr8* depletion (data not shown). The more severe apoptosis phenotype after Dicer1 depletion can be explained by the additional functions of the protein during maturation of small interfering RNAs (siRNAs) or noncanonical miRNAs (Babiarz et al., 2008; Ruby et al., 2007).

Drosha cKO in NPs caused precocious differentiation and exit from the VZ within 24 hours. Similarly *Dgcr8* KD promoted differentiation *in vivo*, showing that MP inactivation was causing the phenotype. In contrast, NPs conditionally depleted for *Dicer1* retained stem cell markers. The observation of two distinct phenotypes after *Dicer1* deletion or MP inactivation suggests that the effect is not resulting from alterations in mature miRNA levels. This was also supported by the fact that the changes caused by *Drosha* and *Dgcr8* deletion were already visible after 24 hours, a time-frame too short to allow for essential shifts in miRNA levels. Analysis of Drosha depleted cells confirmed that mature miRNA levels were unchanged at the time point when Drosha phenotype occurred, which is therefore independent of miRNA loss.

The loss-of-function data showed, that the MP is necessary to maintain stem cell potential and prevent early differentiation. Precocious differentiation and exit from the VZ after MP inactivation was going along with changes in proneural gene mRNA levels. *Neurog2* and its downstream effector *NeuroD1* were increased upon *Drosha* cKO whereas their levels were unchanged after *Dicer1* deletion. Expression of Ngn2 in NPs was sufficient to induce differentiation and exit from the VZ and phenocopied the changes after *Drosha* deletion. Furthermore we were able to rescue the Drosha phenotype via shRNA-mediated KD of *Neurog2*, showing that Ngn2 expression is necessary to induce VZ exit of NPs. These findings demonstrate, that increased Ngn2 levels are sufficient and necessary to induce precocious differentiation and suggest a direct effect of Drosha loss on *Neurog2* levels. It needs to be investigated though if the increase in *NeuroD1* occurs downstream of Ngn2, or whether this is directly dependent on *Drosha* deletion.

Drosha binds and affects transcript stability of *Dgcr8*, by binding to hairpin structures embedded in the *Dgcr8* mRNA (Han et al., 2004). Concordantly we observed an increase in *Dgcr8* levels after *Drosha* deletion, whereas *Dicer1* cKO did not cause this effect. In addition, Drosha and the MP were reported to directly affect mRNA stability in a miRNA independent manner by cleavage of pre-miRNA-like hairpins (Chong et al., 2010; Macias et al., 2012). *Neurog2,* *NeuroD1 and NeuroD6* mRNA were predicted by EvoFold and Mfold algorithms to contain evolutionary conserved hairpins in the 3' UTR. The transcripts were bound by Drosha and in the case of *Neurog2* we specified, that the binding took place via the conserved hairpin structures (Fig. 38). This interaction mediated cleavage of the 3' UTR, as no intact 3' ends of the *Neurog2* transcript were detected in the presence of Drosha. Upon *Drosha* cKO *Neurog2* mRNA containing the 3' UTR as well as the Ngn2 protein were abundant. However, we did not identify the exact cleavage site of the *Neurog2* hairpin. Drosha was also binding to *NeuroD1* and *NeuroD6*, suggesting a general mechanism of proneural gene regulation by the MP. This needs to be confirmed though as we did not formally proof cleavage of *NeuroD1* and *NeuroD6* by the MP.

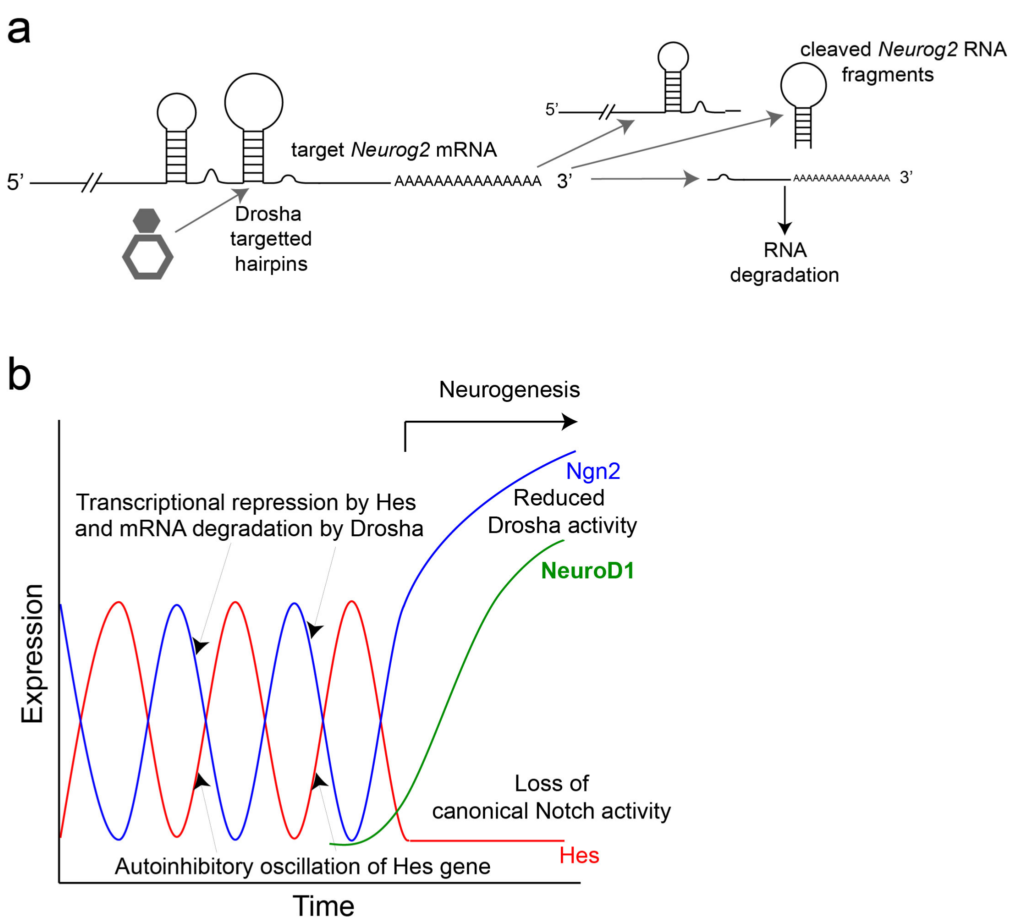

Figure 38. Drosha and the microprocessor regulate proneural gene expression in NPs a. Drosha directly binds *Neurog2* mRNAs in NPs, which results in cleavage of the conserved hairpin localized in the 3' UTR and degradation of the mRNA. **b.** Scheme of dynamic expression of *Hes* and the proneural genes *Neurog2* and *NeuroD1* in NPs. *Hes* genes transcriptionally repress their own levels, which results in an oscillatory expression. Conversely Ngn2 is expressed in an oscillatory fashion in NPs. Drosha prevents accumulation of Ngn2 by destabilization of the mRNA and thus inhibits precocious differentiation of NPs.

Tight temporo-spatial control of embryonic neurogenesis is required to ensure proper development of the cortex, which is achieved by neurogenic transcription factors. The discovery of microprocessor-dependent and Dicer1-independent *Neurog2* mRNA destabilization during embryonic neurogenesis represents a novel regulatory mechanism during forebrain development. This mechanism is crucial to maintain NSCs and prevent early differentiation and is possibly also involved in the regulation of other systems where hypostable transcription factors are at work. Therefore, it would we interesting to investigate other proneural genes that are involved in NP differentiation such as *Atoh1*, *Ascl1* and *Neurog1*. Whereas Ngn1 and Ngn2 are important in development of the dorsal telencephalon Ascl1 is expressed in the subpallium where it controls ventral fate. It is very likely that transcript destabilization through Drosha is a conserved mechanism in NP differentiation and occurs as well in other parts of the brain and not only in the dorsal telencephalon. This assumption is supported by conserved hairpin structures that are predicted for *Neurog1* and *Atoh1*. NeuroD family members are transcriptional targets of proneural genes, which are activated upon neuronal differentiation. Evolutionarily conserved hairpin structures were also predicted in *NeuroD6* and *NeuroD1*, which are potential target sites for the MP. It would therefore be very interesting to investigate if Drosha does not only act at the level of the proneural genes but in addition keeps their target genes in check.

We showed in the CLIP experiment that Drosha is binding *Neurog2* mRNA, which results in cleavage of the 3’ UTR. However, we did not identify the exact cleavage site of the hairpin or determine whether the MP has different binding affinities for *NeuroD1, NeuroD6* and *Neurog2*. These would be interesting points to address in order to identify any domain specific regulation of proneural factors at the post-transcriptional level.

With the Drosha mediated and Dicer1-independent cleavage of the proneural gene *Neurog2* we identified a novel mechanism of NP regulation. In the expression analysis we detected *Drosha* transcript not only in NPs in the VZ but also at high levels in differentiating immature neurons in the CP. It is therefore likely that Drosha is not only important for NSC maintenance but also for differentiation of neurons. The MP potentially regulates proneural factor mRNA stability throughout neuronal commitment, controlling changes in transition from stem cells to basal progenitor cells to neurons. One could therefore investigate Drosha-bound transcripts in various cell types present during cortical development.

In our previous study we focused on specific proneural genes which were predicted to harbour conserved hairpin structures and checked for Drosha binding and regulation. However, there might be a whole array of non-miRNAs in NSCs and potentially neurons that are regulated by the MP. This could be addressed by Drosha CLIP-Seq analysis, which can be performed not only in embryonic but also adult NSCs and other cell populations. Thereby the non-miRNAs bound by the MP can be identified by correlating the data with analysis of miRNA expression by NSCs, which has been performed previously in the lab.

9.2 Published Article

Drosha regulates neurogenesis by controlling Neurogenin 2 expression independent of microRNAs

Philip Knuckles[1,8], Miriam A Vogt[1,2,8], Sebastian Lugert[1,2], Marta Milo[3], Mark M W Chong[4,5], Guillaume M Hautbergue[6], Stuart A Wilson[6], Dan R Littman[4,7] & Verdon Taylor[1,2]

Temporal regulation of embryonic neurogenesis is controlled by hypostable transcription factors. The mechanism of the process is unclear. Here we show that the RNase III Drosha and DGCR8 (also known as Pasha), key components of the microRNA (miRNA) microprocessor, have important functions in mouse neurogenesis. Loss of microprocessor in forebrain neural progenitors resulted in a loss of stem cell character and precocious differentiation whereas Dicer deficiency did not. Drosha negatively regulated expression of the transcription factors Neurogenin 2 (Ngn2) and NeuroD1 whereas forced Ngn2 expression phenocopied the loss of Drosha. *Neurog2* mRNA contains evolutionarily conserved hairpins with similarities to pri-miRNAs, and associates with the microprocessor in neural progenitors. We uncovered a Drosha-dependent destabilization of *Neurog2* mRNAs consistent with microprocessor cleavage at hairpins. Our findings implicate direct and miRNA-independent destabilization of proneural mRNAs by the microprocessor, which facilitates neural stem cell (NSC) maintenance by blocking accumulation of differentiation and determination factors.

miRNAs are small noncoding RNAs that inhibit translation, and destabilize and deadenylate target mRNAs[1,2]. Identity between target mRNA and the 'seed' sequence at the 5′ end of the miRNA is essential to attenuate translational output, whereas incomplete base pairing at the 3′ end of the miRNA allows target heterogeneity[3,4]. miRNAs are generated predominantly through a multistep process. In canonical miRNA processing, a long primary transcript, the pri-miRNA, is cleaved by the microprocessor. The central components of the microprocessor, DGCR8 and Drosha, form a multimeric complex that binds double-stranded hairpins of pri-miRNAs and cleaves them, releasing the stem-loop pre-miRNA[5–7]. The pre-miRNA is exported from the nucleus and processed to a mature double-stranded miRNA by Dicer[8]. miRNAs are loaded onto the RNA-induced silencing complex (RISC). Some miRNAs are generated independently of the microprocessor, including from pre-miRNA like transcripts called mirtrons released by the splicing machinery[9,10] and from small nucleolar RNAs[11–13]. Some miRNAs are also generated independently of Dicer by the RNase III Argonaute 2 (refs. 14–16). Despite crucial roles in miRNA production, conditional knockout (cKO) of *Dicer1* has no obvious effect on embryonic forebrain neural stem cells, indicating that miRNAs are not critical for cortical neurogenesis but are important for neuronal survival[17,18]. In retinal progenitors, loss of *Dicer1* results in a defect in the transition from early to late progenitor stages[19]. Similarly, *Dgcr8* cKO from neurons results in less cell death than in *Dicer1* mutants, implying functions for noncanonical miRNAs in the brain[18]. However, Dicer also regulates *Alu* RNA levels in retinal pigmented epithelial cells by degradation, preventing their accumulation and toxicity[20].

Development of the mammalian central nervous system is highly controlled. Radial glial stem cells line the lumen of the neural tube, form the ventricular zone and are the major source of neurons throughout the brain[21]. Radial glial stem cells in the dorsal telencephalon generate basal progenitors, a committed intermediate cell type that populates the subventricular zone[22]. Basal progenitors generate neurons that migrate to superficial layers of the forming cortex. Notch signaling activates *Hes* genes, maintains stem or progenitor cells and represses neurogenesis by suppressing transcription of proneural genes including *Ascl1*, *Atoh1* and *Neurog* genes[23]. Paradoxically, proneural genes are expressed by ventricular-zone progenitors at low levels. The proneural basic helix-loop-helix factors control neurogenic differentiation and immature neuronal migration through a cascade of transcriptional regulation[24]. Hes proteins are in an unstable autoregulatory feedback loop, which results in oscillating expression[25]. In turn, mRNAs of the proneural factors are also hypostable, and the factors themselves are regulated post-transcriptionally[25,26]. Although much is known about the regulation of the neurogenic transcription factors at the transcriptional level[27,28], little is known about post-transcriptional regulation. mRNA degradation and destabilization have crucial roles in preventing aberrant accumulation of neurogenic factors and abnormal neurogenesis. Hence, the regulated stability

[1]Department of Molecular Embryology, Max Planck Institute of Immunology, Freiburg, Germany. [2]Embryology and Stem Cell Biology, Department of Biomedicine, University of Basel, Basel, Switzerland. [3]National Institute for Health Research Cardiovascular Biomedical Research Unit, Sheffield Teaching Hospitals National Health Service Trust, University of Sheffield, Sheffield, UK. [4]Molecular Pathogenesis Program, Kimmel Center for Biology and Medicine, Skirball Institute of Biomolecular Medicine, New York University School of Medicine, New York, New York, USA. [5]The Walter and Eliza Hall Institute of Medical Research, Parkville, Victoria, Australia. [6]Department of Molecular Biology and Biotechnology, University of Sheffield, Sheffield, UK. [7]Howard Hughes Medical Institute, New York University School of Medicine, New York, New York, USA. [8]These authors contributed equally to the work. Correspondence should be addressed to V.T. (verdon.taylor@unibas.ch).

Received 26 April; accepted 14 May; published online 17 June 2012; doi:10.1038/nn.3139

of the neurogenic transcription factor cascade is critical for normal brain development. The destabilization mechanisms that control proneural mRNAs, including those encoding Ngn2 in the embryonic forebrain, are not clear.

Here we show that, unlike Dicer, the microprocessor is essential during early stages of mammalian forebrain neurogenesis. The microprocessor directly binds to and destabilizes the *Neurog2* mRNA in a Dicer- and miRNA-independent process. Thus, Drosha and the microprocessor regulate the dynamics of proneural factor mRNA degradation, providing molecular inhibition of Ngn2 accumulation, thereby controlling progenitor-cell maintenance and neurogenic differentiation.

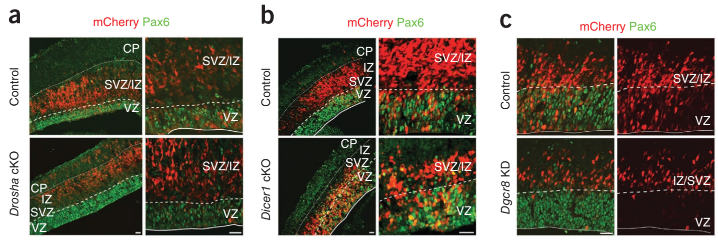

Figure 1 Microprocessor inactivation at E13.5 induces neural-progenitor differentiation and results in a distinct phenotype compared to *Dicer1* cKO. (**a**) Fluorescence images of sections show that *Drosha* cKO neural progenitors exit the ventricular zone (VZ) (by embryonic day 15.5), entering the SVZ/IZ and some precociously migrate to the cortical plate (CP). *Drosha* cKO cells downregulate the progenitor marker Pax6. (**b**) *Dicer1* cKO neural progenitors express the progenitor marker Pax6 and do not precociously exit the VZ. (**c**) shRNA *Dgcr8* knockdown (KD) at embryonic day 13.5 results in downregulation of Pax6 and neural progenitor exit from the VZ, transfected cells monitored by mCherry expression. Dashed lines mark the boundaries between the VZ, SVZ/IZ and CP. All scale bars, 20 μm.

RESULTS

The microprocessor is critical for embryonic neurogenesis

Drosha is expressed in the developing CNS by forebrain progenitors and differentiating neurons in the cortical plate (**Supplementary Fig. 1a**). We assessed Drosha function by cKO of its gene from Notch signaling neural progenitors by expressing Cre recombinase from the *Hes5* regulatory elements in *loxP*-flanked (floxed) *Drosha* embryos (**Supplementary Fig. 1b–d**). *Drosha* cKO resulted in a loss of neural progenitor marker Pax6, precocious exit of cells from the ventricular zone, and entry into the subventricular or intermediate zone (SVZ/IZ). *Drosha* cKO cells migrated to the cortical plate, which is consistent with precocious differentiation (**Fig. 1a**). In contrast, *Dicer1* cKO neural progenitors retained progenitor-marker expression and did not precociously exit the ventricular zone (**Fig. 1b**). Hence, loss of Drosha resulted in a neural progenitor phenotype distinct from one resulting from the loss of Dicer and presumably miRNAs[17,29].

We confirmed our *Drosha* cKO findings using short hairpin RNAs (shRNAs) to knock down *Drosha* in neural progenitors. Progenitors subjected to *Drosha* knockdown had reduced Pax6 and Sox2 expression, and lost radial morphology and contact to the apical surface of the ventricular zone (**Supplementary Figs. 2a–g** and **3**). Neural progenitors of the ventricular zone rely on Notch signaling and express *Hes5* (refs. 30,31). *Drosha* knockdown in neural progenitors resulted in a loss of *Hes5* expression, consistent with loss of both canonical Notch activity and stem or progenitor status (**Supplementary Fig. 4**).

We also expressed a catalytically inactive transdominant-negative Drosha[32] in neural progenitors. Most transdominant negative Drosha–expressing neural progenitors exited the ventricular zone and turned down Pax6 expression (**Supplementary Fig. 2f,g**). To address whether the Drosha effects required the core microprocessor components, we knocked down *Dgcr8* by shRNA expression. *Dgcr8* knockdown resulted in rapid loss of progenitor markers (DGCR8, 17.9 ± 5.8% and control, 36.8 ± 2.6%, ± s.e.m.; $P < 0.001$: **Fig. 1c**) and exit from the ventricular zone, phenocopying the loss of Drosha. Drosha or DGCR8 inactivation did not result in apoptosis at early time points (**Supplementary Fig. 5**). Thus, neural progenitors of the developing forebrain depend upon Drosha and microprocessor function and lose progenitor status upon inactivation.

Inactivation of Drosha does not induce cell-cycle exit

Cell cycle and differentiation in the developing forebrain are intimately connected[33]. Blocking cell cycle induces neural-progenitor differentiation and exit from the ventricular zone[34]. The microprocessor, miRNAs and Dicer have all been linked to cell-cycle regulation in other systems[35,36]. However, *Drosha* knockdown cells remained in the cell cycle, expressing Ki67 (*Drosha* knockdown cells, 35.5 ± 9.2%, control, 36.6 ± 7.0%: **Fig. 2a**) even in the SVZ/IZ. Although reduced in number compared to controls, some cells remaining in the ventricular zone of *Drosha* knockdown mice were proliferating, and this corresponded to an increase in mitotic cells in the subventricular zone (**Fig. 2b**). BrdU incorporation 3 h before killing the mice revealed a moderate reduction in S-phase labeling of *Drosha* knockdown cells (**Fig. 2c,d**). Together with maintained Ki67 expression this suggested slowing of the cell cycle rather than premature exit. Loss of Drosha did not affect the total number of BrdU-labeled cells when cells were labeled 48 h after knockdown (**Fig. 2d**). However, the reduction in the number of BrdU-labeled cells in the apical region of the ventricular zone and a concomitant increase in the subventricular zone was consistent with *Drosha* knockdown inducing a transition from a ventricular zone stem or progenitor cell to a basal progenitor (**Fig. 2e,f**).

Tbr2 is expressed by basal progenitors in the subventricular zone. Tbr2 expression did not increase as a result of *Drosha* knockdown (**Supplementary Fig. 6a–c**). We did not observe differences in Tbr2 expression in the SVZ/IZ when comparing *Drosha* knockdown cells to controls even after 48 h when most *Drosha* knockdown cells had exited the ventricular zone (**Supplementary Fig. 6d**). We found that many *Drosha* knockdown cells had not only exited the ventricular zone and entered the subventricular zone but had migrated to the intermediate zone (**Supplementary Fig. 6b**). Tbr1 and NeuN are associated with postmitotic neurons at this stage, but their expression was not affected by *Drosha* knockdown (data not shown). Hence, reduced Drosha and microprocessor activity promoted a rapid transition of ventricular-zone progenitors to mitotically active subventricular-zone progenitors.

miRNAs levels are not affected by *Drosha* knockdown

The difference in phenotype between microprocessor inactivation and *Dicer1* cKO suggested that the effects induced by Drosha or DGCR8 inactivation may not be the result of changes in mature miRNA levels. Furthermore, the phenotype alterations following conditional disruption of Drosha and DGCR8 expression were evident by 24 h, a timeframe too short to remodel the cellular transcriptome and proteome through changes in miRNA levels. We addressed whether miRNA levels were altered as a result of loss of Drosha. We sorted *Drosha* cKO and control neural progenitors from embryonic day 15.5 (E15.5)

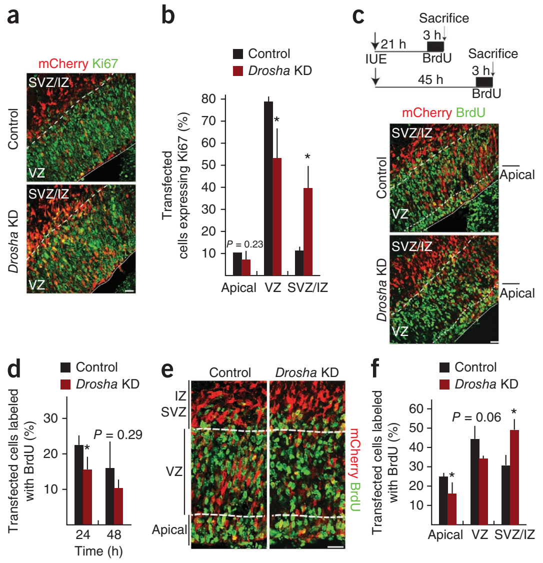

Figure 2 *Drosha* knockdown reduces S-phase labeling but does not induce cell-cycle exit. (**a**) *Drosha* knockdown cells exit the ventricular zone (VZ) but remain in the cell cycle and express Ki67 in the SVZ/IZ. Transfected cells were identified by pCAGGs::mCherry expression. (**b**) Distribution of Ki67-expressing cells throughout the VZ and SVZ/IZ. 'Apical', cells in the apical-most aspect of the VZ. (**c**) Scheme of BrdU labeling procedure of embryonic day (E) 13.5 mice with a BrdU pulse 21 h after electroporation and 3 h before killing them (sacrifice) (top). Staining of embryos 24 h after knockdown (bottom). Dashed lines mark the VZ–SVZ/IZ boundary, dotted lines mark the cells in the apical VZ. Transfected cells were identified by pCAGGs::mCherry expression. (**d**) Quantification of total BrdU-labeled cells 24 h and 48 h after knockdown. (**e**) Magnification of the VZ, SVZ/IZ and the region defined as apical VZ. (**f**) Quantification and distribution of BrdU-labeled cells 24 h after transfection. Apical, apical region of the VZ. *t* test: $^*P < 0.05$. Error bars, s.e.m. For **b**: control, $n = 3$; *Drosha* knockdown, $n = 4$. For **d**,**f**: control, $n = 4$; *Drosha* knockdown, $n = 4$. IUE, *in utero* electroporation. All scale bars, 20 µm.

embryos, isolated small RNAs and generated expression profiles of 381 miRNAs (**Supplementary Fig. 6e**). We detected 187 miRNAs in neural progenitors (cycle threshold value below 32; **Supplementary Table 1**), and their levels were not substantially changed 48 h after *Drosha* cKO ($R^2 = 0.93$; **Fig. 3a**) even though the mutant phenotype was well established. Hence, *Drosha* cKO did not cause global changes in miRNA levels.

To gauge general miRNA stability and address whether mature miRNA levels changed after disrupting microprocessor function, we knocked down *Drosha* or *Dgcr8* in N2A cells and analyzed selected miRNAs by quantitative PCR. The abundance of none of the miRNAs analyzed (miR15a, miR9, miR30d and miR124a) was affected by *Drosha* or *Dgcr8* knockdown (**Supplementary Fig. 7a**,**b**). In agreement with recent reports[37], these data confirm the relative stability of mature miRNAs and that blocking microprocessor function for 24 h does not significantly affect their levels.

Drosha is required for maintenance of NSC self-renewal

NSCs form neurospheres and retain the capacity to self-renew *in vitro*. We addressed the role of Drosha in NSC maintenance by conditional inactivation from spherogenic embryonic forebrain cells. We ablated *Drosha* from NSCs with Cre recombinase–expressing adenovirus (**Supplementary Fig. 6f**,**g**). Sphere-forming potential of *Drosha* cKO NSCs was reduced 45% compared to that in control cells heterozygous for floxed and wild-type *Drosha* alleles ($Drosha^{flox/WT}$) NSCs (**Fig. 3b**). After dissociation and replating, Drosha-deficient NSCs continued to show impaired sphere-forming (self-renewing) ability (**Fig. 3b**). In accordance with the phenotype differences observed by acute depletion of Drosha and Dicer *in vivo*, Drosha-deficient neurospheres showed distinct defects compared to Dicer-deficient neurospheres[38], which could be propagated indefinitely[38].

Microprocessor inactivation induced a rapid loss of neural progenitor status without obvious effects on miRNAs. We compared *Drosha* and *Dicer1* cKO cells 4 d after ablation. *Dicer1* cKO cells had undergone cell death *in vivo* and only fragmented cell debris remained in the SVZ/IZ and cortical plate. *Drosha* cKO brains showed increased cell death over control brains, although cell death was less severe than in the *Dicer1* cKO (**Supplementary Fig. 5a**–**d**). These results are similar to findings after *Dgcr8* cKO in neurons[18] and suggested that the cell death in *Drosha* cKO cells at 4 d may reflect reduced miRNA amounts. We profiled miRNAs in *Drosha* cKO NSCs 5 d after ablation. We detected 135 miRNAs in control NSCs and only 44 miRNAs in Drosha-deficient NSCs 5 d after cKO (**Supplementary Tables 2** and **3**). Expression of remaining miRNAs was dramatically reduced in *Drosha* cKO cells ($R^2 = 0.2091$; **Supplementary Fig. 7c**). Hence, *Drosha* ablation resulted in a delayed reduction in miRNAs and cell death of maturing neurons.

Drosha regulates proneural gene mRNA levels

We analyzed the effects of *Drosha* cKO on NSC gene expression. Ablation of *Drosha* from dorsal telencephalic NSCs reduced *Sox2* mRNA levels, consistent with a loss of neural progenitors in contrast to Dicer1-deficient NSCs, which retain stem-cell markers (**Fig. 3c**)[38]. Drosha regulates DGCR8 expression directly in a miRNA-independent fashion by cleaving hairpins in its mRNA[32]. *Drosha* cKO from NSCs resulted in a 2.8-fold increase in *Dgcr8* mRNA levels, supporting inhibition of the microprocessor (**Fig. 3c**). Proneural transcription factors of the Ngn, Ascl and Atoh families are pivotal regulators of mammalian neurogenesis[39]. Ngn2 is important for neurogenesis in the dorsal forebrain[40] and regulates the expression of downstream effectors including NeuroD1. *Neurog2* mRNA levels were increased tenfold after *Drosha* cKO compared to control cells but were not changed by *Dicer1* cKO (**Fig. 3c**). Consistent with *Drosha* cKO cells losing NSC status and commencing differentiation, mRNA levels of Ngn2 downstream target NeuroD1 were also increased (**Fig. 3c**). We examined the expression of *Ascl1* and *Atoh1* mRNAs, which encode two proneural factors that regulate ventral and dorsal midline neurogenesis, respectively. Neither mRNA was expressed at high levels, nor was the abundance of their mRNAs altered after *Drosha* cKO (data not shown).

We next addressed whether Drosha regulates *Neurog2* mRNA levels in another system. *Drosha* knockdown in N2A cells reduced *Drosha* mRNA levels by > 55% and protein amounts to barely detectable levels (**Fig. 3d** and **Supplementary Fig. 2a**). *Neurog2* mRNA levels were increased 5.3-fold in *Drosha* knockdown N2A cells relative to control cells, indicating that Drosha may directly regulate Ngn2 in neural progenitors (**Fig. 3c**,**d**). We addressed whether *Neurog2* and *Neurod1* mRNAs are regulated *in vivo* after *Drosha* knockdown. We expressed *Drosha* or control shRNAs in dorsal forebrain neural progenitors and also transfected them with an mCherry expression vector for sorting.

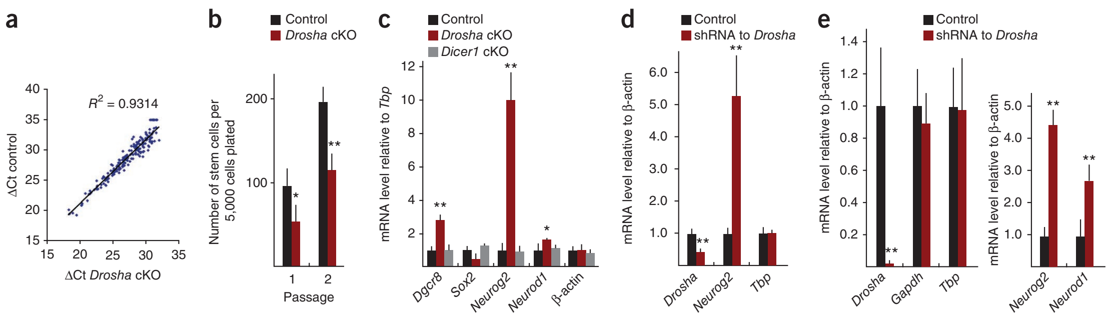

Figure 3 Drosha regulates proneural mRNA levels. (**a**) Change in cycle threshold (ΔCt) plot of relative miRNA expression profiles of control (*Drosha*$^{flox/WT}$) and *Drosha* cKO neural progenitor cells. R^2 = 0.9314 indicates no change in miRNA levels 24 h after *Drosha* cKO. (**b**) *Drosha* cKO NSCs *in vitro* (neurospheres) have reduced self-renewal potential and do not recover their potential after passaging. (**c**) qrt-PCR analysis of *Drosha* cKO and *Dicer1* cKO neurospheres demonstrating loss of progenitor-associated *Sox2* and increased Ngn2 and NeuroD1 mRNA levels following inactivation of *Drosha* but not *Dicer1*. *Dgcr8* mRNA levels also increased in *Drosha* cKO cells. (**d**) Drosha regulates *Neurog2* mRNA levels also in neuroblastoma N2A cells. (**e**) Drosha mRNA levels are reduced by expression of *Drosha* shRNAs in *in vivo*–electroporated neural progenitors (sorted by flow cytometry); this results in increased *Neurog2* and *Neurod1* mRNA levels in embryonic neural progenitors *in vivo*. *t* test: $*P < 0.05$ and $**P < 0.001$. Error bars, s.e.m. (n = 3).

Twenty-four hours after knockdown we sorted the transfected cells from pools of embryos, isolated mRNA and performed quantitative real-time PCR (qrt-PCR) (**Supplementary Fig. 5e**). *Drosha* mRNA levels were reduced, and expression of both *Neurog2* and *Neurod1* mRNAs increased 4.6-fold and 2.8-fold, respectively (**Fig. 3e**). These findings indicated that Drosha regulates *Neurog2* mRNA levels in neural progenitors.

Microprocessor-depleted progenitors express *Neurog2*

The mRNA and protein levels of the proneural genes are dynamic during NSC commitment and differentiation[25]. We analyzed the expression of Ngn2 after *Drosha* knockdown *in vivo* and found almost twice as many Ngn2-expressing cells compared to controls (**Fig. 4a**,**b**). *Dgcr8* knockdown resulted in a similar increase in Ngn2-expressing cells indicating that the elevated *Neurog2* mRNA levels caused by microprocessor inactivation translated into increased protein expression (**Fig. 4b**). Ngn2 is stabilized in differentiating neurogenic progenitors to induce commitment and is reduced by the time precursors have entered the subventricular zone. Most control neural progenitors that expressed Ngn2 were restricted to the ventricular zone (**Fig. 4a**). By contrast, many *Drosha* knockdown and *Dgcr8* knockdown cells (data not shown) in the SVZ/IZ retained weak Ngn2 expression in an ectopic basal location (**Fig. 4a**). This suggested that loss of microprocessor activity resulted not only in an increase Ngn2 protein but also extended expression of *Neurog2* into later stages of the neurogenic lineage.

To test whether increased amounts of Ngn2 result in activation of downstream targets, we generated a *Neurod1* promoter construct that drives mCherry expression (*NeuroD*∷*mCherry*) (**Fig. 4c**). After transfection, *NeuroD*∷*mCherry* is expressed in cells within the SVZ/IZ but not in the ventricular zone, consistent with endogenous *Neurod1* expression (**Fig. 4d**). We expressed *NeuroD*∷*mCherry*, pCAGGs∷eGFP (transfection reporter expressing eGFP) and either *Drosha* or control shRNA constructs in neural progenitors *in vivo* and analyzed activation of the *Neurod1* promoter (mCherry expression). Many control transfected cells (expressing an shRNA directed against *Renilla* luciferase–GFP) and predominantly those in the SVZ/IZ, expressed mCherry (*NeuroD*∷*mCherry*), consistent with an onset of neurogenic differentiation (**Fig. 4d**). Control cells (GFP-expressing) in the ventricular zone did not express mCherry (*NeuroD*∷*mCherry*) as these cells presumably remained as uncommitted ventricular-zone progenitors. The majority of the *Drosha* knockdown cells activated *NeuroD*∷*mCherry*, and expression of this transgene was particularly prominent in the cells in the SVZ/IZ. In addition, the number of neural progenitors in the apical ventricular zone that expressed mCherry (*NeuroD*∷*mCherry*) increased 2.7-fold (*Drosha* knockdown, 4.0 ± 0.6% and control, 1.5 ± 1.0%; $P < 0.05$). This was consistent with the increased expression of Ngn2 leading to precocious activation of *Neurod1* transcription by Drosha-depleted neural progenitors.

Expression of Ngn2 phenocopies *Drosha* knockdown

We postulated that microprocessor inactivation stabilized *Neurog2* mRNA and increased translation of Ngn2 protein, initiating neurogenesis by activation of targets. We addressed whether increased Ngn2 expression is sufficient to induce neural-progenitor differentiation and exit from the ventricular zone. Expression of Ngn2 resulted in a loss of stem or progenitor markers including Pax6 and induced exit of neural progenitors from the ventricular zone, similar to inactivation the microprocessor (**Fig. 5a**). Even the few remaining cells in the ventricular zone turned down Pax6 expression after Ngn2 expression (Ngn2, 49.2 ± 12.7% and control, 25.1 ± 2.5%; $P < 0.05$: **Fig. 5b**). We co-transfected neural progenitors *in vivo* with *NeuroD*∷*mCherry*, pCAGGs∷eGFP and either pCAGGs∷Ngn2 or control pCAGGs∷empty constructs. Ngn2 expression induced the *Neurod1* promoter not only in SVZ/IZ cells but also ectopically in neural progenitors in the ventricular zone (**Fig. 5c**). Like Drosha and microprocessor inactivation, Ngn2 expression was not sufficient to induce Tbr2 expression *in vivo* (Ngn2, 42.2 ± 3.6% of transfected cells and control, 43.5 ± 3.6%; P = 0.68). Hence, Ngn2 is sufficient to induce neural progenitor exit from the ventricular zone, activate a neurogenic differentiation program and phenocopy loss of microprocessor activity.

We addressed whether Ngn2 expression was necessary for the ventricular-zone exit induced by the loss of Drosha and whether shRNA-mediated *Neurog2* knockdown could rescue the phenotype change. We knocked down *Drosha* and at the same time *Neurog2* using two independent shRNA constructs and analyzed neural progenitors after 24 h. *Drosha* and *Neurog2* double knockdown neural progenitors resembled control scrambled shRNA–expressing

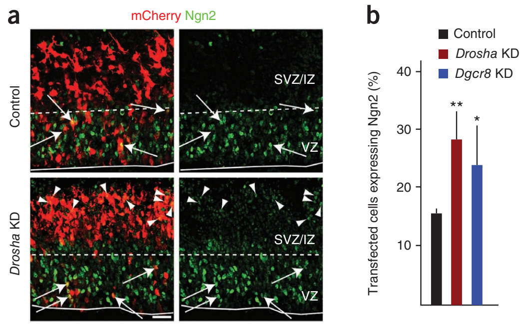

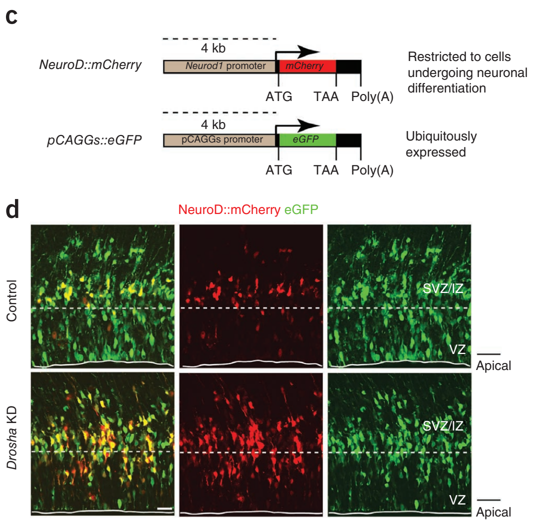

Figure 4 *Drosha* knockdown induces Ngn2 protein expression and activation of neurogenesis. (**a**) *Drosha* knockdown (KD) cells express Ngn2 in the ventricular zone (VZ) (arrows) and retain expression ectopically into the SVZ/IZ (arrowheads) unlike control cells. (**b**) Quantification of Ngn2-expressing cells after *Drosha* and *Dgcr8* knockdown relative to control. (**c**) *NeuroD::mCherry* and *pCAGGs::eGFP* transfection reporter constructs. (**d**) *Drosha* knockdown cells induce *Neurod1* promoter activity (red) in the VZ. IZ. *t* test: $*P < 0.05$ and $**P < 0.001$. Error bars, s.e.m. (control, $n = 5$; *Drosha* knockdown, $n = 5$). All scale bars, 20 μm.

neural progenitors and showed a normal ventricular–subventricular zone distribution (**Supplementary Fig. 8**). Thus, Ngn2 not only can phenocopy the loss of microprocessor function but is a major effector in the Drosha loss-of-function phenotype.

Neurog2 mRNA contains hairpins bound by microprocessor

Drosha cKO, *Drosha* knockdown and *Dgcr8* knockdown resulted in similar phenotypes distinct to that caused by the ablation of *Dicer1* from neural progenitors. We speculated that the microprocessor has miRNA-independent functions in neural progenitors that modulate differentiation. *In silico* analysis revealed that the last 350 bases in the 3′ untranslated region (3′ UTR) of the *Neurog2* mRNA contain multiple evolutionarily conserved hairpin structures (EvoFold) (**Fig. 6a**). These hairpins were reminiscent of pri-miRNAs and thus were potential targets of the microprocessor. We examined whether the microprocessor bound *Neurog2* mRNA in neural progenitors by performing cross-linked immunoprecipitation (CLIP) (**Supplementary Fig. 9a**). We expressed Flag-tagged Drosha or Flag-tagged transdominant negative Drosha in N2A cells and Flag-tagged GFP as a control and analyzed bound RNAs after CLIP by qrt-PCR. As controls, *Dgcr8* but not *GAPDH* mRNA were precipitated by CLIP with Drosha and transdominant negative Drosha (**Fig. 6b** and **Supplementary Fig. 9b**). Endogenous *Neurog2* mRNA associated with Drosha and transdominant-negative Drosha. Thus, Drosha interacts with *Neurog2* mRNA, supporting potential destabilization. Algorithms predict conserved secondary stem-loop structures in *Neurod1* and *Neurod6* mRNAs, downstream determination factors and targets of proneural genes. *Neurod1* and *Neurod6* mRNAs also associated with Drosha and transdominant negative Drosha in N2A cells (**Fig. 6b**).

We assessed whether *Neurog2* mRNAs with intact 3′ ends were present in cultured NSCs. To detect potential deadenylated (and cleaved) RNA transcripts we performed *in vitro* RNA polyadenylation before 3′ rapid amplification of cDNA ends (RACE) rt-PCR using an anchored oligo(dT) RACE primer and an *Neurog2*-specific 5′ primer to generate amplicons that spanned the putative hairpin cleavage region of the mRNA. NSCs expressed Ngn2 at low levels and its mRNA could be detected with primers directed to the open reading frame (**Fig. 3c**). However, we did not detect *Neurog2* transcripts containing the 3′ end of the mRNA in *Drosha* heterozygous NSC cultures, which is consistent with transcript cleavage (**Fig. 6c**). In contrast, we detected intact *Neurog2* transcripts in *Drosha* cKO neurospheres (**Fig. 6c**). The total increase in full-length *Neurog2* mRNA

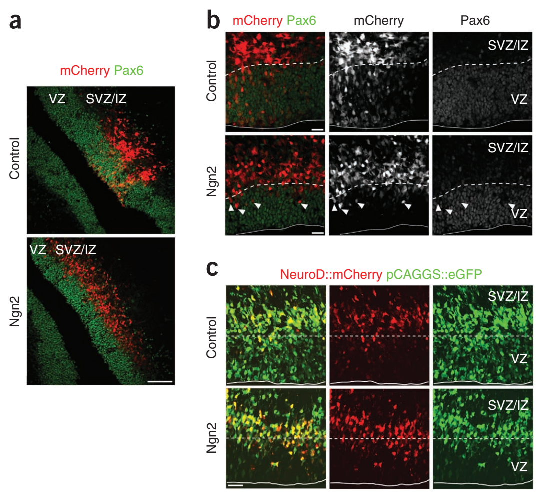

Figure 5 Expression of Ngn2 phenocopies Drosha inhibition and microprocessor inactivation and induces *NeuroD::mCherry* expression. (**a**) Expression of Ngn2 in ventricular zone (VZ) neural progenitors induces exit from the VZ, entry into the subventricular zone (SVZ/IZ) and loss of Pax6 expression similar to *Drosha* knockdown. (**b**) Magnification of Ngn2-expressing cells in the VZ (arrowheads) that do not express Pax6 compared to control transfected cells in the VZ, where most retain Pax6 expression. (**c**) Expression of Ngn2 leads to an activation of the *NeuroD::mCherry* reporter in a similar fashion to the inactivation of Drosha and microprocessor. Many cells migrate to the SVZ/IZ and the remaining Ngn2 over expressing cells in the VZ express *NeuroD::mCherry*. *t* test: $*P < 0.05$. Error bars, s.e.m. (control, $n = 3$; Ngn2, $n = 3$). All scale bars, 20 μm.

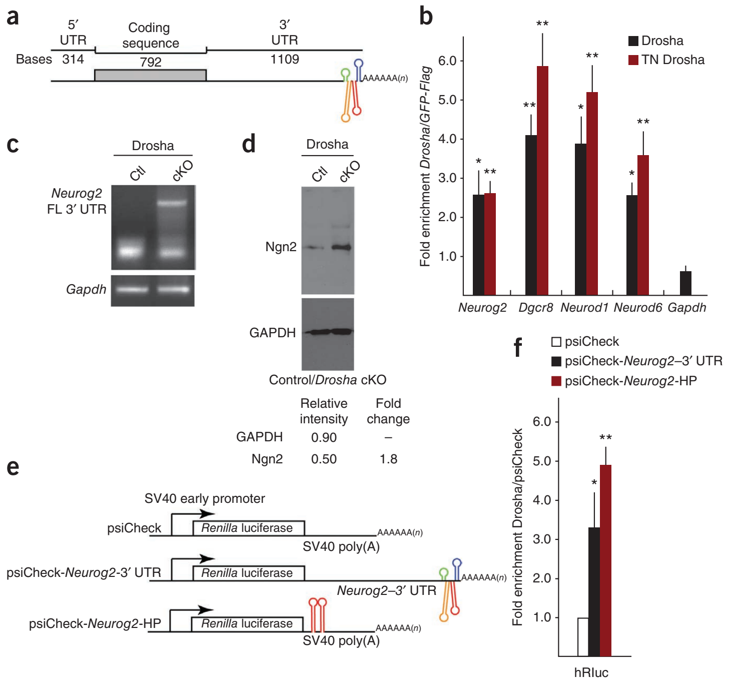

Figure 6 Drosha interacts and destabilizes hairpins within *Neurog2* mRNA. (**a**) Schematic representation of the mouse *Neurog2* mRNA. *Neurog2* mRNA contains a 3′ UTR of 1,109 bases with evolutionarily conserved hairpin structures (EvoFold prediction). (**b**) qrt-PCR analysis of *Neurog2, Dgcr8, Neurod1, NeuroD6* and *Gapdh* transcripts precipitated by CLIP from N2A cells with *Drosha* and transdominant negative (TN) Drosha. Values are fold enrichment over control CLIP-precipitated (Flag-GFP) transcripts. Statistical analysis of CLIP-precipitated products corrected relative to input RNA concentrations compared to Flag-GFP CLIPed samples. Agarose gel analysis of the amplicons is shown in **Supplementary Figure 9b.** (**c**) 3′-RACE analysis of full-length 3′ *Neurog2* mRNA (FL 3′ UTR) in control (Ctl: *Drosha*$^{flox/WT}$) and *Drosha* cKO neurospheres. (**d**) *Drosha* cKO translated into increased Ngn2 protein levels in neurospheres relative to control (Ctl: *Drosha*$^{flox/WT}$) neurospheres. Data were quantified by densitometry using ImageJ software, standardized to GAPDH levels. (**e**) Scheme of the mouse *Renilla* luciferase constructs expressing mRNAs containing either synthetic SV40 polyadenylation sequences (psiCheck), psiCheck–*Neurog2–3′* UTR or a synthetic SV40 polyadenylation sequences containing a tandem repeat of the *Neurog2* hairpin (bases 2,044–2,202) (psiCheck–*Neurog2*–hairpin). (**f**) qrt-PCR analysis of humanized *Renilla* luciferase (*hRluc*) mRNA from psiCheck–*Neurog2–3′* UTR and psiCheck–*Neurog2*–hairpin CLIP-precipitated from N2A relative to psiCheck. Values are fold enrichment over CLIP-precipitated (Flag-Drosha) psiCheck transcripts. Statistical analysis of CLIP-precipitated products corrected relative to input RNA concentrations compared to Flag-Drosha CLIP-precipitated samples. *t* test: $^*P < 0.05$ and $^{**}P < 0.001$. Error bars, s.e.m. For **b** and **f**, $n = 3$.

translated into an almost twofold increase in Ngn2 protein in *Drosha* cKO NSCs compared to heterozygous controls (**Fig. 6d**). These data suggested that *Neurog2* transcripts in NSC are normally destabilized by the microprocessor leading to reduced Ngn2 protein expression.

Neurog2 mRNA hairpin conveys microprocessor association

We addressed whether the 3′ UTR of the *Neurog2* mRNA and its hairpin structures bind the microprocessor. We inserted the entire *Neurog2* 3′ UTR downstream of the *Renilla* luciferase coding region in the dual reporter system psiCheck2 or two copies of the hairpin (bases 2,044–2,202) into the SV40 synthetic polyadenylation sequence and expressed these in N2A cells (**Fig. 6e**). We performed CLIP with Flag-tagged Drosha and qrt-PCR for *Renilla* luciferase mRNA. The full-length *Neurog2* 3′ UTR containing *Renilla* luciferase mRNA associated with Drosha and was precipitated by CLIP from transfected N2A cells (**Fig. 6f**). The *Neurog2* RNA hairpin alone was sufficient to convey mRNA binding to the microprocessor, whereas the SV40 synthetic polyadenylation sequence of psiCheck did not interact with the microprocessor. These data indicate that the conserved hairpin (bases 2,044–2,202) in the 3′ UTR of *Neurog2* transcripts is sufficient to convey binding of an mRNA to the microprocessor.

DISCUSSION

Our results are consistent with a new function for the microprocessor components Drosha and DGCR8 in neurogenesis in addition to miRNA biogenesis. We propose that the microprocessor destabilizes *Neurog2* mRNA, thereby regulating neural stem or progenitor cell maintenance independently of Dicer activity. Recent evidence supports alternate functions for Drosha and the microprocessor in the regulation of the cellular proteome in a cell- and tissue-specific manner by directly targeting and destabilizing hairpin-containing mRNAs[32,41–43]. The archetypal demonstration of this function is the cleavage of *Dgcr8* mRNA in an autoregulatory feedback mechanism[32]. Although it has been claimed that mRNA cleavage by Drosha may be specific for *Dgcr8* (ref. 44), comparison of *Drosha* and *Dicer1* cKO cells uncovered many microprocessor targeted mRNAs that are destabilized in a cell-specific manner[42]. Here we describe miRNA-independent regulation of *Neurog2* mRNA that reflects the endogenous instability of *Neurog2* transcripts in neural progenitors (**Supplementary Fig. 10a**).

NSCs depend on canonical Notch signaling and Hes proteins to block neurogenesis. Hes proteins and their mRNAs are hypostable and are regulated through an autoinhibitory oscillatory feedback mechanism (**Supplementary Fig. 10b**)[45]. Hes proteins (fluctuating amounts) bind to and repress proneural gene expression, including that encoding Ngn2. Ngn2 expression in forebrain neural progenitors is hypostable but upon loss of stem-cell status it accumulates, activates downstream targets and drives progenitors into differentiation[39,46]. Although Hes proteins are important for the inhibition of *Neurog2* transcription, it is unclear how *Neurog2* mRNAs are held in check and destabilized. We found that microprocessor activity in neural progenitors regulates both *Neurog2* mRNA and Ngn2 protein levels and thus neurogenesis. This suggests a key role for the microprocessor-dependent regulatory mechanism in NSCs, preventing precocious accumulation of Ngn2 synergistic with transcriptional regulation by Notch (**Supplementary Fig. 10b**). However, a reduction in microprocessor activity on the *Neurog2* mRNA could regulate the onset of differentiation of NSCs. As Ngn2 and its downstream targets are in an autoregulatory cascade, even moderate changes in *Neurog2* mRNA stability and half-life could affect fate.

The microprocessor is involved in early stages of miRNA biogenesis, and Dicer, in their maturation[47]. *Dicer1* cKO did not result in neural-progenitor differentiation in the forebrain or upregulation of Ngn2, consistent with previous reports and substantiating that the microprocessor has functions independent of miRNAs[17,29]. In addition, the rapid and dramatic phenotypic changes we observed were not associated with global changes in mature miRNA expression levels. This suggests that miRNAs are relatively stable in neural progenitors. miRANDA predicts several miRNAs that could potentially target *Neurog2* mRNA. Either these miRNAs were not expressed by neural progenitors, or their expression was not altered by microprocessor inactivation. We also showed that the conserved hairpins in *Neurog2* are sufficient to convey microprocessor association. Although we cannot formally exclude that accumulation of pri-miRNAs may have miRNA-independent functions in gene regulation, we phenocopied the Drosha and microprocessor inhibition phenotypes by forced expression of Ngn2. This suggested that Ngn2 regulation is a key element of the Dicer-independent function of the microprocessor in neural progenitors.

Our findings were reminiscent of the microprocessor cleavage of pri-miRNA–like hairpins in protein-coding mRNAs described previously[32,41–43] and provide a physiological relevance for this alternate function. EvoFold and Mfold algorithms predict that mRNAs encoding Ngn2, NeuroD1 and NeuroD6 all contain evolutionarily conserved hairpins that could be microprocessor targets. We show Drosha association with the mRNAs encoding NeuroD1 and NeuroD6 and transcript profiling of Drosha-deficient neural progenitors revealed increases in *Neurod1* and *Neurod6* as well as *Dgcr8* and *Fmr1* mRNAs (data not shown). *Fmr1* has been identified in a tiling microarray screen for Drosha-regulated mRNAs in *Drosophila melanogaster*[48]. We suggest that microprocessor action on target mRNAs in neural progenitors contributes to regulation of differentiation (**Supplementary Fig. 10b**).

Drosha-deficient neural progenitors downregulate progenitor markers, consistent with increased Ngn2 expression and activation of differentiation. They also migrate rapidly to the SVZ/IZ, similar to neural progenitors where Ngn2 expression is forced from a ubiquitous promoter. Ngn2 regulates the expression of Rnd2, which controls migration in the forebrain[46]. Although both *Drosha* knockdown and Ngn2 expression resulted in *Neurod1* activation, neither induced expression of the basal progenitor marker Tbr2. This suggests that Tbr2 expression requires additional mechanisms that are not activated and are potentially independent of Ngn2 and Drosha. Alternatively, the absence of precocious Tbr2 expression by microprocessor-deficient and Ngn2-expressing neural progenitors may reflect the rapid kinetics of the differentiation phenotype. Notably, neuroepithelial cells can generate neurons without generating Tbr2-expressing basal progenitors[49]. It remains to be determined whether Drosha is also involved in this process during development.

We provide to our knowledge the first evidence for a direct mechanism through which Drosha and the microprocessor can regulate neural progenitor maintenance and differentiation during development. How does *Neurog2* mRNA and protein accumulate in neural progenitors to initiate differentiation under normal differentiation? Although *Drosha* and *Dgcr8* mRNA levels are prominent in neural progenitors in the ventricular zone, their expression is somewhat reduced in cells within the SVZ/IZ and where Ngn2-expressing cells accumulate. Furthermore, NeuroD1 and NeuroD6 expression also increases in this region[39]. Thus, microprocessor expression and activity may be downregulated as neural progenitors commit to differentiation enabling Ngn2 to accumulate through a positive feedback autoregulation on its own promoter. In addition, microprocessor function may be controlled at target hairpins by cell- and tissue-specific expression of regulatory proteins that could include RNA-binding proteins that compete with the microprocessor. This remains to be explored but opens a potentially new avenue for post-translational proteome regulation. Precedent for this is found in the function of Lin28, which blocks microprocessor cleavage of a subset of pri-miRNAs[50]. Our data indicate the multifaceted functions of Drosha in the regulation of mRNA expression. The full pallet of neural progenitor mRNAs regulated by the microprocessor in this way remains to be uncovered.

METHODS

Methods and any associated references are available in the online version of the paper.

Note: Supplementary information is available in the online version of the paper.

ACKNOWLEDGMENTS

We thank N. Kim (Seoul National University) for *Drosha* constructs, F. Guillemot (UK National Institute for Medical Research) for *Neurog2* and shRNA constructs, and P. Herrare for *beta2/NeuroD* promoter, members of the Taylor laboratory for helpful discussions, and F. Sager for excellent technical assistance. P.K. and S.L. were PhD students of the International Max Planck Research School Molecular and Cellular Biology and of the Faculty of Biology, University of Freiburg, M.A.V. is a PhD student of the Department of Biomedical Science, University of Sheffield. This work was supported by the Deutsche Forschungsgemeinschaft (TA–310–1, TA–310–2 and SFB592 to V.T.).

AUTHOR CONTRIBUTIONS

P.K. and M.A.V. performed the experiments, analyzed the data and wrote the paper, S.L. cloned the *Hes5::Cre* construct and performed neurosphere assays, M.M. analyzed the miRNA array data, M.M.W.C. and D.R.L. provided the floxed *Drosha* mice, G.M.H. and S.A.W. helped with the CLIP analysis. V.T. designed the project, performed experiments, analyzed the data and wrote the paper.

COMPETING FINANCIAL INTERESTS

The authors declare no competing financial interests.

Published online at http://www.nature.com/doifinder/10.1038/nn.3139.
Reprints and permissions information is available online at http://www.nature.com/reprints/index.html.

1. Eulalio, A., Huntzinger, E. & Izaurralde, E. Getting to the root of miRNA-mediated gene silencing. *Cell* **132**, 9–14 (2008).
2. Filipowicz, W., Bhattacharyya, S.N. & Sonenberg, N. Mechanisms of post-transcriptional regulation by microRNAs: are the answers in sight? *Nat. Rev. Genet.* **9**, 102–114 (2008).
3. Lewis, B.P., Burge, C.B. & Bartel, D.P. Conserved seed pairing, often flanked by adenosines, indicates that thousands of human genes are microRNA targets. *Cell* **120**, 15–20 (2005).
4. Lai, E.C. Micro RNAs are complementary to 3′ UTR sequence motifs that mediate negative post-transcriptional regulation. *Nat. Genet.* **30**, 363–364 (2002).
5. Gregory, R.I. *et al.* The Microprocessor complex mediates the genesis of microRNAs. *Nature* **432**, 235–240 (2004).
6. Han, J. *et al.* The Drosha-DGCR8 complex in primary microRNA processing. *Genes Dev.* **18**, 3016–3027 (2004).
7. Denli, A.M., Tops, B.B., Plasterk, R.H., Ketting, R.F. & Hannon, G.J. Processing of primary microRNAs by the microprocessor complex. *Nature* **432**, 231–235 (2004).
8. Chendrimada, T.P. *et al.* TRBP recruits the Dicer complex to Ago2 for microRNA processing and gene silencing. *Nature* **436**, 740–744 (2005).
9. Okamura, K., Hagen, J.W., Duan, H., Tyler, D.M. & Lai, E.C. The mirtron pathway generates microRNA-class regulatory RNAs in *Drosophila*. *Cell* **130**, 89–100 (2007).
10. Ruby, J.G., Jan, C.H. & Bartel, D.P. Intronic microRNA precursors that bypass Drosha processing. *Nature* **448**, 83–86 (2007).

11. Babiarz, J.E., Ruby, J.G., Wang, Y., Bartel, D.P. & Blelloch, R. Mouse ES cells express endogenous shRNAs, siRNAs, and other Microprocessor-independent, Dicer-dependent small RNAs. *Genes Dev.* **22**, 2773–2785 (2008).
12. Yang, J.S. & Lai, E.C. Alternative miRNA biogenesis pathways and the interpretation of core miRNA pathway mutants. *Mol. Cell* **43**, 892–903 (2011).
13. Ender, C. *et al.* A human snoRNA with microRNA-like functions. *Mol. Cell* **32**, 519–528 (2008).
14. Cheloufi, S., Dos Santos, C.O., Chong, M.M. & Hannon, G.J. A dicer-independent miRNA biogenesis pathway that requires Ago catalysis. *Nature* **465**, 584–589 (2010).
15. Cifuentes, D. *et al.* A novel miRNA processing pathway independent of Dicer requires Argonaute2 catalytic activity. *Science* **328**, 1694–1698 (2010).
16. Yang, J.S. *et al.* Conserved vertebrate mir-451 provides a platform for Dicer-independent, Ago2-mediated microRNA biogenesis. *Proc. Natl. Acad. Sci. USA* **107**, 15163–15168 (2010).
17. De Pietri Tonelli, D. *et al.* miRNAs are essential for survival and differentiation of newborn neurons but not for expansion of neural progenitors during early neurogenesis in the mouse embryonic neocortex. *Development* **135**, 3911–3921 (2008).
18. Babiarz, J.E. *et al.* A role for noncanonical microRNAs in the mammalian brain revealed by phenotypic differences in Dgcr8 versus Dicer1 knockouts and small RNA sequencing. *RNA* **17**, 1489–1501 (2011).
19. Georgi, S.A. & Reh, T.A. Dicer is required for the transition from early to late progenitor state in the developing mouse retina. *J. Neurosci.* **30**, 4048–4061 (2010).
20. Kaneko, H. *et al.* DICER1 deficit induces Alu RNA toxicity in age-related macular degeneration. *Nature* **471**, 325–330 (2011).
21. Anthony, T.E., Klein, C., Fishell, G. & Heintz, N. Radial glia serve as neuronal progenitors in all regions of the central nervous system. *Neuron* **41**, 881–890 (2004).
22. Gotz, M. & Huttner, W.B. The cell biology of neurogenesis. *Nat. Rev. Mol. Cell Biol.* **6**, 777–788 (2005).
23. Kageyama, R., Niwa, Y., Shimojo, H., Kobayashi, T. & Ohtsuka, T. Ultradian oscillations in Notch signaling regulate dynamic biological events. *Curr. Top. Dev. Biol.* **92**, 311–331 (2010).
24. Gohlke, J.M. *et al.* Characterization of the proneural gene regulatory network during mouse telencephalon development. *BMC Biol.* **6**, 15 (2008).
25. Kageyama, R., Ohtsuka, T., Shimojo, H. & Imayoshi, I. Dynamic regulation of Notch signaling in neural progenitor cells. *Curr. Opin. Cell Biol.* **21**, 733–740 (2009).
26. Masamizu, Y. *et al.* Real-time imaging of the somite segmentation clock: revelation of unstable oscillators in the individual presomitic mesoderm cells. *Proc. Natl. Acad. Sci. USA* **103**, 1313–1318 (2006).
27. Guillemot, F. Spatial and temporal specification of neural fates by transcription factor codes. *Development* **134**, 3771–3780 (2007).
28. Miyata, T., Kawaguchi, D., Kawaguchi, A. & Gotoh, Y. Mechanisms that regulate the number of neurons during mouse neocortical development. *Curr. Opin. Neurobiol.* **20**, 22–28 (2010).
29. Makeyev, E.V., Zhang, J., Carrasco, M.A. & Maniatis, T. The MicroRNA miR-124 promotes neuronal differentiation by triggering brain-specific alternative pre-mRNA splicing. *Mol. Cell* **27**, 435–448 (2007).
30. Lutolf, S., Radtke, F., Aguet, M., Suter, U. & Taylor, V. Notch1 is required for neuronal and glial differentiation in the cerebellum. *Development* **129**, 373–385 (2002).
31. Imayoshi, I., Sakamoto, M., Yamaguchi, M., Mori, K. & Kageyama, R. Essential roles of Notch signaling in maintenance of neural stem cells in developing and adult brains. *J. Neurosci.* **30**, 3489–3498 (2010).
32. Han, J. *et al.* Posttranscriptional crossregulation between Drosha and DGCR8. *Cell* **136**, 75–84 (2009).
33. Salomoni, P. & Calegari, F. Cell cycle control of mammalian neural stem cells: putting a speed limit on G1. *Trends Cell Biol.* **20**, 233–243 (2010).
34. Nguyen, L. *et al.* p27kip1 independently promotes neuronal differentiation and migration in the cerebral cortex. *Genes Dev.* **20**, 1511–1524 (2006).
35. Cheung, T.H. *et al.* Maintenance of muscle stem-cell quiescence by microRNA-489. *Nature* **482**, 524–528 (2012).
36. Wang, Y. & Blelloch, R. Cell cycle regulation by MicroRNAs in embryonic stem cells. *Cancer Res.* **69**, 4093–4096 (2009).
37. Gantier, M.P. *et al.* Analysis of microRNA turnover in mammalian cells following Dicer1 ablation. *Nucleic Acids Res.* **39**, 5692–5703 (2011).
38. Kawase-Koga,, Y. *et al.* RNaase-III enzyme Dicer maintains signaling pathways for differentiation and survival in mouse cortical neural stem cells. *J. Cell Sci.* **123**, 586–594 (2010).
39. Guillemot, F. Cellular and molecular control of neurogenesis in the mammalian telencephalon. *Curr. Opin. Cell Biol.* **17**, 639–647 (2005).
40. Nieto, M., Schuurmans, C., Britz, O. & Guillemot, F. Neural bHLH genes control the neuronal versus glial fate decision in cortical progenitors. *Neuron* **29**, 401–413 (2001).
41. Ganesan, G. & Rao, S.M. A novel noncoding RNA processed by Drosha is restricted to nucleus in mouse. *RNA* **14**, 1399–1410 (2008).
42. Chong, M.M. *et al.* Canonical and alternate functions of the microRNA biogenesis machinery. *Genes Dev.* **24**, 1951–1960 (2010).
43. Karginov, F.V. *et al.* Diverse endonucleolytic cleavage sites in the mammalian transcriptome depend upon microRNAs, Drosha, and additional nucleases. *Mol. Cell* **38**, 781–788 (2010).
44. Shenoy, A. & Blelloch, R. Genomic analysis suggests that mRNA destabilization by the microprocessor is specialized for the auto-regulation of Dgcr8. *PLoS ONE* **4**, e6971 (2009).
45. Shimojo, H., Ohtsuka, T. & Kageyama, R. Oscillations in notch signaling regulate maintenance of neural progenitors. *Neuron* **58**, 52–64 (2008).
46. Heng, J.I. *et al.* Neurogenin 2 controls cortical neuron migration through regulation of Rnd2. *Nature* **455**, 114–118 (2008).
47. Kim, V.N., Han, J. & Siomi, M.C. Biogenesis of small RNAs in animals. *Nat. Rev. Mol. Cell Biol.* **10**, 126–139 (2009).
48. Kadener, S. *et al.* Genome-wide identification of targets of the drosha-pasha/DGCR8 complex. *RNA* **15**, 537–545 (2009).
49. Noctor, S.C., Martinez-Cerdeno, V., Ivic, L. & Kriegstein, A.R. Cortical neurons arise in symmetric and asymmetric division zones and migrate through specific phases. *Nat. Neurosci.* **7**, 136–144 (2004).
50. Heo, I. *et al.* TUT4 in concert with Lin28 suppresses microRNA biogenesis through pre-microRNA uridylation. *Cell* **138**, 696–708 (2009).

ONLINE METHODS

Animals and administration of thymidine analogs. *Hes5::GFP*, floxed *Drosha* and floxed *Dicer1* mice have been described elsewhere[51–53]. Adult mice 8–12 weeks of age were used in the experiments. Mice were maintained on a 12-h day-night cycle with adequate food and water under specific pathogen-free conditions and according to Max Planck Institutional and German Federal regulations and under license numbers H-05/01, 0-06/02, G-09/18, G-09/19 and G-08/26 (Ethical Commission Freiburg, Germany). The day of vaginal plug was considered as embryonic day 0 (E0). Bromodesoxyuridine (BrdU; Sigma) 50 mg/kg body weight, was administered by intraperitoneal (i.p.) injection 3 h before killing the mice.

In utero **electroporation for overexpression in neural progenitors** ***in vivo*****.** Female C57BL/6J, floxed *Drosha* and floxed *Dicer1* mice were anesthetized with isoflurane 13.5 d after detection of vaginal plug and their uteri were exposed. For the injection of DNA constructs, a microinjector (Pneumatic Pico Pump, WPI Rnage) and Borosilicate glass capillaries (Kwick-Fil; Hampton Research) were used. The capillaries were pulled in a micropipette puller (Sutter Instrument Co.). The tip of the capillaries was broken and sharpened using a capillary sharpener (Bachofer). The capillaries were back end–loaded with 10 μl of the plasmid. Plasmid stocks were prepared under endotoxin-free conditions. Plasmids were dissolved in sterile PBS at a high concentration (2–4 μg/μl). A fast green contrast dye (10%) was added to the plasmids to visualize targeted area of the telencephalon. The overexpression or knockdown vectors were electroporated in a molecular excess of 3:1 with the transfection reporter vector (pCAGGs::mCherry or pCAGGs::eGFP). Mice were anesthetized with 1–2% isoflurane (Baxter) in a constant flow of O_2 and secured on a heated operating table. Body temperature was monitored continually. The fur was removed from the abdomen using depilation cream. Throughout the operation the peritoneal cavity was moistened with sterile HBSS to prevent drying. The uterine horns containing the embryos (E13.5) were manipulated under sterile conditions by hand. A cold light source was used to illuminate the developing embryos. We injected 1–2 μl of DNA solution (3–4 μg) into the lateral ventricles of each embryo. The embryos were electroporated (Electro Square Pavator, BTX; Harvard Apparatus) with ten pulses of 40 V and a pulse length of 50 ms at 950-ms intervals. The anode of the electrode was oriented toward the injected side. After injection and electroporation, the uterus was returned into the abdomen, the muscle and the skin sutured and the females allowed to recover under a heating lamp with constant observation and were given free access to postoperative analgesic (Temgesic jelly). The animals were sacrificed after a defined time by cervical dislocation or CO_2 inhalation and the embryos isolated and prepared for sectioning.

Expression plasmids and constructs. Full-length cDNAs for mCherry and eGFP were subcloned into pCAGGs expression vectors, the Ngn2 cDNA including the endogenous UTRs was a gift from F. Guillemot. pSuper-shDrosha and pSuper-shDGCR8 were obtained from Addgene; pSuper-shGFP was a gift of D. Messerschmitt and pSuper-shRenilla was cloned according to the manufacturer's instructions (Oligoengine). pCK-Drosha-WT-Flag and pCK-TN-Drosha-Flag expression constructs (TN, transdominant negative) have been described previously[32] and *Hes5::Cre* was generated by cloning a Cre-recombinase cDNA into the ATG of the *Hes5* transgene as described previously[51]. *NeuroD::mCherry* reporter was generated by cloning an mCherry cDNA downstream of the *NeuroD* promoter (Beta2) in the pBS-Beta2 plasmid. The mouse *Neurog2* 3′ UTR and tandem copies of the hairpin fragment bases 2044–2202 of the mouse *Neurog2* mRNA were amplified by PCR and cloned into the NotI site of psiCheck2 vector (Promega) 3′ to the open reading frame of the *Renilla* luciferace.

In situ **RNA hybridization.** Brains were isolated, frozen in OCT compound (TissueTech), and 20 μm cryostat sections were made and postfixed in 4% PFA. *In situ* RNA hybridization was performed as described previously[54]. A digoxigenin (DIG)-labeled RNA probe for Drosha (amplified from mouse cDNA using primers fwd 5′-TAATGATCCGGACCTTCGAG-3′ and rev 5′-CTTAGAAAGGCAATGCTCCG-3′) using the procedures described previously[54]. Expression was detected by colorimetric reaction using NBT (nitro-blue tetrazolium chloride) and BCIP (5-bromo-4-chloro-3-indolylphosphate p-toluidine) as reaction substrates and images taken using an Axioplan microscope (Zeiss) with an Axiocam charge-coupled device (CCD) camera (Zeiss).

Fluorescence-activated cell sorting (FACS), neurosphere cultures and immunohistochemistry and terminal deoxynucleotidyl transferase dUTP nick end labeling (TUNEL). Brains of electroporated embryos were transferred to L15 medium (Gibco) and the electroporated area of the brain microdissected and mechanically dissociated in the presence of L-cysteine and papain. Cells were sorted by FACS, gating on mCherry$^+$ or GFP$^+$ cell populations depending on the experiment. Neurosphere cultures were established from E13.5 floxed *Drosha*, floxed *Dicer1* and control embryo brains in the presence of FGF2 and EGF as described previously[51,55]. Cre recombinase–expressing adenovirus (adeno-Cre) infection and analysis of neurosphere number were performed as described previously[56]. For histology, embryos were collected, and the brains were fixed in 4% paraformaldehyde (PFA) solution in 0.1 M phosphate buffer overnight. Brains were cryoprotected in a 30% sucrose solution in 0.1 M phosphate buffer for 24 h, embedded and frozen over dry ice in OCT (TissueTEK). Horizontal sections (20 μm) were collected on Superfrost glass slides (Thermo Scientific) and stored at −20 °C until use. For immunostaining, sections were incubated overnight at 4 °C with the primary antibody diluted in blocking solution of 2% normal donkey serum (Jackson ImmunoResearch), 0.1% Triton X-100 in PBS. Sections were washed three times in PBS and incubated at room temperature for 3 h with the corresponding secondary antibodies in blocking solution. When signal amplification was needed, sections were washed and incubated for 1 h at room temperature in streptavidin-FITC (Jackson ImmunoResearch; 1:400) and counterstained with DAPI (1 μg/ml). For BrdU detection, sections were treated with 2 M HCl at 37 °C for 15 min before primary antibody incubation. HCl-treated sections were then equilibrated in borate buffer (0.1 M, pH 8.5) for 10 min. For Ki67, Ngn2 and Tbr2 detection, antigens were recovered at 80 °C for 30 min in sodium citrate solution (10 mM, pH 6.0). Stained sections were embedded in mounting medium containing diazabicyclo-octane (DABCO; Sigma) as an anti-fading agent and visualized using a Zeiss LSM510 confocal microscope. Antibodies and conditions used for immunolabeling were rat anti-BrdU (1:500; OBT0030, AbD Serotec), rabbit anti–cleaved Caspase3 (1:200; 5A1E, Cell Signaling), rabbit anti-Drosha (1:1000; D2881, Cell Signaling), rabbit anti-Drosha (1:100; ab12286, Abcam), mouse anti–γ-tubulin (1:25; D2881, Sigma), mouse anti-GAPDH (1:10,000; 6C5, Calbiochem), guinea pig anti-GLAST (1:200; AB1782, Chemicon), rat anti-Ki67 (1:25; TEC-3, Dako), mouse anti-Ngn2 (1:500; MAB3314, R and D), rabbit anti-Pax6 (1:300; PRB-278P, Covance), mouse anti-Sox2 (1:500; AB5770, Chemicon), rabbit anti-Tbr2 (1:1000; ab23345, Abcam) in combination with FITC- or Cy3-conjugated donkey anti–species specific immunoglobulin antibodies (1:1,000; Jackson ImmunoResearch). For TUNEL labeling of DNA, an *In situ* Cell Death Detection Kit (Roche) was used according to the manufacturer's instructions. Sections were analyzed with an Axioscope (Zeiss) or confocal (Zeiss LSM510) fluorescence microscope. Fragmented cell debris lacking DAPI stained nuclei was visualized with either an Axioscope (Zeiss) or confocal (Zeiss LSM510) fluorescence microscope and 3D reconstruction. Images were acquired using Axiovision or Zeiss LSM 4.2 (Zeiss) and processed with ImageJ 1.33 or Photoshop CS4 (Adobe) software.

RNA analysis and ***Neurog2*** **3′ RACE fragment detection.** Total RNA was isolated from FACS-sorted electroporated cells or adeno-Cre–infected neurospheres using mirVANA total RNA isolation kits (Ambion) according to the manufacturer's instructions. RNA purity and quantity were verified using a Bioanalyser 2100 RNA chips (Agilent). miRNA profiling was performed on TaqMan arrays (Invitrogen) with 500 ng of purified RNA according to the manufacturer's instructions. Expression analysis was performed using the comparative cycle threshold (Ct) method. For 3′ RACE of *Neurog2* fragment detection, total RNA was 3′ polyadenylated using poly(A) polymerase (NEB) following the manufacturer's instructions. We used 1 μg of total RNA for cDNA synthesis using the Superscript III First-Strand kit for rt-PCR (Invitrogen), priming the reaction with an anchored 3′ RACE oligo(dT) primer. PCR amplification from cDNA was performed using Kappa2G polymerase (Peqlab) with forward *Neurog2*-specific primers and an anchor binding primer. Resulting fragments, including *Neurog2* full-length 3′ UTR RNAs, were visualized by standard gel electrophoresis cloned and sequenced. *Gapdh* was amplified as a control using mRNA-specific primers. The primers used were β-actin fwd 5′-AAGGCCAACCGTGAAAAG

AT-3′ and rev 5′-GTGGTACGACCAGAGGCATAC-3′, 3′ RACE oligo-dT fwd 5′-GACCACGCGTATCGATGTCGACTTTTTTTTTTTTTTTTTV-3′, 3′ RACE anchor 5′-GACCACGCGTATCGATGTCGAC-3′, 3′ RACE forward 5′-TTGTAGGCTTTTGTAAGGGTTG-3′, *Drosha* fwd 5′-CTATGATCGGGGGAGAACG-3′ and rev 5′-CCGGTGCCTGTGTCTCTC-3′, *Dgcr8* fwd 5′-GGCGAATGGAGGAAAAATATG-3′ and rev 5′-AGGCAATGGCTCTGTAGGTG-3′, *Dgcr8* (CLIP) fwd 5′-GCCACAGGTGGAAGAAGAA-3′ and rev 5′-ACACTGGCGGCTTAGTCAA-3′, *Gapdh* fwd 5′-AGTGATGGCATGGACTGTGGTC-3′ and rev 5′-TCCATGACAACTTTGGCATTGTGG-3′, *Neurod1* fwd 5′-CGCAGAAGGCAAGGTGTC-3′ and rev 5′-TTTGGTCATGTTTCCACTTCC-3′, *Neurog2* fwd 5′-GACATTCCCGGACACACAC-3′ and rev 5′-AGTCTCAGATTTGACGAACATCC-3′, *Neurog2* (CLIP) fwd 5′-AGGAGGGAGGATTGCTTC-3′ and rev 5′-GGCATCTGCTCTATTCCCA-3′, *hRluc* fwd 5′-TGATCGGAATGGGTAAGTCC-3′ and rev 5′-GGCCTTGATCTTGTCTTGGT-3′, *Sox2* fwd 5′-TCCAAAAACTAATCACAACAATCG-3′ and rev 5′-GAAGTGCAATTGGGATGAAAA-3′, and *Tbp* fwd 5′-CGGTCGCGTCATTTTCTC-3′ and rev 5′-GGGTTATCTTCACACACCATGA-3′.

Quantitative real-time PCR analysis of gene and miRNA expression. For RNA isolation, cells were lysed directly in Trizol (Invitrogen) reagent. RNA was prepared according to the manufacturer's instructions. We used 1 μg of total RNA for cDNA synthesis by oligo(dT) priming and Superscript III first strand kit (Invitrogen). For quantitative rt-PCR, we used the comparative Ct method with Roche Universal probes performed on a 7300 Real-Time PCR System (Applied Biosystems). TATA-binding protein, β-actin and *Gapdh* mRNA levels were measured as endogenous controls and for quantification. For mature miRNA quantification, SYBR green–based Ncode system (Invitrogen) was used following the manufacturer's instructions and normalized to *U6* RNA.

Cross-linked RNA immunoprecipitation. N2A cells were transfected using Lipofectamine 2000 (Invitrogen) according to manufacturer's instructions with p3X-Flag-GFP or pCK-Drosha-WT-Flag or pCK-TN-Drosha-Flag and trypsinized after 48 h. The cells were then fixed in 3% formaldehyde in PBS for 10 min and lysed by sonication (10 pulses for 10 s). Immunoprecipitation was performed overnight at 4 °C using anti-Flag M2 Affinity Gel (Sigma-Aldrich). After collection by centrifugation at 2,000*g* and washing 3–4 times with lysis buffer, the complexes were reverse cross-linked, and RNA was extracted using Trizol reagent (Invitrogen) according to the manufacturer's instructions. Isolated RNA was treated with RNase-free DNase I (Roche) to remove any genomic DNA contamination. First-strand cDNA was generated using BioScrip (Bioline) and random hexamer primers followed by real-time PCR using SensiMix SYBR kit (Bioline).

Quantification and statistical analysis of the data. Randomly selected, stained cells were analyzed with fixed photomultiplier settings on a Zeiss LSM510 confocal microscope. Data are presented as average percentages of co-labeled cells. Statistical comparisons were conducted by two-tailed unpaired Student's *t*-test. Significance was established at $P < 0.05$. In all graphs, error bars, s.d.

51. Basak, O. & Taylor, V. Identification of self-replicating multipotent progenitors in the embryonic nervous system by high Notch activity and Hes5 expression. *Eur. J. Neurosci.* **25**, 1006–1022 (2007).
52. Harfe, B.D., McManus, M.T., Mansfield, J.H., Hornstein, E. & Tabin, C.J. The RNaseIII enzyme Dicer is required for morphogenesis but not patterning of the vertebrate limb. *Proc. Natl. Acad. Sci. USA* **102**, 10898–10903 (2005).
53. Chong, M.M., Rasmussen, J.P., Rudensky, A.Y. & Littman, D.R. The RNAseIII enzyme Drosha is critical in T cells for preventing lethal inflammatory disease. *J. Exp. Med.* **205**, 2005–2017 (2008).
54. Stump, G. *et al.* Notch1 and its ligands Delta-like and Jagged are expressed and active in distinct cell populations in the postnatal mouse brain. *Mech. Dev.* **114**, 153–159 (2002).
55. Giachino, C., Basak, O. & Taylor, V. Isolation and manipulation of mammalian neural stem cells *in vitro*. *Methods Mol. Biol.* **482**, 143–158 (2009).
56. Nyfeler, Y. *et al.* Jagged1 signals in the postnatal subventricular zone are required for neural stem cell self-renewal. *EMBO J.* **24**, 3504–3515 (2005).

doi:10.1038/nn.3139